NASA Contractor Report 2920

Calibration of Transonic and Supersonic Wind Tunnels

T. D. Reed, T. C. Pope, and J. M. Cooksey

CONTRACT NAS2-8606
NOVEMBER 1977

NASA

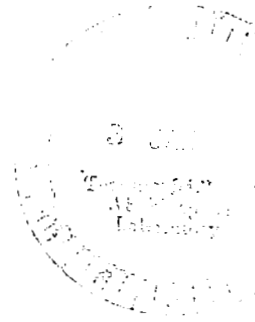

NASA Contractor Report 2920

Calibration of Transonic and Supersonic Wind Tunnels

T. D. Reed, T. C. Pope, and J. M. Cooksey
Vought Corporation
Dallas, Texas

Prepared for
Ames Research Center
under Contract NAS2-8606

National Aeronautics
and Space Administration

**Scientific and Technical
Information Office**

1977

FOREWORD

In April, 1970 a report was issued by an ad hoc NASA-USAF group on transonic scale effects and testing techniques. This report assessed transonic testing techniques and recommended, among other things, that a transonic wind-tunnel calibration manual be written which reviewed the state-of-the-art. This was viewed as a necessary step toward the development of more accurate and standardized tunnel calibration procedures.

For this purpose, the present manual was jointly funded by: (1) the U. S. Navy through the Office of Naval Research, (2) the U. S. Air Force through the Air Force Flight Dynamics Laboratory and Arnold Research Organization, (3) NASA through the Washington Headquarters and the Lewis, Langley and Ames Research Centers. The contract was administered by NASA Ames. Mr. F. W. Steinle served as technical monitor.

A rough draft of this manual was reviewed by personnel of NASA Ames Research Center and Arnold Research Organization. The comments of the various reviewers were compiled by Mr. F. W. Steinle at Ames and Mr. F. M. Jackson at ARO. The manual was improved considerably by the constructive comments that were received, and we wish to thank all those involved for their time and efforts.

Our thanks go to Mr. C. J. Stalmach of the Vought Corporation for the discussion of hot wires and films which is given in Appendix I. Finally, we wish to acknowledge the superior typing and secretarial assistance provided by Ms. F. H. Deason.

TABLE OF CONTENTS

LIST OF ILLUSTRATIONS

NOMENCLATURE*

A	amplitude of sinusoidal oscillation, or probe interference function introduced in Eq. (3.D.1)
B	function introduced in Eq. (3.D.1) as a measure of probe-crossflow interference
B_M	fixed error limit for Mach number, Eq. (4.D.2)
B_γ	estimated uncertainty limit for ratio of specific heats, Eq. (4.D.2)
B_{P_∞}	estimated uncertainty limit for static pressure, Eq. (4.D.2)
C	Chapman-Rubesin viscosity parameter
ΔC_{D_G}	drag coefficient increment produced by a linear pressure gradient in the test section
ΔCp	RMS value of fluctuating static pressure coefficient
$\Delta Cp(n)$	RMS fluctuating static pressure coefficient per unit band width at frequency n.
D	diameter of a transverse, cylindrical, probe support
D_s	distance between centers of slots in tunnel wall
d	diameter of static pressure probe
d_1	diameter of Pitot probe
d_o	orifice diameter
$F(n)$	nondimensional spectral function which is a measure of the intensity of static pressure fluctuations per unit band width at the frequency n, $\Delta Cp = \int_o^\infty F(n)dn$
f	frequency of oscillation
f_p	frequency of static pressure fluctuations
f_r	fineness ratio of probe nose ($2L_n/d$)
H	total head or stagnation pressure in test section

*Separate lists of symbols appear in Appendices I and II.

H_s	total head in settling chamber
H'	Pitot pressure at $\alpha = 0$ (either subsonic or supersonic)
H_2, $\overline{H}_2$	time-averaged, total pressure behind a normal shock
$\langle H_2' \rangle$	RMS of fluctuating total pressure behind a normal shock
K	slot parameter, Eq. (3.6.7)
L_m	model length
L_n	nose length
l_o	distance from cone-cylinder juncture to nearest static pressure orifice
ℓ	distance from a static pressure orifice to beginning of a probe enlargement, e.g., flare or support
M_c	Mach number based on static pressure in plenum chamber
M	Mach number in test section
$\dot{m}_w$	mass flow per unit area through ventilated wall
$\dot{m}_\infty$	mass flow per unit area in freestream of test section
n	reduced frequency of static pressure fluctuations, $f_p W_T/U_\infty$
n_d	general designation for direction normal to a wall
P	static pressure in freestream of test section
$\langle P' \rangle$	RMS of fluctuating static pressure
$P_m(t)$	measured, unsteady static pressure
P_s	static pressure in settling chamber
$P_t(t)$	true, unsteady static pressure of undisturbed freestream
$\overline{P}_t(t)$	time-averaged, true static pressure
P_w	static pressure measured on a probe or tunnel sidewall
q'	indicated dynamic pressure, $H'-P$
q_i	incompressible definition of dynamic pressure, $H-P$
q_s	dynamic pressure in settling chamber
q_∞	dynamic pressure of freestream in test section
R	porosity parameter, Eq. (3.G.5)

R_s	viscous parameter for flow through slots
Re	Reynolds number
Re_x	Reynolds number based on wetted length
S	wing reference area, or width of a strut support for a probe
S_y	compressible yawmeter sensitivity, Eq. (3.E.2)
S_y^*	incompressible yawmeter sensitivity, Eq. (3.E.1)
T	period of sinusoidal oscillation
t	time
U(t)	total, unsteady velocity along a probe axis
U_M	total uncertainty interval for Mach number, Eq. (4.D.3)
U_∞	velocity of freestream in test section
u_s	velocity of sound source
u_τ	turbulent friction velocity, $(\tau_w/\rho)^{1/2}$
V	model volume
$V_n(t)$	total, unsteady velocity normal to a probe axis
v_n	average velocity normal to a ventilated wall
W_s	width of slots
W_T	square root of cross-sectional area of test section
x	Cartesian coordinate measured along the tunnel axis
Y	Cartesian coordinate measured normal to the tunnel sidewalls
z	Cartesian coordinate measured normal to the top and bottom walls of tunnel

Greek Letters

α	angle of attack
β	$(1 - M^2)^{1/2}$
γ	ratio of specific heats
δ	angle between orifice planes of a yawmeter
η	azmuthal angle or polar coordinate angle

θ	semi-vertex angle of a cone
θ_w	tunnel wall angle (positive for divergent walls)
μ_e	viscosity coefficient at edge of boundary layer
μ_w	viscosity coefficient at wall temperature
ρ	density of gas
σ_m	standard deviation in Mach number along tunnel centerline
τ	wall porosity
τ_w	shear stress at a solid wall
ϕ	perturbation velocity potential, Eq. (3.6.1)
ψ	yaw angle
ω	angular velocity, rad/sec

I. INTRODUCTION

I.A. Background

The use of a wind tunnel for aerodynamic measurements requires a knowledge of the test environment. Furthermore, a definite relationship obviously exists between the accuracy with which the test conditions are known and the uncertainty in the final results. The demand for increased wind tunnel data accuracy follows naturally from the demand for improved full scale vehicle performance and accuracy of performance prediction. A sustained effort has been directed toward improving the accuracy of test data from existing wind tunnel facilities. In addition, requirements have been established for new wind tunnel facilities with more complete simulation capabilities.

The results of one of the first comprehensive test programs to study the correlation of wind tunnel data from several transonic facilities were reported by Treon et al. in Ref. (1). Since the same model, instrumentation and support sting were used in each of the three tunnels, this unique series of tests allowed a comparative evaluation of the effects of facility flow environment and calibration upon data agreement. The results of this series of tests, using state-of-the-art techniques and instrumentation, were considered good but deficient relative to current goals.

The purpose of this report is to review the current state-of-the-art of wind tunnel calibration techniques and instrumentation, evaluate the expected results and, where possible, recommend improvements. This program was carried out by (1) acquiring information from eighty-eight wind tunnel facilities by means of a comprehensive questionnaire, (2) a detailed literature search, (3) personal visits and telephone conversations, and (4) independent analyses.

This report documents the results of these investigations. In addition to the above background information, Section I also presents (1) a brief historical sketch of attempts to improve wind tunnel flow quality and calibration procedures and (2) a summary of tunnel calibration tasks. Section II discusses tunnel variables and how uncertainty in the measurements of various flow quantities affect test results. The details of measuring static and total pressures, temperature, flow angularity, flow unsteadiness, and humidity are all discussed in Section III. This section also includes a review of the

transonic-wall-interference problem, the use of standard models, and the role which optical methods can have during tunnel calibrations. Section IV discusses the various types of errors in calibration measurements and their effects on final results. In addition to presenting conclusions and recommendations, a summary of the questionnaire results is given in Section V. The manual concludes with four appendices. Appendices I and II review, respectively, the use of hot-wires/films and laser Doppler velocimeters. Appendix III discusses the effects of vibration on a cylindrical, static pressure probe. Finally, Appendix IV summarizes the characteristics of tunnels for which questionnaires were received.

I.B. Historical Sketch

The need for good flow quality in wind tunnel was recognized by the earliest investigators. As reported by Pritchard in Ref. (2), the Council of the Royal Aeronautical Society agreed in 1870 to provide funds for the construction of "a suitable and well-finished instrument having the means of instantly setting various plane surfaces at any desired angle and capable of registering both horizontal and vertical forces simultaneously for all degrees of inclination. The results to be published for the benefit of the Society." As a result of this action, the first wind tunnel was constructed by Wenham and Browning, and a series of tests on flat plates were undertaken.

A later report on the results noted that "these experiments would have been more satisfactory had a steady and continuous current been obtained, but the fluctuations carried by each arm of the fan, as it revolved, exerted an appreciable influence on the result," The need for improved flow quality was also recognized by later experimentors, e.g., see Ref. (3).

Dr. Ludwig Mach (son of Ernst Mach) constructed a tunnel at Vienna in 1893 with a test section of 18 x 25-cm which was used for flow observation and photography. This apparatus used a wire screen over the inlet to straighten the flow. In 1896, Sir Hiram Maxim constructed a 91 x 91-cm tunnel and used a form of honeycomb to remove fan-induced swirl and straighten the flow upstream of the test section. The Wright brothers' tunnel, constructed in 1901, included both screens and a honeycomb. A tunnel constructed by Dr. A. F. Zahm at Washington in 1901 included screens of cheese cloth and wire to smooth the inlet flow.

Dr. Zahm also was concerned with flow uniformity and the accuracy of calibration of the tunnel velocity. He developed an extremely sensitive manometer for measuring the pressures generated by a Pitot-static tube which was used for velocity measurements. In describing this instrument, he used the term "wind tunnel" for the first time in the literature. Zahm also used a toy balloon moving with the flow to obtain a time-of-flight measurement of the velocity.

Another calibration procedure used by Zahm involved measurement of the force on a "pressure plate" or drag plate at the same time the flow velocity was measured. This method allowed determination of the flow velocity during later tests by observing the force on the pressure plate, Ref. 4.

Additional discussion of early wind tunnels and measurement techniques is also given in an article by Goin (Ref. 5).

From the beginning, the development of wind tunnel facilities has usually been a precursor of improved flight vehicles as outlined by Goethert in Ref. 6. The development of new and improved wind tunnels has, in turn, required new calibration procedures, techniques and instrumentation in the struggle to provide experimental data with the accuracy required by vehicle designers.

I.C. Calibration Procedures

Both the quality of the wind tunnel flow environment and the accuracy with which this environment is known contribute to the accuracy of aerodynamic measurements. The total uncertainty in aerodynamic data is the result of a large number of error sources, as is discussed in Sections II.B.2 and IV.

Figure I.C.1, from Ref. (7), illustrates the many sources of error and the manner in which errors propagate to a typical test result such as drag coefficient. Considering the total number of error sources, the necessity to minimize those due to tunnel calibration is obvious. This flow diagram is helpful since it isolates the facility flow environment and calibration elements which are discussed herein.

Both the quality of the flow and the accuracy with which the flow conditions are known are considered as part of the calibration contribution. It is suggested that the calibration effort include the following elements:

1. Initial evaluation of performance characteristics and flow quality, and determination as to need for corrective action.
2. Determination of optimum tunnel operational parameters such as wall angle and porosity, control system performance, etc.
3. Diagnostic measurements to investigate a specific flow problem or deficiency.
4. Measurement of mean, unsteady and spatial distributions of test section flow conditions for the selected tunnel configuration and various operating conditions.
5. Standard model tests for inter-facility comparisons.
6. Periodic re-evaluation of basic tunnel calibration for control or monitoring purposes. This may be accomplished in part by tests on a standard facility model.

Considering the above task descriptions, it can be observed that flow quality improvements, verification tests and basic tunnel calibrations are intimately related. The accuracy requirements may vary, depending upon the type of calibration task and the primary purpose of the facility, but are most stringent for items 4 and 6 since errors in the measurements can contribute directly to the random or fixed error in the final data.

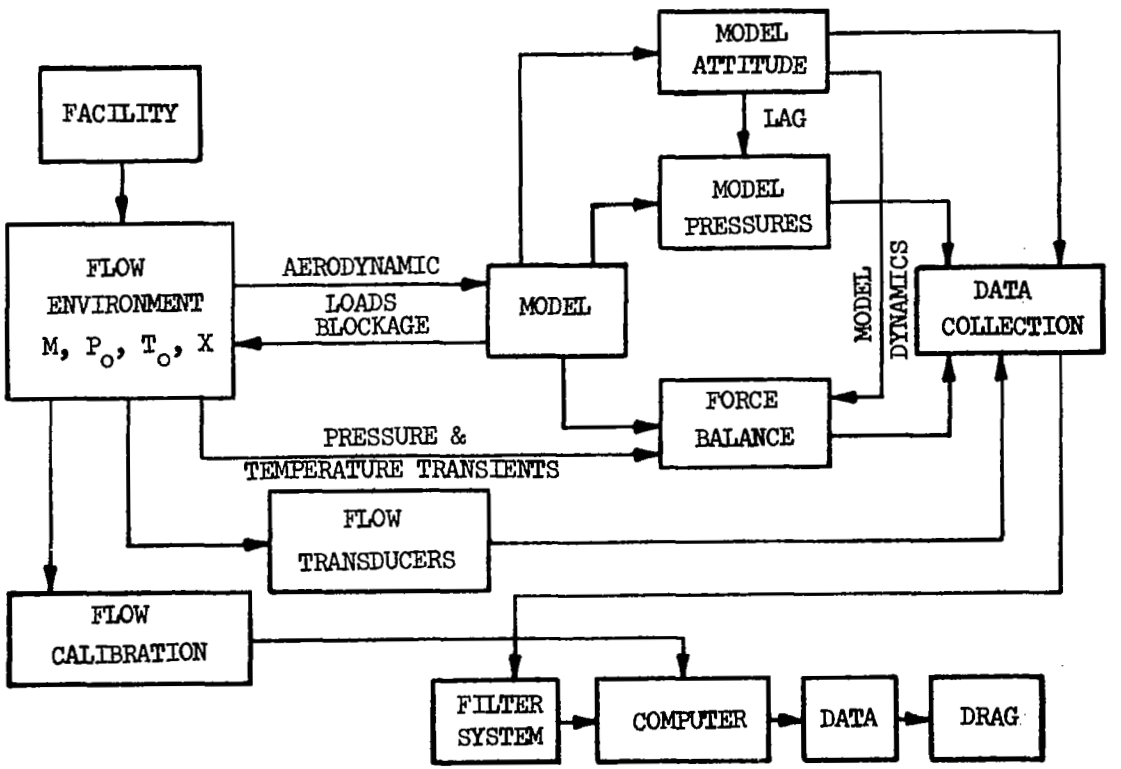

Figure I.C.1. DATA AND ERROR FLOW DIAGRAM, Ref. 7

I. References

1. Treon, S. L., Steinle, F. W., Hagerman, J. R., Black, J. A. and Buffington, R. J.: "Further Correlation of Data From Investigations of a High-Subsonic-Speed Transport Aircraft Model in Three Major Wind Tunnels," AIAA Paper 71-291, Albuquerque, New Mexico, 1971.

2. Pritchard, J. L.: "The Dawn of Aerodynamics," Journal of the Royal Aeronautical Society, V. 61, March 1957.

3. Randers-Pehrson, N. H.: "Pioneer Wind Tunnels," V. 93, No. 4, Smithsonian Miscellaneous Collections.

4. Bird, K. D.: "Old Tyme Wind Tunnels," Perspective Sept.-Oct., 1957, Cornell Aeronautical Laboratories, Inc.

5. Goin, K. L.: "The History, Evolution, and Use of Wind Tunnels," AIAA Student Jour., Feb. 1971.

6. Goethert, B. H.: Transonic Wind Tunnel Testing, pp 2-31, Permagon Press, New York, 1961.

7. Picklesimer, J. R., Lowe, W. H., and Cumming, D. P.: "A Study of Expected Data Precision in The Proposed AEDC HIRT Facility," AEDC-TR-75-61, August, 1975.

II. TUNNEL VARIABLES

II.A.1 Types of Tunnels

The material presented herein is directed toward wind tunnels operating in the Mach number range from 0.4 to 3.5. The modes of operation of the various facilities surveyed include: (1) continuous flow, (2) blowdown, and (3) intermittent.

In the case of intermittent tunnels, e.g., a Ludwieg tube, the very short run times require special provisions for measurement and recording systems. Pressure measurements can be accomplished using either high-response pressure transducers or a capture system which permits measurements of pressure after the run. However, the same basic procedures must be followed in order to calibrate the facility as for a long-run-time facility. Thus, the special problems associated with the short run times of intermittent tunnels are not discussed, but the general discussions of calibration procedures are applicable.

Although transonic tunnels with high-aspect-ratio (2-D) test sections are generally operated at higher Reynolds numbers, this type of tunnel is not discussed separately because they share the same calibration problems as symmetrical tunnels.

Discussions of the various topics are of a general nature where possible. Subdivisions into transonic and supersonic areas are made where dictated by the peculiarities of these regions. Further subdivisions are made, as appropriate, in discussions of details.

II.B. OPERATIONAL PARAMETERS

II.B.1 Pressure Control

Pressure controls are incorporated in some form in all wind tunnels (with the possible exception of supersonic, indraft tunnels). The methods of control are obviously different for transonic and supersonic wind tunnels and for intermittent, blowdown and continuous wind tunnels. This section is limited to discussions of pressure control systems as they influence tunnel calibration programs and the effects of variations introduced by these systems on tunnel flow quality and measurement accuracy.

Continuous Wind Tunnels

Continuous wind tunnels may be either pressure tunnels or atmospheric-vented tunnels. For the pressure or variable density wind tunnel, the stagnation pressure is determined by the static or wind-off pressure and the pressure added by the fan or compressor drive system. The drive system pressure ratio may be controlled by varying compressor speed, blade angle, or guide-vane angle.

Vented tunnels usually operate at atmospheric stagnation pressure, but some facilities of this type operate at atmospheric test section static pressure or the atmospheric vent may be located at some other part of the tunnel circuit so that neither the stagnation nor the static pressure is atmospheric. The drive system is controlled by the same techniques as for the pressure tunnel to achieve the desired pressure ratio across the nozzle and test section.

For supersonic tunnels the Mach number (and all Mach dependent test section conditions) are determined by the nozzle geometry and stagnation conditions. The supersonic nozzle is not normally considered a static pressure control (although it does perform that function). Several tunnels include automatic control of nozzle geometry. The pressure control is simplest for the atmospheric-stagnation-pressure, supersonic tunnel since the prime function of the drive system is to create the pressure ratio necessary to start and maintain nozzle flow. For pressure tunnels, both the tunnel pressurization and main drive system control the stagnation pressure.

Transonic tunnel operation requires additional control of the test section static pressure. In addition to control of compressor pressure ratio, the static pressure is controlled by some type of plenum evacuation system. At supersonic Mach numbers above about 1.4 a variable geometry, convergent-divergent nozzle is usually used. Also, a specified Mach number can be attained over a range of tunnel pressure ratios by other control variables. Tunnel pressure ratio may therefore be one of the variables investigated for tunnel flow optimization, in terms of both flow uniformity and minimum power consumption. Plenum evacuation can be accomplished by ejector flaps which use the main stream flow to pump the plenum, or auxiliary pumping systems can be used.

Almost all of the continuous tunnels responding to the questionnaire use manual control of total and static pressure, although several have available automatic systems to indicate the measured test conditions to the operators, and a few include closed-loop, automatic control. The response of a continuous tunnel, particularly a large one, to control inputs is influenced by the time constants involved. These time constants are a function of the circulating air mass, the rotational inertia of the main drive, etc., and are generally large. A beneficial effect of the large time constants is that short-term disturbances tend to be heavily attenuated and smoothed. Precise, smooth control is possible by manual control, but changes in level require a longer period than for small time constant systems. Fluctuations in the controlled pressure tend to occur at the system natural frequency, which is the inverse of the time constant. The period of these fluctuations can be very long - up to 10-15 seconds. In order to obtain a measurement of the mean value of tunnel flow conditions, measurements over at least one period are required.

Blowdown Wind Tunnels

The control systems for blowdown wind tunnels can have a significant effect on tunnel flow quality. In addition to the automatic stagnation pressure control system, automatic control systems are used in a majority of the transonic, blowdown wind tunnels for Mach number control also.

The stagnation pressure control for a blowdown wind tunnel uses a control valve between the storage reservoir and the stilling chamber to control pressure in the chamber. Constant stagnation pressure is the normal mode of operation,

but the system can also be computer or program controlled to maintain constant Reynolds number as the stagnation temperature drops during the run, or the pressure may be increased linearly with time to investigate Reynolds number effects, explore flutter boundaries, etc. In general, the functional capability of the stagnation pressure system has become more sophisticated with the introduction of digital computer control.

From the flow quality standpoint, the most important performance parameter of the system is the accuracy of pressure control or, in more specific terms, the variance of the stagnation pressure about the mean level. The period of this variation is typically about 1 second and the current state-of-the-art appears to be about a 0.1 percent standard deviation; much larger perturbations, up to 1/2%, can easily result due to electrical noise, mechanical friction or misadjustment of the control computer. The stagnation pressure control system must operate continuously to overcome the disturbance created by the decreasing reservoir pressure. Thus a controller of higher order than that used for a continuous tunnel pressure control is usually required to achieve the desired accuracy. A simple regulator is normally inadequate.

The shock system generated downstream of the blowdown-wind-tunnel control valve may introduce excessive flow unsteadiness. Test-section flow angularity may also vary with valve position (and therefore, time). Thus, the entire flow channel, from the storage reservoir to the stilling chamber, must be considered when designing the stagnation pressure control system. Considerable work has been accomplished in recent years to identify and correct flow problems caused by the stagnation pressure control system. Corrective measures have included choked-flow devices in series downstream of the valve, specialized valves, acoustic silencers and honeycombs in the stilling chamber.

A second pressure control system used in transonic tunnels, the Mach number control, functions to maintain a desired Mach number by controlling static pressure as a function of stagnation pressure. Almost all blowdown, transonic tunnels use a choked throat downstream of the test section to control subsonic Mach numbers. The primary advantage of this control mode is that the Mach number is determined by the test section geometry (at a fixed model angle of attack) and is therefore independent of fluctuations in stagnation pressure.

Automatic control of the downstream throat area is used in a number of facilities. Automatic control is highly desirable in order to maintain constant Mach number during model attitude variations and simultaneously maintain optimum plenum evacuation. More sophisticated operational modes are available under computer control, such as Mach number sweeps, etc. The performance of this system also directly influences the variation of the test section Mach number. Current best performance appears to be about 0.001, but larger variations are possible at subsonic speeds, particularly at high model-pitch rates.

In the absence of perturbations introduced by the Mach or static pressure control loop, small variations in stagnation pressure cannot necessarily be taken into account by simultaneous measurement of the two pressures because of phase lag and attenuation errors.

An important procedural difference in making calibration measurements in a blowdown tunnel is that runs should be made at each calibrated Mach number where all tunnel variables are held constant during an entire blowdown, in order to detect time or valve position dependent effects. If a traversing angularity probe is moved along the tunnel centerline during the run, for example, time-dependent effects will be obscured by the spatial variations and vice versa.

Intermittent (Impulse) Wind Tunnels

Intermittent wind tunnels are considered to be those that operate in a basic blowdown mode, but with a run time of about 4 to 5 seconds or less. The Ludwieg tunnel is a typical facility of this class. The Ludwieg principle can be applied to either a supersonic or a transonic wind tunnel. Pressure control is limited to the initial charge tube pressure and is therefore relatively straightforward. An advantage of the Ludwieg tunnel is that the stagnation pressure downstream of the initial expansion tube is constant (neglecting viscous effects). The primary calibration measurement problems associated with the Ludwieg tunnel obviously arise from the short test duration.

II.B.2 Calibration Accuracy, Flow Uniformity and Relationship to Model Testing

The calibration of a transonic wind tunnel is significantly more difficult than calibration of a supersonic tunnel due primarily to the ventilated test section walls. The ventilated walls and the basic nature of transonic flow prevent the determination of test section conditions from tunnel or nozzle geometry alone, as is the case with a calibrated supersonic tunnel nozzle. A measurement of test section static pressure, in addition to stagnation pressure, is required during calibration and routine test operations. Further, for fixed test section geometry, the model or other apparatus in the test section can influence the Mach number. These factors require that the tunnel calibration provide a relation between the static pressure distribution in the test section and a reference pressure measured in the plenum chamber or on the ventilated wall.

Transonic tunnel calibration is further complicated by the additional degrees of freedom provided by a ventilated wall, i.e., at each Mach number, the optimum wall angle, wall porosity (for adjustable porosity walls), plenum evacuation flow rate, tunnel pressure ratio, and choke control position must all be determined. Criteria for optimum adjustment include uniformity of Mach number and, at supersonic speeds, shock and expansion-wave cancellation characteristics which are usually evaluated based on tests of cone-cylinder models. At subsonic speeds, in addition to minimizing variations in Mach number distribution, other criteria for optimization are tunnel noise level and forces on a standard model. A recent report by Jackson (Ref. 1) provides a comprehensive discussion of the procedures employed in selecting transonic tunnel parameters to minimize Mach number variations.

Many of the transonic tunnels surveyed determine the wall angle based on shock and expansion wave cancellation at supersonic speeds, and this angle is often maintained constant at all Mach numbers, while others adjust the wall angle according to a Mach number schedule. In general, adjustment of wall angle with Mach number will provide a more uniform flow.

A typical optimization problem at subsonic Mach numbers is balancing of plenum evacuation and choke area for a choke-controlled blowdown tunnel. The average test section Mach number can be attained with an infinite number of combinations of plenum pumping and choke area. For example, the criterion usually chosen is to minimize downstream Mach number increases or decreases from

the upstream value. Downstream disturbances in Mach number are undesirable because they can create bouyancy effects further upstream. Since the disturbance magnitude is extremely sensitive to changes in plenum pumping at subsonic Mach numbers below about 0.85, the optimum pumping is determined during calibration and maintained constant for routine testing. The test section Mach number is controlled by varying the choke area which does not alter the downstream disturbance.

A similar upstream disturbance occurs at Mach numbers near 1.0. Therefore, one of the purposes of a calibration program is to determine the region of flow along the test section within which the Mach number deviation does not exceed various limits such as ± 0.001, ± 0.002, etc. Jackson (Ref. 1) has suggested the following criteria be adopted as an industry standard for "good flow quality" in transonic tunnels. For subsonic flows, 2σ deviations in centerline Mach number should be less than 0.005 and less than 0.01 in the case of supersonic flows. Of course, the minimum Mach number deviation is indicative of the best distribution and therefore flow quality for a given test section length and set of tunnel conditions. Jackson's flow quality criteria are shown in Fig. 2.B.1 as a function of Mach number. Recent calibration data from the AEDC-PWT 16T Transonic Tunnel is also included for comparison.

Morris and Winter (Ref. 2) have suggested even more stringent requirements for supersonic tunnels. These investigators have suggested the maximum allowed variations in (1) flow angularity be ± 0.1 deg and (2) Mach number be ± 0.003 at $M = 1.4$, ± 0.005 at $M = 2$, ± 0.01 at $M = 3$.

It should be noticed that criteria based on the standard deviation do not distinguish between random or periodic variations and mean flow gradients. Thus, in addition to standard deviation criteria, consideration must be given to empty-tunnel static pressure gradients. The static pressure distribution along the test section must be either constant (within acceptable limits) or any gradient must be known and repeatable to a sufficiently high degree of accuracy so that bouyancy corrections can be made to attain the required accuracy in measurements of model drag. It is therefore of interest to investigate, in a systematic manner, the effects of test section pressure gradient on drag measurement accuracy and how this relates to flow quality requirements.

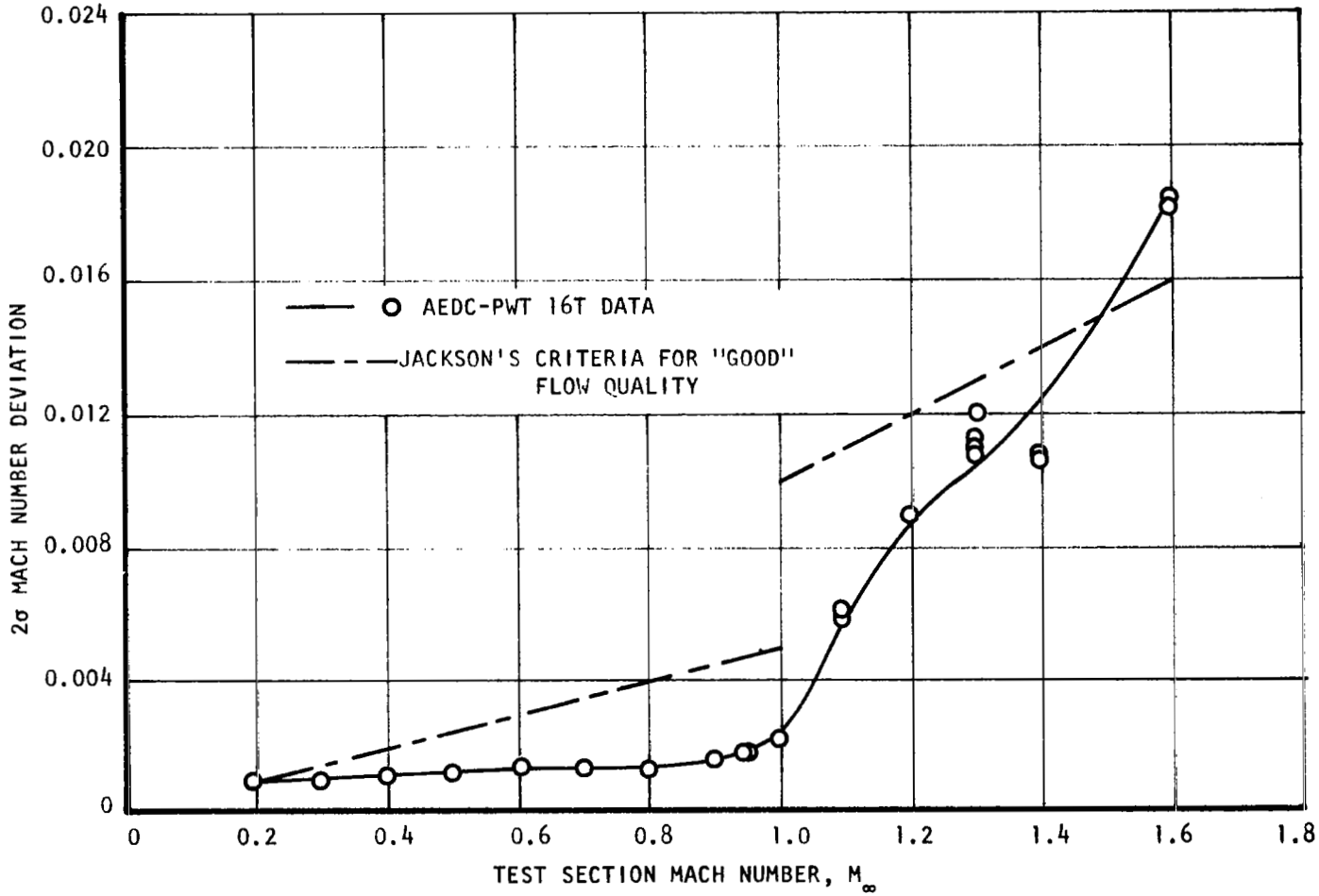

Figure 2.B.1 JACKSON'S FLOW QUALITY CRITERIA FOR TRANSONIC TUNNELS, Ref. 1.

The bouyancy drag coefficient resulting from a linear static pressure gradient (Ref. 3) can be stated as

$$\Delta C_{D_G} = - \frac{V}{S} \frac{1}{q_\infty} dP/dx \ , \qquad (2.B.1)$$

where V is the model volume, S is wing reference area, q_∞ is the average test section dynamic pressure, dP/dx is the pressure gradient and ΔC_{D_G} is the drag coefficient increment produced by the pressure gradient.

Utilizing the above equation, Isaacs (Ref. 4) investigated the effects of bouyancy on the drag of typical, transport aircraft models in a 2.44-m (8-ft) wind tunnel. Based on model values of the parameter V/S ranging from 0.069 to 0.208 meter (0.23 to 0.68 ft), Isaacs determined that $\frac{1}{q_\infty} \frac{dP}{dx}$ should be known to an accuracy of 0.00047 to 0.0014 per meter (0.00014 to 0.00043 per ft) in order to know ΔC_{D_G} to an accuracy of 0.0001, i.e., one drag count.

In a study of bouyancy effects on drag measurement accuracy in supersonic wind tunnels, Morris and Winter (Ref. 2) determined the allowable pressure gradient for a bouyancy drag of 1% of the model drag. Based on an assumed, rectangular-wing, aircraft model and Eq. 2.B.1, the allowable pressure gradient in terms of $\Delta P/H$ over the model length was found to range from 0.002 at $M = 1.4$ to 0.0005 at $M = 3.0$. The corresponding Mach number gradient over the model length was approximately 0.4% of the average Mach number. The estimated drag coefficient of the configuration considered indicated 1% of ΔC_D was 0.00023 at $M = 1.4$ and 0.00013 at $M = 3.0$. On a per-drag-count basis, the allowable Mach number gradient, in percent of average Mach number, was then 0.17% at $M = 1.4$ and 0.31% at $M = 3.0$.

Bouyancy effects may be evaluated in a generalized way by taking into account both model configuration variables and Mach number effects. Assuming a specific heat ratio of 1.4, the relations

$$\frac{P}{H} = (1 + 0.2\ M^2)^{-3.5} \qquad (2.B.2)$$

$$\frac{q_\infty}{H} = 0.7\ M^2(1 + 0.2\ M^2)^{-3.5} \qquad (2.B.3)$$

may be used to write Eq. (2.B.1) as

$$C_{D_G} = \frac{V}{S}\left[\frac{2}{M(1+0.2\ M^2)}\right]\frac{dM}{dx} \quad . \tag{2.B.4}$$

Where H and q_∞ are considered constant at their average values. If the Mach number gradient is assumed to be linear, $\frac{dM}{dx}$ may be written as $\Delta M/\Delta x$ with Δx taken as the model length, L_m. ΔM is then the Mach number variation per model length. Eq. (2.B.4) becomes

$$\Delta C_{D_G} = \frac{V}{SL_m}\left[\frac{2}{M(1+0.2\ M^2)}\right]\Delta M \quad . \tag{2.B.5}$$

The parameter V/SL_m is a nondimensional configuration parameter and is therefore independent of model scale. Figure 2.B.2 shows the allowable Mach number gradient, over the model length, for a bouyancy-induced, drag coefficient error of 0.0001 as a function of the configuration parameter V/SL_m. Owing to this extreme sensitivity of drag measurements accurate to within one count, there are a number of problems in achieving this goal. For example, if the random, short wavelength variations in Mach number are too large, the mean gradient may be obscured and difficult to define. One approach is to use empty-tunnel pressure distributions, measured during calibrations, to integrate over the model length. However, this procedure can be in error because of lack of exact repeatability of tunnel flow conditions. In the case of transonic tunnels, the model may induce departures from empty-tunnel calibrations, e.g., Parker (Ref. 5). In addition, Jackson (Ref. 1) has found that a change in unit Reynolds number from 4.1×10^6 to 15.8×10^6 (per meter) can cause an increase of 0.003 in tunnel Mach number, see Fig. 2.B.3. This is an effect that is frequently ignored during transonic tunnel calibrations.

The data of Fig. 2.B.2 are also shown in Fig. 2.B.4 with the Mach number gradient expressed in percent of the average Mach number. Points derived from the criteria suggested by Morris and Winter (Ref. 2) for supersonic flow are shown on Fig. 2.B.4 for comparison. This comparison indicates the model configuration used by Morris and Winter to establish flow uniformity criteria had a value of approximately 0.05 for V/SL_m.

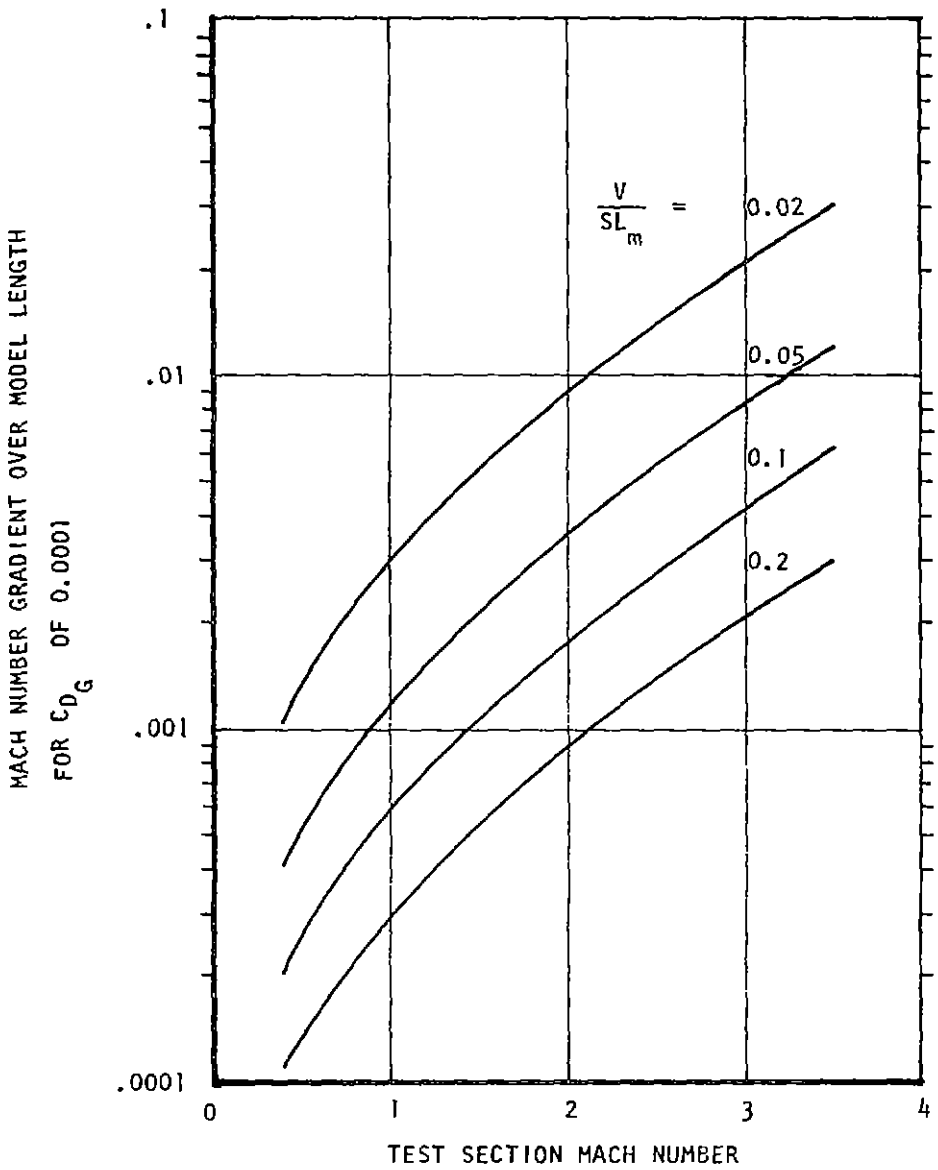

Figure 2.B.2 ALLOWABLE LINEAR MACH NUMBER GRADIENT OVER MODEL LENGTH FOR BOUYANCY DRAG COEFFICIENT CONTRIBUTION OF 0.0001

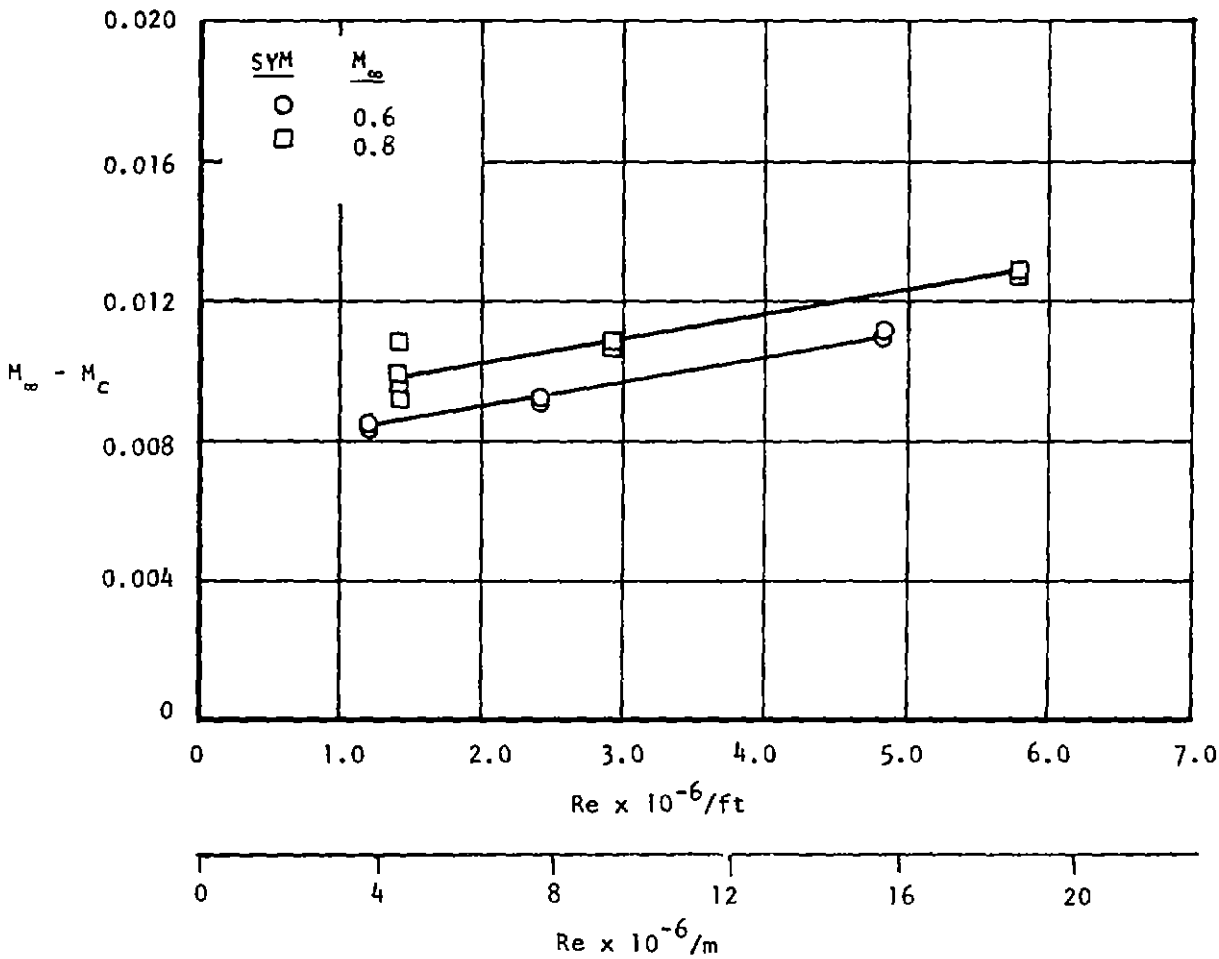

Figure 2.B.3 EFFECTS OF REYNOLDS NUMBER ON CALIBRATION OF THE PWT-16T TUNNEL AT M_∞ = 0.6 AND 0.8 FOR θ_w = 0 AND τ = 6%

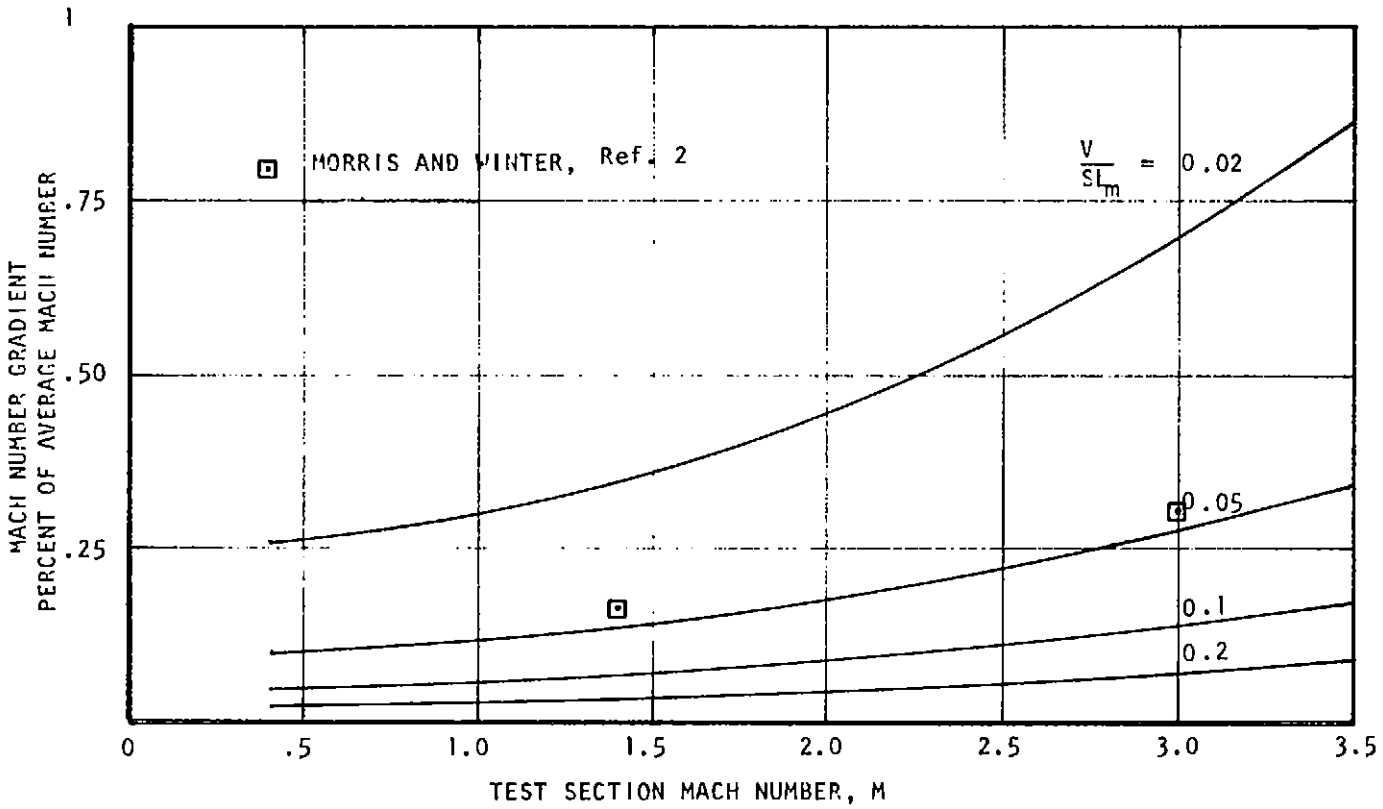

Figure 2.B.4. MACH NUMBER GRADIENT OVER MODEL LENGTH AS PERCENT OF AVERAGE MACH NUMBER FOR BOUYANCY DRAG COEFFICIENT OF 0.0001

The value of the parameter V/SL_m for several aircraft typical of fighter, attack and transport configurations are listed below.*

Aircraft	V/SL_m
F-15	0.054
F-16	0.048
YF-17	0.043
A-7	0.071
DC-8	0.061
DC-9	0.088
DC-10	0.083
B-747	0.065
B-727-100	0.076
B-727-200	0.056
C-141A	0.055
C-5A	0.078

The above data demonstrates the variation in V/SL_m with aircraft type is not large, at least for conventional configurations, and that the model configuration selected by Morris and Winter (Ref. 2) is representative of supersonic fighter aircraft. It is anticipated that V/STOL configurations would have a larger value of V/SL_m than the aircraft listed above and would therefore be more sensitive to Mach number gradient effects.

*Due to the approximate values used for some of the aircraft volumes, the values of V/SL_m should be regarded as approximate.

II.B. References

1. Jackson, F. M.: "Calibration of the AEDC-PWT 16-Ft Transonic Tunnel at Test Section Wall Porosities of Two, Four, and Six Percent," AEDC-TR-76-13, Jan. 1976.

2. Morris, D. E. and Winter, K. G.: "Requirements for Uniformity of Flow in Supersonic Wind Tunnels," RAE Tech Note AERO 2340 (1954).

3. Glauert, H.: "Wind Tunnel Interference on Wings, Bodies and Ailerons," A.R.C. R&M 1566 (1933).

4. Isaacs, D.: "Calibration of the R.A.E. Bedford 8-ft. x 3-ft. Wind Tunnel at Subsonic Speeds, Including a Discussion of the Corrections Applied to the Measured Pressure Distribution to Allow for the Direct and Blockage Effects due to the Calibration Probe Shape," A.R.C. R&M 3583 (1969).

5. Parker, R. L.: "Flow Generation Properties of Five Transonic Wind Tunnel Test Section Wall Configurations," AEDC-TR-75-73, Aug. 1975.

II.C. FLOW PARAMETERS AND UNCERTAINTY RELATIONSHIPS

The proper measurement of stream properties to allow the accurate determination of the various flow parameters is necessary for the meaningful interpretation of wind tunnel test results. For example, the desirability of a Mach number accuracy of 0.001 has been suggested (i.e., Ref. 1). The necessity of such a requirement may be illustrated by the afterbody data of Fig. 2.C.1. This data appears to have substantial scatter but may be correlated using Mach number measurements with a precision of 0.001 as shown in Fig. 2.C.2.* It also may be noted that for a typical fighter aircraft configuration the transonic drag rise is such that a Mach number uncertainty of 0.001 is "equivalent" to 0.0002 (2 counts) in drag coefficient. Similarly, other parameters must be computed to high degrees of accuracy. The sensitivities of the several flow parameters to the various measurements are presented in this section to illustrate the consequences of measurement uncertainty on accuracy.

II.C.1. Pressures

The pressure of a fluid is one of its most significant properties. The knowledge of static and stagnation pressures in a wind tunnel is necessary to define characteristic flow conditions such as Mach number and Reynolds number and to properly normalize the various data coefficients. The following discussion concerns the measurement of these two pressures.

Static Pressure: During transonic operation static pressure is obtained from a reference pressure (wall or plenum) and a predetermined relation (calibration) of this pressure to the test section static pressure. During supersonic operation static pressure is usually obtained from stagnation pressure and the Mach number previously obtained during calibration of the facility with the particular nozzle setting.

*Figures 2.C.1 and 2 were obtained through private communication with Mr. Jack Runkel, NASA Langley Research Center. This requirement for a Mach number accuracy of at least 0.001 is also substantiated by the recent nozzle-afterbody tests reported by Spratley and Thompson (Ref. 17).

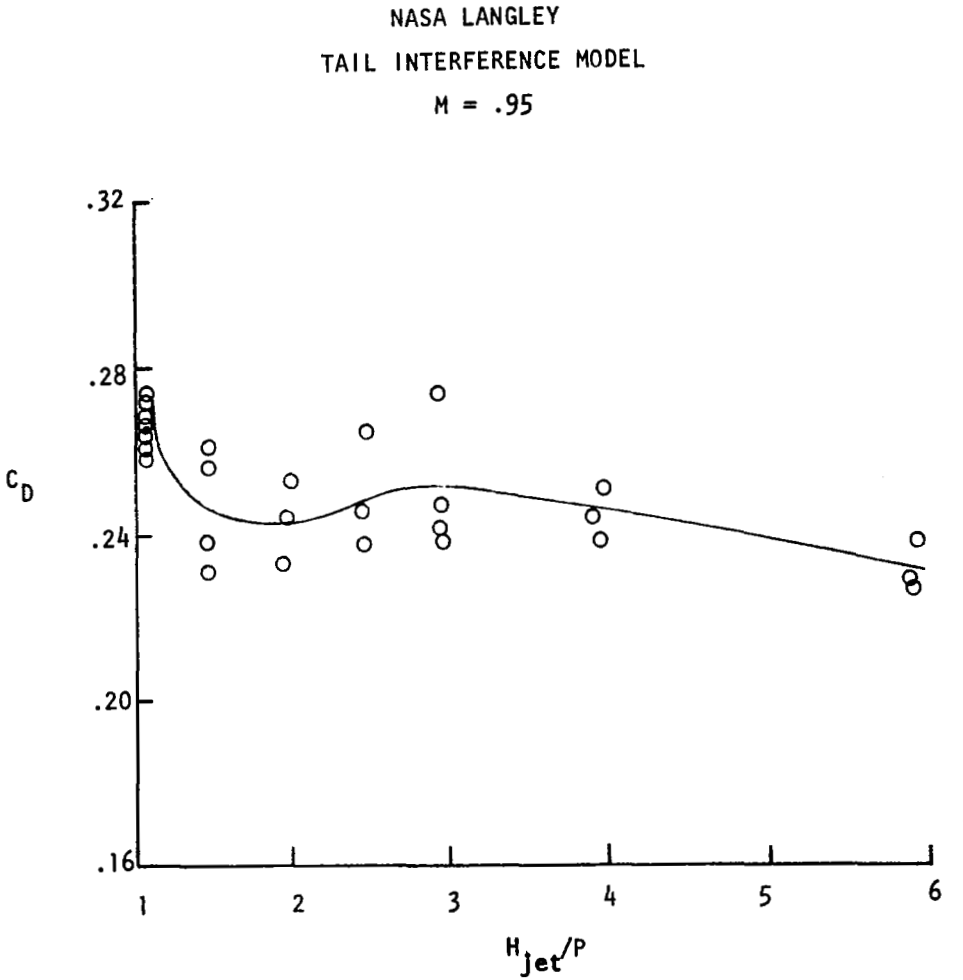

Figure 2.C.1 AFTERBODY DRAG DATA AT AN AVERAGE MACH NUMBER OF 0.95

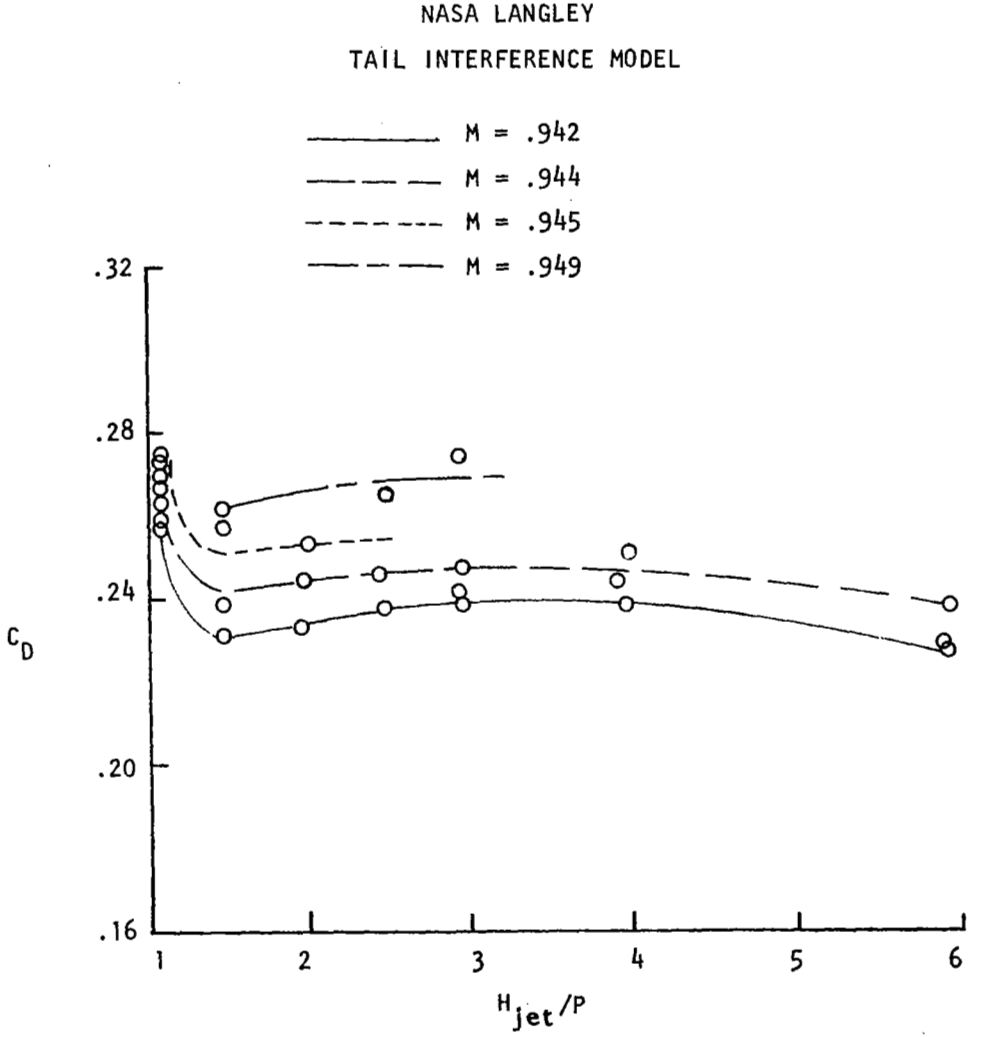

Figure 2.C.2 AFTERBODY DRAG DATA WITH TUNNEL MACH NUMBER GIVEN TO THREE DECIMALS

In the transonic region a static pressure probe or array of probes may be used to relate the reference and test section static pressures. With regard to the higher Mach numbers it has been illustrated (Ref. 2), that the uncertainty in Mach number may be related to uncertainties in static P_∞, isentropic total, H_s, and Pitot, H_2, pressures by the following relations (assuming the ratio of specific heats is 1.4):

$$\frac{\partial H_s}{H_s} - \frac{\partial P_\infty}{P_\infty} = \frac{\partial M}{M}\left(\frac{7M^2}{M^2+5}\right)$$

$$\frac{\partial H_s}{H_s} - \frac{\partial H_2}{H_2} = \frac{\partial M}{M}\left[\frac{35\,(M^2-1)^2}{(M^2+5)(7M^2-1)}\right]. \qquad (2.C.1)$$

If it is assumed that the total pressure is measured in the stilling chamber with no error $\left(\frac{\partial H_s}{H_s} = 0\right)$, the above equation becomes

$$\frac{\partial P_\infty}{P_\infty} + \left(\frac{7M^2}{M^2+5}\right)\frac{\partial M}{M} = 0 \qquad (2.C.2)$$

and

$$\frac{\partial H_2}{H_2} + \frac{35\,(M^2-1)^2}{(M^2+5)(7M^2-1)}\,\frac{\partial M}{M} = 0 \qquad (2.C.3)$$

Solving for $\frac{\partial M}{M}$ in the first equation and substituting into the latter, the following expression is obtained.

$$\frac{\partial H_2}{H_2} - \frac{5\,(M^2-1)^2}{M^2\,(7M^2-1)}\,\frac{\partial P_\infty}{P_\infty} = 0 \qquad (2.C.4)$$

which yields

$$\frac{\partial H_2}{\partial P_\infty} = \frac{H_2}{P_\infty} \frac{5\,(M^2-1)^2}{M^2(7M^2-1)} \quad . \tag{2.C.5}$$

Since $$\frac{H_2}{P_\infty} = \left[\frac{6M^2}{5}\right]^{3.5} \left[\frac{6}{7M^2-1}\right]^{2.5}$$, then $$\frac{\partial H_2}{\partial P_\infty} \tag{2.C.6}$$

can be simplified to:

$$\frac{\partial H_2}{\partial P_\infty} = \left[\frac{6M^2}{5}\right]^{3.5} \left[\frac{6}{7M^2-1}\right]^{2.5} \left[\frac{5\,(M^2-1)^2}{M^2(7M^2-1)}\right]. \tag{2.C.7}$$

Hence the ratio of uncertainty of Pitot-to-static pressure becomes a simple function of Mach number and is shown in Fig. 2.C.3. It may be noted that the ratio becomes 1 near M = 1.6. Thus, for a specified error in Mach number at an M < 1.6, the error in static pressure may be greater than the error in Pitot pressure.* For Mach numbers greater than 1.6 the reverse is true. This occurs because the static pressure becomes very small at high Mach numbers, and small absolute errors in the measurement of P_∞ produce relatively large errors in calculated Mach number. For example, Fig. 2.C.3 shows that at Mach 3 the absolute error in Pitot pressure can be approximately seven times the static pressure error for the same error in calculated Mach number. Thus the use of static pressure for the determination of Mach number is generally restricted to Mach numbers less than 1.6; while Pitot pressure is employed (with stagnation pressure) at higher Mach numbers.

*Also see Fig. 2.C.9, p.39.

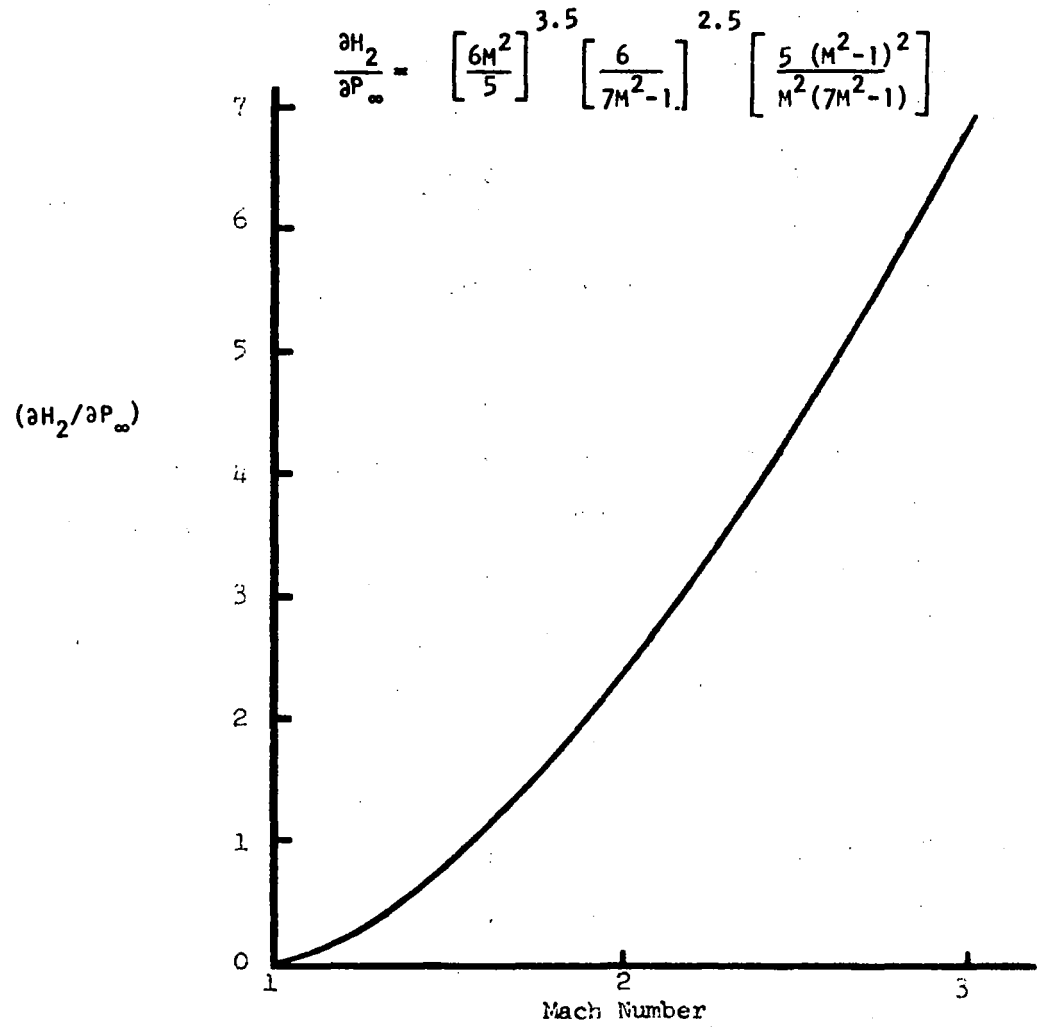

Figure 2.C.3 THE UNCERTAINTY OF PITOT-TO-STATIC PRESSURE AS A FUNCTION OF MACH NUMBER

Stagnation Pressure: The pressure of the test medium is measured with the fluid at rest either in the settling chamber or by means of a total head tube.

The settling chamber (isentropic stagnation) pressure, H_s, is generally used for both transonic and supersonic operation. Because of the aforementioned sensitivity of Mach number to static pressure, after-shock total (Pitot) pressure, H_2, is employed above a nominal 1.6 Mach number.

Dynamic Pressure: Dynamic pressure, q, is perhaps the most frequently employed flow parameter used to normalize wind tunnel data. Thus the accuracy of q is directly reflected in the accuracy of coefficient data. In most instances, after static pressure has been obtained by measurement (transonic) or by inference (supersonic) it is used with Mach number to compute q from

$$q = \frac{\gamma}{2} M^2 P_\infty \, . \tag{2.C.8}$$

In the transonic range, both P_∞ and H_s are measured. Errors in either affect Mach number. Fig. 2.C.4 shows the sensitivity of q to H_s which results solely from Mach number error as determined from the following.

Since $q = \frac{\gamma}{2} M^2 P_\infty$,

$$\frac{\partial q}{\partial H_s} = \gamma M P_\infty \frac{\partial M}{\partial H_s} \, , \tag{2.C.9}$$

and $$(\partial q/q)/(\partial H_s/H_s) = \frac{H_s}{q} \frac{\partial q}{\partial H_s} = \frac{2H_s}{\gamma M^2 P_\infty} \left(\gamma M P_\infty \right) \frac{\partial M}{\partial H_s} = 2 \, (\partial M/M)/(\partial H_s/H_s) \, .$$

It will subsequently be illustrated (see Section II.C.3) that

$$\partial M/(\partial H_s/H_s) = \frac{5}{7M} (1 + .2M^2) \, ,$$

which leads to the results

$$(\partial M/M)/(\partial H_s/H_s) = \frac{1}{7M^2} (M^2 + 5) \, . \tag{2.C.10}$$

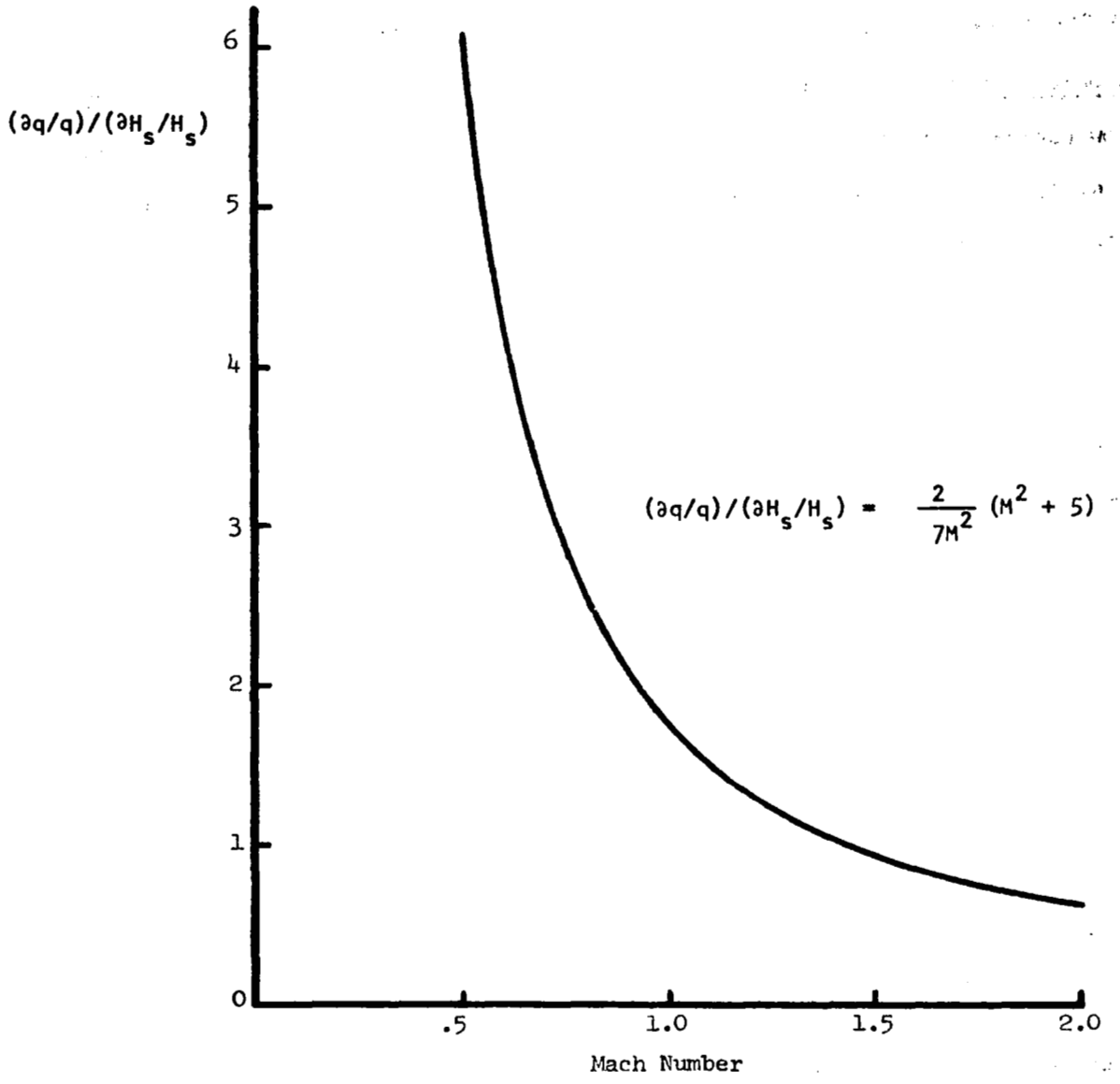

Figure 2.C.4 THE SENSITIVITY OF DYNAMIC PRESSURE TO STAGNATION PRESSURE ERROR, TRANSONIC OPERATION

Equation 2.C.10 may be substituted into the preceding equation to obtain

$$(\partial q/q)/(\partial H_s/H_s) = \frac{2}{7M^2}(M^2 + 5) \ . \qquad (2.C.11)$$

Errors in P_∞ affect q by means of the P_∞ term and the erroneous Mach number as illustrated in Fig. 2.C.5. From $q = \frac{\gamma}{2} M^2 P_\infty$:

$$\frac{\partial q}{\partial P_\infty} = \gamma M P_\infty \frac{\partial M}{\partial P_\infty} + \frac{\gamma}{2} M^2 \qquad (2.C.12)$$

$$(\partial q/q)/(\partial P_\infty/P_\infty) = \gamma M P_\infty \frac{\partial M}{\partial P_\infty} \frac{P_\infty}{q} + \frac{\gamma}{2} M^2 \frac{P_\infty}{q} \qquad (2.C.13)$$

$$= \frac{2}{M} (\partial M/(\partial P_\infty/P_\infty)) + 1 \ . \qquad (2.C.14)$$

It will be shown in Section II.C.3 that

$$\partial M/(\partial P_\infty/P_\infty) = -\frac{5}{7M}(1 + .2M^2) , \qquad (2.C.15)$$

which upon substitution yields

$$(\partial q/q)/(\partial P_\infty/P_\infty) = 1 - \frac{2}{7M^2}(M^2+5) \ . \qquad (2.C.16)$$

During supersonic operation, calibrated Mach numbers are known for the facility geometry setting and are employed with H_s for q determination. However, an error in defining the calibrated Mach number will affect q as shown in Fig. 2.C.6. The function illustrated in this figure was obtained as follows:

$q = \frac{\gamma}{2} M^2 P_\infty$, from Eq. 2.C.8.

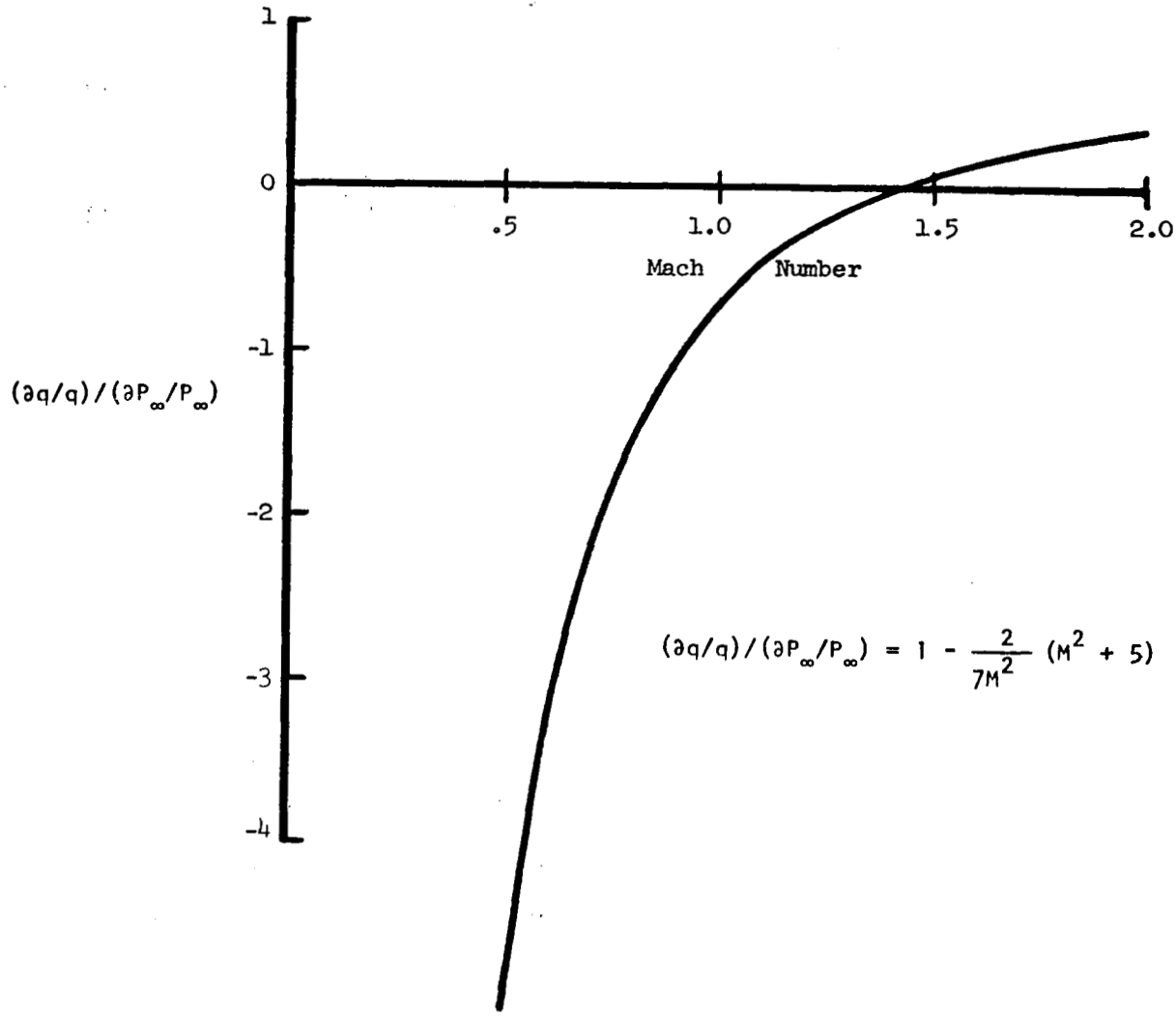

Figure 2.C.5 THE SENSITIVITY OF DYNAMIC PRESSURE TO STATIC PRESSURE ERROR, TRANSONIC OPERATION

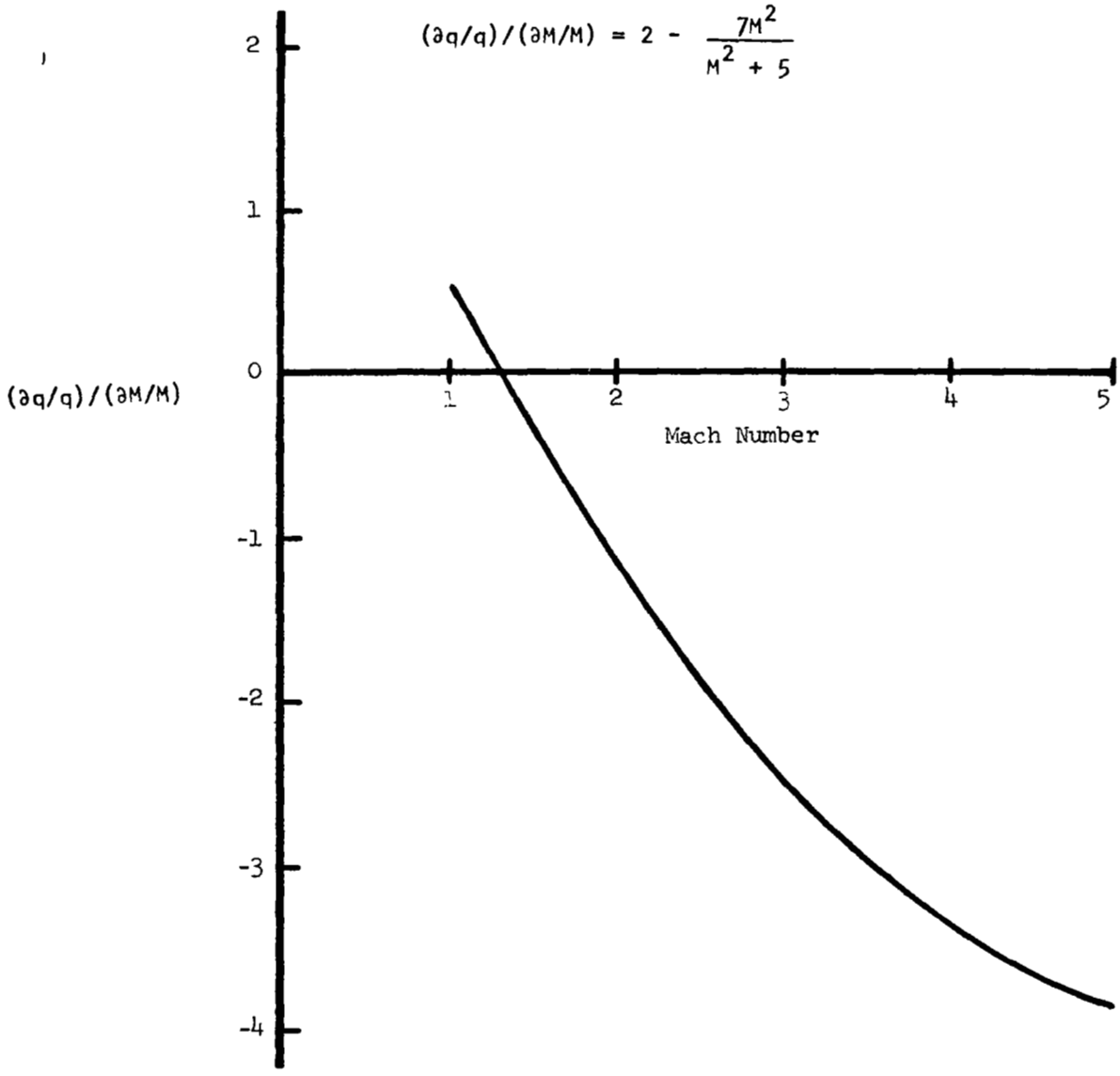

Figure 2.C.6 THE SENSITIVITY OF DYNAMIC PRESSURE TO MACH NUMBER ERROR, SUPERSONIC OPERATION

$$\therefore \quad \frac{\partial q}{\partial M} = \gamma M P_\infty + \frac{\gamma}{2} M^2 \frac{\partial P_\infty}{\partial M} \tag{2.C.17}$$

$$(\partial q/q)/(\partial M/M) = \frac{M}{q}\left(\gamma M P_\infty + \frac{\gamma}{2} M^2 \frac{\partial P_\infty}{\partial M}\right) \tag{2.C.18}$$

$$= 2 + (\partial P_\infty/P_\infty)/(\partial M/M) \tag{2.C.19}$$

As shown in Section II.C.3,

$$\partial M/(\partial P_\infty/P_\infty) = -\frac{5}{7M}(1 + .2M^2), \tag{2.C.20}$$

hence

$$(\partial M/M)/(\partial P_\infty/P_\infty) = -\frac{5}{7M^2}(1 + .2M^2). \tag{2.C.21}$$

Then

$$(\partial q/q)/(\partial M/M) = 2 - \frac{7M^2}{5(1 + .2M^2)}, \tag{2.C.22}$$

or

$$(\partial q/q)/(\partial M/M) = 2 - \frac{7M^2}{(M^2 + 5)}. \tag{2.C.23}$$

In a similar manner, errors in H_s can be shown to have a one-to-one relationship with errors in q.

At low subsonic Mach numbers, the pressure ratio P_∞/H_s approaches unity, so that determination of the Mach number and dynamic pressure from measurements of the individual pressures becomes increasingly inaccurate. At these low Mach numbers (below about 0.4) a preferred procedure is to measure the differential $(H_s - P_\infty)$ directly with a low range transducer and to compute the dynamic pressure from:

$$q = (H_s - P_\infty)/(1 + \frac{M^2}{4} + \frac{M^4}{40} + \ldots). \tag{2.C.24}$$

At low Mach numbers, only the first term of the series is usually required. For example, the error is only 0.14 percent at M = 0.5 using only the first term. At M = 1.0, the first three terms yield results accurate to 0.1 percent.

II.C.2 Temperature

As a fundamental state property, stream (static) temperature is of substantial importance in establishing the character of the fluid flow. Thus an accurate value of temperature is required in wind tunnel testing to determine several correlation parameters which define the nature of the flow.

The determination of static temperature in a gas stream conventionally involves an indirect measurement. Stagnation temperature is a convenient measurement to make since it is relatively easy to obtain, and there are established procedures for computing static temperature from the stagnation value and flow Mach number. Figure 2.C.7 illustrates the relation of stagnation-to-static temperature for a perfect gas ($\gamma = 1.4$) in an adiabatic process. This relation ($T_o/T = 1 + \frac{\gamma-1}{2} M^2$) is used in wind tunnels which operate at moderate pressures and temperatures and where real gas effects are negligible. It can be seen that an error in the measurement of stagnation temperature, T_o, is directly reflected in the static temperature.

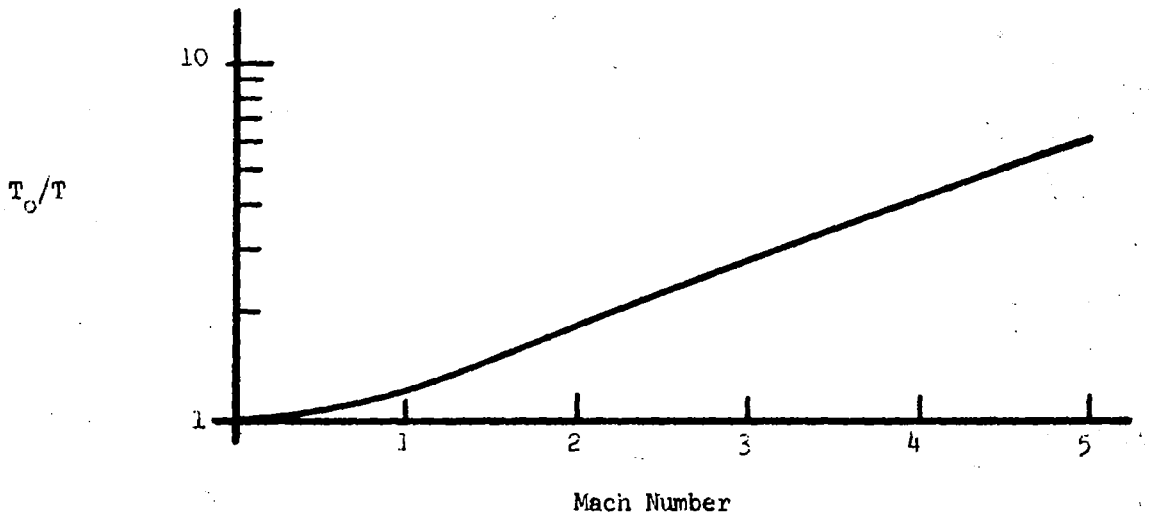

Figure 2.C.7 THE RELATION OF STAGNATION TO STATIC TEMPERATURE AS A FUNCTION OF MACH NUMBER

II.C.3 Mach Number

As previously discussed Mach number is computed using settling chamber pressure and either static pressure or after-shock (Pitot) stagnation pressure. In the transonic region, Mach number is computed from

$$M = \left\{ 5 \left[\left(\frac{H_s}{P_\infty} \right)^{2/7} - 1 \right] \right\}^{1/2} . \qquad (2.C.25)$$

The sensitivity of Mach number to settling chamber pressure measurement can be derived by obtaining the partial derivative of the above expression with respect to H_s, i.e.,

$$\frac{\partial M}{\partial H_s} = \frac{1}{2} \left\{ 5 \left[\left(\frac{H_s}{P_\infty} \right)^{2/7} - 1 \right] \right\}^{-1/2} \left\{ \frac{10}{7} \left(\frac{H_s}{P_\infty} \right)^{-\frac{5}{7}} \frac{1}{P_\infty} \right\} \qquad (2.C.26)$$

$$\frac{\partial M}{\partial H_s} = \frac{5}{7M} \left(\frac{H_s}{P_\infty} \right)^{-\frac{5}{7}} \frac{1}{P_\infty} . \qquad (2.C.27)$$

This expression may be non-dimensionalized to obtain

$$\partial M/(\partial H_s/H_s) = \frac{5}{7M} \left(\frac{H_s}{P_\infty} \right)^{\frac{2}{7}} \qquad (2.C.28)$$

or

$$\partial M/(\partial H_s/H_s) = \frac{5}{7M} (1 + .2M^2) . \qquad (2.C.29)$$

Similarly, the non-dimensional sensitivity of Mach number to P_∞ is found to be

$$\partial M/(\partial P_\infty/P_\infty) = - \frac{5}{7M} (1 + .2M^2) , \qquad (2.C.30)$$

which illustrates that

$$\partial M/(\partial P_\infty/P_\infty) = - \partial M/(\partial H_s/H_s) . \qquad (2.C.31)$$

The relation of stagnation pressure behind a normal shock, H_2, to H_s as a Mach number function is:

$$\frac{H_2}{H_s} = \left[\frac{6M^2}{M^2 + 5}\right]^{3.5} \left[\frac{6}{7M^2 - 1}\right]^{2.5} \qquad (2.C.32)$$

This relation will not yield an explicit expression for Mach number, therefore, the sensitivity of Mach number to H_2 was evaluated using a numerical, finite interval approach. As previously shown

$$\partial M/(\partial H_s/H_s) = -\partial M/(\partial H_2/H_2) \ . \qquad (2.C.33)$$

These sensitivities are illustrated in Fig. 2.C.8.

This figure consistently shows a larger Mach number error per percent error in H_s and H_2 than per percent error in H_s and P_∞. However, when nominal values of H_s, P_∞ and H_2 are substituted appropriately, the relative magnitude of Mach number error per N/m^2 error in the measurement illustrates the superiority of H_2 over P_∞ at supersonic speeds (see Fig. 2.C.9).

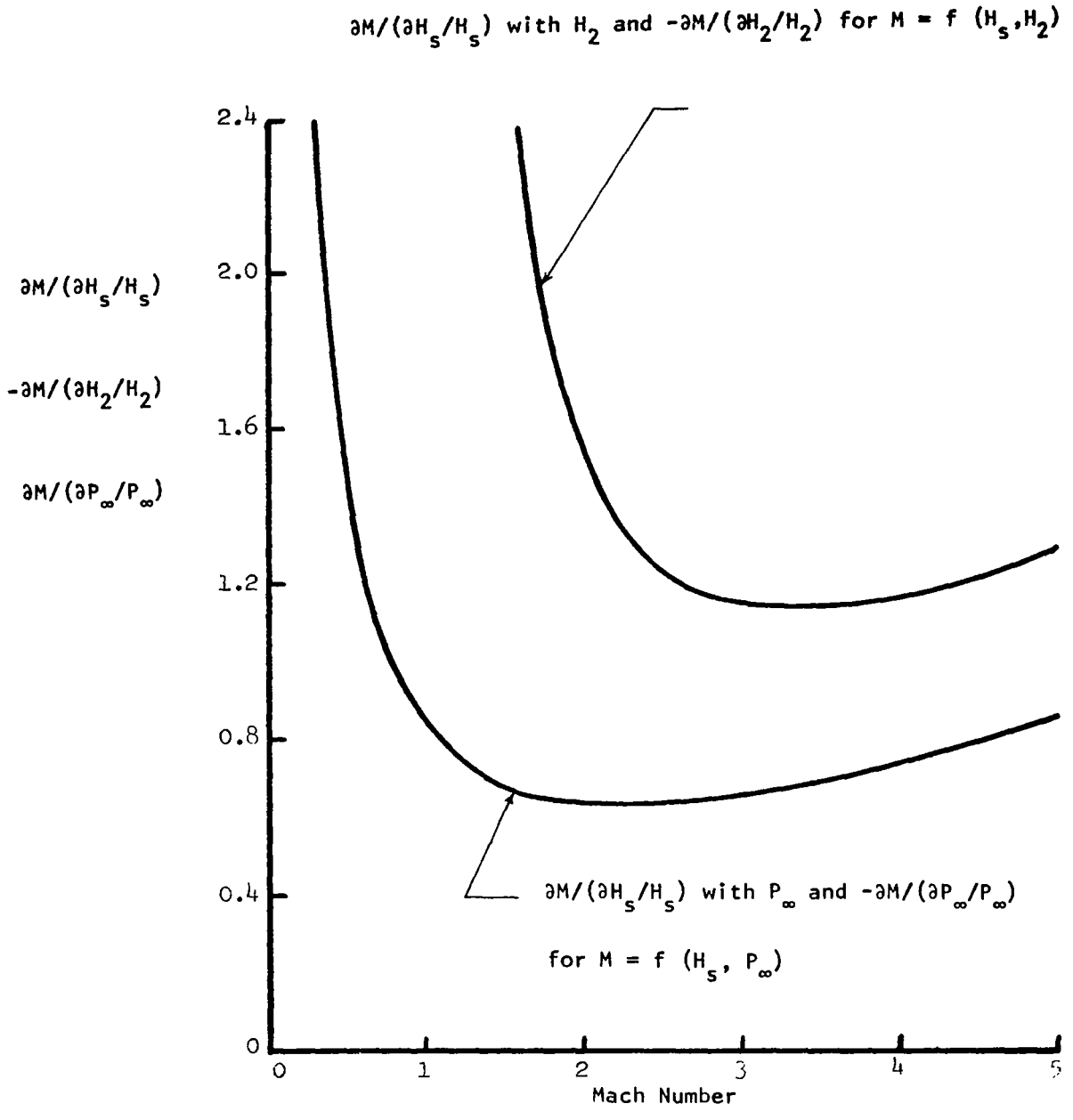

Figure 2.C.8 THE SENSITIVITY OF MACH NUMBER TO STATIC PRESSURE AND STAGNATION PRESSURE ERROR

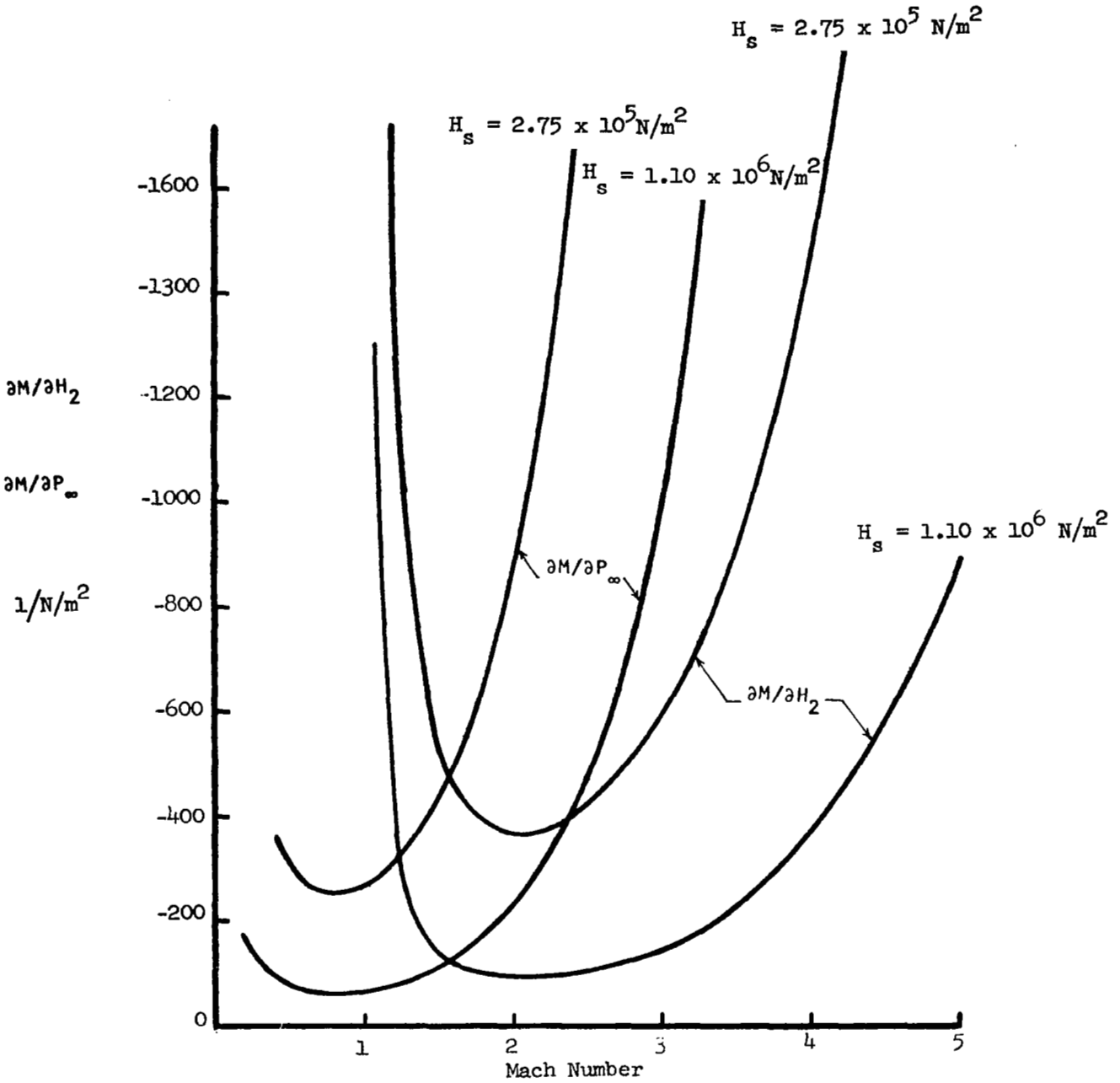

Figure 2.C.9 THE SENSITIVITY OF MACH NUMBER TO STATIC PRESSURE AND STAGNATION PRESSURES

II.C.4 Flow Angularity and Curvature

Flow angularity and curvature can result from nozzle contour errors, irregularities or discontinuities in the internal surfaces of a tunnel, in-flow or out-flow due to leakage, and swirl or curvature propagated from upstream of the nozzle or contraction. The resulting non-uniformity produces local perturbations in the flow which result in gradients or variations in flow properties including static pressure, and therefore, Mach number (see Fig. 2.C.10). Thus steps are taken to dissipate these disturbances by means appropriate to the particular tunnel configuration. These corrective actions include nozzle contour corrections, installation of honeycombs in regions of low Mach number flow, and more recently, perforated plates in regions where an uncontrolled, high-pressure-ratio shockdown would generate additional undesirable perturbations (Ref. 4).

Because of the acute sensitivity of certain model configurations to non-uniformity of flow such as local flow direction and Mach number, it is necessary to define via calibration any flow anomalies that may exist in the test section. Probes for measuring flow angularity are discussed in Section III.E.

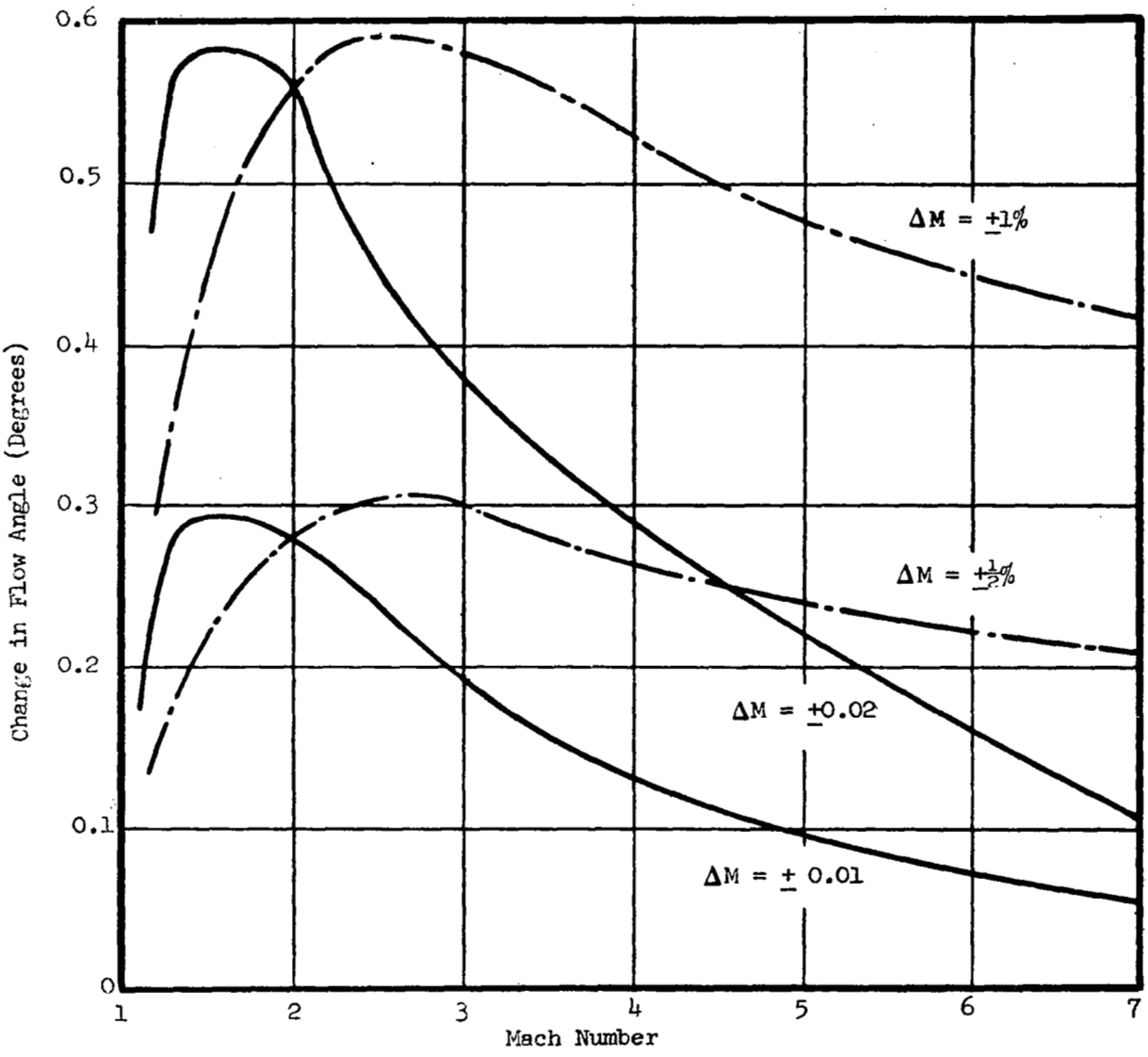

Figure 2.C.10 CHANGE IN FLOW DIRECTION WITH INCREMENT OF MACH NUMBER, Ref. 3

II.C.5 Reynolds Number

The ratio of inertial to viscous forces in the test medium is obtained from wind-tunnel measurements as a dimensional unit Reynolds number given by

$$R/\ell = \frac{\rho U}{\mu} \quad . \tag{2.C.34}$$

This can be expressed in units of m^{-1} in terms of T_o, M and P_∞ as follows:

$$R/\ell = 2.29 \times 10^6 \quad \frac{P_\infty M}{T_o^2} (1 + .2M^2)^2 \left(\frac{T_o}{1 + .2M^2} + 110.3 \right), \tag{2.C.35}$$

or if P_∞ is replaced with H_s,

$$R/\ell = 2.29 \times 10^6 \quad \frac{H_s M}{T_o^2 (1 + .2M^2)^{1.5}} \left(\frac{T_o}{1 + .2M^2} + 110.3 \right). \tag{2.C.36}$$

Since R/ℓ is a linear function of P_∞ and H_s, the sensitivity to these parameters is one-to-one; that is, a given error in either of these will be reflected in the same percent error in R/ℓ. However, in the transonic range P_∞ and H_s are used to obtain Mach number which is also a variable in the above expressions. Thus errors in P_∞ and H_s can be reflected in R/ℓ through errors in M. Figures 2.C.11 and 2.C.12 illustrate these sensitivities for selected unit Reynolds numbers (5, 25, 50 & 100 x 10^6/meter) at a nominal stagnation temperature of 311 ^oK (100 ^oF). The sensitivity of Reynolds number to measurements of stagnation temperature is shown in Fig. 2.C.13.

In tunnels where calibrated Mach numbers are obtained and considered constant for subsequent operation with the same facility configurations, any errors in Mach number due to calibration or a dissimilar configuration will contribute to errors in R/ℓ. This effect is shown in Fig. 2.C.14.

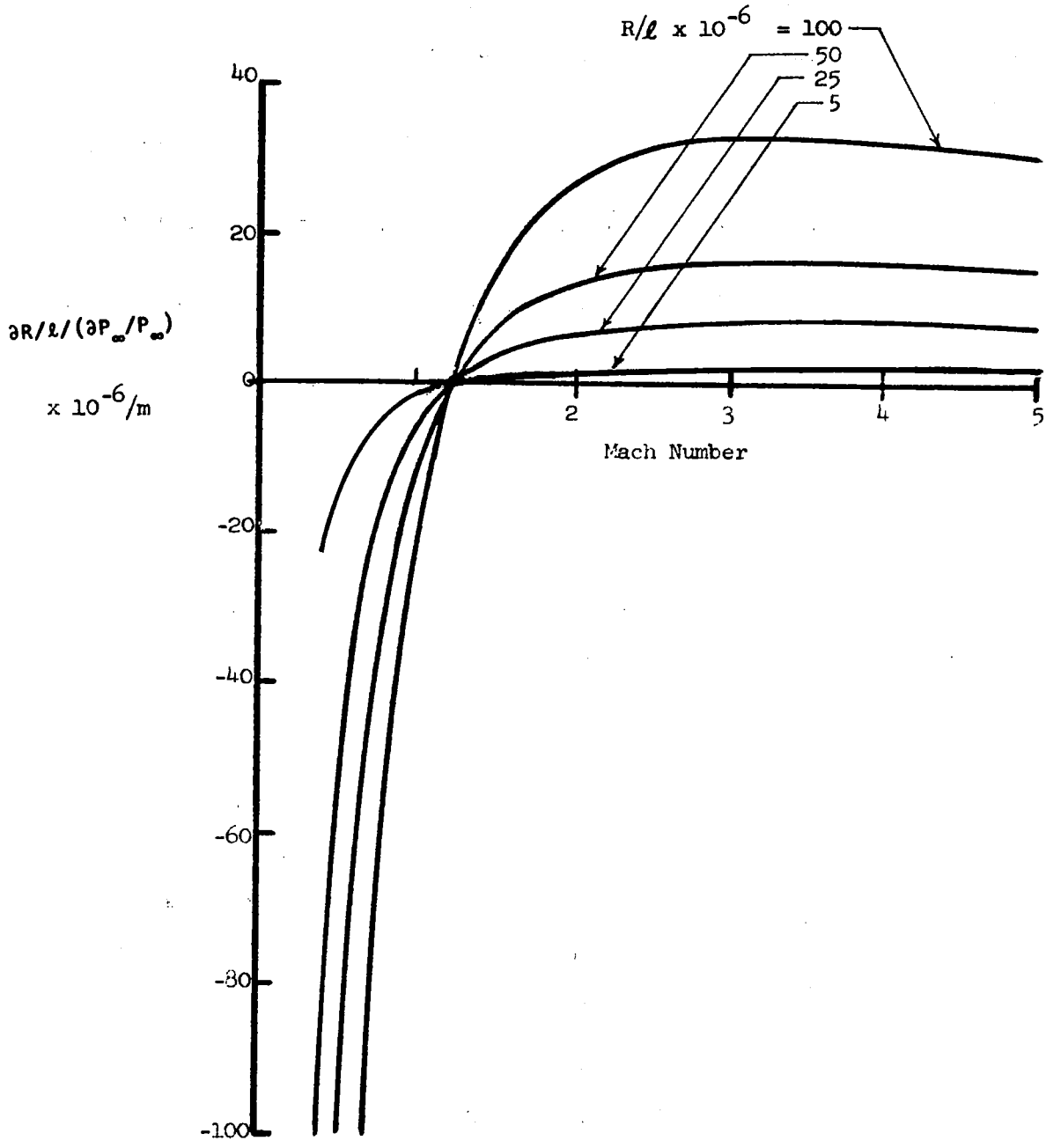

Figure 2.C.11 THE SENSITIVITY OF UNIT REYNOLDS NUMBER TO STATIC PRESSURE ERROR

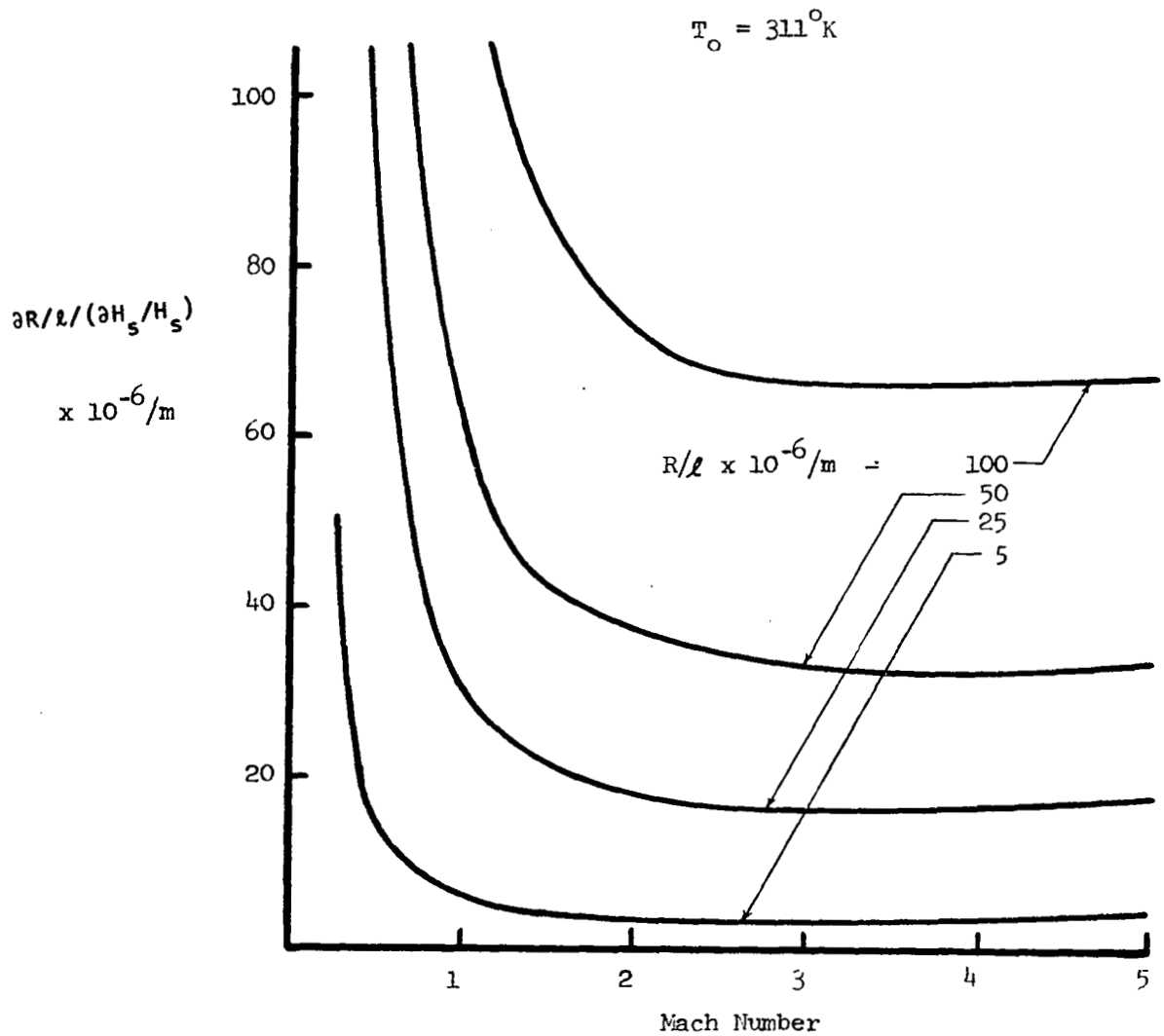

Figure 2.C.12 THE SENSITIVITY OF UNIT REYNOLDS NUMBER TO STAGNATION PRESSURE ERROR

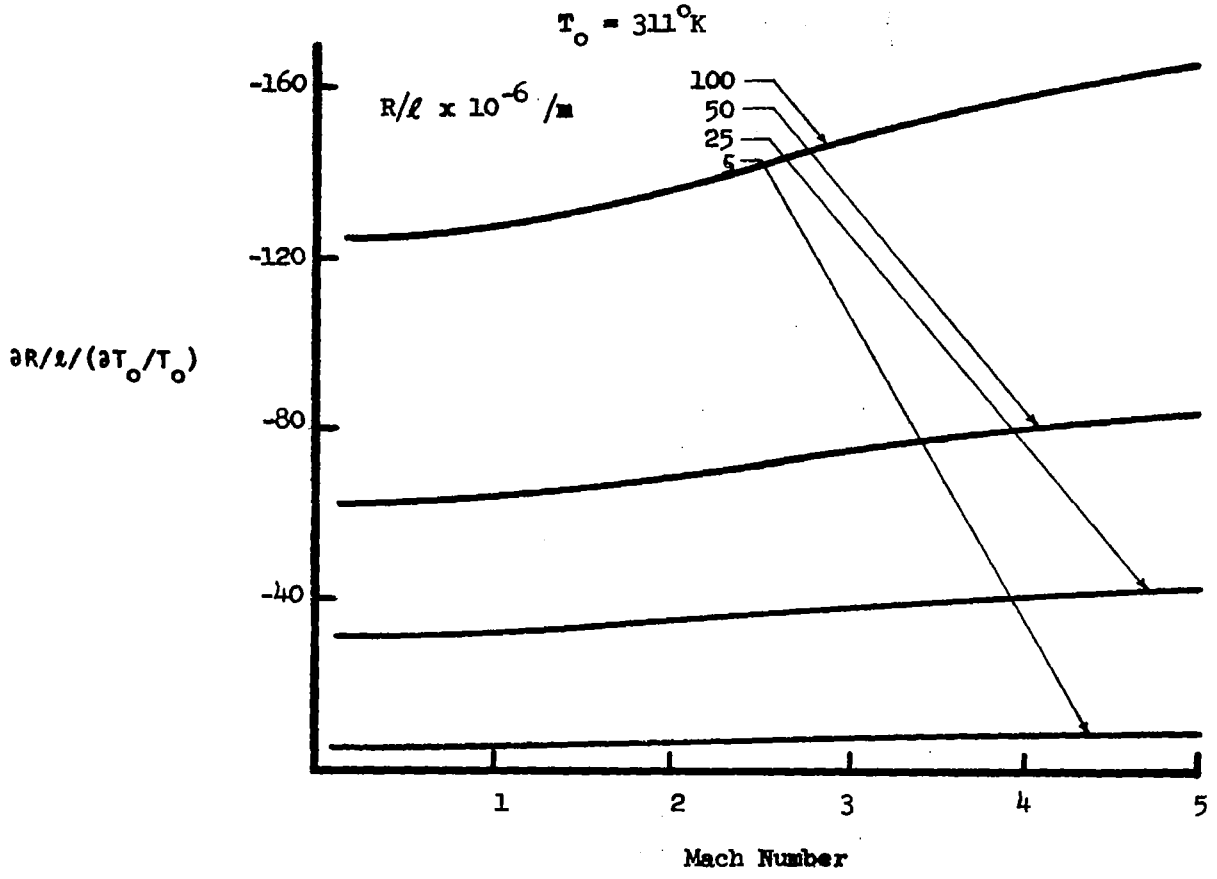

Figure 2.C.13 THE SENSITIVITY OF UNIT REYNOLDS NUMBER TO STAGNATION TEMPERATURE ERROR

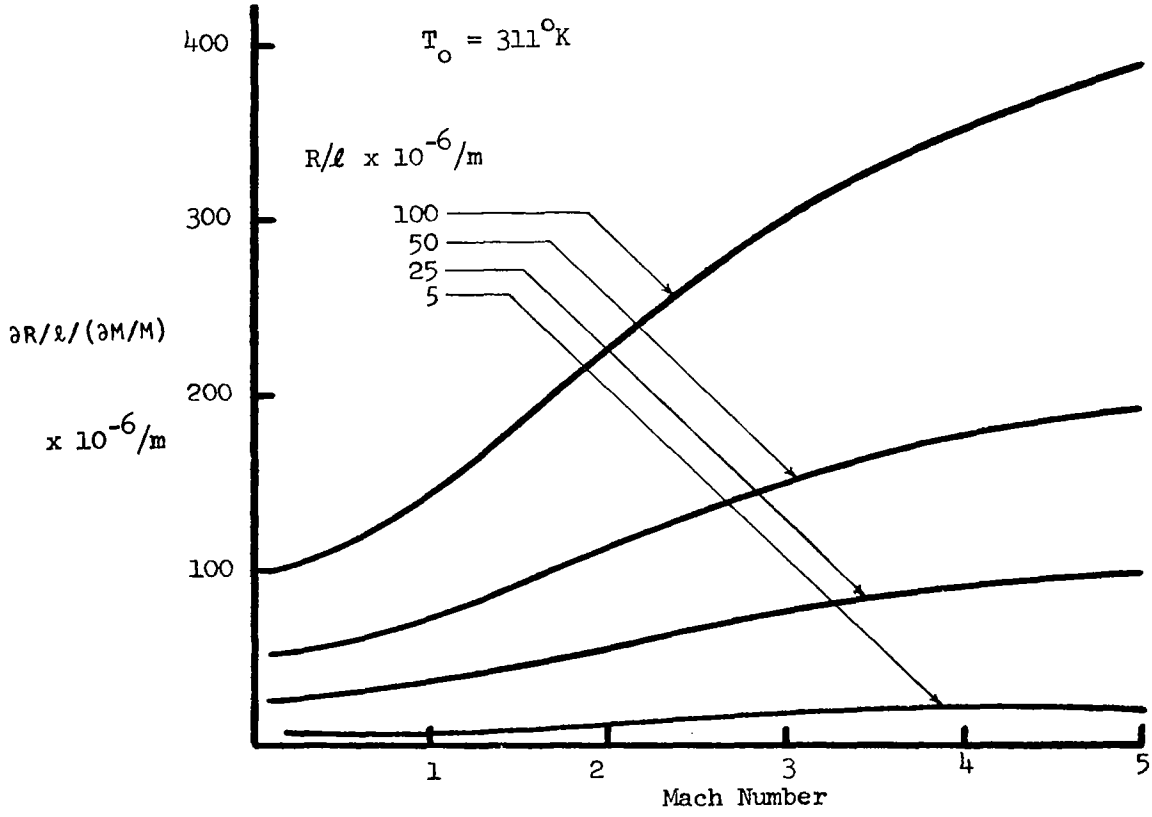

Figure 2.C.14 THE SENSITIVITY OF UNIT REYNOLDS NUMBER TO MACH NUMBER ERROR

II.C.6. Unsteadiness, Turbulence and Noise

Large, continuous flow tunnels often have small-amplitude, low-frequency oscillations in the mean flow conditions. For example, the 11-Ft Transonic Tunnel at NASA Ames has a characteristic period of approximately 10 seconds. Of course, this type of variation should be calibrated and used to establish routine testing procedures.

According to Westley (Ref. 5), measurements in AEDC, Langley, and Modane wind tunnels indicate the maximum axial and transverse turbulence intensities are approximately 1.0% and 0.4% for Mach numbers near one. In Part II.2 of Ref. 6, it is noted that wind tunnel turbulence has been used at NLR (Netherlands) and ONERA (France) to excite model flutter modes.* However, Timme (Ref. 7) cautions that turbulence not only can mask the initiation of flutter, but may also excite response modes which are not true flutter modes. Also, Timme points out that Mabey (RAE) found the transonic buffet boundary to be very sensitive to flow unsteadiness. In addition, freestream turbulence introduces errors in static pressure measurements (see Section III.D) and affects boundary layer transition, separation phenomena at leading and trailing edges, and shock-boundary layer interactions.

The following are known to be sources of noise in transonic wind tunnels:

1. porous walls which can generate distinct frequencies known as edgetones and/or organ tones,
2. slotted walls which generate broad-band disturbances due to shearing in the slots between the moving air in the test section and the air in the surrounding plenum chamber,

*A preferred procedure would appear to be a controlled excitation of the model via either a mechanical excitor, pressure pulse generator, or loudspeakers.

3. reverberation of tunnel walls,
4. plenum chamber surges,
5. turbulent boundary layers along the tunnel walls,
6. diffuser flow instability,
7. compressors in continuous wind tunnels,
8. control valves in blowdown wind tunnels,
9. vibration of tunnel sidewalls,
10. working section cutouts, and
11. model supports and struts.

The noise sources, which usually dominate at various Mach numbers, are indicated in Figs. 2.C.15 and 16.

It is noted in the review paper by Westley (Ref. 5) that $C_{L_{max}}$, buffet onset, transonic drag rise, boundary layer transition and separation, skin friction drag, shock shapes and locations, etc., may all be affected by tunnel-generated noise. Hence, wind tunnel data will not be representative of free-flight conditions in cases where this is true. Our present state of knowledge does not allow a quantitative definition of the complex interactions between turbulence, noise, and aerodynamic testing in wind tunnels. The fundamental objective of current research in this area is to obtain a better understanding of this phenomena via a systematic testing program which uses standardized instrumentation. A list of 25 recommendations concludes the paper by Westley (Ref. 5). These recommendations mainly consist of:

(1) decisions which need to be made to standardize instrumentation and test procedures, and
(2) new experimental programs.

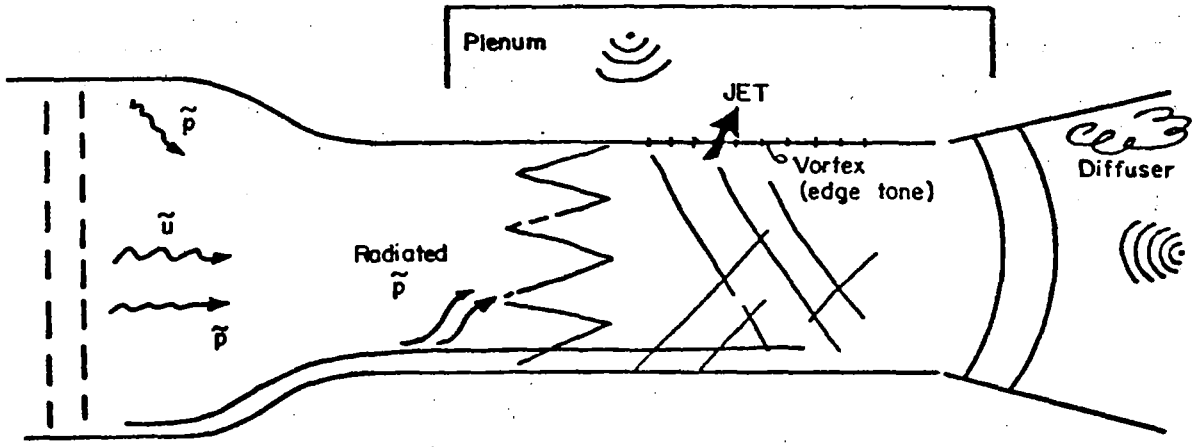

$M_\infty < 0.3$	TURBULENCE $\tilde{u}$ (valves, compressor)	← Dominant Source
	DIFFUSER $\tilde{p}$	← " "
$0.3 < M_\infty < 1$	WALL HOLE RESONANCE	← " "
	JET NOISE	← " "

Figure 2.C.15 FLOW DISTURBANCES IN TRANSONIC TUNNELS, Ref. 5

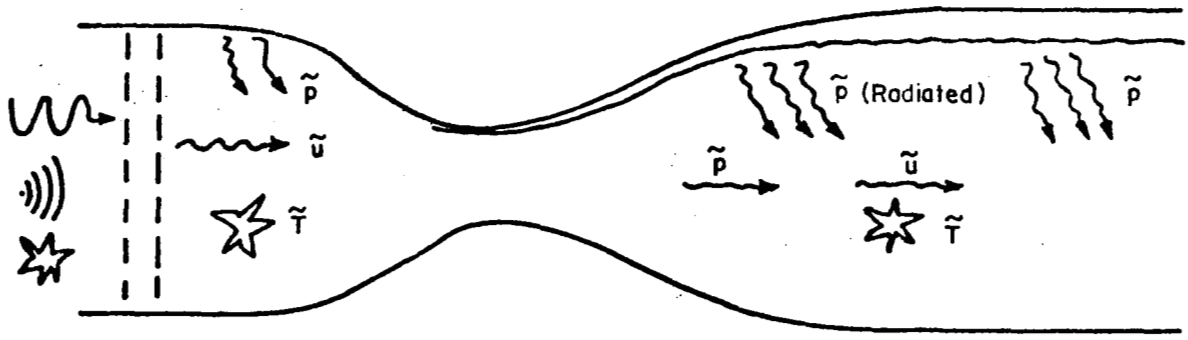

SUPERSONIC – HYPERSONIC

M_∞ = 1 – 3	VORTICITY (turbulence)	$(\tilde{u})$	← Usually Dominant
	NOISE	$(\tilde{p})$	
	ENTROPY (temp. spots)	$(\tilde{T})$	
M_∞ = 3 – 10 20 (cold flow)	RADIATED NOISE	$(\tilde{p})$	← Usually Dominant
M_∞ > 10 Arc tunnels Shock " MHD "	ENTROPY	$(\tilde{T})$	?

Figure 2.C.16 FLOW DISTURBANCES IN SUPERSONIC AND HYPERSONIC TUNNELS, Ref. 5

One of the primary recommendations is that standard instrumentation be adopted to measure free-stream disturbances. This problem of noise measurements in transonic tunnels is discussed in Section III.F.

II.C.7 Humidity

The acceleration of air from rest involves the reduction of static pressure and temperature. Such expansion to even moderate speeds results in the rapid approach to water-vapor saturation. Figure 2.C.17 illustrates this condition in terms of the ratio of the relative humidity of the stream to that of air at rest as in a reservoir. The extent of the effect of condensation on aerodynamic test data, and thus the amount of condensation which can be tolerated, has not been firmly established (Ref. 8). For example, the investigation reported by Norton, et al. (Ref. 9) indicates very little difference in data obtained on the same model in moist air as compared with that obtained in dry air.

In the absence of a water surface or a precipitant (such as a droplet or foreign nuclei), humid air can be cooled well beyond the theoretical saturation point before condensation occurs. This is because the process is time dependent and the rate of expansion (which defines the temperature history of the flow and is usually related to the tunnel size) defines the amount of supercooling that can be attained. Supercooling of as much as 100 ^{o}C has been experimentally measured using substantial temperature gradients (100 ^{o}C/cm), e.g., Ref. 10; and theoretical work has been accomplished which indicates that the saturation vapor pressure may be exceeded by a factor of 4, Ref. 11. It has been demonstrated that supercooling of 30 ^{o}C can be accomplished with negligible likelihood of condensation, Ref. 12. However, even with this tolerance, it may be seen in Figure 2.C.18 that for an arbitrary dew point of 2 ^{o}C extreme reservoir temperatures would be required to avoid condensation at low supersonic Mach numbers. Therefore, it is generally not practical (because of airstream stagnation temperature limits, such as those of Ref. 8) to employ reservoir heating as a means for avoiding condensation. In practice, air dryers are usually used to reduce dew points to as low as practical; although this may be above the stream temperature, the total water content is small, and condensation effects are negligible.

As noted by Pope and Goin (Ref. 12), the effect which humidity has on tunnel Mach number depends on whether the flow is subsonic or supersonic. In the case of subsonic flow, water vapor tends to increase the Mach number and

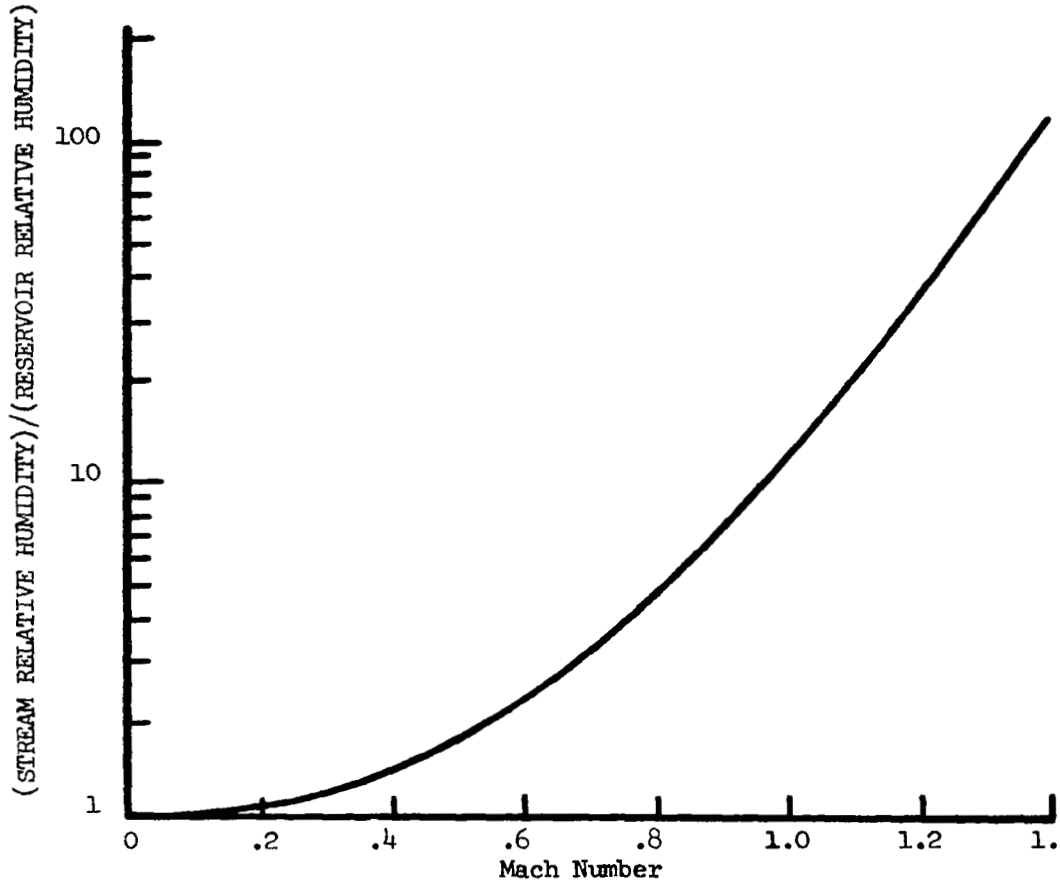

Figure 2.C.17 THE RATIO OF RELATIVE HUMIDITY IN THE STREAM TO RESERVOIR AS A FUNCTION OF MACH NUMBER

Assumptions:

Dew Point Temperature = 2 C
Allowable Supercooling = 30 C
Allowable Stream Temperature = -29 C

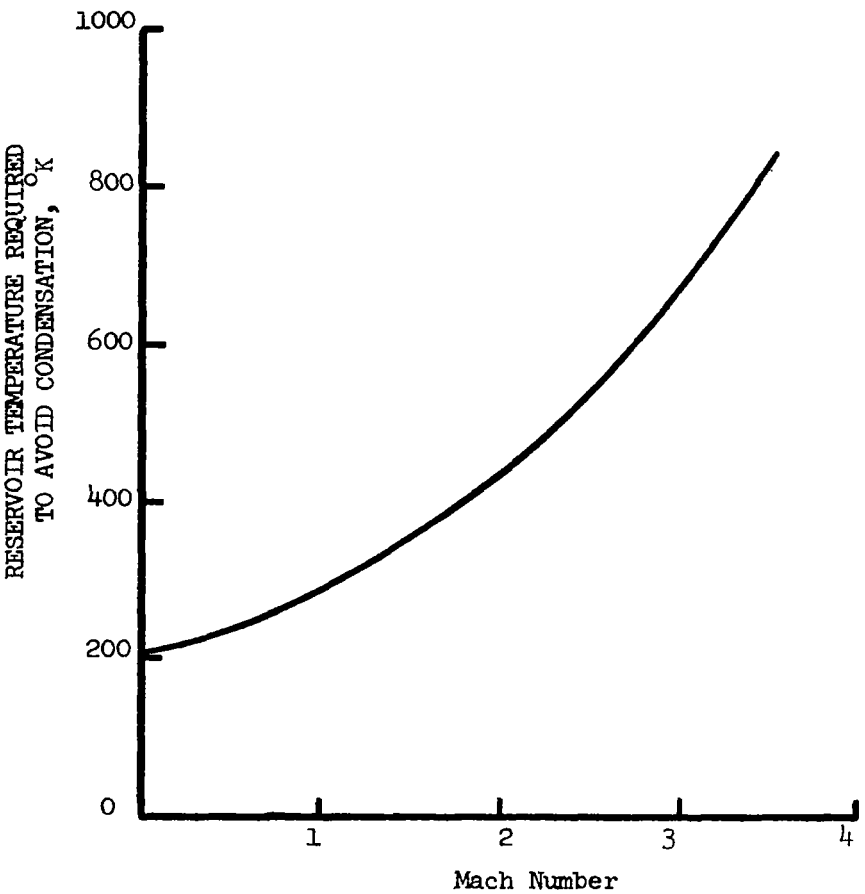

Figure 2.C.18 RESERVOIR TEMPERATURE REQUIRED TO AVOID CONDENSATION, Ref. 10

reduce static pressure; whereas, the opposite occurs in supersonic flow. This effect has also been substantiated by analyses at AEDC.* These results indicate a negative Mach number gradient occurs when moisture condenses in supersonic flow.

The absence of condensation during tunnel calibration (i.e., empty tunnel) does not preclude the possibility of local condensation in proximity of a model during production testing. It has been observed in the AEDC Aerodynamic Wind Tunnel 4T (Transonic 4T) that transonic force data is unaffected by moisture content until condensation can be seen (a nominal water-vapor content of 0.002 gm/gm of air). However, tests involving surface pressure measurements are more sensitive, and experience at AEDC indicates this type of transonic testing should be conducted with humidity $\leq$ 0.0015 gm H_2O/gm air.** An additional procedure for reducing the effect of humidity in transonic tunnels is to adjust wall angle according to the test medium dew point, e.g., Ref. 8. In the supersonic regime, experience at NASA Ames has shown that 0.0004 gm H_2O/gm of air is a good rule-of-thumb for model tests with $M < 3.5$.† For example, mass flow through an inlet model is found to vary about 1% at $M = 3.0$ when the moisture content varies from 0.0002 to 0.001. Because of the facility variables which affect the allowable moisture content, it is desirable to establish the level which can be tolerated in a particular facility by conducting tests on a representative configuration and varying only humidity. This type of test was included in the work reported by Corson, et al. (Ref. 8).

---

* Private communication, Mr. J. D. Gray, AEDC.

** Private communication, Mr. J. Gunn, AEDC.

† Private communication, Mr. F. W. Steinle, NASA Ames.

II.C.8 Test Mediums

Air is almost universally used as the test medium in transonic and supersonic wind tunnels. Although these facilities have different operating characteristics with the air being subjected to different pressure and temperature levels during the various cycles, it is generally allowable to consider the gas to be ideal. Real gas effects may become relevant at extreme conditions such as in a Ludwieg tube facility (Ref. 6). Departures from the ideal gas relations may occur when other test mediums are employed. However, it has been found that the ideal relations are suitable for the very low temperature nitrogen used in the Langley 1/3-Meter Transonic Cryogenic Tunnel (Ref. 14).

Recent transonic wind tunnel tests of airfoils have indicated an effect of varying γ , Refs. 15 and 16. Although no effect was detected for subcritical flows, a systematic reduction in local peak Mach numbers was observed for supercritical flows. Tuzla, et al. (Ref. 16) suggest this trend is associated with the effects of γ on transonic-shock/boundary-layer interactions. This is relevant to the calibration of empty, transonic tunnels if a conventional, static-pressure probe is used to measure freestream Mach number in different test gases. As discussed in Section III.D.2, a transonic shock always forms on a conventional static-pressure probe. If variations in γ can affect supercritical pressure distributions, this may also change the location on a probe at which freestream pressure exists. Research on this phenomena is continuing at NASA Ames.

II.C. References

1. Hill, Jacques A. F. et al, "Mach Number Measurements in High Speed Wind Tunnels," MIT, Naval Supersonic Laboratory Technical Report 145, February 1956.

2. Thompson, J. S. and Holder, D. W., "Notes on Wind Tunnel Pressure Measurements from the Operator's Point of View," RAE TN Aero. 2547, February 1958.

3. Raney, D. J., "Flow Direction Measurements in Supersonic Wind Tunnels," Her Majesty's Stationery Office, London 1956.

4. Cooksey, J. M. and Arnold, J. W., "Flow Quality Improvements in a Blowdown Wind Tunnel Using a Multiple Shock Entrance Diffuser," AIAA Journal, Vol. 10, No. 9, September 1973.

5. Westley, R.: "Problems of Noise Measurements in Ground-Based Facilities With Forward-Speed Simulation (High-Speed Windtunnel Noise)," AGARD-AR-83, Sept. 1975.

6. MiniLaWs Working Group, "A Further Review of Current Research Aimed at the Design and Function of Large Windtunnels," AGARD-AR-83, Sept. 1975.

7. Timme, A., "Effects of Turbulence and Noise on Wind-Tunnel Measurements At Transonic Speeds," AGARD-R-602, April 1973.

8. Corson, Blake, W., et al. "Calibrations of the Langley 16-foot Transonic Tunnel with Test Section Air Removal," NASA TR R-423, August 1974.

9. Norton, Harry T. Jr., Runckel, Jack F., and Pendergraft, Odis C. Jr., "Transonic Performance of Two Convergent-Divergent Ejector Nozzles Designed for Corrected Secondary Flows of 3 and 9.4 Percent," NASA TM X-909, 1964.

10. Lundquist, G. A., "Recent Experimental Work at NOL on Condensation in Compressible Flows," Geophysical Research Paper No. 37, ARDL, July 1955.

11. Oswatitsch, K. I., Z. A. M. M. 22, 1, 1942, English Trans.; British R.T.P. Trans. No. 1950, MAP.

12. Pope, A. and Goin, K. L., High Speed Wind Tunnel Testing, Wiley, 1965.

13. - , Survey Response from NASA Langley 16 Ft. Transonic Dynamics Tunnel.

14. Adcock, Jerry B., Kilgore, Robert A. and Ray, Edward J., "Cryogenic Nitrogen as a Transonic Wind Tunnel Test Gas," AIAA Paper 75-143, January 1975.

15. Gross, A. R. and Steinle, F. W.: "Pressure Data from a 64010 Airfoil at Transonic Speeds in Heavy Gas Media of Ratio of Specific Heats from 1.67 to 1.12," NASA TM X-62468, Aug. 1975.

16. Tuzla, K.; Wai, J. C.; and Russell, D. A.: "γ-Effects on 2-Dimensional Transonic Aerodynamics," Proc. AIAA 9th Aerodynamic Testing Conference, June 1976.

17. Spratley, A. B., Thompson, E. R., and Kennedy, T. L.: "Reynolds Number and and Nozzle Afterbody Configuration Effects on Model Forebody and Afterbody Drag," AIAA Paper 77-103, January 1977.

III. CALIBRATION PROCEDURES AND INSTRUMENTATION

A. Settling Chamber Pressure

As discussed in Section II.A., the reservoir total pressure is a fundamental variable which is usually measured directly in the settling* chambers of both transonic and supersonic tunnels. The Mach number and dynamic pressure in the settling chamber are determined by the contraction ratio, A_o/A^*, where A_o is the cross sectional area at the settling chamber and A^* is the choked throat area corresponding to the test section Mach number. The maximum stilling chamber Mach number normally occurs at Mach 1.0 in a transonic-supersonic tunnel. At a contraction ratio of 10, for example, the corresponding stilling chamber Mach number is 0.058. The flow may be considered incompressible and the ratio of dynamic to stagnation pressure determined from

$$\frac{q_s}{H_s} = \frac{H_s - P_s}{H_s} = 1 - \left(\frac{P_s}{H_s}\right), \qquad (3.A.1)$$

where (P_s/H_s) is defined by the settling chamber Mach number. At a contraction ratio of 10, the stilling chamber dynamic pressure is 0.235 percent of the stagnation pressure. Thus, the error in measured total head, induced by using a static orifice in place of a Pitot probe, would be 0.235 percent. This would contribute a Mach number error of 0.002. Therefore, if a Mach number accuracy of 0.001 is to be achieved and static orifices are used to measure settling chamber pressure, the error must be eliminated via calibration with Pitot probes.

When using a Pitot probe to calibrate total pressure in a settling chamber, the probe must be located downstream of any screens, honeycombs, etc., since these items can cause significant pressure losses, Ref. 1. Also, the chamber cross section should be surveyed for variations in total pressure. If a single value of total pressure is to be used (as is commonly done) and its contribution to Mach number error is to be less than 0.001, then 2σ of spatial variations in total pressure must be less than 0.05 percent ($\pm\Delta M = 0.0005$ at $M = 0.80$). Unfortunately, this is not only near the state-of-the-art of pressure measurement accuracy, it is also very difficult to achieve this uniformity in practice. Thus, the decision as to what is an acceptable amount of nonuniformity in settling chamber pressure must be left to individual judgment. This decision

* The terms "settling chamber" and "stilling chamber" are used interchangeably.

should be based on the particular facility characteristics* and the type of tests which are conducted in that facility.

Once the spatial variations in settling chamber pressure are judged to be acceptable, it is suggested that an appropriate average be defined based on measurements in the central portion of the flow. For example, in the 16 ft. Transonic Tunnel at NASA Langley, four Pitot probes have been mounted in the central portion of the flow to define an average (Ref. 2). In general, initial calibrations require more measurements in order to establish a suitable average. However, once the average total pressure is determined for the range of operating conditions, a simple wall mounted tube (or a static orifice) can be calibrated to relate its measurements to the average. By following this procedure, routine testing can be accomplished without any unnecessary obstructions in the central portion of the flow.

Although a wide variety of Pitot probe nose geometries have been used in low speed flows, simple steel tubing with an internal to external diameter ratio $\geq$ 0.5 and a square-cut nose will measure total pressure in the settling chamber with negligible error.** A Pitot probe with this diameter ratio is unaffected by flow angles of 10 degrees or less, Ref. 3. Assuming that reasonable care is taken to align the probe with the flow, this type of probe will provide adequate accuracy even if considerable turbulence exists in the settling chamber. This conclusion is substantiated by the following discussion.

The problem of Pitot probe measurements in an incompressible, turbulent flow has been examined by Becker and Brown (Ref. 4). These authors have analyzed data for four different probe geometries: (1) spherical-nosed probe (a sphere on a tubular support), (2) a hemispherical-nosed tube, (3) a square-nosed tube, and (4) sharp-lipped probes made by conically tapering the exterior of a tube. The results of their semi-empirical analysis for square-nosed probes indicates the following. In an isotropic, turbulent flow with a turbulence intensity of 5 percent, a square-nosed probe with a diameter ratio

---

*A number of supersonic tunnels have fixed-contour, sliding block nozzles which are routinely operated off design. These nozzles can have significant total pressure losses which can only be determined by Pitot surveys within the test section. However, the average test section total pressure could be related to stilling chamber pressure via calibration tests.

**This assumes the nose is free of burrs. Finishing of orifices is briefly discussed in Section III.D.4.

of 0.5 will capture the total pressure with an error of $0.56 \times 10^{-4} q$. For a given amount of turbulence, the error decreases with increasing diameter ratio. This accuracy is more than ample for most tunnels since hot-wire measurements at AEDC in the settling chamber of the Aerodynamic Wind Tunnel (4T), Ref. 5, indicate the longitudinal component of the turbulence intensity is of the order of one percent for $0.3 < M < 1.2$. Assuming isotropic turbulence, this means the total turbulence intensity is approximately 1.73 percent. Thus, the suggested square-nosed probe can be used in most settling chambers with confidence.

The above described accuracy analysis ignores a number of other possible sources of error. It is assumed the probe nose is long enough to isolate it from any effects of downstream geometry. Becker and Brown (Ref. 4) suggests the nose length be greater than six probe diameters. Also, the effect of changes in the internal diameter is ignored.* In order to eliminate internal geometry as a variable, Becker and Brown suggest the internal diameter be constant for a distance of three probe diameters. In addition, the probe should be located more than two diameters from the nearest wall in order to avoid a reduction in measured pressure (e.g., Ref. 3, p. 12).

Finally, the probe should be designed and mounted to minimize vibration. Winternitz (Ref. 6) has presented a simplified procedure for designing cantilevered, circular cylinders to avoid oscillations induced by vortex shedding. Ower and Pankhurst (Ref. 7, p. 54) observe that for a cylinder with a diameter of 0.8 cm (5/16 in.) the vortex shedding frequency in air is 40 Hz at 1.5 m/sec and 160 Hz at 6 m/sec. Hence, they conclude resonance between vortex frequency and the natural frequency of the probe is unlikely in most wind tunnel applications. However, in some cases this could be a problem at the low speeds characteristic of stilling chambers. Thus, probes for measurements in the stilling chamber should be designed to avoid this phenomenon.

*The problem of internal geometry changes causing biasing of measured mean pressures in fluctuating flows is briefly discussed in Ref. 3, p. 105.

III.A. References

1. Loehrke, R. I. and Nagib, H. M.: "Experiments on Management of Free-Stream Turbulence," AGARD-R-598, Sept. 1972.

2. Corson, B. W., Jr.; Runckel, J. F.; and Igoe, W. B.: "Calibration of the Langley 16-Foot Transonic Tunnel with Test Section Air Removal," NASA TR-R-423, Aug. 1974.

3. Bryer, D. W. and Pankhurst, R. C.: Pressure-Probe Methods for Determining Wind Speed and Flow Direction, National Physical Laboratory, Her Majesty's Stationery Office, London, 1971.

4. Becker, H. A. and Brown, A. P. G.: "Response of Pitot Probes in Turbulent Streams," Jour. Fluid Mech., Vol. 62, Part 1, 8 Jan. 1974.

5. Credle, O. P.: "An Evaluation of the Fluctuating Airborne Environment in the AEDC-PWT 16-Ft Transonic Tunnel," AEDC-TR-69-236, Nov. 1969.

6. Winternitz, F. A. L.: "Effects of Vibration on Pitot Probe Readings," The Engineer, Vol. 201, 30 Mar. 1956, pp. 273-275 and 6 April 1956, pp. 228-290, London.

7. Ower, E. and Pankhurst, R. C.: The Measurement of Air Flow, Pergamon Press, London, 1966.

III. B. TOTAL TEMPERATURE

The total temperature is normally monitored in the stilling chamber during routine tunnel operation. Since the difference between total and static temperature is small at low velocities, a shielded, high-recovery thermocouple probe is not usually necessary. In fact, data obtained by Stickney (Ref. 1) for these two types of probes show that the recovery factors are nearly identical (≈ 0.999) for temperatures near ambient and $M < 0.2$. Thus, Pope and Goin (Ref. 2) note that in many cases the total temperature can be measured in the stilling chamber, with satisfactory accuracy, by using a simple bare-wire thermocouple junction.* A schematic of this type of temperature probe is shown in the upper part of Figure 3.B.1. Measurements by Stickney (Ref. 1) indicate that such unshielded temperature probes have a much shorter response time compared to more elaborate, shielded probes. In the case of blowdown tunnels where total temperature can vary rapidly, this is an essential advantage. For example, if tests are conducted at constant Reynolds numbers, the total temperature must be monitored continuously so that total pressure can be controlled automatically. Also, small wire thermocouples with time constants of the order of 0.1 sec. are typically required. For example, a 0.13 mm (0.005 in.) diameter wire has a time constant** of 0.1 sec. in air at ambient temperature and pressure and a velocity of 19.8 m/sec (65 ft/sec). Whereas, for the same conditions, a 0.53 mm (0.021") diameter wire has a 1.0 sec time constant, e.g., Ref. 4.

In response to the questionnaire, the majority of tunnel operators indicated they do in fact use the bare-wire thermocouple for total temperature measurements. Estimated accuracies varied from ±0.56°C to ±1.1°C (±1°F to ±2°F). Based on the relations presented in Section II.C.2, an uncertainty in total temperature of 1°C will cause, at $M = 1$, a maximum uncertainty of 0.5 percent at a Reynolds number per meter of 33 million. For most testing purposes this is acceptable. However, few tunnels (transonic or supersonic) appear to have been calibrated for temperature gradients which may exist across and along the flow.

---

*A comprehensive discussion of thermocouple principles, circuits, electromotive force tables, stability and compatibility data, installation techniques, etc. may be found in Ref. 3.

**The time constant is here defined as the time required to reach 63.2% of an instantaneous temperature change.

Typical Bare-Wire Probe

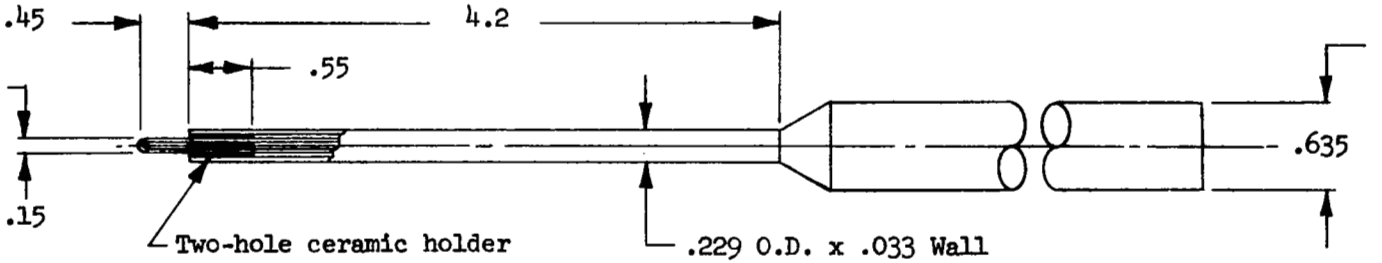

All Dimensions In Centimeters

AEDC-PWT 16T Probe (Ref. 5)

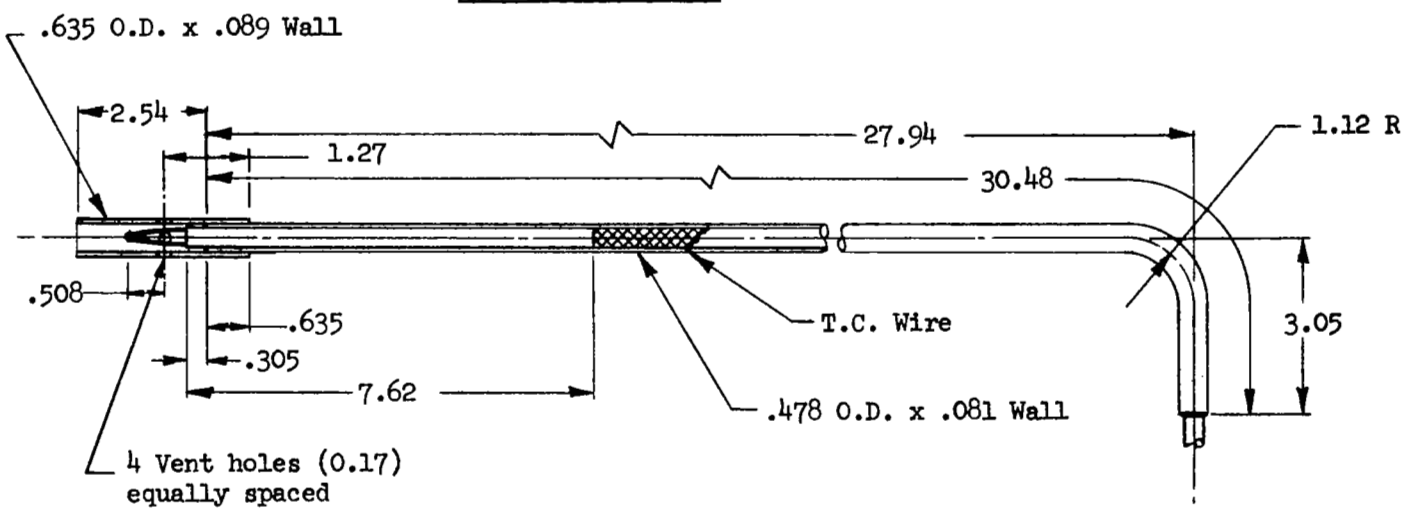

Figure 3.B.1 TOTAL TEMPERATURE PROBES

One of the most complete and extensive calibration of temperature gradients in a transonic tunnel has been done in the AEDC Propulsion Wind Tunnel (16T), Ref. 5. The temperature calibration was done to investigate the effects of a special-purpose, cryogenic cooling system which consists of a liquid nitrogen system to chill the coolant in the tunnel cooler and a liquid air system for direct injection into the tunnel airstream. A rectangular array of shielded temperature probes was located in the nozzle contraction region and in the test section. A schematic of a typical probe is shown in Figure 3.B.1.* Since the recovery factor of all thermocouple probes need to be calibrated for Mach and Reynolds number effects (Ref. 1), the raw temperature data were first corrected for these effects by Robson (Ref. 5). Subsequently, the temperature of the flow through the central portion of the nozzle entrance section was defined by an average of thirteen temperatures measured over a 2 x 3.5 m (6 x 11 ft) rectangular region. The temperature of the test section flow was defined by an average of 17 temperatures obtained over a 2 x 2 m (6 x 6 ft) portion of the core. The difference between these two temperatures was used to define a temperature calibration parameter which relates temperature at the nozzle entrance to test section temperature. In this case, the test section flow was found to be approximately 1.1°C (2°F) lower than the nozzle flow. Deviations of ±8°F were obtained across both the nozzle and the test section over a Mach number range 0.2 to 0.8 and $-22°C < T_o < 21°C$. These detailed temperature measurements were made because of the anticipated nonuniformities produced by the special cooling system.** Although smaller temperature gradients usually exist in tunnels without special cooling or heating systems, this example illustrates the procedure required to accurately calibrate wind tunnel temperatures. For routine testing, a single temperature probe can be related to the average stilling chamber temperature via calibration in order to eliminate the disturbing effects of an unnecessary thermocouple grid.

---

*Robson (Ref. 5) states that the copper-constantan thermocouples used in this probe are generally considered to have a systematic error of ±2.2°C (±4°F).

**Temperatures in the 1/3-Meter Transonic Cryogenic Tunnel at NASA Langley have also been surveyed using a grid of thermocouple probes, Ref. 6.

Additional information on the design and calibration of total temperature probes can be found in Refs. 7-10. Also, Bate (Ref. 11) has reviewed the problem of errors in thermocouple measurements based on experience in the DFVLR wind tunnels in West Germany.

III. B. References

1. Stickney, T. M.: "Recovery and Time-Response Characteristics of Six Thermocouple Probes in Subsonic and Supersonic Flow," NACA TN 3455, July 1955.

2. Pope, A. and Goin, K. L.: High-Speed Wind Tunnel Testing, Wiley, New York, 1965.

3. American Society for Testing and Materials (ASTM), Committee E20: Manual on the Use of Thermocouples in Temperature Measurement, ASTM Special Technical Publication No. 470, Philadelphia, Pa., 1974.

4. The Omega Temperature Measurement Handbook, Omega Engineering, Inc., Stamford, Conn., 1975.

5. Robson, G. D.: "Test Section Temperature Calibration of the AEDC PWT 16-Ft Transonic Tunnel at Stagnation Temperatures from -30 to 30°F," AEDC-TR-69-2, Feb. 1969.

6. Polhamus, E. C.; Kilgore, R. A.; Adcock, J. B.; and Ray, E. J.: "The Langley High Reynolds Number Wind-Tunnel Program," Astro. & Aero., Oct. 1974.

7. Benedict, R. P.: Fundamentals of Temperature, Pressure, and Flow Measurements, Wiley, New York, 1969.

8. Baker, H. D.; Ryder, E.A.; and Baker, N. H.: Temperature Measurement in Engineering, Vol. II, Wiley, New York, 1961.

9. Volluz, R. J.: "Handbook of Supersonic Aerodynamics, Section 20, Wind Tunnel Instrumentation and Design," NAVORD Rept. 1488 (Vol. 6), 1961.

10. Dean, R. C., Jr.: Aerodynamic Measurements, MIT Gas Turbine Lab., Eagle Enterprises, New York, 1953.

11. Bate, J.: "Temperature Measurements in Wind Tunnels," RAE Lib. Transl. No. 1736, AD 922 120, Farnborough, Hants, England, June 1974.

III.C. PITOT PRESSURES

Use of Pitot Pressures for Calibration

As described in Section II.C.1, when M > 1.6 the uncertainty in calculated test section Mach number is less if the calculation is based on Pitot pressure rather than freestream static pressure. Thus, most supersonic tunnels have been calibrated via Pitot probe surveys and assuming an isentropic expansion from the stilling chamber. In the past, investigators such as Hill (Ref. 1) and Hill, et al. (Ref. 2) have reported that measurements in small, supersonic tunnels (<0.5 m) of the ratio of total pressure in the test section to reservoir pressure exhibit a range of 0.998 $\pm$ 0.003. This type of result leads to the conclusion that nonisentropic expansion effects are negligible at normal operating temperatures and pressures in a properly designed supersonic tunnel, i.e., one in which the empty tunnel is free of shocks. However, large continuous tunnels are often operated at relatively high humidity levels in order to increase the operating time prior to dryer saturation. For example, Maxwell and Hartley (Ref. 3) found in the AEDC-PWT 165 Tunnel that when the humidity was 0.002 gm H_2O/gm of dry air, the average total pressure of the test section was 2 to 6% lower than the reservoir pressure. This loss was reduced 50% by decreasing tunnel humidity to 0.001.*

In addition to water vapor condensation, oblique shocks and real gas effects can cause a loss in total pressure. Also, large tunnels can have nonuniformities in total pressure caused by incomplete mixing in the stilling chamber,** and small tunnels can have losses caused by axial velocity gradients (e.g., Ref. 4). With this number of possible causes of total pressure variation, it is recommended that operators of both transonic and supersonic tunnels make calibration measurements to validate the assumption of uniform total pressure. This can be accomplished in subsonic flow via a Pitot probe, since it can be used directly to compare test section total pressure with reservoir pressure. In supersonic flow, another independent pressure must be measured such as freestream static, surface pressure on a cone or wedge, or Pitot pressure behind an oblique shock. Once a choice is made, the two pressures and the ratio of specific

---

* These results were obtained with $2.0 < M < 4.75$, $3.1\ N/cm^2 < H_s < 9.1\ N/cm^2$, $55\ ^oC < T_o < 78\ ^oC$.

** This can be determined during settling chamber calibration, Section III.A.

heats can be used to calculate the test-section Mach number and total pressure.

Barry (Ref. 5) has discussed in detail the errors that occur in computed Mach number when using pressures measured with total, static, conical, and wedge probes. A significant conclusion, obtained by Barry (Ref. 5) and Thompson and Holder (Ref. 6), is that the Mach number computed from a pressure ratio involving the isentropic stagnation pressure is less sensitive to measurement errors. For this reason, an isentropic stagnation pressure probe has been designed and tested by Goodyer (Ref. 7). The probe consists of a Pitot tube mounted on the surface of a curved cylinder of circular cross section. The Pitot tube senses the impact pressure of a stream tube which has been slowed to subsonic speed by isentropic compression along the leading edge of the curved cylinder. A sketch of the probe is shown in Figure 3.C.1. The independent experimental results of Couch (Ref. 8) indicate that this type of probe permits measurements of absolute stagnation pressures with an accuracy of 99.8 percent in a Mach number range of 1.4 to 2.2. Beyond a Mach number of 2.2, the pressure recovery decays and the probe ceases to offer any advantage over a conventional probe. However, for Mach numbers less than 2.2 the stagnation pressure probe can be used for direct measurement of total pressure loss. Also, for the case of equal uncertainty in measured pressures and $1.6 < M < 2.2$, the analysis of Barry (Ref. 5) indicates the most accurate calibration of Mach number would be obtained by using the isentropic probe in conjunction with a conventional pitot probe.

If a supersonic tunnel engineer elects not to use a Goodyer probe because of its limited Mach number range, the next most accurate tunnel calibration procedure is to measure Pitot pressures in the freestream and on a wedge, Ref. 5. This procedure has been used at a number of facilities with success. Perhaps the most sophisticated use of this method has been developed at the AEDC Propulsion Wind Tunnel, Ref. 3. A variable angle wedge with a movable pitot tube near each surface is used in the 16S facility. The purpose of the variable angle feature is to optimize the wedge angle and thereby eliminate uncertainty in effective angle caused by changes in boundary layer growth. In effect, this feature eliminates wedge angle uncertainty in the calculation of Mach number. The complete Mach number probe includes two conventional Pitot

Dimensions In Centimeters

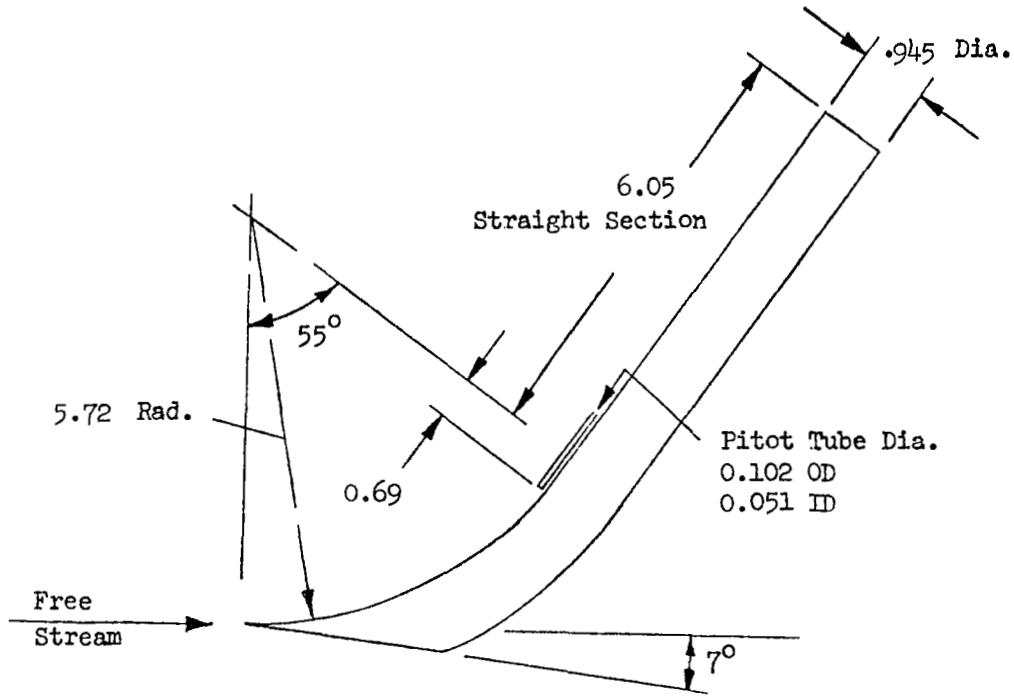

Figure 3.C.1. ISENTROPIC STAGNATION PRESSURE PROBE, Ref. 8

probes located outboard and aligned with the leading edge of the wedge. A plan view of this Mach number probe is shown on the right in Fig. 3.C.2. One of these probes has been used on a sting to calibrate the empty test section of 16S. These same data have been used to calibrate a retractable version of the probe which is mounted in the ceiling of the test section. When fully extended, the wedge centerline is 58.4 cm (23 in.) from the ceiling. This permits routine Mach number measurements without the uncertainty of an isentropic expansion assumption. The interested reader may refer to Reference 3 for additional details.

A second type of Mach number probe has been employed in Tunnel A at the AEDC Von Karman Facility. This probe measures static pressure on the surface of a retractable disk. The supporting arm is a 15 deg included-angle wedge and has a small Pitot probe mounted below the disk. A schematic of this probe is shown on the left in Figure 3.C.2. Although this probe is susceptible to leading edge and angle of attack errors, it may be calibrated by conventional, sting mounted probes and has the important feature of simplicity.*

In the case of intermittent tunnels, e.g., a Ludwieg Tube, a different type of Mach number probe is required because of the short run-time and the possibility of rapid changes in test-section flow. The AGARD Technical Working Group, which is responsible for selection and design of the Large European High-Reynolds-Number Transonic Windtunnel (LEHRT), has recommended the probe shown in Fig. 3.C.3. As reported by Ross and Hartzuiker (Ref. 9), this miniature probe utilizes high-frequency-response pressure transducers for measurement of both Pitot and static pressures and is designed to be used in the small-scale pilot LEHRT facilities. The primary purpose of this probe is to monitor temporal changes in mean Mach number. Dougherty (AEDC) has pointed out to the present authors that measurements of static pressure fluctuations with this probe will have a limited frequency response and thus should not be used to calibrate static pressure fluctuations associated with noise and/or turbulence. However, the fluctuating Pitot pressures can be used for this purpose; see Section III.F. for further discussion of measurements of unsteady flow disturbances.

Pitot Probes for Freestream Calibration

Although a wide variety of Pitot nose geometries have been used, the simple cylindrical tube with square-cut nose is adequate for freestream calibrations. For an internal to external diameter ratio of 0.125, the tests of Gracey (Ref. 10)

*Compared to the other two Mach number probes, this type of probe has an additional disadvantage. Barry's analysis (Ref. 5) shows the uncertainty in calculated Mach number is greater when there is equal uncertainty in measured pressures.

Tunnel A

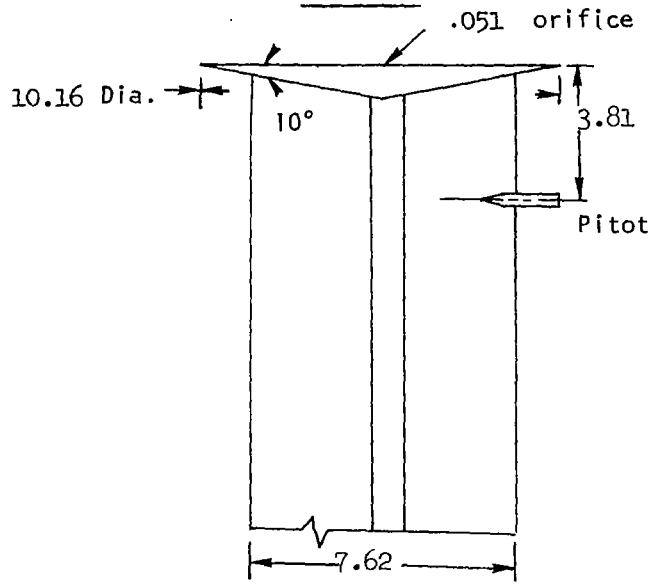

1. Disk not presently calibrated with $\mathbf{C}_L$ probe data.

Tunnel 16 S

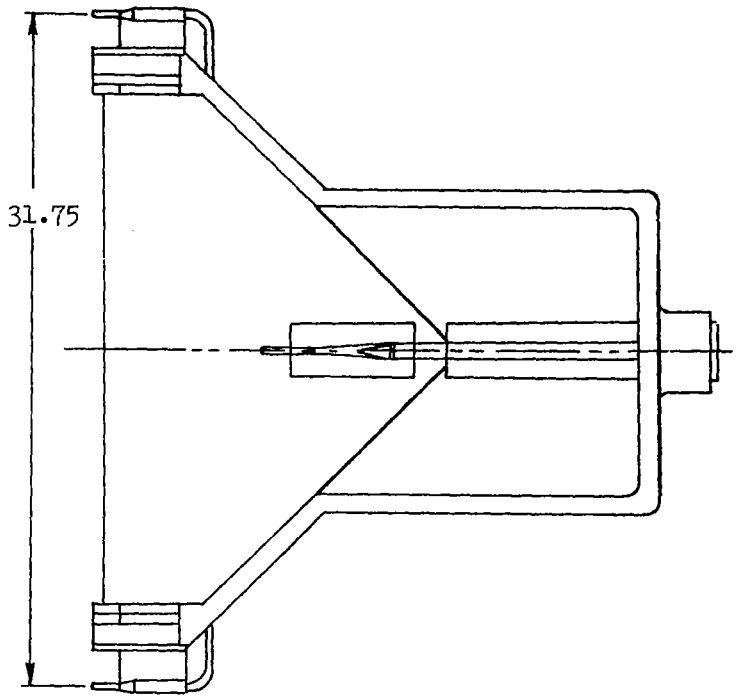

1. Variable angle (10°-26°) pitot wedge probe mounted on ceiling; extends center of wedge 58.4 cm from ceiling.
2. Calibrated with identical wedge located at tunnel $\mathbf{C}_L$.

Dimensions In Centimeters

Figure 3.C.2. AEDC SUPERSONIC MACH NUMBER PROBES

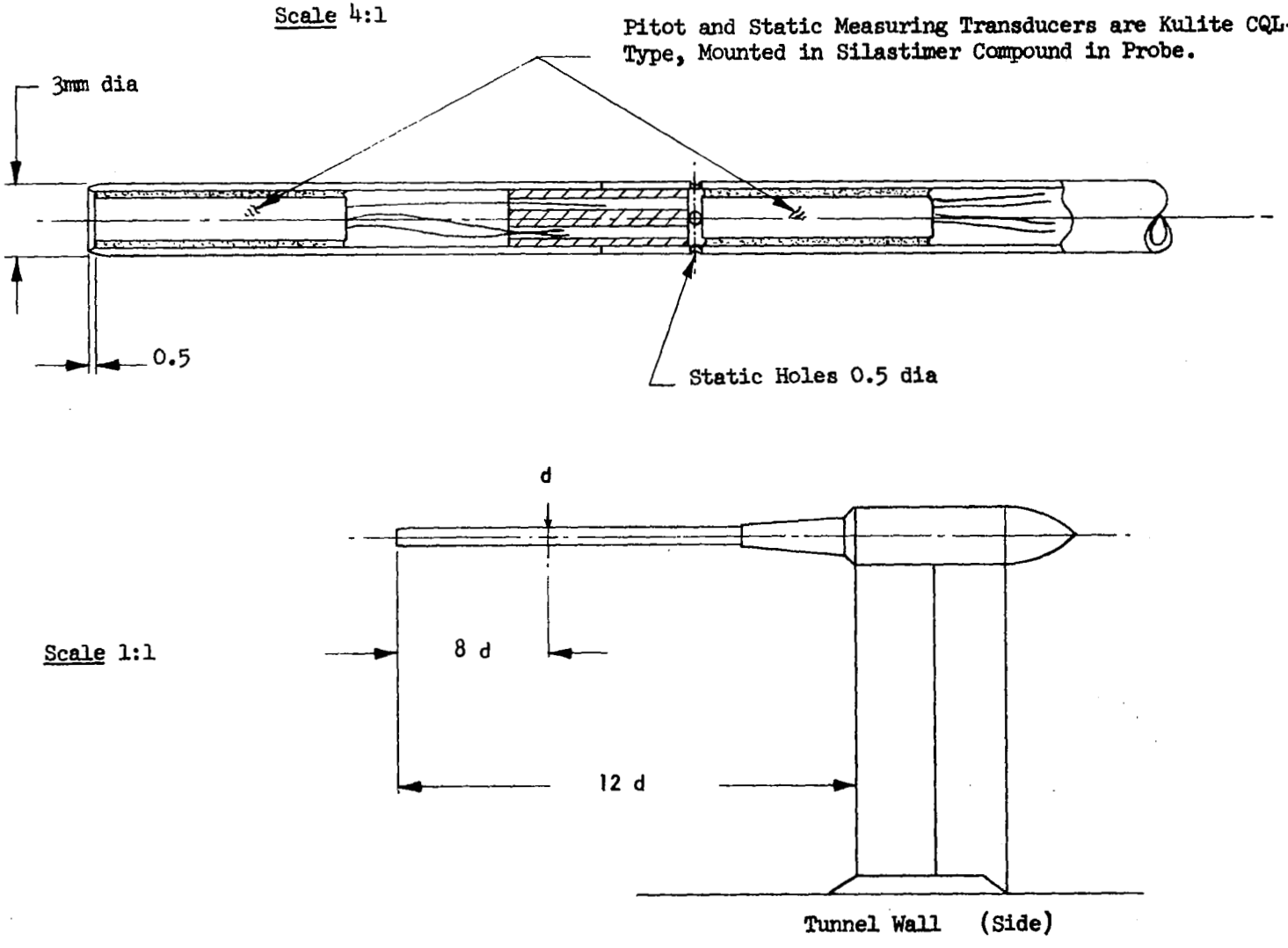

Figure 3.C.3 MACH NUMBER PROBE FOR SMALL PILOT LEHRT FACILITIES, Ref. 9

demonstrated that total pressure measurements with this probe will be in error by 0.01q' at an angle of attack of 11 degrees and M = 0.26 and 1.62. This same accuracy was attained at $\alpha = \pm 23^{\circ}$, M = 0.26 and $\alpha = \pm 29^{\circ}$, M = 1.62 by increasing the diameter ratio to 0.96. The angle of attack range was increased even more by using internal bevelling to increase the diameter ratio to near one. However, since flow angularity in empty test sections seldom exceeds 1 or 2 degrees, a tube with a straight impact opening and a diameter ratio of 0.5, or more, will provide impact pressures with negligible error. (Of course, this assumes the probe is free of burrs.)

Effects of Various Parameters on Pitot Probes

Size:

Early experiments with Pitot probes showed measured pressures to be independent of probe size, e.g., Ref. 11. Thus, sizing is usually guided by the size of facility and Mach number at which the probe is to be used. When total pressure gradients are present, a Pitot probe senses an impact pressure corresponding to a displacement towards the higher pressure, Ref. 12. This effect decreases with probe size and with increasing wall thickness. However, Livesey (Ref. 13) found that a conical nose Pitot, with a sharp edge at the opening, is best for use in a transverse pressure gradient since it exhibits a negligible displacement error. But since cones cannot be used very close to walls, two dimensional boundary layer measurements are usually made with Pitot probes having very small, flattened-oval openings and a square-cut nose, e.g., Refs. 11 and 12.

Analysis of data for the simple, circular Pitot tube indicates the measured pressure is independent of Reynolds number (based on inside radius of the opening) when it is greater than 100, Ref. 12.

Mach number:

In dry air, the Pitot tube has generally been found to be insensitive to Mach number and will reliably provide the freestream stagnation pressure at subsonic speeds and the stagnation pressure behind a normal shock at supersonic speeds.

Turbulence:

The incompressible analysis of Becker and Brown (Ref. 14) indicates that a circular tube Pitot with square-cut nose is relatively insensitive to turbulence. However, these authors suggest that the length of the constant diameter

opening be at least three diameters. The intent is to eliminate surging of the flow, in response to turbulence, and thus assure the existence of stagnation conditions prior to changes in internal geometry. When the results of Becker and Brown are viewed in light of the data obtained by Gracey (Ref. 10), which demonstrates decreasing flow angle sensitivity of Pitot probes with increasing Mach number, one may conclude that circular tube Pitot probes are unaffected by low levels of turbulence. Since the turbulence intensity in most empty tunnels is less than two percent, the recommended Pitot probes (i.e., circular tubes with internal/external diameter ratios > 0.5) can be used with confidence to calibrate transonic and supersonic wind tunnels.

Rakes, Arrays and Supports:

In subsonic flows, impact pressure can be successfully measured with an orifice in a circular cylinder mounted normal to the flow, e.g., Ref. 12. Thus, Pitot probes are generally considered to be insensitive to support arrangements. However, near Mach one the bow shock generated by a support could conceivably interfere with the probe shock. The resulting pressure measured behind the shock interactions would be expected to differ from the normal shock pressure. Thus, at transonic speeds the nose of the Pitot probe should extend far enough forward to avoid this problem. A tube length at least 12 times the support thickness is recommended. At subsonic speeds, Dudziniski and Krause (Ref. 15) have observed that the effect of proximity of a transverse cylindrical supporting strut is negligible if the strut is two or more strut diameters downstream from the Pitot tube tip. For supersonic applications, Pope and Goin (Ref. 16, p. 353) note that the Pitot tube length is usually 15 to 20 tube diameters.

When several Pitot probes are used in a rake or an array, the measured pressures may be affected by interactions between the bow waves on adjacent tubes. Bryer and Pankhurst (Ref. 12) note that experiments at $M = 1.6$ indicate the gap between Pitot probes may be as small as one diameter without causing significant error. As Mach number decreases toward one, the separation distance must be increased. In subsonic flow, the spacing of Pitot probes is generally not considered to be critical, e.g., Ref. 17.

III.C. References

1. Hill, J. A. F.: "On the Calibration of Supersonic Wind Tunnels," Jour. Aero. Sci., Vol. 22, No. 6, June 1955.

2. Hill, J. A. F.; Baron, J. R.; Schindel, L. H.: "Mach Number Measurements in High-Speed Wind Tunnels," MIT Naval Supersonic Laboratory Tech. Rept. 145, Jan. 1956 (Also available as AGARDograph 22, Oct. 1956).

3. Maxwell, H. and Hartley, M. S.: "Aerodynamic Calibration Results for the AEDC-PWT 16-Ft. Supersonic Tunnel at Mach Numbers from 1.50 to 4.75," AEDC-TR-69-102, May 1969.

4. Murphy, J. S.: "Evidences of an Inherent Error in Measurement of Total-Head Pressure at Supersonic Speeds," Aero. Engr. Rev., Nov. 1953.

5. Barry, F. W.: "Determination of Mach Number From Pressure Measurements," Trans. ASME, April 1956.

6. Thompson, J. S. and Holder, D. W.: "Notes on Wind Tunnel Pressure Measurements from the Operator's Point of View," R.A.E. Tech. Note Aero. 2547, Feb. 1958.

7. Goodyer, M. J.: "A New Probe for the Direct Measurement of Stagnation Pressure in Supersonic Flow," R.A.E. Tech. Rept. 73122, March 1974.

8. Couch, L. M.: "Effects of Geometric Variables on the Performance of a Probe for Direct Measurement of Free-Stream Stagnation Pressure in Supersonic Flow," NASA TN D-7887, May 1975.

9. Ross, R. and Hartzuiker, J. P.: "Recommended Flow Quality Measurements in LEHRT Pilot Facilities," AGARD Technical Working Group AC/243 (PG.7/WG.1) Action 61, June 2, 1975.

10. Gracey, W.: "Wind-Tunnel Investigation of a Number of Total-Pressure Tubes at High Angles of Attack," NACA Rept. 1303, Jan. 1956.

11. Folson, R. G.: "Review of the Pitot Tube," Trans ASME, Oct. 1956.

12. Bryer, D. W. and Pankhurst, R. C.: Pressure-Probe Methods for Determining Wind Speed and Flow Direction, National Physical Laboratory, Her Majesty's Stationery Office, London, 1971.

13. Livesey, J. L.: "The Behavior of Transverse Cylindrical and Forward Facing Total Pressure Probes in Transverse Total Pressure Gradients," Jour. Aero. Sci., Vol. 23, p. 949, Oct. 1956.

14. Becker, H. A. and Brown, A. P. G.: "Response of Pitot Probes in Turbulent Streams," Jour. Fluid Mech., Vol. 62, Part 1, 8 Jan. 1974.

15. Dudziniski, T. J. and Krause, L. N.: "Effect of Inlet Geometry on Flow-Angle Characteristics of Miniature Total-Pressure Tubes," NASA TN D-6406, July 1971.

16. Pope, A. and Goin, R. L.: High-Speed Wind Tunnel Testing, Wiley, 1965.

17. Chew, W. L., Jr.: "Calibration of Five Total Pressure and Temperature Survey Rakes at Speeds from M = 0.2 to 1.0," AEDC TN-59-37, May 1959.

III.D. TEST SECTION STATIC PRESSURES

As discussed in Section II.C.1, measurement of static pressure is fundamental to transonic wind tunnel calibration. It is currently standard practice to measure settling chamber pressure and empty-tunnel static to calibrate subsonic and transonic tunnels when $M < 1.6$. Typically, an average of static pressure data, measured along the centerline, is used to calibrate a reference pressure. In order to avoid interference, it is generally considered good practice not to measure this reference pressure with a probe permanently mounted in the test section. Thus, the reference pressure is usually measured either in the plenum chamber or at sidewall orifices located in the forward portion of the test section. Once calibrated, the reference pressure is used to control Mach number during routine operation.

The best location to measure the reference static pressure appears to be a matter of opinion. All of the larger tunnels (> 2.4 m), which responded to the questionnaire, use plenum chamber measurements. The survey indicated smaller tunnels use either upstream orifices or plenum chamber measurements. A total of the responses indicated a majority of approximately 2:1 preferred to use plenum chamber measurements.

Advantages of using plenum chamber data are: (1) it is relatively insensitive to location at which the pressure is measured, and (2) it avoids having to contend with erosion and/or contamination of orifices. However, experience with tunnel wall piezometer rings in a number of tunnels has proven orifice deterioration is not a significant problem. At supersonic Mach numbers, the plenum chamber pressure is generally lower than freestream static pressure, and the difference increases with increasing Mach number, becoming increasingly more significant at Mach numbers exceeding 1.4. In contrast, test-section-wall

pressures are generally higher than freestream static pressure at supersonic Mach numbers. In the Vought High Speed Wind Tunnel (with walls slightly converged), tunnel-wall pressure is closer to freestream static than plenum pressure when $1 < M < 1.6$. Thus, this tunnel is calibrated using tunnel-wall pressures because smaller departures from freestream static offer the possibility of greater accuracy in Mach number calibration. In general, a more accurate tunnel calibration may be expected when the reference pressure is closer to freestream static pressure.

In the case of subsonic Mach numbers, test-section-wall and plenum pressures generally agree very closely. A possible exception to this general conclusion is that models, with large blockage ratios (i.e., > 2%), may reduce plenum chamber pressure below the calibrated, empty-tunnel values at high subsonic Mach number, e.g., Parker (Ref. 57). As is well known, inclined holes, such as used in the AEDC transonic tunnels, are designed to inhibit excessive inflow from the plenum to the test section, but ventilated tunnels with slots or normal holes are more vulnerable to this type of departure from empty-tunnel calibration. In addition, the plenum chamber pressure may lag freestream pressure during rapid changes in model orientation.

III.D.1. Transonic Survey Pipes

Responses to the questionnaire indicate that 31 out of 53 transonic tunnels have used long pipes to survey centerline static pressure. The results of the centerline static pressure survey are usually averaged over one or more lengths of the test section and used to calibrate a reference pressure. In routine tests, a calibrated length is selected which most closely matches the location and length of a particular model. An alternate procedure is to construct a number of calibration curves to relate the reference pressure to several stations along the centerline. By locating the aerodynamic center of a model at

a station which has been calibrated, the local Mach number at that station can be used in data reduction.* This method is used in transonic tests at NASA Ames** and is considered to be important for measurements of Mach number at which a model encounters transonic drag rise. In low supersonic tests ($M < 1.6$), the nose of the model is usually located at one of the calibrated stations for more accurate wave drag measurements. In either case (i.e., calibrations of the reference static pressure with an average along the centerline or with pressures measured at particular locations), buoyancy corrections are usually applied by using centerline pressure measurements obtained in the empty tunnel.

Guidelines for the installation of a long survey pipe are presented in Reference 1. Some rules of thumb are:

1. The nose of the pipe should be a small angle cone or ogive and should be located well upstream in the subsonic portion of the tunnel nozzle, e.g., in the 11-ft. Transonic Tunnel at NASA Ames the nose of the pipe extends into the settling chamber and is supported under tension.

2. In order to minimize pipe sway, the pipe should be loaded with a large tensile force, and if appropriate, an upward moment should be applied at the downstream support.

---

* In cases where a measured-average is used to calibrate a tunnel, a variation on this procedure would be to account for local departures from the average.

** Private communication, Mr. F. W. Steinle, NASA Ames.

3. In the case of very long pipes, three or four cables should be attached to further control pipe sag and vibration.
4. All support cables should be free of obstructions, and all turnbuckles and cable attachment fixtures should be located behind the tunnel walls.
5. Cables near or within the test section should be swept back at an angle of approximately 30 deg to the centerline.

Although a number of tunnel calibrations have been conducted with the nose of the pipe located in the test section near the beginning of uniform ventilation (e.g., Refs. 1 and 2), the preferred arrangement is with the nose well upstream so that it is always in subsonic flow, Ref. 3. This arrangement minimizes disturbances caused by the nose (e.g., no bow shock) and assures that no transonic shock passes over the orifices.

A properly-designed, static-pressure survey pipe requires no transonic calibration curve* and supplies simultaneous data throughout the length of the test section. In transonic tunnels, boundary layer growth on the pipe does not usually induce any longitudinal Mach-number gradients because of the ventilated walls feature.** In contrast, the disadvantages of the long pipe are:

1. sag can cause the pipe to be inclined to the flow which in turn can cause erroneous static pressure data,
2. vibration can induce errors, see Appendix III,

---

* This conclusion is often sustained by demonstration that a plot of pipe measured static pressure versus plenum chamber pressure is smooth through transonic Mach numbers.

** However, as a rule of thumb, the blockage ratio of the pipe should be kept less than 0.5%, Ref. 6.

3. disturbances generated by supports may introduce errors, and

4. its bulk makes it difficult to use for surveys off centerline.*

Orifices are a source of error, which is often overlooked when using a long fixed pipe. An example of significant orifice-induced error has been discussed by Isaacs (Ref. 5). This tunnel calibration probe is shown in Fig. 3.D.1. The orifices have a diameter of 0.076 cm (0.030 in.) and were ground and deburred with particular care to prevent chamfer of the opening. However, static pressure variations as large as 0.3% of the dynamic pressure were observed. The fact that the errors were indeed orifice errors was ascertained by moving the probe along the tunnel centerline. A repeatable pattern in the variation of measured static pressure was observed. Figure 3.D.2 shows a comparison of data obtained at two different tunnel locations with $M = 0.74$.

This example illustrates the need for caution when using a fixed, static pressure survey pipe; particularly when the pressure at a given tunnel station is obtained with only one orifice. It is suggested that tunnel operators, who use such pipes, check the orifice problem by translating the pipe for at least one high subsonic and one supersonic Mach number. If a problem is detected, this source of error may be reduced by manifolding four or more orifices together at a given station. A second alternative is to translate the pipe either forward or rearward and take several measurements at a given station with different orifices. Either of these procedures would improve the accuracy of static pressure calibrations. Also, it is

*A second pipe, mounted on the floor, has been used for subsonic calibration measurements in the 11-Foot Transonic Wind Tunnel at NASA Ames.

Dimensions In Centimeters

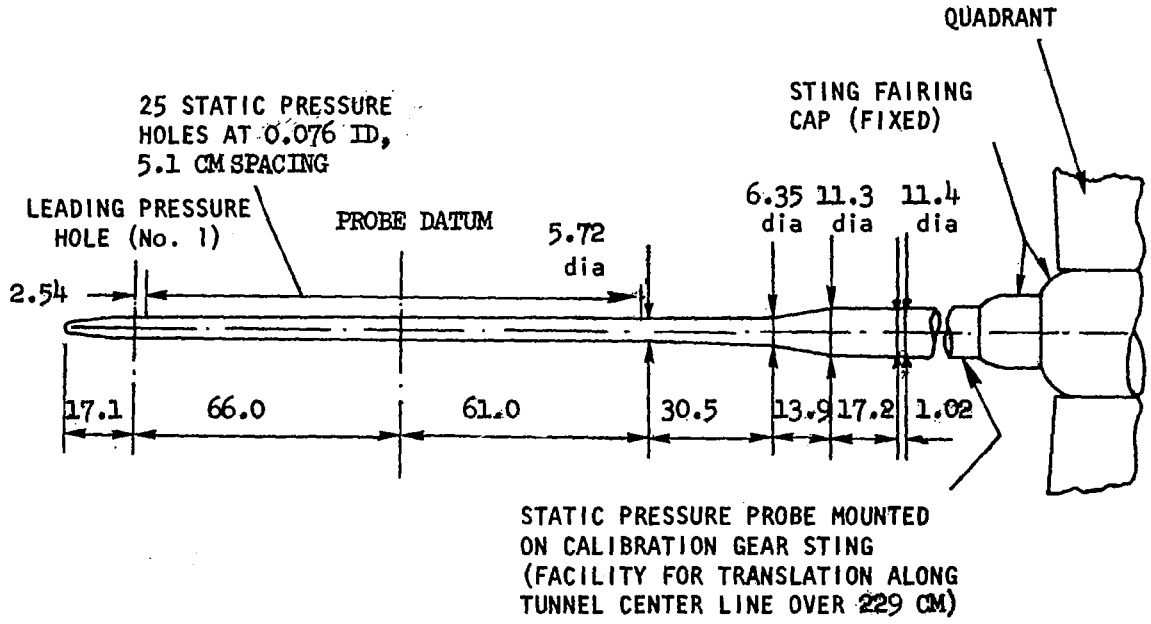

Figure 3.D.1. R.A.E. SUBSONIC STATIC-PRESSURE PROBE

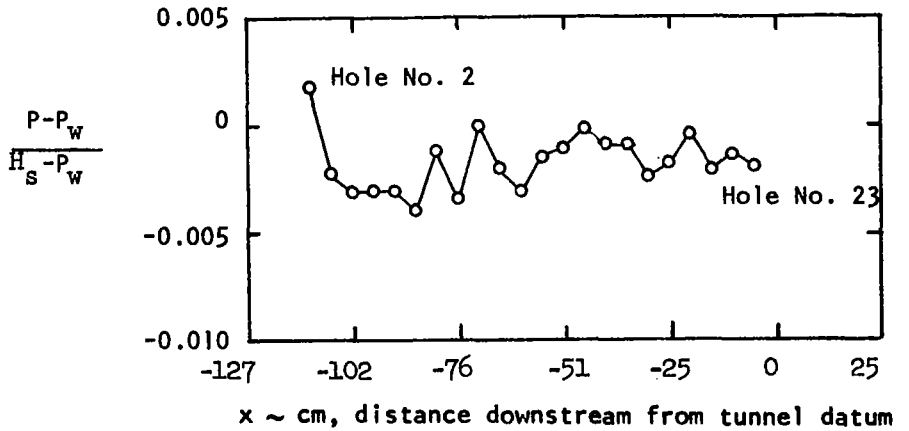

(a) PROBE DATUM 53 CM UPSTREAM OF TUNNEL DATUM

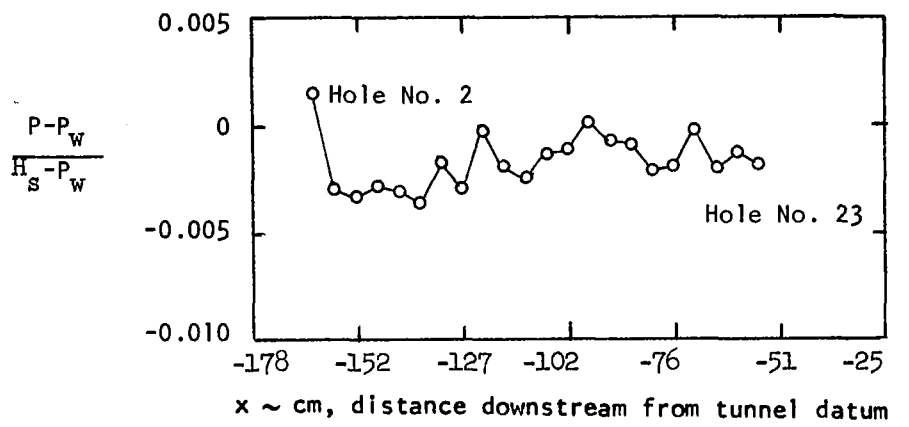

(b) PROBE DATUM 104 CM UPSTREAM OF TUNNEL DATUM

Figure 3.D.2. TYPICAL PRESSURE DISTRIBUTIONS ALONG PROBE AT TWO LOCATIONS ON TUNNEL CENTERLINE, M = 0.74(choked), $R/\ell = 19.7 \times 10^6$ PER METER

generally considered good practice not to place orifices directly in line with each other, since a disturbance at an upstream orifice can propagate downstream and induce errors at a downstream orifice.

As noted by Pope and Goin (Ref. 6), the static pipe is seldom used to calibrate closed-wall supersonic tunnels. The pipe not only alters the Mach number because of the reduced area ratio but also interferes with the expansion pattern which is required for uniform flow.*

*However, a static pipe has been used quite successfully for Mach numbers up to two at AEDC in the Aerodynamic Wind Tunnel (4T), Ref. 7. For example, at M = 1.6 the 2 σ variation in measured centerline Mach numbers was only .007 and at M = 1.99 was 0.008. This application of a static pipe was made possible by the unique features of this tunnel, viz., adjustable porosity (0-10%), wall angle, and plenum pumping.

III.D.2. Transonic Static Pressure Probes

In cases where variations of Mach number transverse to the flow had been calibrated, respondents to the questionnaire indicated that such variations are often larger than longitudinal variations along the centerline. These data were obtained with conventional probes which, as discussed later, are subject to asymmetrical wall interference when moved off centerline and M exceeds 0.85. Although these transverse variations may be partly the result of transonic wall-probe interference, the calibration of such variations is obviously important, particularly for testing winged models. In the past, transonic tunnel operators have traditionally concluded that if (1) the tunnel wall parameters are set to minimize Mach number variations along the centerline and (2) the average of the centerline pressures agrees closely with the plenam chamber pressure (for $M < 1$), then the transverse variations in Mach number are negligible. This conclusion is based on the comparison between two averages, and, in general, does not justify the assumption of negligible transverse gradients. Thus, wind tunnel calibration should include off-centerline measurements as a standard part of the calibration procedure. For this reason, one of the primary advantages of conventional static pressure probes is mobility as contrasted to the long, static pressure, survey pipe.

Questionnaire results also reveal that the most popular transonic static pressure probe is a 10 deg apex-angle cone-cylinder with orifices located ten or more cylinder diameters (calibres) downstream of the shoulder. This criterion for orifice location appears to have originated with the tests conducted by Holder, et al. (Ref. 8). These investigators conducted a systematic, experimental study of the effects of nose geometries and orifice location on static pressure measurement at $M = 1.6$. A summary of these data is presented in Fig. 3.D.3. The conclusion is that the measured static pressure is within 0.5% of the reference pressure when $l_o \geq 10d$. As noted in the figure, the reference pressure,

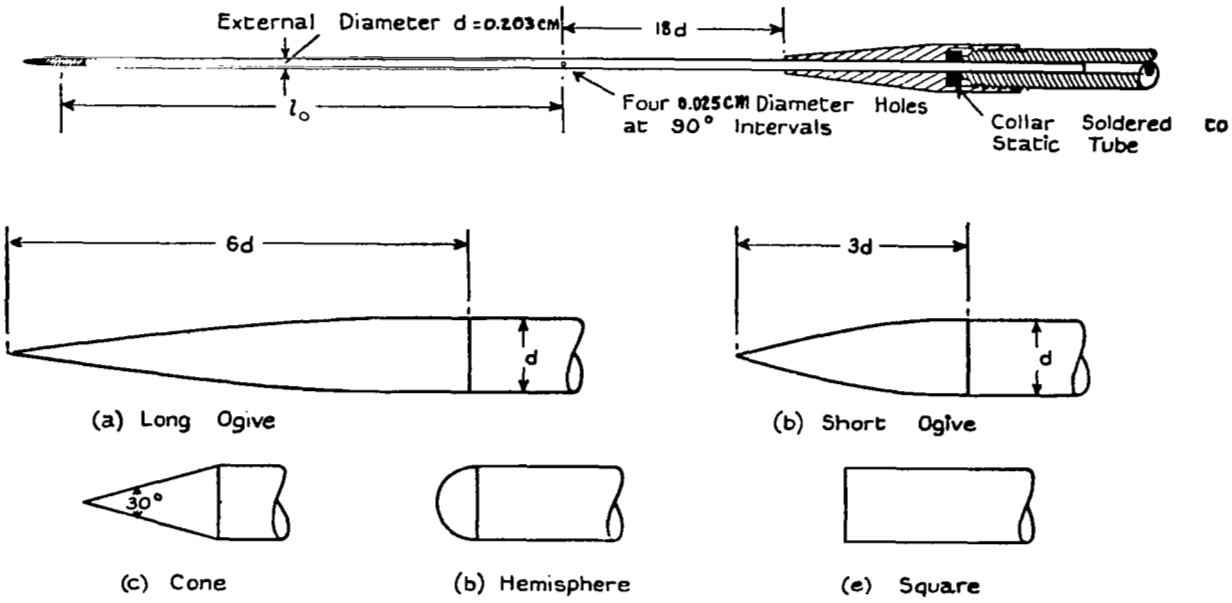

General arrangement of the static tubes and the nose shapes tested.

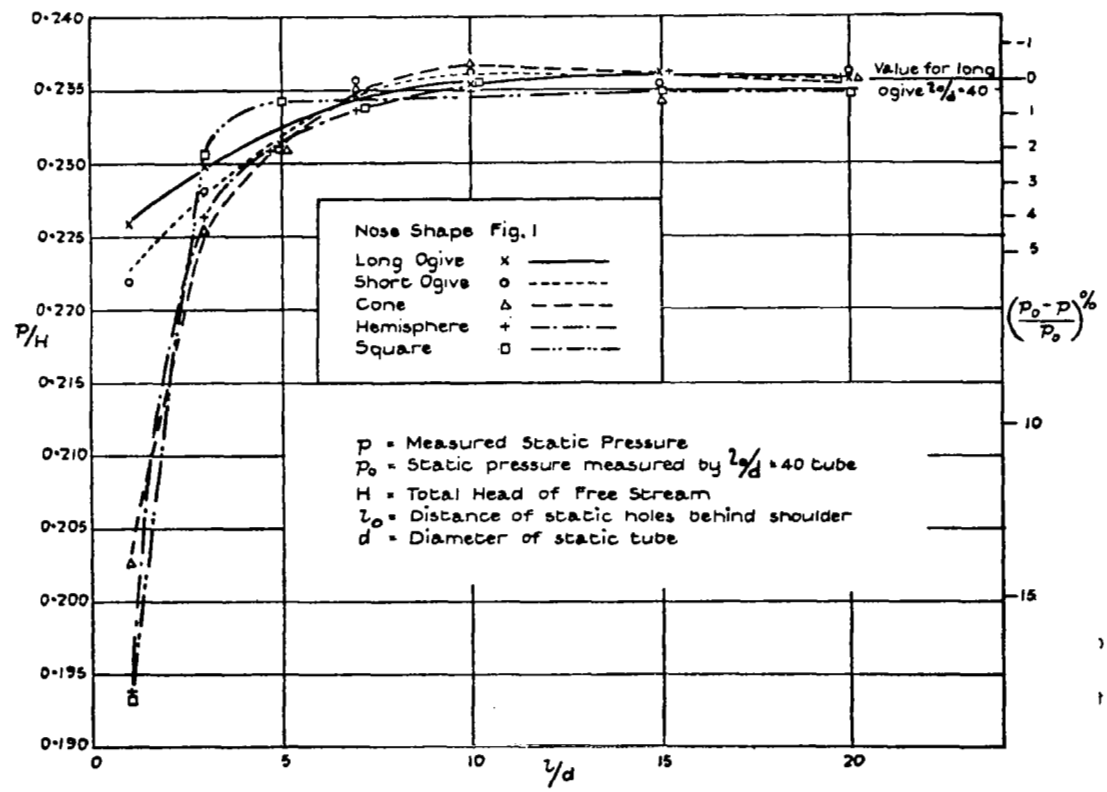

Figure 3.D.3 VARIATION OF STATIC-PRESSURE READING WITH POSITION OF STATIC HOLES AND NOSE SHAPE AT M = 1.6, Ref. 8

which was assumed to be true freestream static, was obtained with the long ogival nose and orifices located 40 calibres downstream.

High subsonic (M = 0.6 to 0.9) data indicate probe pressure generally returns to freestream levels (within 0.5% of q) at l_o/d values of 4 to 6 calibres, Ref. 9. The exact location is dependent on nose geometry. For example, transonic data presented by Ritchie (Ref. 10) for a static pressure probe, with a nose corresponding to the long ogive shown in Fig. 3.D.3, indicate negligible measurement error when orifices are located only two calibres downstream of the nose-cylinder juncture.

However, since the overexpansion at the shoulder extends farther downstream in the supersonic case, Gracey (Ref. 9) concluded orifices located 10 or more diameters downstream would sense freestream pressure with "small-error" at both subsonic and low supersonic speeds. The consensus of transonic tunnel operators seems to agree with Gracey.

As noted by Davis and Graham (Ref. 11), in the past the data obtained by Estabrooks (Ref. 12) for a cone-cylinder has been used, almost universally, as a standard for transonic interference-free data. Although the purpose of these measurements was to investigate wall effects, the results are also pertinent to probe design and performance. Estabrooks obtained data on a 20^o apex angle cone-cylinder in the AEDC-PWT 16T tunnel with a model blockage ratio of 0.008% and M = 0.7 to 1.4. A cursory examination of these data indicates orifices located seven calibres downstream of the cone-cylinder juncture, will allow accurate measurements of freestream static pressure throughout the transonic speed regime. The data were unaffected by varying freestream Reynolds number per meter from 4.5 to 12.7 million ($1.36 \times 10^6 < Re/ft < 3.87 \times 10^6$). The fact that freestream static pressure cannot be measured at any one location, as $M \rightarrow 1.0$, will be established in the following discussion.

When the same cone-cylinder model was tested in the AEDC-PWT 1T tunnel, blockage was 2%, and in this case considerable wall interference was observed. In the Mach number range of 0.95 to 1.05, Estabrooks concluded the dominant wall interference effect was reflections of supersonic expansion waves (originating at the shoulder) back to the model as compression waves. In order to explain this phenomena, a discussion was given concerning too low a resistance to inflow from the plenum to the test section. Unfortunately, Estrabrooks appeared to be unaware of the transonic shock which forms near the shoulder of this type of body and moves rearward with increasing Mach number. Although compression waves (generated by inflow) may have been present, interpretation of this data must account for passage of a transonic shock when $0.90 < M < 1.05$. Thus, the effects of this shock on the measured pressure distributions were misinterpreted as solely wall interference. For example, the existence of a shock immediately aft of the shoulder is clearly indicated (Fig. 3.D.4) for the 20 deg cone-cylinder at $M = 0.95$. Data for this configuration at $M = 0.975$ are less definitive possibly because of a bifurcated shock or boundary layer separation, either of which reduces the pressure gradient produced by the shock.* As the Mach number is increased to one, the shock moves rearward and off the instrumented portion of the cylinder. This type

*Although the Reynolds number based on wetted length is approximately 2.55×10^6 near $x/d = 4$, it is not clear that the boundary layer is turbulent because of the shoulder expansion which thins and stabilizes the boundary layer. However, even if the boundary layer is turbulent, the transonic shock can cause separation if the local Mach number exceeds 1.3 (e.g., Refs. 13 and 14). The measured pressure ratio at the shoulder does indeed indicate a local Mach number near 1.3. It is also relevant to here note that Hsieh (Ref. 15) found the laminar boundary on a hemisphere-cylinder separated near $M = 0.80$.

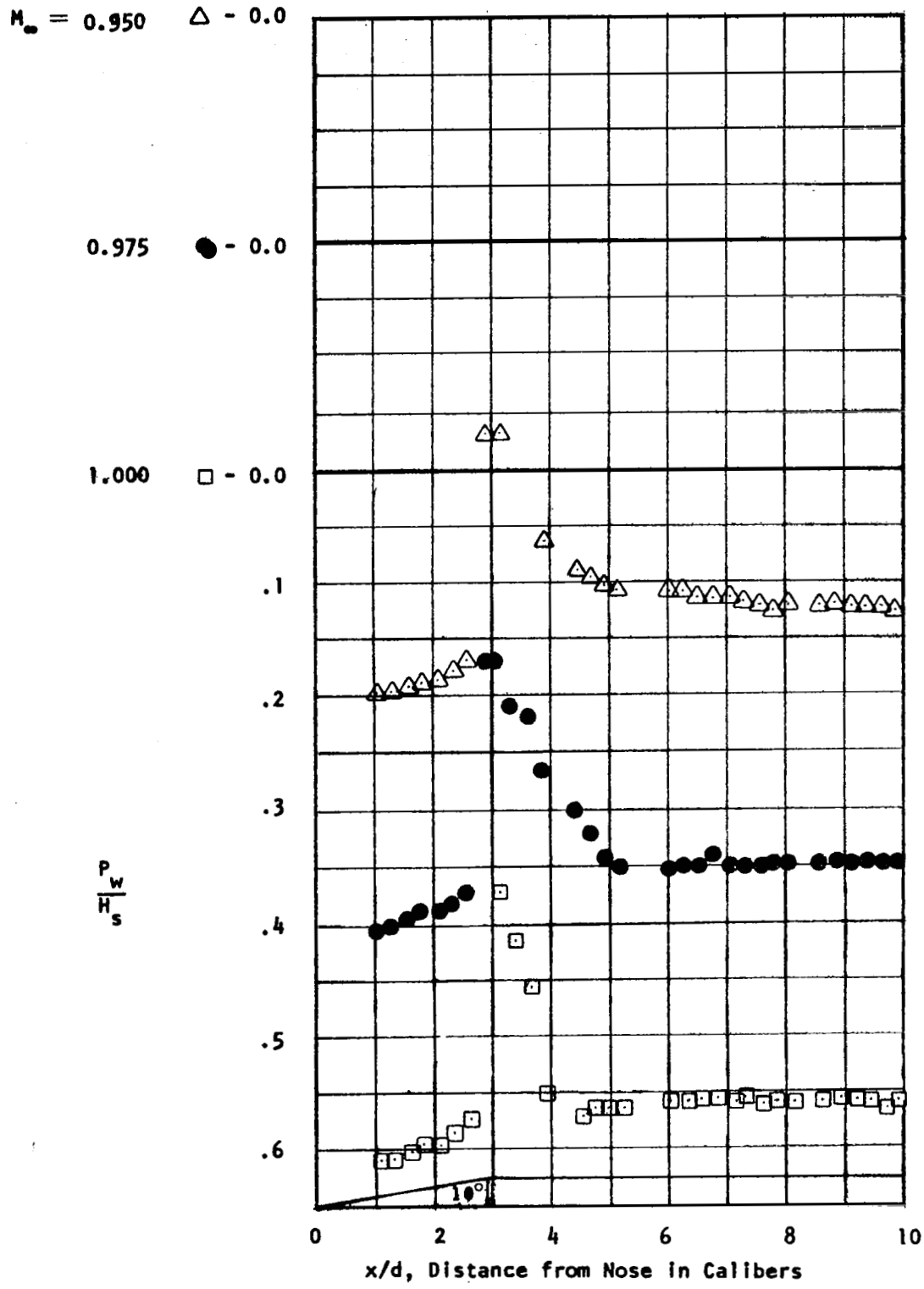

Figure 3.D.4 TRANSONIC PRESSURE DISTRIBUTIONS ON A 20 DEG CONE-CYLINDER WITH 0.008% BLOCKAGE, Ref. 12

of phenomena may be clearly seen in the schlieren photographs presented by Page (Ref. 16) for a 14 deg apex cone-cylinder with a blockage ratio of 0.005%. A rather general conclusion is that the transonic shock will move off a cylindrical probe as $M \rightarrow 1$, and merge with the sting and/or support shocks, provided there is no wall interference.

Movement of a transonic shock on axisymmetric bodies can now be calculated via the computer program of South and Jameson (Ref. 17). This program provides a solution to the complete potential equations for steady transonic flow. Thus, in order for these solutions to be applicable to real bodies there must be no boundary layer separation (e.g., Ref. 15), and in the case of wind tunnel probes, the body must be free of wall interference.

The existence of boundary layer separation on cone-cylinders in transonic flow has been investigated by Robertson and Chevalier (Ref. 18). Cone-cylinder models with a blockage ratio of 0.5% and 1.2% were tested with $M = 0.5$ to 1.17 in the AEDC-PWT 1T tunnel. These investigators found that the boundary layer separated at the cone-cylinder juncture when the cone apex angle was 40 deg or more and $M < 0.85$. In general, as cone apex angle increased, the Mach number for boundary layer attachment increased Although surface pressures were only measured a distance of four calibres downstream of the shoulder, the freestream static pressure was attained in most cases within less than four calibres. This was found to be true for both sizes of models with apex angles ranging from 20 to 60 deg.

The primary exception to this observation occurs when a transonic shock locates near an orifice. If the shock is forward of the orifice,

the measured static pressure will tend to be higher than freestream. The exact amount depends on strength of the shock and distance from orifice. Correspondingly, the pressure will be low if the shock is located near, but downstream of, the orifice. Since the transonic shock moves rearward with increasing Mach number, all stations along a probe's stem are affected. For example, schlieren photographs obtained by Robertson and Chevalier show the transonic shock on a 20 deg cone-cylinder model initially forms near the shoulder at M = 0.8, and increases in strength and moves rearward as Mach number increases. The rate of movement of this shock is affected by model blockage and the extent of the supersonic zone on a given model.

The effect of wind tunnel blockage on movement of the transonic shock may be seen in the M = 1 data of Estabrooks (Ref. 12). By varying the size of cone-cylinder models to obtain wind tunnel blockage ratios from 0.5% to 4%, the transonic shock moved forward from x/d ≈ 5 to less than 4 at M = 1. This effect of blockage may also be seen in the schlieren pictures of Page (Ref. 16) which compare the transonic shock locations on the same model in two different slotted-wall tunnels with blockage ratios of 0.25% and 0.005%. Further evidence of this phenomena may also be found in the data of Capone and Coates (Ref. 19) and Couch and Brooks (Ref. 20). For example, the surface pressure data of Capone and Coates provide an excellent illustration of transonic shock movement on a 20 deg cone-cylinder. In this case, the model was tested in the Langley 16-Foot Transonic Tunnel and had a blockage ratio of 0.198%. A sample of this data is reproduced in Fig. 3.D.5. Here we see the transonic shock move from x/d ≈ 3.25 at M = 0.90 back to x/d ≈ 10.5 at M = 1.025. Measurements at the next higher Mach number, M = 1.04, indicated the shock had moved past the instrumented portion of the cylinder.*

*Reflection of the bow shock back onto the cylinder was not observed until $M \geq 1.10$.

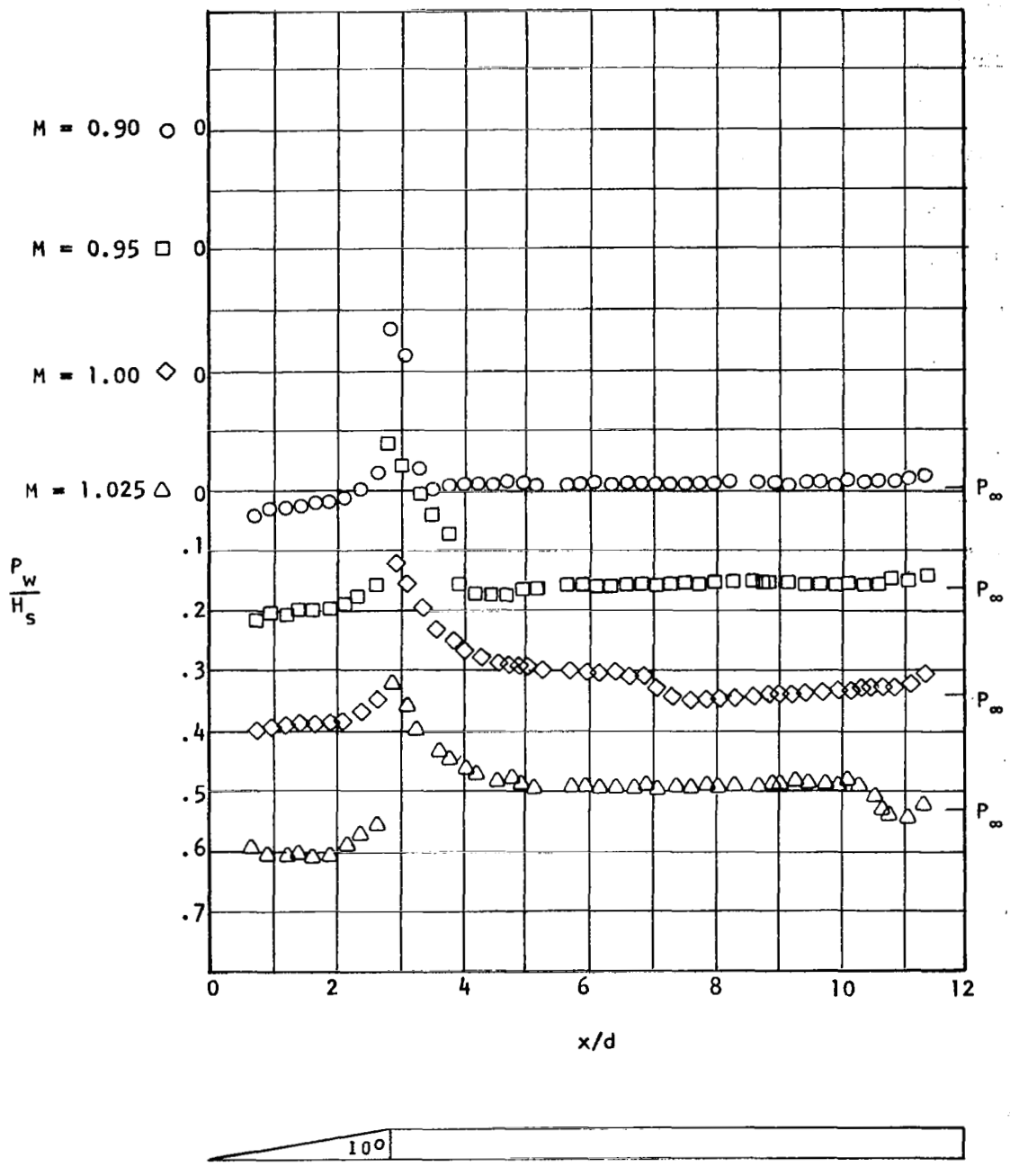

Figure 3.D.5 TRANSONIC PRESSURE DISTRIBUTIONS ON A 20 DEG CONE-CYLINDER, REF. 20.

Similar measurements for a 40 deg cone-cylinder, with the same blockage, showed the shock was at x/d = 10.5 when M = 1.04. Thus, the larger expansion at the cone-cylinder juncture and the correspondingly larger pocket of supersonic flow resulted in a retarded movement of the transonic shock.

Based on these various results, it appears that a 20 deg apex cone-cylinder must have a cross-sectional area less than 0.01% of the tunnel area in order to avoid retarding the rearward movement of a transonic shock with increasing Mach number. This conclusion is based on measurements made only at tunnel centerlines. When the probe is moved off centerline, closer to a wall, even smaller sizes would be necessary to avoid wall interference.* Also, some asymmetry of the shock may be expected. Thus, a non-perturbing flow measurement technique, such as a laser Doppler velocimeter, appears to be very desirable for tunnel calibrations in the range $0.95 < M < 1.05$.

Recently, Newman and Klunker (Ref. 21) and South and Keller (Ref. 22) have performed calculations for transonic flows about airfoils and axisymmetric bodies which include wind tunnel walls in the boundary conditions. These calculations show the shock moves forward when the open-jet boundary condition is applied, i.e., $P_w = P_\infty$. Similarly, the shock moves rearward, compared to the free-air solution, when the solid wall boundary condition is applied. In light of the foregoing discussion, this implies that either slotted or perforated walls act more like open-jets as the size of transonic models is increased. This phenomenon is apparently a result of larger pockets of supersonic flow which impress lower pressures at the walls. This in turn draws in more air from the plenum chamber and apparently shifts the model flow pattern toward the open-jet boundary condition.

---

* This may partially explain the transverse Mach number gradients reported by some of the questionnaire respondents.

As regards static pressure probe design, small angle cones can be used to minimize strength of the transonic shock. In addition, the smaller expansion angle will generate less wall interference for a given probe diameter and the boundary layer will remain attached at the cone-cylinder juncture. A separated boundary layer is undesirable because it introduces disturbances which are convected downstream and can cause additional errors in static pressure measurements (see Eq. 3.D.1, p. 98). Thus, in the past the 10 deg apex angle cone-cylinder probe has served as a convenient compromise between optimum transonic performance and ease of construction.*

The problem of orifice-transonic shock interference, which is characteristic of cone-cylinder probes, may be avoided by locating orifices on very small-angle cones. This was demonstrated by Sutton (Ref. 24) who compared the transonic surface pressures on a 3 deg included-angle cone with a conventional 10 deg cone-cylinder having 0.021% tunnel blockage. These probes are shown in Fig. 3.D.6. The corresponding surface pressures are shown in Fig. 3.D.7. for $0.9 \leq M \leq 1.02$. The oscillation in calculated Mach number, based on the cylinder surface pressure, is caused by passage of the transonic shock. However, it is relevant to note that transonic shock effects can be confined to a small Mach number range (e.g., $\Delta M = 0.02$) when using a carefully designed 10 deg cone-cylinder probe at the tunnel centerline. In contrast, the 3 deg cone provides a monotonically increasing pressure and decreasing Mach number throughout the transonic range.

Unfortunately, the 3 deg cone is reported by Gracey (Ref. 9) to be sensitive to flow misalignment. For angles of attack between ± 1 deg, pressure

---

* The AGARD needle probe described in Reference 23 has a cone apex angle of approximately 12 deg and four 0.3 mm orifices located 11.3 calibres downstream of the shoulder.

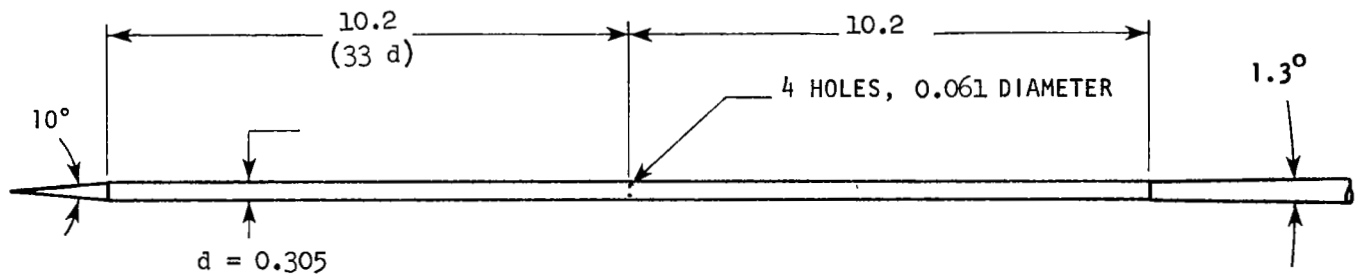

(a) CONE-CYLINDER STATIC HEAD

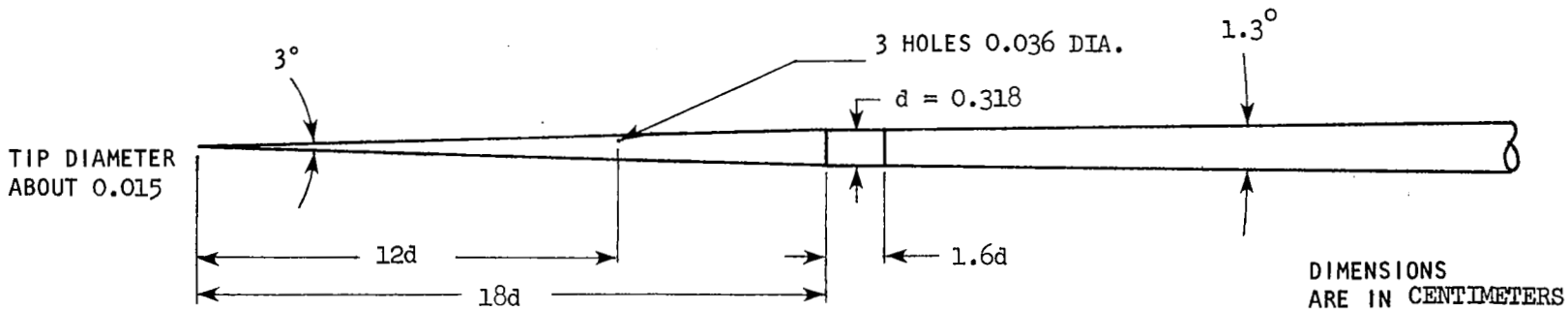

(b) 3° CONE STATIC HEAD

Figure 3.D.6. DIMENSIONS OF THE R.A.E. STATIC PRESSURE PROBES

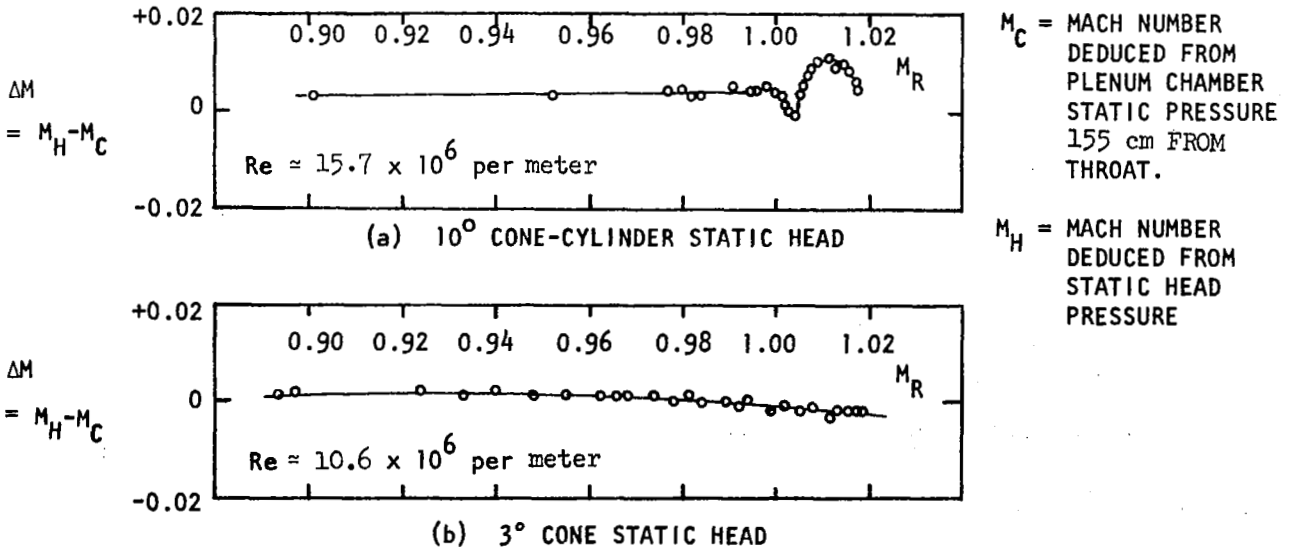

Figure 3.D.7. TRANSONIC CHARACTERISTICS OF THE TWO R.A.E. PROBES

measurements on a 3 deg cone in the Langley 8-ft. Transonic Tunnel indicate variations of approximately 0.02 q_i near M = 1. These results were the same for a 0.033 cm (0.013 in.) orifice located either 12.7 or 17.8 cm (5 or 7 in.) from the tip. Thus, a small-angle cone can be used to calibrate wind tunnels near M = 1, but its sensitivity to flow angularity can make it difficult to resolve Mach number variations as small as 0.001.*

Effects of Various Parameters on Static Pressure Probes

Size:

As found by Couch and Brooks (Ref. 20), cone-cylinder bodies with a tunnel blockage ratio of only 0.03% can have cylinder surface pressures which depart significantly from freestream static near M = 1. Therefore, for accurate tunnel calibrations along the centerline and near M = 1, static pressure probes with blockage ratios larger than 0.01% are not recommended. The wall-interference-free performance of such probes can be caluclated using the South and Jameson computer program (Ref. 17). If for some reason a larger probe is required, centerline blockage effects can be estimated by theoretical analysis, e.g., Refs. 21, 22 and 26. Wall reflected disturbances can also be detected by having orifices at more than one station and checking monotonicity of the data with increasing distance from the nose. Pope and Goin (Ref. 6) suggest moving the model off centerline and/or using a schlieren system.

Once the probe diameter is selected, at least four orifices with a diameter of 0.051 cm (.02 in.) should be located 10 or more calibres downstream of the nose-cylinder juncture. Finally, errors induced by orifice size are discussed in Section III.D.4.

*Additional transonic measurements of flow angularity with a 3 deg conical probe are reported by Wright, et al. (Ref. 25).

Reynolds Number:

At Reynolds numbers characteristic of transonic tunnels (i.e., Re/m > 5 million), static pressure probes are usually unaffected by this variable, provided the probe boundary layer is attached.

Turbulence:

In contrast to the Pitot probe, static pressure probe data can be affected by turbulence. The desired quantity is the static pressure associated with the mean flow. Bryer and Pankhurst (Ref. 27) note that when the turbulence scale is large, compared to the probe dimensions, the measured static pressure will tend to be low and is proportional to the dynamic pressure of the turbulence normal to an orifice. If the turbulence scale is small, the measured static pressure will be high. The following equation has been derived by Siddon (Ref. 28) to relate the error in measured,mean static pressure to the dynamic pressure generated by a turbulent flow.

$$P_m - P_t = A\,\rho(U^2 + \overline{(u')^2}) + B\,\rho(V_n^2 + \overline{(v'_n)^2}) \qquad (3.D.1)$$

If the orifices are located so there are no nose and/or support stem-induced errors, then A = 0. B is a measure of the crossflow-induced error in measured static pressure. When a probe is inclined at an angle α in a steady flow, Eq. (3.D.1) may be written as

$$P_m - P_t = 2q(A\cos^2\alpha + B\sin^2\alpha) \qquad (3.D.2)$$

This type of measurement was performed in subsonic flow by Siddon with a standard, classical probe. The probe had: (1) an ellipsoidal nose, (2) a diameter of 0.305 cm (0.12 in.), and (3) six orifices located 8 1/2 diameters downstream from the nose. For this probe, B was found to be -0.55.

A special probe, designed to measure unsteady crossflow and fluctuating static pressure, was also tested by Siddon. This probe, which had a circumferential slit for sensing static pressure, was found to have a B value of -0.23. According to Siddon, the difference in B values is primarily caused by the difference in orifice arrangement. Additional measurements in a rotating-inclined nozzle, a turbulent channel flow, and a round turbulent jet indicated B varied over the range -0.46 to -0.35. Thus, the magnitude of crossflow-induced errors varies with probe design and turbulence scale and intensity. Bryer and Pankhurst (Ref. 27, p. 43) suggest that probes be calibrated in flows with turbulence closely matching those in which the probe will be used. This is obviously an area which needs further research.

Yaw:

When several orifices (4 or more) are located around the probe circumference, flow angularity causes the measured static pressure to be low. This can be readily seen from the pressure distribution about a circular cylinder normal to a flow (e.g., see Appendix III). Bryer and Pankhurst (Ref. 27) note that the yaw-induced static pressure error of this type of probe is typically 0.01 P_∞ when yawed 3 deg. The error, in a particular case, is dependent on nose geometry and orifice location. Ritchie (Ref. 10) reported yaw-induced errors generally increase with Mach number. Thus, for a given allowed error in measured static pressure, the permissible variation in flow misalignment decreases. Gracey (Ref. 9), Ritchie (Ref. 10), and Rittenhouse (Ref. 29) have reported on static pressure probes designed to minimize yaw sensitivity. These probes utilize only two orifices located 30 to 40 degrees from the windward meridian. Although these probes have small errors at transonic speeds and yaw angles up to ± 8 deg, they require knowledge of the stream direction. Since this is not usually known during wind tunnel calibrations, this type of probe cannot be recommended. Hence, the conventional

probe with four or more orifices is preferred. Particularly since the flow angularity in the central core of many contemporary transonic and supersonic tunnels is less than one degree, the conventional probe will usually have negligible error due to yaw.* For example, Ritchie (Ref. 10) found a two degree angle of attack caused less than 0.2% error in measured static pressure through-out the transonic Mach number range. (These results were obtained with a probe having an ogival nose (f_r = 12) and orifices located 12 1/2 calibres from the nose.) However, this is another reason for minimizing flow angularity in the empty tunnel, i.e., not only will model testing results be more representative of free-flight phenomena, but the tunnel calibration will be more accurate.

Rakes and Support Interference:

The effects of a support flare on base pressures have been investigated by Chevalier (Ref. 30) over a Mach number range of 0.70 to 1.60. Based on the experimental results at M = 1, a flare located approximately 15 flare diameters downstream of the orifices will not interfere with static pressure probe readings. An 11 deg flare (semiangle) located at this distance from the orifices will have negligible effect on the flow at the orifices throughout the transonic speed regime. The required distance for no interference decreases with smaller flare angles and increasing Mach number.

Interference caused by a cylindrical strut normal to the probe axis has been investigated by Krause and Gettelman (Ref. 31) for M = 0.3 to 0.9. These authors found that a distance of 14 strut diameters between static probe orifices and the strut was required for negligible interference at these speeds.

*It is conceivable that a static pressure probe could be calibrated for yaw errors. Static pressure readings could then be corrected for measured flow angles. However, most tunnels do not have sufficient flow angularity to warrant this procedure, and few operators would consider it practical.

Perhaps the most stringent requirements for distance between orifices and a strut have been reported by Nichols (Ref. 32). For the case of a static pressure probe mounted on a double wedge strut support, the transonic measurements of Nichols indicate orifices should be located 32 strut diameters ahead of the strut. These data are shown in Fig. 3.D.8.

General criteria for probe survey rakes have been suggested by Gray (Ref. 33) and are presented in Fig. 3.D.9. The separation criterion for adjacent static and pitot probes in subsonic flow is based on the data of Krause and Gettelman (Ref. 31). In supersonic flows, Gray recommends spacing adjacent probes so that the neighboring bow shock intersects a static pressure probe 15 probe diameters downstream of the orifices. The objective is to prevent disturbances caused by shock-wave/laminar-boundary-layer interaction from affecting the pressure measured at the orifices. Since the criterion becomes impractical when $M < 2$, Gray recommends the flow deflection across the Pitot shock be kept less than 3 deg at its intersection with the static probe, and furthermore, the probes should be spaced so the intersection is 5 or more static probe diameters downstream of the orifices.

For Mach numbers between 0.9 and 1.2, rakes must be used with caution because of increased blockage and near-normal shock waves. Also, rakes are notorious for inducing crossflow in the plane of the rake at high subsonic Mach numbers, see Section III.E. In this Mach number range the following alternative is recommended: employ a single, static pressure probe (or combination Pitot-static probe* for validating the isentropic expansion assumption) with a slender ogival ($L_n \approx 6d$) or very small angle conical (≈ 5 deg) nose and a sting type support which satisfies the criteria suggested by Gray.

*Here it is relevant to note Bryer and Pankhurst (Ref. 27, p. 41) are of the opinion that combination probes are in general less accurate than single-purpose instruments.

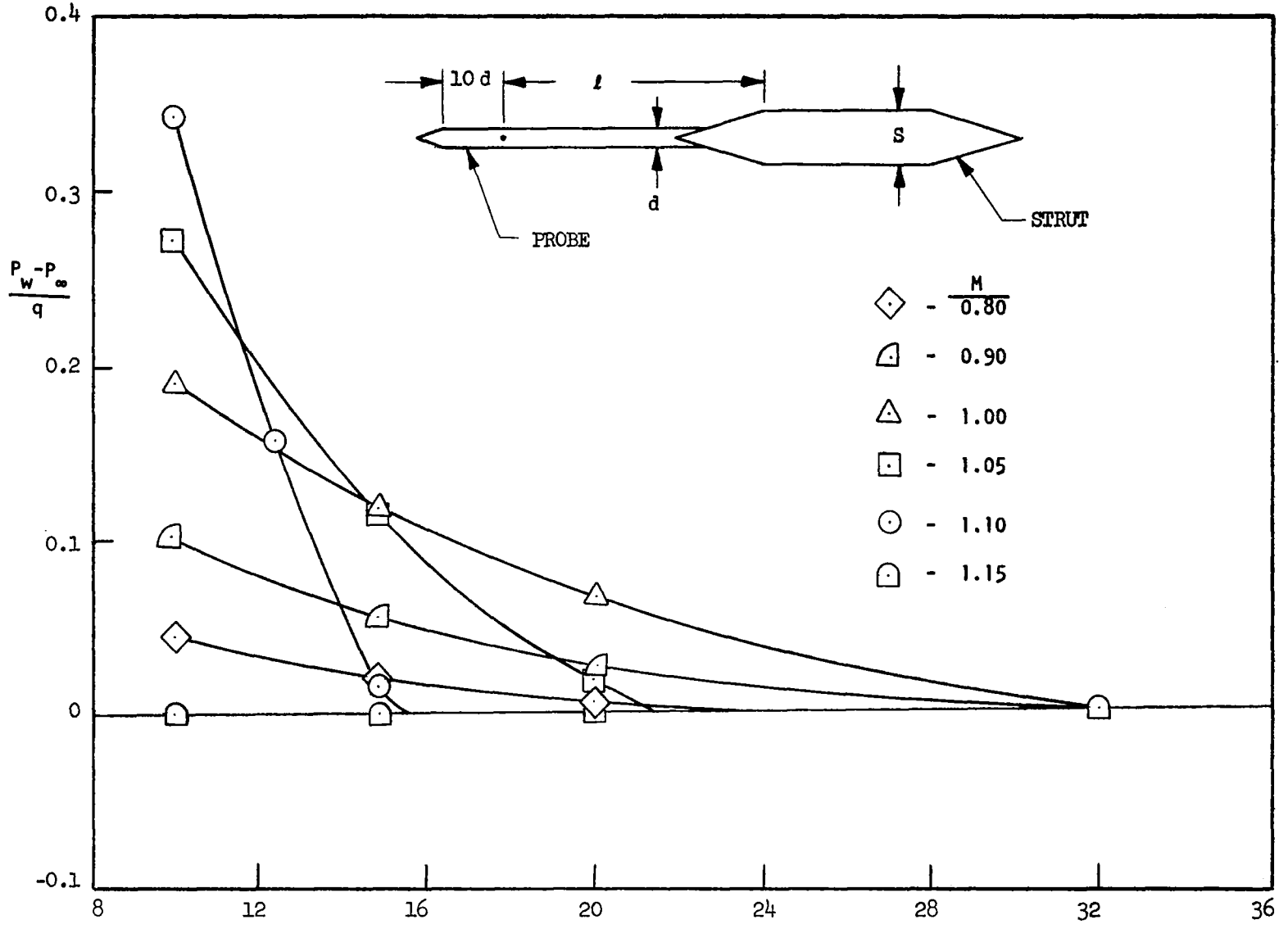

Figure 3.D.8 EFFECT OF ORIFICE LOCATION UTILIZING A DOUBLE WEDGE SUPPORT STRUT, REF. 32.

$$l_o \geq \begin{cases} 10\ d & \text{for } M < 1.6 \\ 16\ d & \text{for } M > 1.6 \end{cases}$$

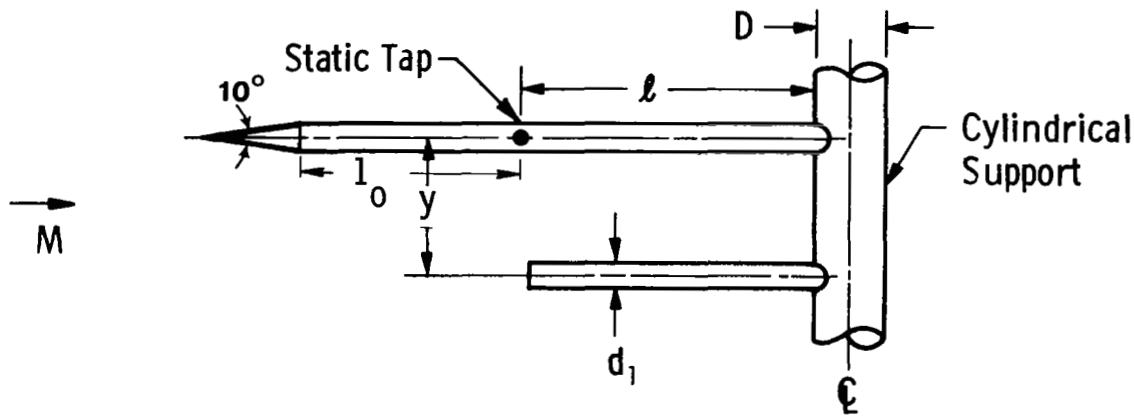

For negligible support interference:

$\ell/D \geq 14$, all values of M

For negligible adjacent probe interference:

(1) $M \leq 0.9$: $y/d_1 \geq 6$

(2) $M \geq 1.2$:

Determined by the intersection of bow wave with static probe

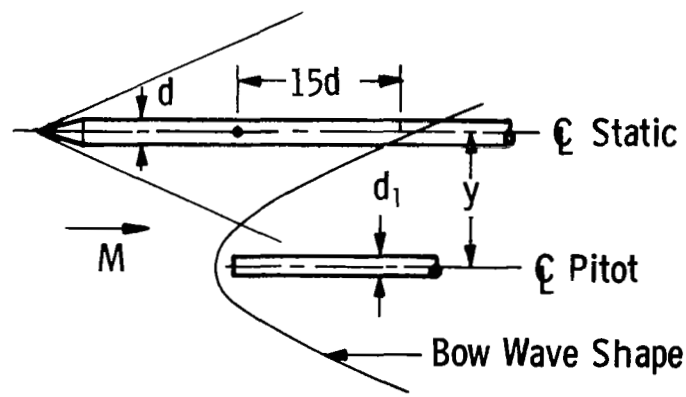

Figure 3.D.9 GENERAL CRITERIA FOR PROBE SURVEY RAKES, Ref. 33

III.D.3. Supersonic Static Pressure Probes

Although Barry (Ref. 34) has shown that supersonic Mach number calculations based on Pitot and freestream static pressure are not as accurate as the Mach probes described in Section III.C, this approach is often used because of its familiar use in subsonic flows and its ease of construction. In addition, it does provide a method for calculating M which does not depend on the assumption of an isentropic expansion from stilling chamber to test section.

Walter and Redman (Ref. 35) measured pressure distributions on a 7 deg included angle cone-cylinder at Mach numbers 1.55 and 2.87.* These data indicate the surface pressure on the cylinder returns to freestream static beyond 10 calibres from the shoulder. In general, as Mach number increases the overexpansion increases and longer distances from the shoulder are required. Increasing cone angle has a similar effect.

Pressure distribution data on cone-cylinder-flare configurations at speeds up to M = 4.5 have been reported by Washington and Humphrey (Ref. 36). Data obtained on a blunt nosed, 10.3 deg cone-cylinder at M = 4.5 and zero yaw indicate the surface pressure returns to within two percent of freestream static at nine calibres downstream of the shoulder.

In the case of yaw, the data of Reference 36 show the circumferentially averaged pressure is below freestream static. For a given yaw angle, the average pressure decreases further as Mach number increases. In general, increasing the number of orifices about the circumference will decrease yaw sensitivity. However, Gray (Ref. 37) and others have noted that surface

---

* This data is also presented in Reference 6.

pressure on long cylinders, measured approximately ± 40 deg circumferentially from the windward location, provides a close approximation to freestream static for M less than 4.0. Thus, this type of probe can be used to eliminate yaw-induced errors in static pressure.

As discussed previously, since most tunnels have small flow angularity in the empty test section, it is unlikely that yaw induced errors will be significant. But this must be determined by the user. If static pressure is being used to calibrate Mach number and an accuracy of 0.1% is desired, then small yaw-induced errors may be important. In which case, a static probe with two orifices located circumferentially 70 - 80 deg apart can provide a more accurate measurement. This can be accomplished by rotating the probe to locate the windward generator (highest pressure) and then rotating the probe until the two orifices agree.*

In order to avoid support-interference, Gray (Ref. 37) recommends the cylinder diameter be constant for at least 8 diameters downstream of the orifices. Any subsequent enlargement in diameter should be restricted to no more than a 10 deg flare (semiangle). Additional criteria for rake arrangements are given in Fig. 3.D.9.

In the past, Pitot pressures and surface pressures on conical probes have frequently been used in supersonic flows to calculate Mach number, e.g., Refs. 38 and 39. Also, an extremely accurate conical static pressure probe is briefly discussed by Pope and Goin (Ref. 6). This probe design has a short (1.78 cm) 8 deg conical tip followed by a long (16.26 cm) 1 deg included-angle cone. Orifices encircle the 1 deg cone at three locations.

---

*This assumes no orifice-induced errors.

The error in measured static pressure is reported to be of the order of 0.1% of true freestream pressure when M = 1.8 to 3.5. Thus, these data represent some of the most accurate static-pressure measurements in supersonic flow.

However, Gray (Ref. 37) has recently reviewed the merits and limitations of supersonic static-pressure probes. Cone-cylinder, sharp cone, and planar probes were considered. Based on the effects of Mach number, angle of attack, and Reynolds number, Gray concluded that the cone-cylinder probe is, in general, superior for use at Mach numbers below 4.

In this Mach number range, the Reynolds numbers of most supersonic tunnels are large enough for viscous corrections to be negligible. This effect can be estimated by calculating the equivalent inviscid pressure from an expression suggested by Gray (Ref. 37) for cone-cylinders probes in flows with Mach number less than 5.

$$\frac{(P_w)_{meas}}{(P_w)_{inviscid}} = 1 + 0.25\,\bar{x} \quad , \tag{3.D.3}$$

where $\bar{x} \equiv M^3/(Re_{l_o}/C)^{1/2}$

$C \equiv (\mu_w/\mu_e)\,(T_e/T_w)$, Chapman-Rubesin viscosity parameter.

For a given configuration, the viscous interaction coefficient decreases with increasing Mach number. For example, the hypersonic experiments of Peterson and George* (Ref. 40) indicate a coefficient of 0.08 is appropriate for a 20 deg cone-cylinder probe at M = 7.2 and 14.0.

*These investigators, among others, have noted that static-pressure probes should not be used in flows with large axial or transverse pressure gradients.

In order to simultaneously minimize the effects of viscous interaction and nose overexpansion at supersonic speeds, it is recommended that orifices be located at least 16 calibres downstream of the shoulder. In cases where correction is judged to be necessary, the interested reader may refer to Gray's discussion (Ref. 37) of a procedure for correcting the measured pressure for viscous interaction and obtaining a better estimate of the inviscid, static pressure.

Since cone-cylinder probes are relatively long, they not only have small rigidity but also cannot be used in pressure gradients. In addition, they are sensitive to yaw. For this reason, shorter supersonic static pressure probes have been investigated, e.g., Refs. 41, 42, and 43. This work has focused on the idea of designing a probe to have at least one station where the circumferentially averaged surface pressure remains a constant fraction of freestream static regardless of Mach number or angle of incidence.

The probes designed by Donaldson and Richardson (Ref. 41) and Pinckney (Ref. 42) are conventional bodies of revolution, whereas the probes of Smith and Bauer (Ref. 43) have noncircular cross-sections. Measurements at M = 0.2 indicate the noncircular probes of Smith and Bauer are completely insensitive to flow angles of ± 6 deg. Beyond this angle of attack range, boundary layer separation becomes a factor, and errors increase rapidly. Since the yaw sensitivity of conventional, circular probes increase with Mach number, these probes may or may not offer an advantage for supersonic applications. Pinckney reports freestream static pressure can be determined with his calibrated probe to within 2 percent for incidence angles of ± 7 deg and M = 2.5 and 4.0. Better results have been reported by Donaldson and Richardson. Using a 50 deg included angle cone-cylinder probe with 24 orifices located 0.88 diameters

downstream of the shoulder, these investigators found the probe measured 0.793 P_∞, and the freestream static pressure could be determined to within 1.2 percent over the Mach number range 1.1 to 2.5. These results were obtained for zero yaw. By adjusting their calibration factor to 0.763, freestream static could be calculated to within 3 percent for incidence angles up to 18 deg in any plane. This represents the smallest yaw sensitivity of any supersonic static pressure probe known to the authors.*

As is well known, theoretical solutions for surface pressure distributions on probes can assist the placement of orifices to measure freestream static pressure. Based on comparisons of measured and predicted surface pressures on a hemisphere-cylinder probe, Hsieh (Ref. 44) concluded the South and Jameson program (Ref. 17) can be used successfully up to M = 1.3. Beyond this Mach number, a method of characteristics algorithm is recommended for axisymmetric probes. A rather large number of such programs are currently available. For examples, the interested reader may refer to the paper by Hsieh (Ref. 44). For non-axisymmetric probes, a number of finite difference solutions for three-dimensional, supersonic, inviscid flows are available, e.g., Marconi, et al. (Ref. 45).

Finally, the use of multiple probes in rake arrangements for surveying supersonic tunnels is well known. Rakes can be successfully employed to calibrate supersonic tunnels by applying the design criteria of Gray, Fig. 3.D.9, and avoiding reflections of bow shock waves off the tunnel walls.

---

* Donaldson and Richardson also found a conventional, single bore, internal plenum provided less yaw sensitivity than an annular plenum.

III.D.4. Orifice-Induced Static Pressure Errors

Errors in static pressure measurements, caused by variations in orifice geometry, have been investigated in a number of studies, Refs. 46-52. The relevant geometric variables are: (1) hole diameter, (2) ratio of hole depth to diameter, (3) the relative size of the cavity or tube connecting to the hole, (4) inclination of hole axis relative to the surface normal, (5) the condition of the hole entry, i.e., whether the edges are square, rounded, chamfered, or have burrs.

Ideally, the measuring hole should be infinitesimally small so as to not disturb the adjacent flow. Shaw (Ref. 47) noted that the basic error caused by finite-sized orifices consisted of three contributions. Firstly, dipping of the streamlines into the orifice causes a divergence of streamlines which results in a higher pressure in subsonic flow. Secondly, an eddy (or system of eddies) is generated within the hole. (An approximate analysis by Nestler (Ref. 51) has shown how the turning of such an eddy can generate increased pressures.) And finally, a Pitot effect occurs at the downstream edge of the hole. These three phenomena cause the measured pressure to be too high. Although the severity of these phenomena decrease with hole size, Rainbird (Ref. 49) observed that holes with diameters less than 0.038 cm (.015 in.) are difficult to produce with sharp edges and negligible burrs. Also in short duration tunnels, the time required for pressure equilization in typical measurement systems becomes excessive.

Based on a study of orifice errors in turbulent pipe flow, Shaw (Ref. 47) and Franklin and Wallace (Ref. 50) have verified that the effect of hole size scales with the local wall shear stress (τ_w) and fluid density (ρ) and viscosity (μ), viz.,

$$\frac{P_{meas} - P_{true}}{\tau_w} = f\left(\frac{d_o}{\nu}, \frac{\tau_w}{\rho}\right) \qquad (3.D.4)$$

In addition, the actual magnitude of errors are a function of a number of other parameters. For example, Shaw (Ref. 47) and Livesey, et al. (Ref. 48) found the relative depth of the hole to also be a significant parameter. In general, the measured pressure decreases towards the true value as the ratio of hole length to diameter decreases. However, as hole length/diameter decreases below 2, Livesey, et al. noted a relatively large cavity (14 d_o) behind the hole caused a negative error in measured static pressure.* In contrast, Rainbird (Ref. 49) and Shaw both used a cavity behind the hole with a diameter of only $2d_o$. With this arrangement, Shaw's data indicate a decreasing static pressure error as the length of the hole decreases from 1.5 d_o to 0.5 d_o.** Shaw also systematically studied the effects of burrs and discovered that burrs of the order of $d_o/127$ can cause errors as large as occur with variations in smooth hole size, i.e., the solid curve in Fig. 3.D.10.

Rayle (Ref. 46) found, as expected, inclining the axis of holes toward the oncoming flow increases the measured pressure. By inclining the hole downstream, a reduced pressure is measured. Rayle also studied the effects of varying edges of an orifice. In general, rounding of the edges resulted in higher pressure; whereas, chamfering produced small negative errors. As observed by Benedict (Ref. 53), the flow over a rounded edge does not immediately separate but instead is guided into the hole with a resulting recovery of part of the dynamic pressure. In the case of a chamfered or countersunk hole, the flow will separate at the upstream sharp edge, but

---

* Similarly, Livesey, et al. also note that a contraction in tubing diameter ($< d_o$) will cause a higher pressure.

** Rainbird used a fixed ratio of hole length to orifice diameter of 3.

it also accelerates along the sloping downstream edge which results in a reduced pressure. Rayle concluded a 0.076 cm (0.030 in.) hole with a 0.038 cm (0.015 in.) deep countersink should provide a static pressure near the true value. Finally, Rayle's experiments with water and air flows covered a Mach number range of 0 to 0.8. This data demonstrates orifice-induced errors increase with Mach number.

A summary of subsonic data obtained by Franklin and Wallace (Ref. 50) and the supersonic data obtained on a 25^{o} apex-angle cone by Rainbird (Ref. 49) is presented in Fig. 3.D.10. Rainbird suggested the scatter in his data could be attributed to variations in the ratio of hole diameter to boundary layer displacement thickness. However, the subsonic data of Franklin and Wallace failed to indicate any effect of this ratio. Furthermore, Nestler (Ref. 51) demonstrated orifice-induced errors could not be correlated by the ratio of hole diameter to boundary layer momentum thickness. The problem is compounded further by the hypersonic wind tunnel data discussed by Cassanto (Ref. 52). In this case, the diameters of square-edged and chamfered (60^{o}) orifices on an 18 deg cone were varied, respectively, from 0.076 - 0.635 cm (0.03 - 0.25 in.) and 0.152 - 0.635 cm (0.06 - 0.25 in.). For a freestream Mach number of 8 ($M_{local} = 6.37$), the measured pressure was insensitive to orifice diameter (decreasing slightly - less than 3 percent - with increasing diameter). Thus, the effects of Mach number on orifice-induced errors in static pressure needs additional research.

Questionnaire results indicate static orifice diameters typically range from 0.025 cm (0.01 in.) on small-angle cones to 0.228 cm (0.09 in.) on wind tunnel walls. In order to minimize static hole errors*, it is recommended

*Of course, a flush-mounted pressure transducer is preferable whenever possible.

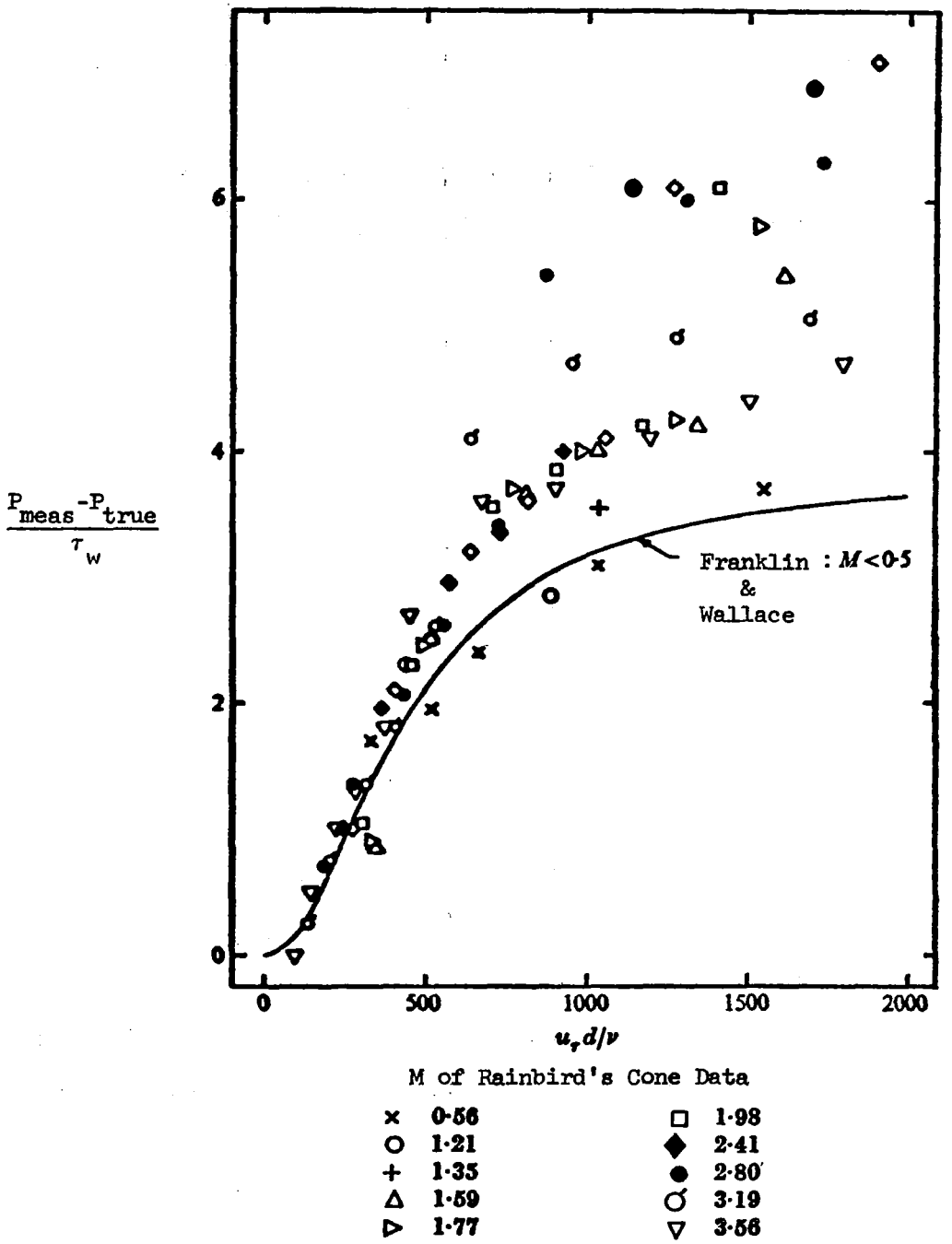

Figure 3.D.10 ORIFICE-INDUCED STATIC PRESSURE ERRORS, Ref. 50

that a square-edge orifice with a diameter of 0.051 cm (0.020 in.) be adopted as an industry standard. Since Rainbird (Ref. 49) has demonstrated this size of orifice can be used with satisfactory results in a blow-down tunnel, it can be used in most facilities. Ideally, the length of the hole should be restricted to the order of 1/2 of an orifice diameter, Ref. 47. However, such thin wall orifices are fragile and, thus, subject to damage. Hence, Gray (Ref. 33) recommends the hole length be greater than two orifice diameters. The diameter of a connecting line, behind the hole, should be restricted to the order of two orifice diameters, Refs. 47, 49, 50 and 33.

Of course, these last two criteria presuppose an installation which is accessible from the back side, e.g., a tunnel wall. In the case of a long, static pressure survey pipe, tubing of the appropriate size is swaged or sweat soldered in a receiving hole and then ground or machined down flush with the outside surface of the pipe. Here again an orifice diameter of 0.051 cm (0.020 in.) can be used, and larger diameter connecting lines may be used to reduce response time.

In the case of a conventional static-pressure probe, a ratio of hole depth to orifice diameter of less than one is not only possible but is frequently the case. For example, a probe wall thickness of 0.033 cm (0.013 in.) is typical for 0.318 cm (1/8 in.) OD stainless steel tubing. Therefore, the recommended orifice size would provide a hole length to diameter ratio of 0.65. Also, static pressure errors of probes may be reduced by designing them to have laminar flow at the orifices. Although the existing correlations of orifice errors are for turbulent flows, it appears probable that a laminar flow will

---

* Of course, a flush-mounted pressure transducer is preferable whenever possible.

dip into an orifice less than a turbulent flow. A laminar flow probe can be obtained by properly sizing the probe and polishing the external surface to 0.25 microns (10μ in.). For example, a 0.318 cm (1/8 in.) diameter probe, with orifices located 10 calibres downstream, would have a local Reynolds number of 1.25 million for a freestream unit Reynolds number of 39.4 million per meter. In general, if noise data is available for a given facility, the correlation of Benek and High (Ref. 54) can be used to estimate Reynolds numbers at which boundary layer transition occurs in order to judge whether a laminar flow probe is feasible.

Since the data of Shaw (Ref. 47) indicate static pressure measurements are very sensitive to burrs, considerable care must be taken to assure a smooth, sharp-edged orifice. This may be done by beginning the hole with drill bits several sizes smaller than the desired final hole size and progressively increasing the hole size. Also, short flute drill bits should be used to minimize flexing and a drill guide (of the same metal) clamped over the orifice location can be of considerable help. Finally, slower rates of drill feed will produce smaller burrs, and pressurizing the hole, during final drilling, with compressed air will aid the removal of burrs. Finishing of the orifice can be done with a drill shank and an appropriate polish. The finished orifice should be inspected for burrs with a microscope, and when possible, measured objectively, e.g., a Talysurf instrument.

Consideration should be given to the possibility of using an electrical discharge machine or a laser to manufacture smooth orifices. To the authors' knowledge, no comparative study of different processes for production of orifices has been made.

III.D.5. A General Purpose Static Pressure Probe

As discussed in Section III.D.1, the long, static pressure survey pipe, with nose located in the settling chamber, is preferred for centerline calibrations of transonic tunnels. This arrangement not only provides a large amount of simultaneous data but also prevents the passage of a transonic shock over the orifices. However, the questionnaire results indicate a large number of transonic tunnel operators (primarily smaller facilities) continue to use conventional probes. As mentioned previously in Section III.D.2, an advantage of inexpensive, classical probes is their mobility and the consequent ease of performing flow surveys off centerline. For the benefit of tunnel operators who wish to continue using this type of probe, the following probe design is suggested for calibrating transonic and supersonic tunnels.

The basic probe design is presented in Fig. 3.D.11. An ogive nose with an effective fineness ratio of 12 is suggested for two reasons: (1) overexpansion at the nose is minimal (e.g., see Fig. 3.D.3) which also minimizes the extent of the supersonic pocket at supercritical speeds and thus wall interference, (2) at supersonic speeds, the bow shock is attenuated by an ogive nose shape (e.g., Ref. 19); thus, this design also reduces wall interference at supersonic speeds.

It should also be noted that the nose design specifies a distributed roughness for boundary layer tripping. The objective of this feature is to prevent shock-induced, boundary layer separation at all speeds. An additional benefit is reduced sensitivity to Reynolds number. Examples of a boundary layer transition strip on this type of probe may be found in the report by Ritchie (Ref. 10). The size of grit and length of strip required for a particular application can be designed via the criteria of Braslow and Knox (Ref. 55) and Braslow, et al. (Ref. 56).

PROBE DIAMETER SHOULD BE SELECTED TO OBTAIN A TUNNEL BLOCKAGE $\leq$ 0.005% FOR TRANSONIC APPLICATIONS

RECOMMENDED ORIFICE SIZE ~ 0.051 CM (0.020 IN.)

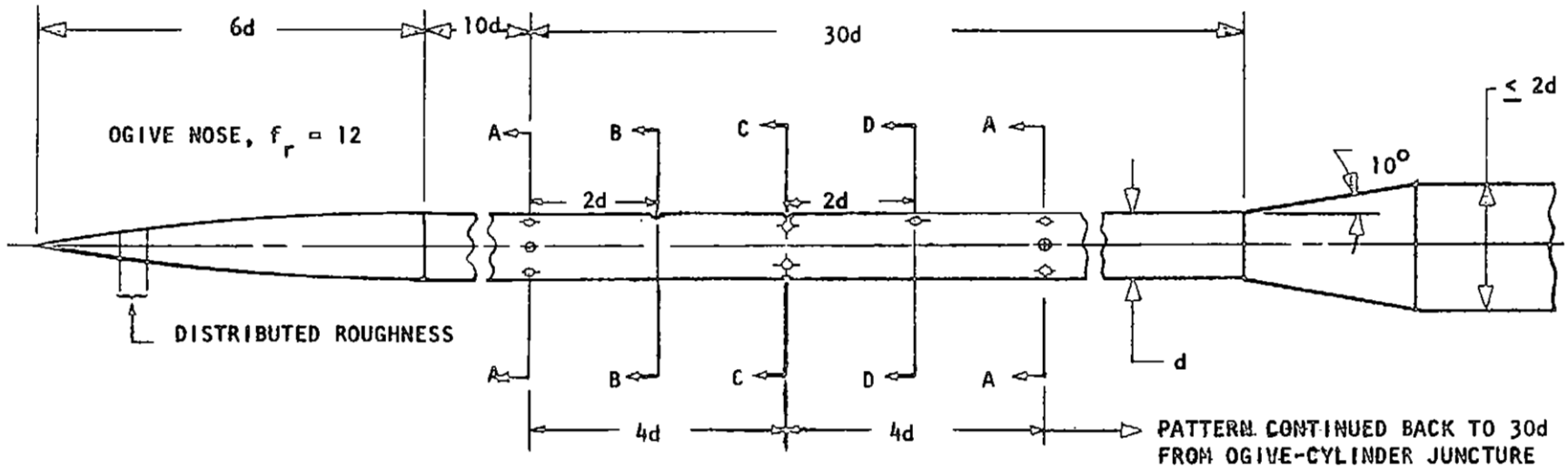

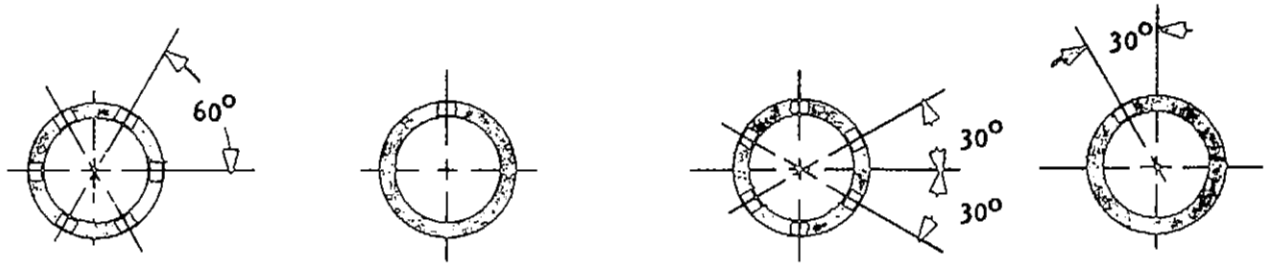

VIEW A-A
6 ORIFICES
60° APART

VIEW B-B
SINGLE ORIFICE

VIEW C-C
6 ORIFICES
ROTATED 30° FROM VIEW A-A

VIEW D-D
SINGLE ORIFICE
ROTATED 30°
FROM VIEW B-B

Figure 3.D.11 TRANSONIC/SUPERSONIC STATIC PRESSURE PROBE

An orifice diameter of 0.051 cm (0.020 cm) is recommended for static pressure ports along the cylinder.* The probe is designed to obtain primary static pressure data at stations having six orifices in order to average out the effects of any probe asymmetries, orifice errors, and small flow inclinations. The purpose of the single orifices is to assist in locating the position of either a transonic shock and/or the reflection of a bow shock (or any other disturbances) back onto the probe. The additional data will aid determination of where surface pressure equals freestream static. This feature will allow the probe to be used off centerline where wall interference increases.

Finally, the flare angle should be 10 deg or less in order to minimize interference near Mach one. The effects of this flare, as well as the wall-interference-free transonic performance of this probe, can be calculated via the South-Jameson computer code (Ref. 17). In the Mach number range of 0.95 to 1.00, it is necessary to keep probe blockage $\leq$ 0.01% in order to realize wall-interference-free performance at a tunnel centerline. If the probe is used with higher blockage and/or off centerline, wall proximity effects on shock location and surface pressure distribution can be estimated using the computer program of South and Keller (Ref. 22). In the case of supersonic applications ($M > 1.3$), probe blockage can be two orders of magnitude larger without any deleterious effects. It is only necessary to apply the criteria of Gray (Fig. 3.D.9) and avoid wall reflections of bow shocks. The interference-free performance can be computed with a number of existing asisymmetric method of characteristics codes.

---

* A hardened, stainless steel is recommended for durability and corrosion resistance in order to maintain orifice integrity and minimize long-term abrasion by particles in the flow.

III.D. References

1. Dick, R. S.: "The Influence of Several Cable-Type Supports Upon the Static Pressures Along the Centerline Tube in a Transonic Wind Tunnel," AEDC-TN-54-26, Feb. 1955.

2. Jackson, F. M.: "Supplemental Calibration Results for the AEDC Propulsion Wind Tunnel (16T)," AEDC-TR-70-163, Aug. 1970.

3. Jacocks, J. L. and Hartley, M. S.: "Calibration of the AEDC-PWT 4-Ft. Transonic Tunnel with Modified Walls," AEDC-TR-69-134, June 1969.

4. Jackson, F. M.: "Calibration of the AEDC-PWT 16-Ft Transonic Tunnel at Test Section Wall Porosities of 2, 4, and 6%," AEDC TR-76-13, Jan. 1976.

5. Isaacs, D.: "Calibration of the R. A. E. Bedford 8 ft. x 8 ft. Wind Tunnel at Subsonic Speeds, Including a Discussion of the Corrections Applied to the Measured Pressure Distribution to Allow for the Direct and Blockage Effects Due to the Calibration Probe Shape," ARC R. & M. No. 3583, Feb. 1968.

6. Pope, A. and Goin, K. L.: High-Speed Wind Tunnel Testing, Wiley, 1965.

7. Gunn, J. A. and Maxwell, H.: "Calibration of the AEDC-PWT Aerodynamic Wind Tunnel (4T) Mach Numbers 1.6 and 2.0 Nozzle Blocks," AEDC-TR-72-111, Sept. 1972.

8. Holder, D. W.; North, R. J.; and Chinneck, A.: "Experiments with Static Tubes in a Supersonic Airstream, Parts I and II," A.R.C. R. & M. No. 2782, July 1950.

9. Gracey, W.: "Measurement of Static Pressure on Aircraft," NACA TN 4184, Nov. 1957, and NACA Report 1364, 1958.

10. Ritchie, V. S.: "Several Methods for Aerodynamic Reduction of Static-Pressure Sensing Errors for Aircraft at Subsonic, Near-Sonic and Low Supersonic Speeds," NASA TR R-18, Feb. 1959.

11. Davis, J. W. and Graham, R. F.: "Wind-Tunnel Wall Interference Effects for 20° Cone-Cylinders," AIAA Jour. Spacecraft and Rockets, Oct. 1973.

12. Estabrooks, B. B.: "Wall-Interference Effects on Axisymmetric Bodies in Transonic Wind Tunnels with Perforated Wall Test Sections," AEDC-TR-59-12, June 1959.

13. Gadd, G. E.: "Interactions Between Normal Shock Waves and Turbulent Boundary Layers," ARC R & M No. 3262, Feb. 1961.

14. Albers, E. E.; Bacon, J. W.; and Mason, B. S.: "An Experimental Inestigation of Turbulent Viscous-Inviscid Interactions," AIAA Paper No. 71-565, June 1971.

15. Hsieh, T.: "Hemisphere-Cylinder in Transonic, $M_\infty = 0.7 \sim 1.0$," AIAA Jour., Oct. 1975.

16. Page, W. A.: "Experimental Study of the Equivalence of Transonic Flow about Slender Cone-Cylinders of Circular and Elliptic Cross Section," NACA TN 4233, April 1958.

17. South, J. C., Jr. and Jameson, A.: "Relaxation Solutions for Inviscid Axisymmetric Transonic Flow Over Blunt or Pointed Bodies," Proc. AIAA Computational Fluid Dynamics Conference, July 1973.

18. Robertson, J. E. and Chevalier, H. L.: "Characteristics of Steady-State Pressures on the Cylindrical Portion of Cone-Cylinder Bodies at Transonic Speeds," AEDC-TDR-63-104, Aug. 1963.

19. Capone, F. J. and Coates, E. M., Jr.: "Determination of Boundary-Reflected-Disturbance Lengths in the Langley 16-Foot Transonic Tunnel," NASA TN D-4153, Sept. 1967.

20. Couch, L. M. and Brooks, C. W., Jr.: "Effect of Blockage Ratio on Drag and Pressure Distributions for Bodies of Revolution at Transonic Speeds," NASA TN D-7331, Nov. 1973.

21. Newman, P. A. and Klunker, E. B.: "Numerical Modeling of Tunnel-Wall and Body-Shape Effects on Transonic Flow Over Finite Lifting Wings," Aerodynamic Analyses Requiring Advanced Computers, Part II, NASA SP-347, Mar. 1975.

22. South, J. C., Jr. and Keller, J. D.: "Axisymmetric Transonic Flow Including Wind-Tunnel Wall Effects," Aerodynamic Analyses Requiring Advanced Computers, Part II, NASA SP-347, Mar. 1975.

23. Sieverdling, C.; Maretto, L.; Lehthaus, F.; and Lawaczeck: "Design and Calibration of Four Probes for Use in the Transonic Turbine Cascade Testing," Von Karman Institute for Fluid Dynamics, Tech. Note 100, May 1974.

24. Sutton, E. P.: "The Development of Slotted Working-Section Liners for Transonic Operation of the R.A.E. Bedford 3-Ft. Wind Tunnel," A.R.C. R. & M. No. 3085, Mar. 1955.

25. Wright, R. H.; Ritchie, V. S.; and Pearson, A. O.: "Characteristics of the Langley 8-Ft. Transonic Tunnel with Slotted Test Section," NACA Report 1389, July 1958.

26. Keller, J. D. and Wright, R. H.: "A Numerical Method of Calculating the Boundary-Induced Interference in Slotted or Perforated Wind Tunnels of Rectangular Cross Section," NASA TR R-379, Nov. 1971.

27. Bryer, D. W. and Pankhurst, R. C.: Pressure-Probe Methods for Determining Wind Speed and Flow Direction, National Physical Laboratory, Her Majesty's Stationery Office, London, 1971.

28. Siddon, T. E.: "On the Response of Pressure Measuring Instrumentation in Unsteady Flow," UTIAS Report No. 136 (AD-682 296), Jan. 1969.

29. Rittenhouse, L. E.: "Transonic Wind Tunnel Results for Five Pressure Probes Designed to Minimize Static-Pressure Sensing Errors," AEDC-TDR-62-48, March 1962.

30. Chevalier, H. L.: "Calibration of the PWT 16-Ft. Transonic Circuit with a Modified Model Support System and Test Section," AEDC TN-60-164, Aug. 1960.

31. Krause, L. N. and Gettelman, C. C.: "Effect of Interaction Among Probes, Supports, Duct Walls and Jet Boundaries on Pressure Measurements in Ducts and Jets," I.S.A. Jour., Vol. 9, Sept. 1953.

32. Nichols, J. H.: "Rake Interference Studies at Transonic Speeds," AEDC-TM-56-1, Feb. 1956.

33. Gray, J. D.: "A Compendium of Flow Measurement Methods and Techniques," AEDC von Karman Gas Dynamics Facility, Notes prepared for a short course at the University of Tennessee Space Institute, Tullhaoma, Tenn., Nov. 1973.

34. Barry, F. W.: "Determination of Mach Number from Pressure Measurements," ASME Trans., April 1956.

35. Walter, L. W. and Redman, E. J.: "Needle Static-Pressure Probes Insensitive to Flow Inclination in a Supersonic Stream," NAVORD Report 3694, March 1954.

36. Washington, W. D. and Humphrey, J. A.: "Pressure Measurements on Four Cone-Cylinder Flare Configurations at Supersonic Speeds," RD-TM-69-11 (AD 699 359), Oct. 1969.

37. Gray, J. D.: "Evaluation of Probes for Measuring Static Pressure in Supersonic and Hypersonic Flow," AEDC-TR-71-265, Jan. 1972.

38. Norris, J. D.: "Calibration of Conical Pressure Probes for Determination of Local Flow Conditions at Mach Numbers from 3 to 6," NASA TN D-3076, Nov. 1965.

39. Vahl, W. A. and Weirich, R. L.: "Calibration of 30^{o} Included-Angle Cone for Determining Local Flow Conditions in Mach Number Range of 1.51 to 3.51.," NASA TN D-4679, Aug. 1968.

40. Peterson, C. W. and George, O. L.: "Wind Tunnel Pressure Probes: New Calibrations for New Geometries and Flow Environments," AIAA Jour., Vol. 13, No. 10, Oct. 1975.

41. Donaldson, I. S. and Richardson, D. J.: "A Short Static Probe with Good Incidence Characteristics at Supersonic Speed," A.R.C. Current Paper No. 1099, 1970.

42. Pinckney, S. Z.: "A Short Static-Pressure Probe Design for Supersonic Flow," NASA TN D-7978, July 1975.

43. Smith, A. M. O. and Bauer, A. D.: "Static-Pressure Probes that are Theoretically Insensitive to Pitch, Yaw and Mach Number," Jour. Fluid Mech., Vol. 44, Part 3, pp. 513-528, 1970.

44. Hsieh, T.: "Hemisphere-Cylinder in Low Supersonic Flow," AIAA Jour., Dec. 1975.

45. Marconi, F.; Yaeger, L. and Hamilton, H. H.: "Computation of High-Speed Inviscid Flows About Real Configurations," NASA SP-347, Mar. 1975.

46. Rayle, R. E.: "Influence of Orifice Geometry on Static Pressure Measurements," ASME Paper No. 59-A-234, Dec. 1959.

47. Shaw, R.: "The Influence of Hole Dimensions on Static Pressure Measurements," Jour. Fluid Mech., Vol. 7, Pt. 4, April 1960.

48. Livesey, J. L.; Jackson, J. D.; and Southern, C. J.: "The Static Hole Error Problem: An Experimental Investigation of Errors for Holes of Varying Diameters and Depths," Aircraft Engr., Vol 34, Feb. 1962.

49. Rainbird, W. J.: "Errors in Measurement of Mean Static Pressure of a Moving Fluid Due to Pressure Holes," DME/NAE Quarterly Bulletin No. 1967 (3), Nat'l. Res. Counc. Canada, Oct. 1967.

50. Franklin, R. E. and Wallace, J. M.: "Absolute Measurements of Static-Hole Error Using Flush Transducers," Jour. Fluid Mech., Vol 42, Pt. 1, June 1970.

51. Nestler, D. E.: "Static Pressure Port Errors in Hypersonic Turbulent Flow," AIAA Paper No. 71-270, Mar. 1971.

52. Cassanto, J. M.: "An Assessment of Pressure Port Erosion Effects," AIAA Paper No. 75-150, Jan. 1975.

53. Benedict, R. P.: Fundamentals of Temperature, Pressure, and Flow Measurements, Wiley, New York, 1969.

54. Benek, J. A. and High, M. D.: "A Method For the Prediction of the Effects of Free-Stream Disturbances on Boundary-Layer Transition," AEDC-TR-73-158, Oct. 1973, also AIAA Jour., P. 1425, Oct. 1974.

55. Braslow, A. L. and Knox, E. C.: "Simplified Method for Determination of Critical Height of Distributed Roughness Particles for Boundary-Layer Transition at Mach Numbers from 0 to 5," NACA TN 4363, 1958.

56. Braslow, A. L.; Hicks, R. M. and Harris, R. V., Jr.: "Use of Grit-Type Boundary-Layer-Transition Trips on Wind-Tunnel Models," NASA TN D-3579, 1966.

57. Parker, R. L., Jr.: "Flow Generation Properties of Five Transonic Wind Tunnel Test Section Wall Configurations," AEDC-TR-75-73, Aug. 1975.

III. E. MEASUREMENT OF FLOW ANGULARITY

The term yawmeter will be used herein to denote probes designed to measure flow angularity in either two or three dimensional flows. A wide variety of yawmeters have been used over the years for different applications. The ones which have been used in transonic tunnels may be divided into three general types: (1) pressure probes, (2) hot wire or film probes, (3) force models instrumented with a very sensitive force balance.* A discussion of pressure probes is given first and is followed by a brief description of two examples of the latter types of yawmeter.

A recent review of the various types of pressure probes and a discussion of the pros and cons of each are given by Bryer and Pankhurst (Ref. 2). These authors classify pressure probe yawmeters into two categories: (1) those consisting of an arrangement of open-ended tubes, and (2) those having a body with pressure sensing orifices. These may be subdivided into probes designed to measure flow angles in one plane (2-D) or two (3-D).

III.E.1. Differential Pressure Yawmeters: 2-D

For flow direction measurements in one plane, three types of yawmeter geometries are most common, viz., two pressure taps on the surfaces of either a wedge or a circular cylinder and two tubes with slanted inlets. A large variety of such probes are available from commercial manufacturers. The circular cylinder yawmeters are not recommended for transonic flows because of their comparatively large interference with the flow and considerable sensitivity to Mach number, Ref. 2. Both the cylinder and wedge have greater susceptibility to error in the presence of velocity gradients because of the larger separation of orifices. Also, Sieverding, et al. (Ref. 3) have found that a 30° (total angle) wedge-shaped yawmeter is Reynolds number dependent in the Mach number range 0.8 to 2.2. In contrast, the two-tube type of yawmeter, generally referred to as a Conrad probe, provides: (1) minimum flow disturbance, (2) adequate sensitivity which is relatively free of Mach number and Reynolds number effects (Refs. 4 and 5), and (3) orifices which are close together for nearly point measurement of flow angularity.

---

*A fourth type, Laser Doppler Velocimeters (LDV), have also been used to measure flow angularity in the AEDC 1T transonic tunnel (Ref. 1). LDV's are discussed in Appendix II of this report.

References 3 and 5 contain calibration results for small tube type yawmeters which were designed to investigate the flow out of transonic turbine cascades and compressors. The objective of Sieverding, et al. (Ref. 3) was to investigate several probe geometries and arrangements which could be used to simultaneously measure total, static, and directional pressures. The two-tube yawmeter, shown in Fig. 3.E.1, was mounted on a rake of rectangular cross section (2.3 mm thickness normal to flow and 6.0 mm parallel to flow). The yawmeter was arranged to measure flow angularity normal to the plane of the rake. A small diameter (1.7 mm), truncated, 25° total apex-angle cone probe was also mounted on the rake. The separation distance between the yawmeter and the conical probe was 16 mm and both nose tips were located 22 mm ahead of the rake. The probes, with this arrangement, were calibrated in the DFVLR/AVA Transonic Wind Tunnel (1m x 1m). The resulting sensitivity of the yawmeter is presented in Fig. 3.E.1. $0.8 \leq M \leq 2.2$.*

A combination Pitot probe and yawmeter was also calibrated with a similar arrangement, but two different companion probes were used. In one case, the companion probe was a 15° cone needle probe (1.5 mm OD) for measuring static pressure, and the second companion probe was a 30° cone probe (1.5 mm OD). The sensitivity of the needle probe was found to be linear over the largest range of angles of yaw ($\pm 10^{\circ}$). The corresponding sensitivity data are also shown in Fig. 3.E.1. The difference in the angle sensitivity of the two-tube yawmeter and the combination probe may be attributed to the difference in the inlet angle.

Sieverding, et al. (Ref. 3) also tested the yawmeter and needle probe combination in the small (135 mm x 50 mm) VKI High Speed Cascade Tunnel C-2. Static pressure measurements along the wall of this facility, with and without the probes, indicated significant blockage when Mach number exceeded 0.90; whereas, a single AGARD needle probe (12.3° cone and 1.5 mm OD) with a standard elbow type support (3 mm OD) located 48 probe diameters downstream showed negligible blockage. Hence, these authors conclude: if a yawmeter (and/or other probes) are to be used in transonic tunnels, the probes and support

*Although these authors did not state the inside diameter of the tubing, the ratio of I.D. to O.D. should be kept greater than 0.6 in order to minimize loss or change of sensitivity with increasing flow angularity, e.g., p. 19 of Ref. 2.

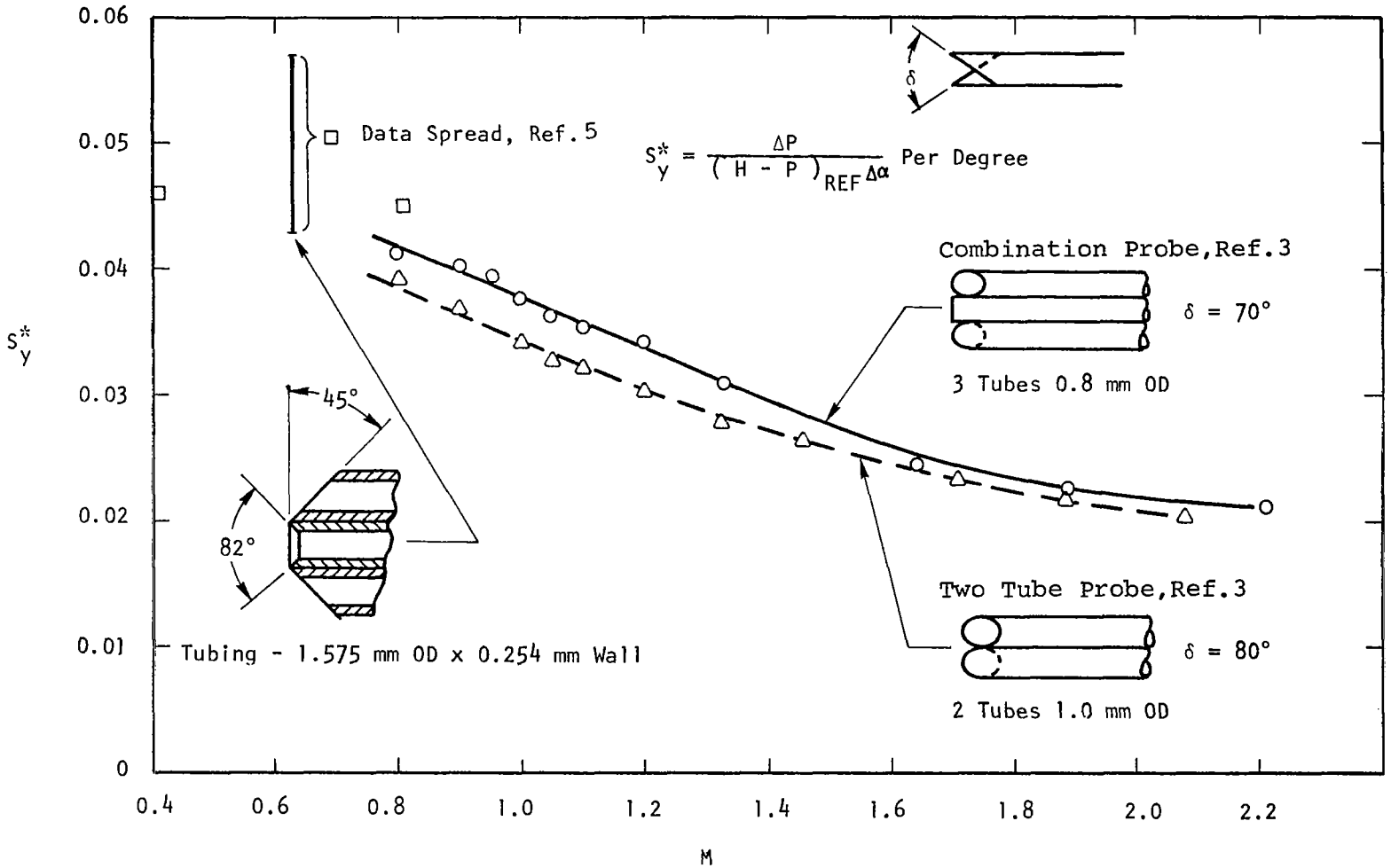

Figure 3.E.1. TWO DIMENSIONAL YAWMETERS

mechanism should be calibrated in a tunnel of size similar to which it is to be used. And most importantly for tunnel calibrations, extreme care must be taken in designing yawmeter supports in order to avoid inducing extraneous flow angularity.

The flow angle sensitivity data of Buzzell (Ref. 5), obtained with a combination Pitot probe and yawmeter, is also shown in Fig. 3.E.1 for M = 0.4, 0.6, and 0.8. These data were obtained with a cobra-styled rake with three combination probes alternating with four single Pitot tubes.* Again, this investigator followed the accepted practice of locating the probe to measure angles normal to the plane of the rake. Mach number sensitivity checks indicated negligible change in yawmeter sensitivity for $0.41 \leq M \leq 0.81$. After this was ascertained, eight rakes were tested at a mean Mach number of 0.6. The resulting spread in data are shown in Fig. 3.E.1.

Vidal, et al. (Ref. 6) have recently reported using a two-tube yawmeter to measure flow angularity in a small (30.5 cm) transonic wind tunnel. The objective of these tests is to compare measurements of flow angularity and static pressure with calculated interference-free transonic flow solutions for a given model, and thereby provide a criterion for adjusting tunnel wall porosity to attain wall-interference-free flow. A planar yawmeter was used because an airfoil, which spans the tunnel, is being used for developmental testing. The yawmeter is similar to the one shown in the lower right portion of Fig. 3.E.1. and was constructed of 0.0635 cm (0.025 in.) OD tubing with each inlet chamfered at 45°. These authors claim that their flow angle sensitivity is such that with a pressure resolution of 0.0007 N/cm^2 (0.001 psi) they can "in principle" resolve angles to within 0.03° in the Mach number range 0.55 to 0.725.**

As noted by Bryer and Pankhurst (Ref. 2), yawmeter sensitivity in low speed flows has traditionally been defined as

$$S_y^* \equiv \partial(\Delta P/q)/\partial\psi \qquad (3.E.1)$$

where ΔP is the pressure difference across the yawmeter. However, these

---

*These rakes were designed to place six of them circumferentially in the stator discharge plane of a compressor.

**Since the original writing of this section, the calibration and use of a new yawmeter design has come to our attention, Lind (Ref. 28). This 2-D yawmeter consists of a two-hole, differential pressure probe placed at the vertex of a forward-swept wing. A yawmeter sensitivity of 0.163 and an accuracy of 0.01 deg is claimed for low-speed flows ($M_\infty \leq 0.17$).

authors note that, for compressible flows, less variation in sensitivity with Mach number is obtained by using the following definition.

$$S_y \equiv \partial(\Delta P/H)/\partial\psi \qquad (3.E.2)$$

An example of this may be found in the paper by Spaid, et al. (Ref. 7). In their experiments with a miniature (1 mm total span) combination Pitot probe and yawmeter, sensitivity, as defined in Eq. (3.E.2), did not vary with $0.8 \leq M \leq 1.0$ and $-30° \leq \psi \leq 30°$. In addition, the supersonic data in Fig. 3.E.1 show much less variation with Mach number when S_y is used. Thus, the compressible definition of yawmeter sensitivity, Eq. (3.E.2), is preferred for transonic and supersonic applications.

III.E.2. Differential Pressure Yawmeters: 3-D

For the general case of flow angularity calibration in an empty tunnel (transonic and/or supersonic), a pyramid yawmeter is recommended. The pyramid geometry has two primary advantages compared to a conical or hemispherical yawmeter. Firstly, the pyramid probe performance is less sensitive to positioning of the orifices. Secondly, it is relatively free of interference between simultaneous measurements of pitch and yaw. In addition, the incompressible flow measurements of Bryer, et al. (Ref. 8) indicate S_y^* for a pyramid probe is comparatively insensitive to Reynolds number and increases slightly (~6%) with increased turbulence.

A typical pyramid yawmeter is shown in Fig. 3.E.2. Here, the ratio of orifice diameter to probe stem diameter is 0.16. In general, it is recommended that this ratio be kept less than 0.20. An additional, suggested constraint is that the diameter of the orifices be no smaller than 0.508-mm (0.02 in.) in order to avoid clogging and excessive time lag problems.* The apex angle was chosen to conform with the recommendation of Bryer and Pankhurst (Ref. 2). These authors suggest that a yawmeter be designed so that the bow shock wave remains detached or attached throughout the range of Mach numbers within which measurements are to be made. Thus, an apex angle of 66° will maintain a detached shock for transonic Mach numbers up to 1.6. (A Mach number of 1.6

*Smaller orifices (0.25 mm) have been used at low speeds (Ref. 9) and supersonic speeds (Ref. 2, P. 57). However, no significant improvement in performance is gained, and clogging and decreased response time can make the probe more expensive to use.

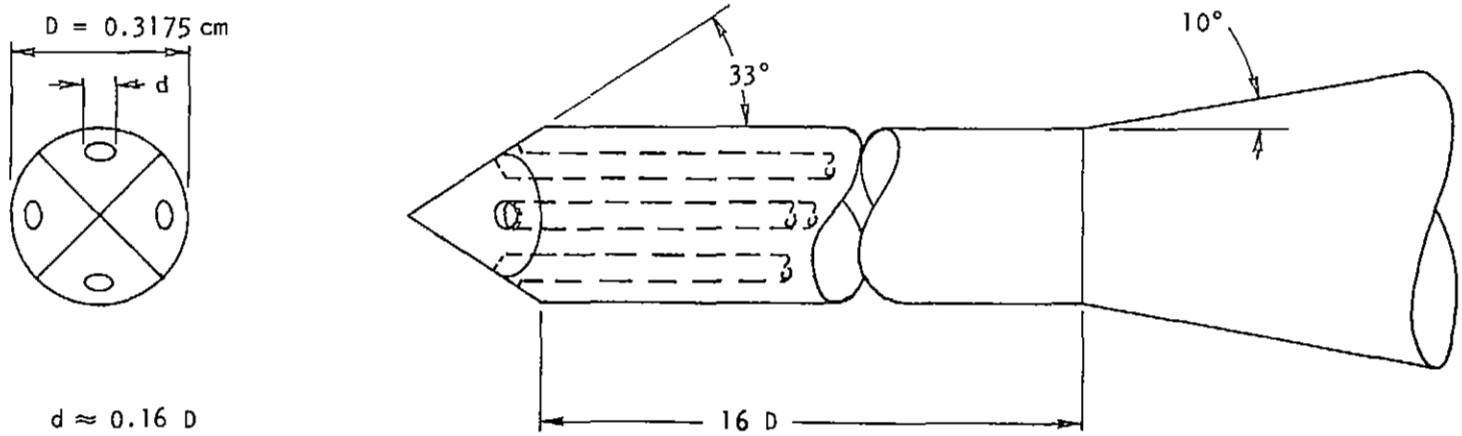

Figure 3.E.2. PYRAMID YAWMETER

is chosen because this represents the upper limit of operation for the majority of transonic tunnels.) Beyond this speed regime, the bow shock will be attached, and the probe can be used in supersonic flows. The purpose of this design feature is to avoid the sudden changes that can occur in the pressure response of sharp-nosed probes near the shock attachment Mach number. Furthermore, Bryer and Pankhurst have noted that the maximum sensitivity of most pointed yawmeters is obtained with an apex angle between 60 and 70 degrees.

Finally, for use in transonic flows the probe stem should extend downstream for a distance of at least 16 diameters. Downstream of this station, the stem can safely be enlarged by a 10° conical flare to mate with the available probe support. Provided a massive, transverse probe support is not used, this design will avoid interference between probe and support at transonic speeds.

The flow angle sensitivity, $\partial(\Delta P/H_s)/\partial\Psi$, of conical and hemispherical-nose probes have been found to increase with Mach number and reach a maximum of about 0.025 at $M \sim 1.5$ (e.g., Ref. 10 and Ref. 2). Further increases in Mach number result in decreasing sensitivity. For example, data for a hemispherical yawmeter with orifices located 45° from the nose indicate a 50% loss in sensitivity at $M = 2.7$, Fig. 35 of Ref. 2. Similarly, theoretical calculations for a 60° conical yawmeter indicate a 70% loss at $M = 3.5$, Fig. 3.E.3.* If we assume similar behavior for the pyramid probe and a maximum sensitivity of 0.025, the smallest change in flow angle which can be detected by a pressure measuring system with a resolution of 3.45×10^{-3} N/cm^2 (0.005 psi) is

$$\Psi_{min} = \frac{3.45 \times 10^{-3} \text{ N/cm}^2}{(0.025)\ H_s} \sim \text{degrees} \qquad (3.E.3)$$

In the case of a transonic tunnel with $T_s = 37.8^{\circ}$C, Re/m = 19.7×10^6, and $M = 1.0$, the settling chamber pressure is 13.79 N/cm^2 (20 psia). Substituting this value for H_s in Eq. (3), we find that a flow angle of 0.01 degree can theoretically be resolved. In practice, the effects of probe and/or support deflections, nonidentical internal geometry of the tubing and passages which

*For this reason, Barry (Ref. 11) and Zumwalt (Ref. 12) explored the use of Pitot probes located near the surface of wedges and cones to provide increased sensitivity at high supersonic Mach numbers. However, for most applications, the conventional surface pressure yawmeters provide adequate sensitivity up to $M = 3.5$.

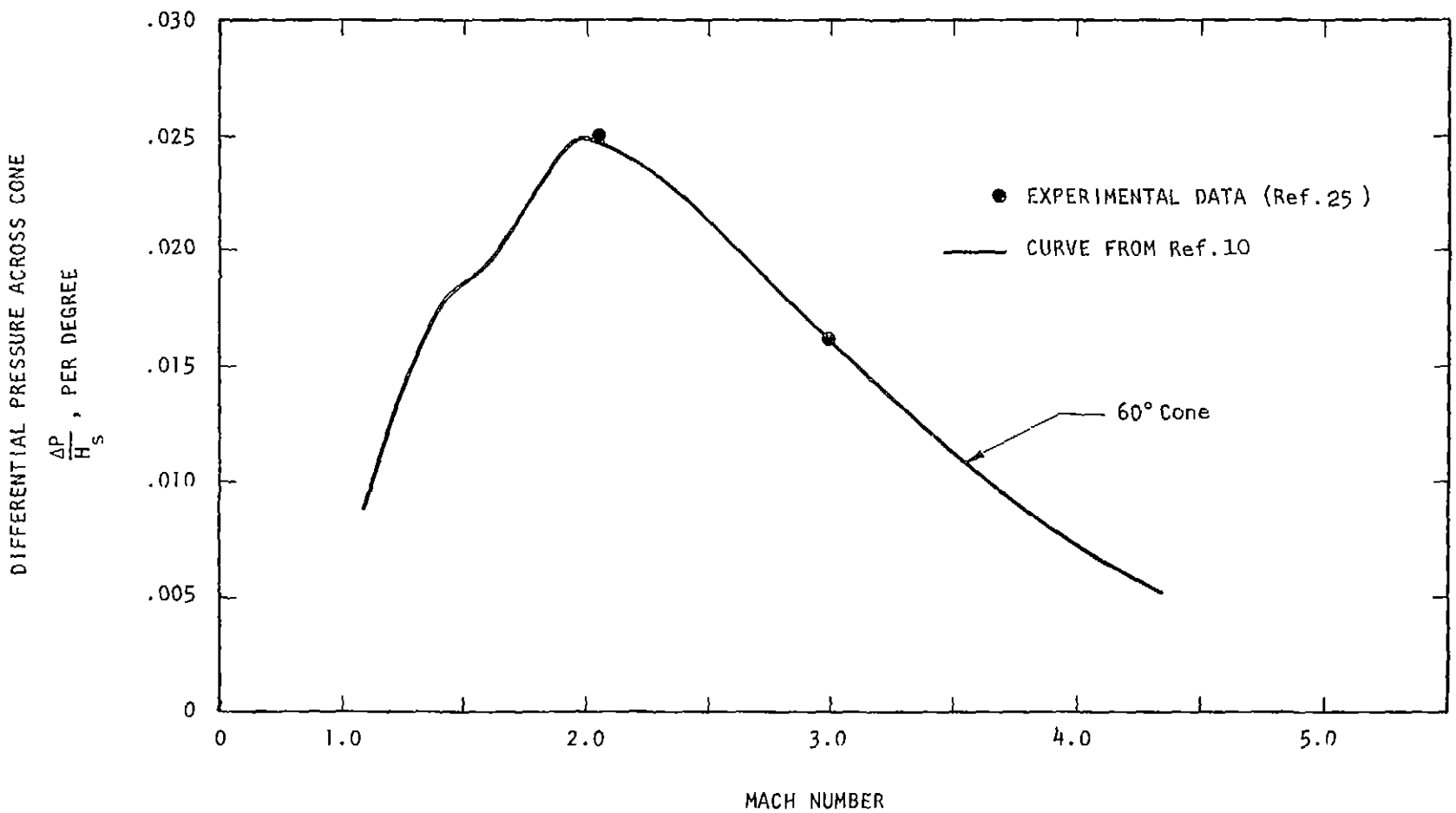

Figure 3.E.3. SENSITIVITY OF 60° CONICAL YAWMETER

connect two orifices to a differential pressure transducer, vibration, turbulence, etc., may prevent the attainment of such accuracy. However, the pyramid probe can provide adequate angle resolution for calibration of most wind tunnels. Especially in light of the fact that the majority of tunnel operators are satisfied with a calibration of (tunnel-empty) flow angles accurate to within 0.1 degree.

If less-accurate, flow angularity measurements are satisfactory and a simultaneous measurement of Pitot pressure is desired, the nose of the pyramid yawmeter may be truncated and an orifice placed in the center of the nose,* e.g., Ref. 9. In the case of subsonic tunnels, this would provide a convenient check on the uniformity of total pressure. In the case of supersonic tunnels, this permits Mach number to be determined simultaneously, e.g., Refs. 14 and 15. Such a probe not only minimizes calibration time but also eliminates any uncertainty in local Mach number at which flow angles are measured.

In summary, the suggested dimensional criteria for a pyramid yawmeter should result in a probe which:

1. has a flow angle sensitivity which is relatively insensitive to extraneous flow variables such as Reynolds number and turbulence,
2. is small enough to map flow angularity in most tunnels with high resolution and minimum interference,**
3. has fast enough pressure response for most applications,
4. has adequate structural stiffness, and
5. can be used to calibrate both transonic and supersonic tunnels.

---

*It is recommended that the lip thickness be kept thin (0.005 cm) and the orifice be beveled at an angle of 15° or more in order to minimize sensitivity of the Pitot probe to flow angularity.

**In large tunnels (≥8 ft) where high resolution of the flow angularity field is not required, the recommended pyramid probe may be scaled up to larger sizes. In any event, probe blockage should be less than 0.1 percent for general calibrations of transonic tunnels. However, near M = 1 values an order of magnitude smaller may be necessary in order to avoid probe-wall interference, see Ref. 13.

Yawmeter Calibration, Rake Interference, and Blockage

As noted by Pope and Goin (Ref. 10, P. 134), all real yawmeters have asymmetries and imperfections which cause the probe to indicate a nonzero ΔP at $\psi = 0$. Thus, a yawmeter should always be calibrated in flow conditions similar to those in which it is to be used. The calibration procedure for differential pressure yawmeters is described in Refs. 10, 14, and 15 and will not be repeated here. However, it is relevant to sound a note of caution here. When calibrating a yawmeter, the center of rotation should be at the nose tip. Also, careful measurements of the angles between yawmeter axis and tunnel axis are essential since these must be subtracted from the flow angles relative to the probe in order to determine flow angularity with respect to the tunnel centerline.

In order to reduce tunnel calibration time, most operators prefer to use probes in rakes or arrays. However, Hartley and Nichols (Ref. 16) conducted tests in the AEDC 16T Tunnel with five 7.62 cm (3 in.) diameter hemispherical yawmeters mounted on a 2.44 m.(8 ft) wide rake. The rake consisted of a 22° (total-angle) wedge with a 7.62 cm (3 in.) wide base and was center mounted on a sting support. The yawmeters were mounted 0.61 m (2 ft) apart with the nose located approximately four diameters ahead of the leading edge of the wedge. The total wind-tunnel blockage of the rake was approximately 1%. These investigators found that the rake induced significant outflow toward the tips of the rake. The induced flow angularity, at the tips of the rake, increased from about 0.5° at M = 0.6 to over 1° at M = 1.1. As Mach number increased from 1.1 to 1.2, the induced flow angularity decreased sharply and exhibited near-interference-free characteristics for $1.2 \leq M \leq 1.5$. A wall-mounted strut support, with the same wedge angle of 22°, was also tested and found to induce even larger outflow from the wall toward the tip.

In both cases, the support-induced flow angularity was ascertained by mounting a single probe on a long sting. The first section of the sting had a diameter of 5.715 cm (2.25 in.) and a length of approximately 16 probe diameters. The second section of sting had a diameter of 7.62 cm (3.0 in.) and a length of over 20 probe diameters which subsequently joined a conical flare and the rest of the sting support mechanism. The sting support system enabled vertical traverses with the sting at zero angle of attack. In addition, the blockage of the single probe was only 0.019%. Thus, the arrangement assured

as near-interference-free, flow angularity measurements as can be expected in a wind tunnel.

An additional conclusion reached by Hartley and Nichols (Ref. 16) is that the rake had negligible effect on flow angles normal to the plane of the rake (i.e., with the rake vertical, the yaw data were valid and with the rake horizontal, the pitch data were valid). Thus, based on these and other similar results, it is possible to use yawmeters in a carefully designed rake arrangement to make two dimensional measurements.* However, for greatest accuracy, a single probe joined to a long sting with a support which is symmetrical about the tunnel centerline is recommended.**

Finally, with regard to wind tunnel blockage at Mach numbers near 1.0, the data of Couch and Brooks (Ref. 13) indicate that even with extremely small values of model blockage (≤ 0.0003) wall interference occurs. Thus, yawmeters for measurements near Mach one must be designed with the utmost care, viz., small probes and long stings, and the resulting data should be scrutinized for any sudden or unexpected variations around M = 1.0.

III.E.3. Hot-Wire/Film Yawmeters

Two hot-wires inclined at an angle with respect to each other and the mean flow have long been used in low speed flows to measure flow angularity (Ref. 17). Three-wire probes have also been used extensively to simultaneously measure pitch and yaw in three dimensional flows. In the past, hot-wires have not been used in transonic flows because they are so easily broken. However, Hortsman and Rose (Ref. 18) have recently demonstrated that low aspect ratio ($\ell/d \sim 100$) tungsten wire probes can be used in transonic flows without a prohibitive breakage problem. Also recently, Johnson and Rose (Ref. 19) have reported using an X-array hot-wire to measure Reynolds stress in a supersonic boundary layer and in a shock-wave/boundary-layer interaction (Ref. 20). Thus, although matching the sensitivities of two or more wires for accurate

*Dudzinski and Krause (Ref. 4) point out that a rake with circular arms is unaffected by angles of attack. Whereas when nonzero yaw angles exist in subsonic and/or transonic flows, noncircular arms can induce larger flow angularity at the nose of the yawmeter and also create undesirable side forces on the rake.

**Another alternative would be to calibrate a rake following the procedure of Ref. 16.

mean flow measurements can be a problem,* there appears to be no prohibitive reason why two and three-wire probes cannot be used as yawmeters. In order to avoid the problem of matching sensitivities of more than one wire, Rosenberg (Ref. 22) has successfully used a single wire probe mounted in a rotatable holder. By rotating an inclined-wire about the axis of the probe's stem and taking data at two distinct orientations, the three components of velocity and mass flux can be determined at a point in a general three-dimensional flow.

In a study of the effects of contouring slotted walls to reduce transonic-wall-interference, Weeks (Ref. 23) has used a hot-film probe for accurate measurement of flow angularity. This work involved the use of airfoil models which spanned the test section of the AFFDL Trisonic Gasdynamics Facility. The required planar measurements of flow angularity were obtained with a split-film, 22^{o} total-angle wedge which was manufactured by Thermo Systems, Inc., according to an AFFDL design. This probe consists of a quartz rod 0.152 cm (0.06 in.) in diameter with the tip ground to a symmetrical wedge. As indicated in Fig. 3.E.4, the rod extends forward 1.27 cm (0.5 in.) from a 0.3175 cm (0.125 in.) diameter support tube. A pair of platinum films, 0.102 cm (0.04 in.) long, are deposited on each side of the apex of the wedge. Four gold-film leads are used to complete the two separate anemometer bridge circuits. The calibrated yaw sensitivity of this probe is shown in Fig. 3.E.4 for $0.85 \leq M \leq 0.95$. Weeks claims that this probe will resolve flow angles to within ± 2 minutes of arc (0.03^{o}). The primary limitation is stated to be probe vibration which was determined experimentally to induce errors ≤ 0.5 minutes of arc.

In summary, since hot-film probes are (1) less delicate, (2) less susceptible to contamination because of their larger size, and (3) can have corrosion resistant coatings, hot-film yawmeters are superior to hot-wire yawmeters. Both hot-wires and hot-films require specialized data processing equipment which may be considered a disadvantage by potential users. However, based on the results obtained by Weeks, hot-film yawmeters appear to offer a viable alternative to differential pressure yawmeters.**

The uses of hot-wires and hot-films are discussed further in Appendix I.

---

* Reference 21 also discusses the fact that the calibration of a hot-wire is susceptible to change with time because of contamination and corrosion. This may require frequent calibration checks.

** Although the authors are not aware of any transient measurements of flow angles with a hot-wire/film, there is no inherent reason why this type of yawmeter can not be used in a continuous-traverse mode. This would provide the advantage of reduced tunnel calibration time, e.g., see discussion of force balance yawmeters.

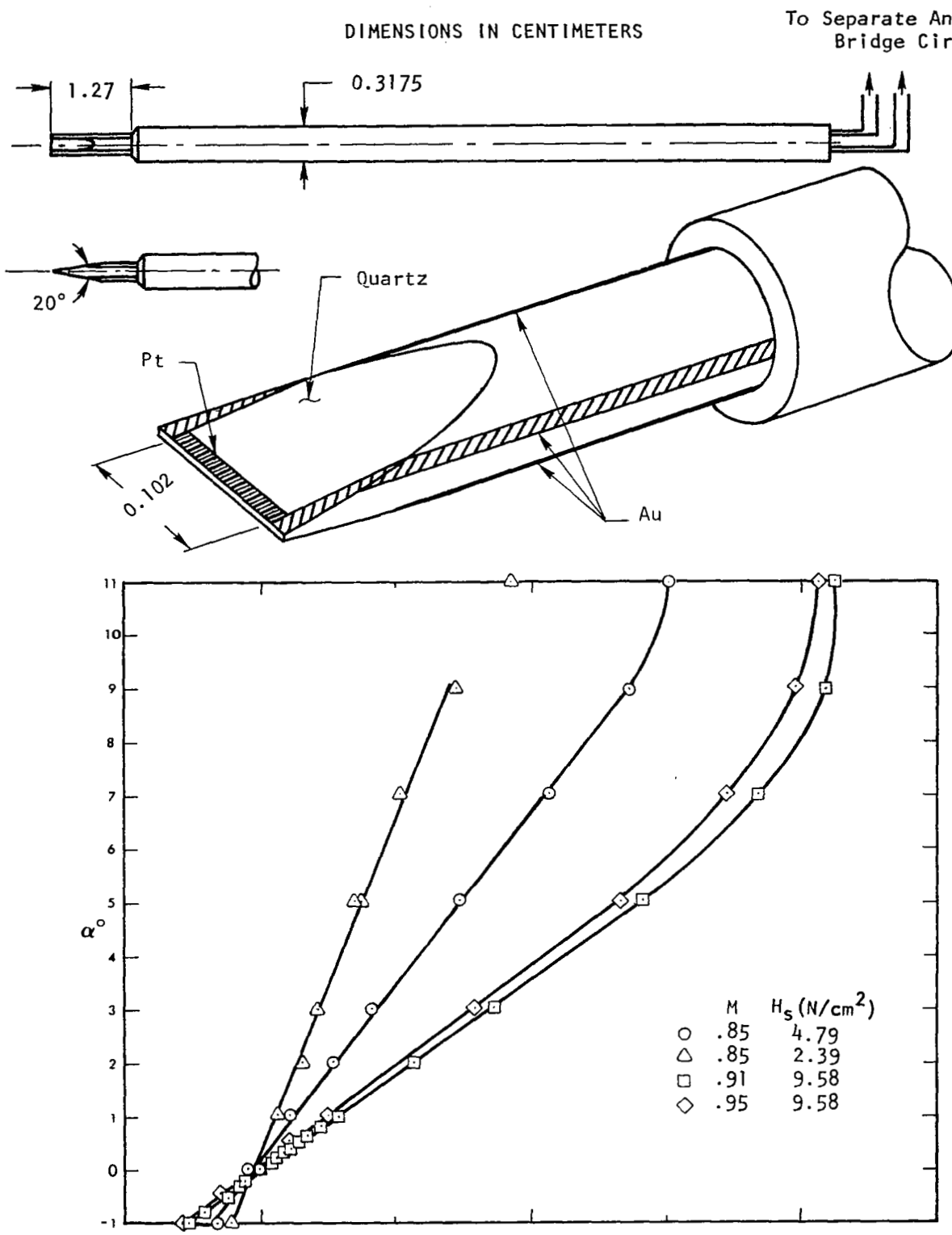

Figure 3.E.4. SPLIT HOT FILM, 20° WEDGE PROBE CALIBRATION BRIDGE VOLTAGE DIFFERENCE VS FLOW ANGLE, REF. 23

Force Balance Yawmeters

The basic procedure of running a wind tunnel force model upright and inverted to determine the average pitch angle is well known and is standard practice in professional wind tunnel testing. However, the use of a small wedge mounted on a sensitive force balance to obtain a measure of tunnel-empty flow angles is new. Maxwell and Luchuk (Ref. 25) have recently reported the results of transonic tests with this type of yawmeter. The probe consists of a 20° included-angle wedge, with a 14.73 cm (5.80 in.) span, mounted on a specially-designed, two-component force balance, Fig. 3.E.5. The force balance was designed to measure normal force and pitching moment with very thin, strain-gauged sections for maximum sensitivity.

The probe was tested in the AEDC Aerodynamic Wind Tunnel (4T) over the Mach number range of 0.6 to 1.3. The calibrated flow angle sensitivities, based on variations of normal force and pitching moment, are shown in Fig. 3.E.6. Although the yaw sensitivity of the pitching-moment mode is approximately 50% larger, Maxwell and Luchuk found that flow angle measurements obtained from either mode were of equal accuracy.

The wedge was supported by the 4T six-degree-of-freedom, captive trajectory system. This permitted the probe to be moved continuously with a variety of movements. Maxwell and Luchuk conclude that flow direction data can be obtained "with an absolute accuracy that is little different from the accuracy with which the probe is aligned." Furthermore, based on comparisons of data obtained with the probe at rest and in motion, reliable and rapid measurements can be made with the probe moving continuously with combined linear and rolling motion. The estimated rms deviations from a mean value of flow angle was $\leq 0.023^{\circ}$ at all measured points. However, $\pm 4^{\circ}$ sweeps in pitch and yaw produced larger variations, viz., $\pm 0.08^{\circ}$ and $\pm 0.25^{\circ}$, respectively. These data were obtained with pitch and yaw rates which varied, respectively, from 1.16 to 1.28 and 1.01 to 1.36 deg/sec.

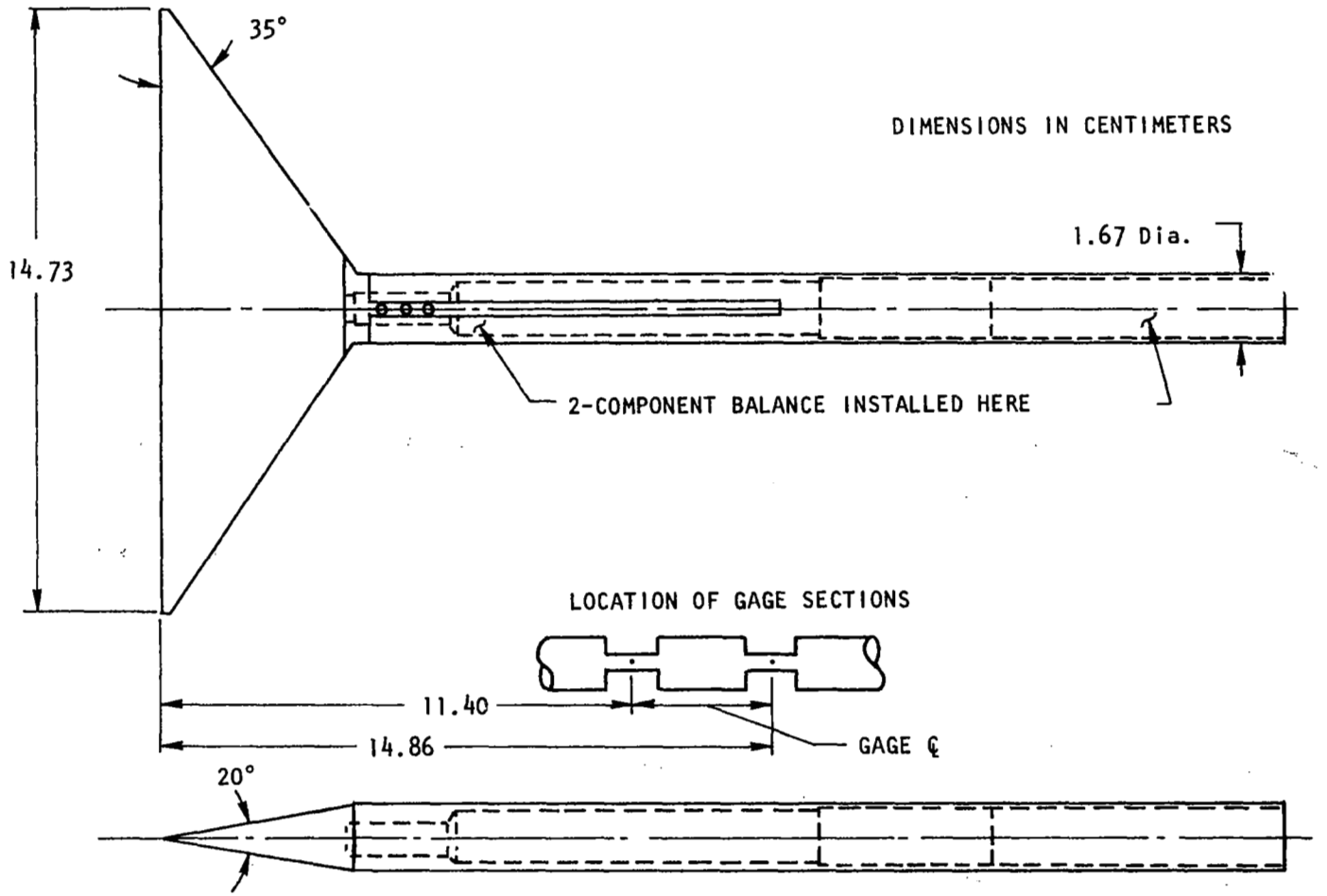

Figure 3.E.5. GEOMETRY OF AEDC FORCE BALANCE YAWMETER

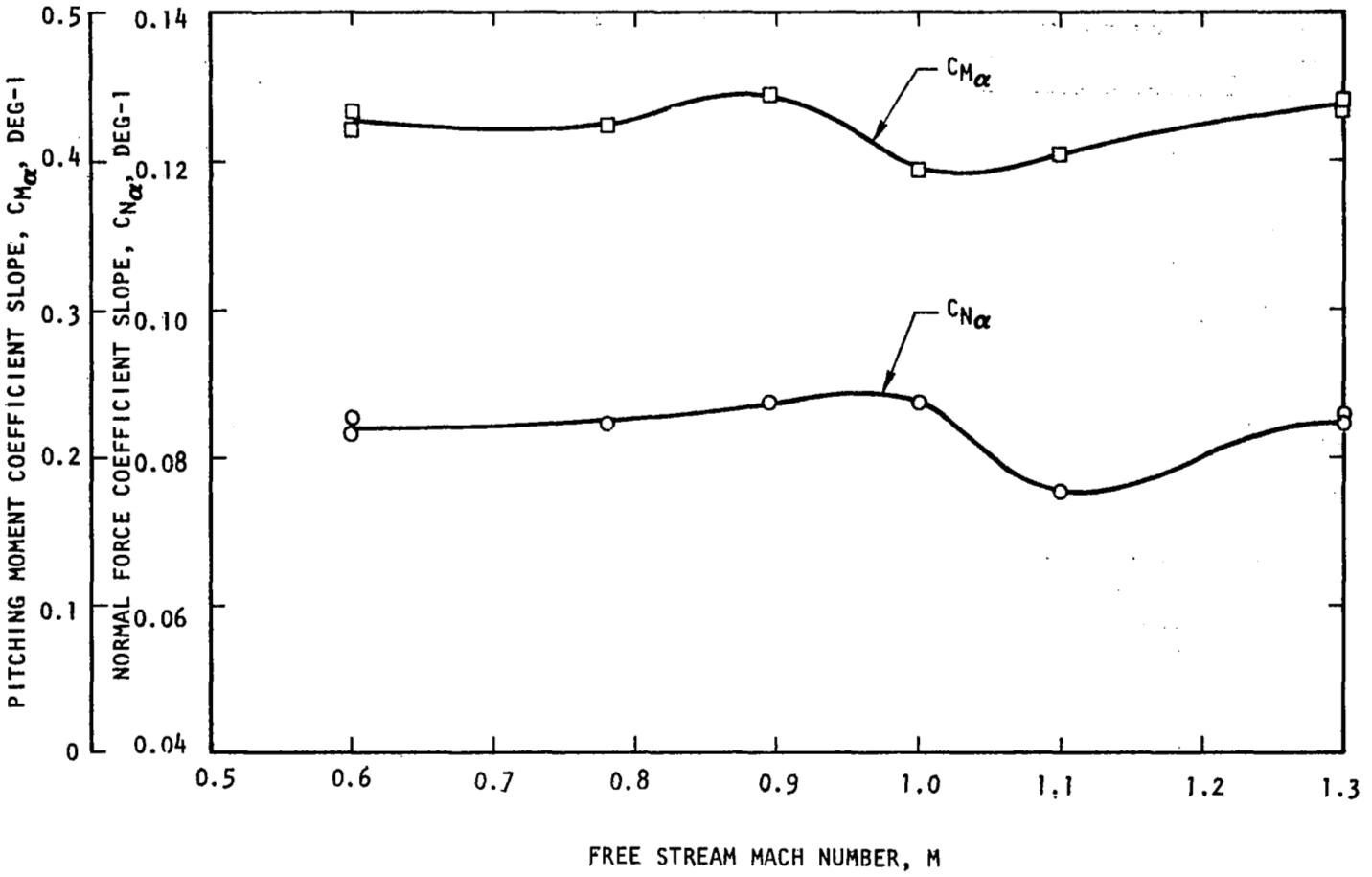

Figure 3.E.6. SENSITIVITY OF THE AEDC FORCE BALANCE YAWMETER

Unfortunately, the Reynolds number dependence of this yawmeter was not investigated. However, some variation of total pressure at M = 0.6 indicated a decreasing sensitivity with increasing unit Reynolds number. At this point, the reader may recall that Sieverding, et al. (Ref. 3) also reported their wedge shaped yawmeter exhibited a Reynolds number dependence.* This implies that wedge shaped yawmeters should be calibrated as a function of Mach number and Reynolds number. Hence, this type of yawmeter will be more tedious to use. Additional disadvantages of the wedge force balance yawmeter is higher initial costs and pitch and yaw must be measured separately.** However, a force balance can be calibrated to relate angular deflection of model and support to changes in loading. This provides a distinct advantage over differential pressure and hot-wire/film yawmeters. In conclusion, the force balance yawmeter's advantage of rapid, continuous measurements of flow angularity appears to outweigh the disadvantages.

---

* Neither of these yawmeters had a boundary layer transition strip. Thus, dependence of wedge-yawmeter sensitivity on Reynolds number could conceivably be reduced by utilizing a grit-type, boundary layer trip.

** A double, intersecting wedge probe with four component force balance has more recently been constructed and tested at AEDC (Summers, Ref. 26). This yawmeter enables pitch and yaw data to be obtained simultaneously in even less time. An improved design, which is less sensitive to unsteady transonic flow, specifies a small, symmetrical centerbody with flat plate wings attached in orthogonal planes, Ref. 27. Recent experience with this type of yawmeter in the AEDC 4T Tunnel indicates simultaneous measurements of pitch and yaw can be obtained at 225 points in less than six minutes and with an accuracy of 0.01 degree.

III. E. References

1. Lennert, A. E.; Hornkohl, J. O. and Kalb, H. T.: "Application of Laser Velocimeters for Flow Measurements," Instrumentation for Airbreathing Propulsion, Progress in Astronautics and Aeronautics, AIAA Vol. 34, MIT Press, 1972.

2. Bryer, D. W. and Pankhurst, R. C.: Pressure-Probes Methods for Determining Wind Speed and Flow Direction, Her Majesty's Stationery Office, London, 1971.

3. Sieverding, C.; Maretto, L; Lehthaus, F. and Lawaczeck, O.: "Design and Calibration for Four Probes for Use in the Transonic Turbine Cascade Testing," VKI TN 100 (AD 922 286), May 1974.

4. Dudzinski, T. J. and Krause, L. N.: "Flow-Direction Measurement with Fixed-Position Probes," NASA TM X-1904, Oct. 1969.

5. Buzzell, W. A.: "Calibration Results for Stationary Pressure Rakes Sensing Yaw Angle Downstream of an Axial Compressor Stage," ARL TR 75-0104, April 1975.

6. Vidal, R. J.; Erickson, J. C. and Catlin, P. A.: "Experiments with a Self-Correcting Wind Tunnel," Windtunnel Design and Testing Techniques, AGARD-CP-174, Oct. 1975.

7. Spaid, F. W.; Hurley, F. X. and Hellman, T. H.: "Miniature Probe for Transonic Flow Direction Measurements," AIAA Jour. Vol. 13, No. 2, Feb. 1975, P. 253.

8. Bryer, D. W.; Walshe, D. E.; and Garner, H. C.: "Pressure Probes Selected for Three-Dimensional Flow Measurement," R.&M. No. 3037, 1958.

9. Schulze, W. M.; Ashby, Jr., G. C.; and Erwin, J. R.: "Several Combination Probes for Surveying Static and Total Pressure and Flow Direction," NACA TN 2830, Nov. 1952.

10. Pope, A.; and Goin, K. L: High-Speed Wind Tunnel Testing, Wiley, 1965.

11. Barry, F. W.: "Comparison of Flow-Direction Probes at Supersonic Speeds," J. Aero. Sci., Sept. 1961, P. 750-752.

12. Zumwalt, G. W.: "Conical Probes for Determination of Local Mach Numbers and Flow Direction in Supersonic Wing Tunnels," SCTM 355-60(71), Sandia Corp., Nov. 1960.

13. Couch, L. M.; and Brooks, Jr., C. W.: "Effect of Blockage Ratio on Drag and Pressure Distributions for Bodies of Revolution at Transonic Speeds," NASA TN D-7331, Nov. 1973.

14. Vahl, W. A. and Weirich, R. L.: "Calibration of 30° Included-Angle Cone for Determining Local Flow Conditions in Mach Number Range of 1.51 to 3.51," NASA TN D-4679, August 1968.

15. Norris, J. D.: "Calibration of Conical Pressure Probes for Determination of Local Flow Conditions at Mach Numbers from 3 to 6," NASA TN D-3076, Nov. 1965.

16. Hartley, M. S.; and Nichols, J. H.: "Effects of Rake Blockage on Flow Angularity Measurements at Transonic Mach Numbers in the AEDC-PWT 16-Foot Transonic Tunnel," Twenty-Fifth Supersonic Tunnel Assoc. Meeting, NASA Langley Research Center, May 1966 (referenced with author's permission).

17. Pankhurst, R. C. and Holder, D. W.: Wind Tunnel Technique, Pitman and Sons, Ltd., 1952.

18. Horstman, C. C. and Rose, W. C.: "Hot-Wire Anemometry in Transonic Flow," NASA TM X-62,495, Dec. 1975.

19. Johnson, D. A. and Rose, W. C.: "Laser Velocimeter and Hot-Wire Anemometer Comparison in a Supersonic Boundary Layer," AIAA Jour. (Tech. Notes), Vol. 13, No. 4, April 1975.

20. Rose, W. C. and Johnson, D. A.: "Turbulence in a Shock-Wave Boundary-Layer Interaction," AIAA Jour., Vol. 13, No. 7, July 195

21. Hot Wire-Hot Film-Ion Anemometer Systems, CAT/FORM 6560375, Thermo-Systems Inc., 1975.

22. Rosenberg, R. E.: "A Three Dimensional Hot-Wire Anemometry Technique Employing a Single Wire Probe," ARL 71-0039, March 1971.

23. Weeks, T. M.: "Reduction of Transonic Slotted Wall Interference by Means of Slat Contouring," AFFDL-TR-74-139, March 1975.

24. Maxwell, H. and Luchuk, W.: "Evaluation of a Wedge on a Force Balance as a Flow Angle Probe," AEDC-TR-74-110, Feb. 1975.

25. Raney, D. J.: "Flow Direction Measurements in Supersonic Wind Tunnels," Aero. Res. Coun. Lond., Current Papers No. 262, 1956.

26. Summers, W. E.; personal communication, AEDC, Feb. 1976.

27. Luchuk, W.: "Flow Angle Measurements Using a 2-Inch Span Cruciform-Wing Force Model," presented at 45th Semi-Annual STA meeting, Albuquerque, N.M., April 1976 (referenced with author's permission).

28. Lind, I. A.: "A Sensitive Flow Transition Probe," KTH Aero Memo FI 175, TRITA-FPT-019, Institutionen for Flygteknik Stockholm, Sweden, July 1975.

III.F. MEASUREMENT OF UNSTEADY FLOW DISTURBANCES

The need for measurements of flow unsteadiness was briefly reviewed in Section II.C.6. The primary objective of noise calibration of a wind tunnel is to obtain a measure of the fluctuations in static pressure and flow angularity that exist in the empty test section. Here a review will be given of the instrumentation that has been used to obtain this type of data. However, before discussing sensors, it is germain to note the amplitudes and frequencies of unsteady static pressure which characterize transonic tunnels.

In the center of transonic test sections the fluctuating pressure coefficient, defined as

$$\Delta C_p \equiv \frac{\langle p' \rangle}{q} \times 100 \quad \text{percent},$$

may range from 0.5% to 5% depending on the tunnel configuration, Mach number, and Reynolds number. Dougherty, et al. (Ref. 1) have noted a value of 0.45% corresponds to a level of sound which is typically radiated from turbulent boundary layers on solid test section walls. However, Hartzuiker, et al. (Ref. 2) have pointed out that ΔC_p actually decreases with increasing Reynolds number and ranges from 0.5% at $Re_x = 5.7 \times 10^6$ to an estimated 0.2% at $Re_x = 1.1 - 1.7 \times 10^8$, see Fig. 3.F.1. McCanless and Boone (Ref. 3) have reviewed noise measurements made in both perforated and slotted test sections. These authors note that in perforated-wall tunnels centerline measurements of ΔC_p tend to be lower (40-60%) than wall measurements; whereas, the opposite trend is found in slotted-wall tunnels. Generally, the edgetones generated by perforated-wall tunnels tend to make these tunnels noisier than slotted-wall tunnels.* For example, ΔC_p data for twelve perforated-wall tunnels range from 1% to 7.4%; whereas, data for five slotted-wall tunnels show a range of 0.5% to 2%, Ref. 3. A peak in ΔC_p is usually measured between $M = 0.70$ and 0.80 for both perforated and slotted-wall tunnels. The frequency spectra of noise at $M = 0.80$ is presented in Fig. 3.F.2 for nine different, continuous tunnels, Ref. 2. These data are representative of solid, perforated, and slotted-wall tunnels and are presented in terms of the Mabey spectrum parameter which is discussed next.

*Recent research indicates there are a number of ways to reduce the level of noise generated by edgetones, Refs. 1 and 4.

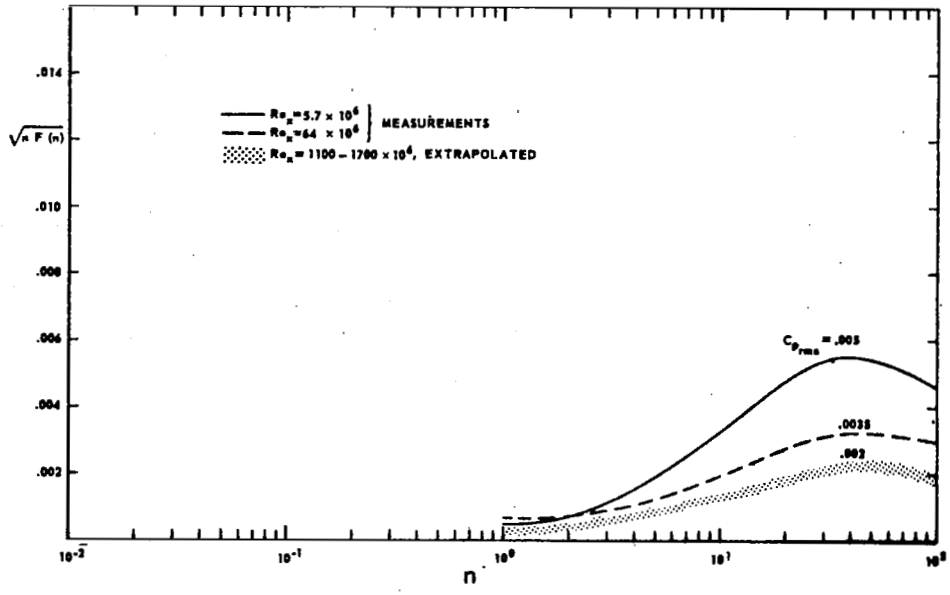

Fig. 3.F.1 FREQUENCY SPECTRA OF NOISE FROM A TURBULENT BOUNDARY LAYER ON A SOLID WALL, Ref. 2

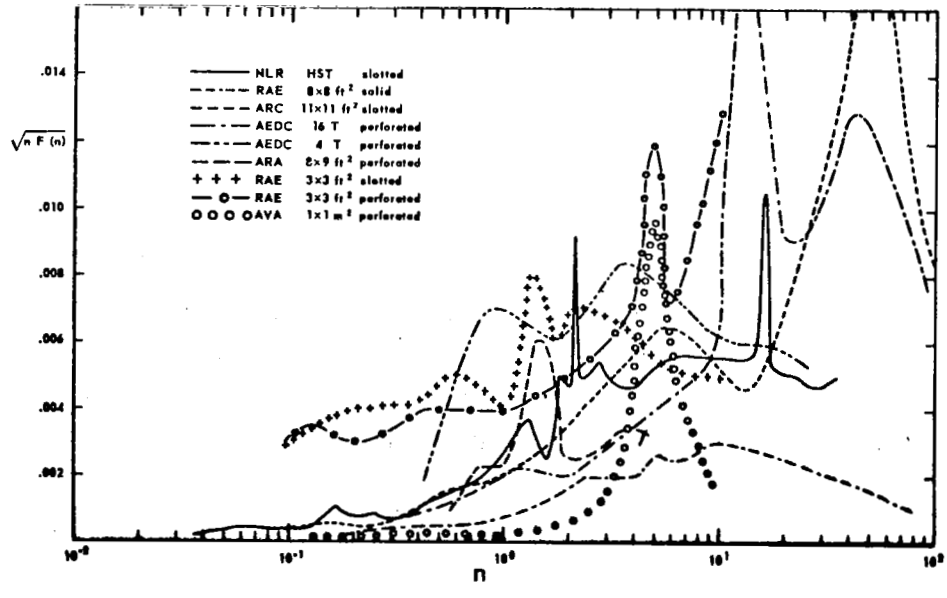

Fig. 3.F.2 NOISE FREQUENCY SPECTRA FOR SOME EXISTING CONTINUOUS WINDTUNNELS AT M_∞ = 0.80, Ref. 2

As noted by Hartzuiker, et al. (Ref. 2)*, flow quality can affect the results of tests on: (1) dynamic stability, (2) static forces and moments, (3) buffet, and (4) flutter. Tests of these quantities generally involve increasingly higher frequencies in the order listed. Apparently, little work has been done to measure fluctuations in flow angularity and correlate these with pressure fluctuations. However, Mabey (Refs. 5-7) and Hartzuiker, et al. (Ref. 2) have found the effects on model tests of both pressure and incidence fluctuations can be correlated by using a spectrum function defined as follows:

$$\Delta C_p^2 = \int_0^\infty F(n)dn \qquad (3.F.1)$$

Here ΔC_p^2 is the mean-squared value of the fluctuating static pressure coefficient, and $F(n)$ is the contribution to ΔC_p^2 per unit bandwidth at the reduced frequency n. Mabey has suggested

$$\sqrt{n\,F(n)} = \Delta C_p(n)\,\sqrt{n/\Delta n} \qquad (3.F.2)$$

can be used to measure windtunnel flow unsteadiness if the reduced frequency is chosen to correspond to a natural frequency of the model, e.g., fundamental wing bending mode, torsion mode, etc. A variety of tests have shown that greater model excitation follows increases in $nF(n)$. Thus, criteria for acceptable flow quality can be established for various types of tests by successively reducing $nF(n)$ until the results approach an asymptote and cease to vary significantly with tunnel flow quality. For example, analyses of buffet measurements on aircraft models with different natural frequencies led Mabey (Ref. 7) to conclude that an acceptable level of flow unsteadiness for the detection of light buffeting is $\sqrt{nF(n)} < 0.002$. Tests at other facilities have confirmed the usefulness of Mabey's spectrum parameter for correlating a variety of dynamic model tests, e.g., Hartzuiker, et al. (Ref. 2). Unfortunately, a precise boundary cannot be drawn to separate acceptable from unacceptable levels of flow unsteadiness. Rather, there is a "gray region" separating flow qualities that are either acceptable or not for a given type of test.

---

*Reference 2 is mainly concerned with estimating the flow quality that will be necessary to make the LEHRT cost-effective in light of the planned 10 sec run time.

However, the utility of including fluctuating pressure measurements in tunnel calibration is now well established.

Condenser microphone measurements on the AEDC 10 deg transition cone, in six different transonic tunnels, indicate 98 percent of the energy of background pressure fluctuations are contained within 0-20 KHz, Ref. 8. However, since there is presently no criterion for an upper limit on frequency beyond which boundary layer transition is unaffected, Westley (Ref. 9) recommends that the frequency range of noise measurements extend at least up to 30 KHz.

Thus, acoustic calibration of transonic tunnels requires instrumentation that can measure dynamic pressures with these ranges of amplitudes and frequencies. The sensors employed should also be relatively insensitive to vibrations of the mounting surface and durable enough not to be easily damaged by either particles in the flow or overloading.

III.F.1. Dynamic Pressure Measurements

A rather wide variety of instrumentation has been used to measure unsteady flow disturbances in wind tunnels. Condenser microphones, strain gage, and piezoelectric dynamic pressure transducers have been employed for noise measurements in stilling and plenum chambers, diffusers, and on test section walls, and models and probes located on the centerline, Refs. 10-15. In addition, hot-wire anemometers have been used to measure flow disturbances in stilling chambers (e.g., Ref. 13) and in the test section of transonic tunnels (e.g., Refs. 9 and 16) and supersonic tunnels (e.g., Ref. 17). Also, laser Doppler velocimeters (LDV) are being used to measure turbulence by an ever increasing number of tunnel operators, Ref. 9.

Unfortunately, this lack of standardization makes it difficult to compare measured levels of flow disturbances. For example, Lewis and Dods (Ref. 18) noted significant variations in the frequency response of 12 different microphones and dynamic pressure transducers. In general, Lewis and Dods found small diameter transducers (0.1 to 0.3 cm) gave higher power-spectral-density values, at all frequencies, than larger diameter transducers (0.5 to 1 cm). Also, the high frequency portion of the spectrum of pressure fluctuations varies with the particular sensor, and as is well known, the rms values will be underestimated when a significant portion of the high frequencies are attenuated. In

addition, when measuring vorticity with hot-wires, hot-films, or an LDV, the data may also vary because of differences in frequency response.

The comparison problem is compounded further by the choice of sensor mounting. Ideally, acoustic pressures should be measured with no relative motion between sensor and the test medium, Ref. 19. However, since this is neither practical nor relevant to wind tunnel model testing, some representative location on a probe, model or tunnel wall must be selected.

The first measurements of wall pressure fluctuations beneath turbulent boundary layers in a wind tunnel were reported by Willmarth in 1956 (Ref. 20). Willmarth (Ref. 21) has recently reviewed the problems of dynamic pressure measurements at tunnel walls and notes that most of these measurements have been made with flush-mounted transducers. Hanly (Ref. 22) has recently studied the effect of sensor flushness on fluctuating-surface-pressure measurements at M = 1.68, 2.0, and 2.5. These tests show spectral pressure measurements are extremely sensitive to flushness with protrusion causing greater error than submergence. Hanly concludes that more repeatable data can be obtained with transducers mounted approximately 0.0254 cm (0.01 in.) beneath a surface orifice. Thus, it is recommended that acoustic measurements at tunnel walls conform to this criterion.

Also, it is relevant to note here that two or more wall-mounted transducers can be used to determine useful correlations between disturbances which may exist in a tunnel, e.g., Refs. 11 and 25. In addition, Boone and McCanless (Ref. 11) have noted that wall data can be used to extrapolate, through M = 1, measurements obtained at the centerline with probes or models which may be subject to oscillating shocks and/or other model-induced unsteadiness near Mach one. However, experience (Ref. 8) with microphone measurements on a 10 deg cone indicates (1) this is not a problem and (2) the real advantage of a wall-mounted sensor is that it can be calibrated with respect to centerline measurements and used as a permanent monitor for assessing any subsequent changes in tunnel flow unsteadiness.

Concerning installation of sensors in perforated walls, Credle and Shadow (Ref. 24) mounted a 0.635 cm (1/4 in.) piezoelectric microphone in the center of an area which was filled and sanded smooth. The radius of the area was

approximately 40 microphone diameters. These investigators stated:

> "This installation technique precluded the measurement of purely near-field influence of the most adjacent upstream holes and allowed for the measurement of what might be considered as the radially integrated average value of pressure fluctuations at the wall surface."

Credle and Shadow also installed an identical, but shielded, microphone in the wall in order to monitor microphone response to wall vibration. In general, it is considered good testing practice to ascertain the component of a microphone's output which is due to vibration. Finally, questionnaire results indicated that strain-gage transducers are most often used for acoustic measurements at wind tunnel walls. Presumably, this is because the instrumentation required to process the signal from a strain gage is readily available at most wind tunnels.

In addition to tunnel wall measurements, tunnel noise calibrations require dynamic pressure data near the center of the test section. Some of the first such measurements in a transonic tunnel were reported by Chevalier and Todd (Ref. 25). In these initial tests, dynamic pressure transducers were mounted on a wedge, a wing probe, and an ogive-cylinder. Later acoustic measurements in the AEDC-PWT 16T and 16S tunnels were performed with condenser microphones and strain gage transducers mounted on a 10 deg included-angle cone, Ref. 10.

A variety of other probe geometries have also been used. For example, an ogive-cylinder and a flat plate have been used in some of the NASA Ames tunnels, Ref. 23. A 10 deg cone-cylinder probe has been used in the 8 x 6-ft. Supersonic Wind Tunnel at NASA Lewis, Ref. 26. As part of a review of probes for acoustic calibration, Boone and McCanless (Ref. 11) considered slender cones, wedges, flat plates, hemispheres, and sharp-tipped, flow-thru, circular cylinders. These authors recommended a 10 deg apex-angle conical probe for wind tunnel acoustic measurements because:

1. cones are not as sensitive to tip flow as wedges and flat plates,
2. the transonic Mach number range, where unstable shock waves occur, is smaller for slender cones than for flat plates, flow-thru cylinders, and hemispheres,
3. a slender cone introduces minimal disturbance to the flow.

As noted by Credle and Shadow (Ref. 24), a smaller angle cone is preferred, but a 10 deg cone is about the minimum angle which will allow installation of

instrumentation under a laminar boundary layer. These same authors also reported that by 1970 the 10 deg cone had become a standard device at AEDC for calibrating wind tunnel flow disturbances.

Up to this time the AEDC acoustic calibration cone had two flats, located 180 deg apart, for flush mounting of sensors. By 1970 experience with this cone indicated satisfactory noise measurements could probably be made with a completely symmetrical cone and two 0.635 cm (1/4 in.) condenser microphones. Furthermore, the surface of the cone was polished to an rms finish of 3 microns* and a traversing Pitot probe mechanism was mounted aft of the cone for boundary layer transition studies, Ref. 27. This subsequently became known as the AEDC transition cone and has now been used to measure dynamic flow quality in over 18 domestic and foreign tunnels, Refs. 8, 28 and 29.

The work of Dougherty with the AEDC transition cone and the correlations of Pate and Schueler (Ref. 30) and Benek and High (Ref. 31) have established a direct relationship between ΔC_p and boundary layer transition. In addition to providing a common measure of dynamic flow quality, Treon, et al. (Ref. 32) reported data from the AEDC transition cone enabled better agreement to be obtained in a series of tests on a transport aircraft model. In these tests, the same model was tested in the AEDC-PWT 16T, the NASA Ames 11-ft. Transonic Wind Tunnel, and the Calspan 8-ft. Transonic Tunnel, and differences in drag coefficients, measured at zero-normal-force, were found to be less when a correction factor was used to account for relative Reynolds number effects between facilities. An effective Reynolds number for the Calspan and Ames tunnels, relative to the AEDC 16T tunnel, was defined on the basis of a common, boundary-layer-transition length. Thus, the utility of a standard acoustic calibration device has been demonstrated. Subsequent to a planned flight calibration, this device will also be useful in correlating tunnel and free-flight conditions.

Because of the demonstrated utility of the AEDC transition cone and its past use in a number of major facilities, Westley (Ref. 9) recommends noise and turbulence levels in transonic tunnels be measured with two 10 deg cones fitted, respectively, with:

*Apparently, the surface finish was later improved to 0.25 microns, Ref. 8.

1. skin-friction gages to determine transition Reynolds numbers and flush-mounted microphones to measure noise levels on the test section centerline,

2. a crossed hot-wire anemometer mounted on the tip (an ONERA design).

The proposal to eliminate the traversing probe mechanism will reduce probe induced noise* and wind tunnel blockage. Although Westley's recommendation is not specific, it is assumed that he is not recommending floating-element skin-friction balances but rather heat transfer devices such as thin-films or thermocouples for transition detection, e.g., Refs. 11, 34 and 35. With regard to hot-wire measurements, Westley expresses a concensus that these instruments are ideal for measuring disturbances in a wind tunnel test section. Because of this importance and the fact that recent research has demonstrated hot-wires can be used effectively in some transonic test sections (Ref. 16), they are discussed separately in Appendix I.

Alternate Acoustic Calibration Probes

Not only would the AEDC transition cone be expensive to reproduce, but noise measurements on it are susceptible to a number of probe-induced errors. Credle and Shadow (Ref. 24) observed that pressure gradients exist on a cone at subsonic and transonic speeds, and hence acoustic measurements are influenced by both static and total pressure gradients. A laminar boundary layer may modulate acoustic disturbances which pass through it to an underlying sensor, Ref. 9. Also, Siddon (Ref. 36) has shown that both axial and lateral fluctuations can cause errors in measurements of ΔC_p with probes. Hence, other probe alternatives may offer some advantages for acoustic calibration of wind tunnels.

The following concise summary of Siddon's work (Ref. 36) is extracted from Willmarth's article (Ref. 21). ---"Siddon has reported construction of an excellent probe for unsteady static-pressure measurements, and he has calibrated it in various contrived flows to remove the errors caused by the interaction

*Credle (Ref. 33) noted earlier that the traversing probe support structure appeared to generate additional noise, based on comparisons with acoustic data obtained on an ogive-cylinder and the AEDC 10 deg cone with flats.

of the body of the probe with streamwise and cross-flow velocity fluctuations. The pressure is transmitted to the diaphragm of a miniature condensor microphone (0.25 dm diam.) inside the probe (0.305 cm diam.) through an annular slit approximately 2 diameters downstream from the tip of the balsa wood, ogive nose. A 0.318 cm (1/8 in.) collar around the probe, downstream of the slit, was carefully positioned to make the steady pressure at the slit equal to the free-stream static pressure when there is no cross flow. The probe-collar compensation was checked at zero angle of attack in a flow with sinusoidal axial velocity fluctuations and was found adequate.

"Siddon's unique achievement is the development of a compensation scheme to cancel the pressure fluctuations produced by cross-flow fluctuations. His scheme is based upon an earlier transducer in which piezoelectric force-sensing elements were used to measure lift fluctuations of a small airfoil, which are proportional to velocity fluctuations normal to the airfoil when the angle-of-attack fluctuations are small. In the present case Siddon used an arrangement of four piezoelectric Bimorph plate elements in an I-beam configuration to measure the orthogonal bending moments produced by cross-flow-induced transverse forces on the nose of the probe. If quasi-steady, slender-body, aerodynamic theory is applicable, the transverse force will be proportional to the instantaneous transverse velocity at the nose. The two electrical signals representing the orthogonal components of transverse velocity were each squared and summed with analog-computer elements to obtain a signal proportional to the square of the transverse velocity. A fraction of this signal was added to the pressure measured by the condensor microphone to give (approximately) the true static-pressure fluctuations that would have existed in the absence of the probe.

"Siddon calibrated the probe in a flow produced by a jet of air passed through a rotating inclined nozzle. The probe slit was placed at the point where the static pressure is constant (the intersection of the nozzle axis and the axis of rotation). At that point any fluctuating pressure signals from the condensor microphone were assumed to be produced by cross-flow interaction with the probe. These signals were cancelled by addition of the proper fraction of the square of the transverse velocity.

"Siddon concluded that the error in the pressure produced by cross-flow interaction in turbulence was less than 20 percent. Thus, reasonably accurate measurements of fluctuating pressure could be made as long as the assumption of quasi-steady flow was not violated and the time lag between the transverse-force signal from the probe nose and the pressure measured at the annular slit was not important. Generally, this requires that the spatial scale of the pressure fluctuations be much larger than the probe dimensions.* As a result of his work Siddon was able to conclude that in many practical circumstances where only root-mean-square pressure fluctuations were measured with probes like Strasberg's (Ref. 37), the correction for cross-flow interaction is likely to be small. Owing to differences in the corrected and uncorrected wave forms, one must use the corrected pressure when instantaneous values are desired; even when the corrected and uncorrected root-mean-square pressures are the same."

Thus, for a number of aerodynamics and acoustic reasons, as well as simplicity and economy, Westley (Ref. 9) notes that a number of operators of transonic and supersonic tunnels are measuring fluctuating static and pitot pressures. He recommends that these types of acoustic probes be developed and standardized. Dynamic static pressure probes should be developed for high speed flows and probably should follow the Siddon type design.

In the case of dynamic Pitot probes, a series of design studies at NASA Langley has culminated in a design which appears to be satisfactory for acoustic calibration of wind tunnels, Refs. 38, 35 and 14. A schematic of the probe reported in Ref. 14 is shown in Fig. 3.F.3. Briefly, it consists of two 0.318 cm (1/8 in.) diameter piezoelectric transducers mounted in tandem. The probe diameter of 0.635 cm (1/4 in.) was selected because mean pressure measurements indicate the pressure is nearly constant across the center of a flat-faced disk in supersonic flow. The diaphragm of the exposed transducer is covered with a thin coating of RTV rubber to reduce vulnerability to damage by particles in the flow. The purpose of the shielded rear transducer is to serve as an acceleration (or vibration) monitor. The signal from this transducer is subtracted from the exposed transducer in order to account for the effects

*The underlining was inserted by the present authors to point out that the size of the AEDC transition cone may induce errors in noise measurements.

All Dimensions in Centimeters

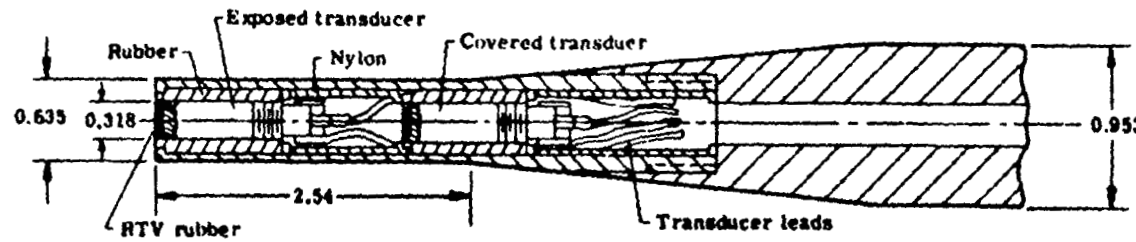

Figure 3.F.3. SMALL PIEZOELECTRIC DYNAMIC PRESSURE PROBE, Ref. 14

of probe vibration.* In order for this technique to be valid, Anders, et al. (Ref.14) noted that the two transducers must be matched to give identical outputs for given acceleration levels.

In conjunction with the probe, a hot wire was also used in the stilling chamber and test section of a small Mach 5 wind tunnel at NASA Langley. Assuming purely acoustical disturbances, the following relation was used to relate the fluctuating static pressures obtained from the hot wire to fluctuating Pitot pressures.

$$\left[\frac{\langle H'_2\rangle}{\bar{H}_2}\right]^2 = \left(\frac{\langle P'_\infty\rangle}{\gamma \bar{P}_\infty}\right)^2 \left[1 - \frac{4}{M^2}\left(\frac{V_\infty}{u_s - V_\infty}\right) + \frac{4}{M^4}\left(\frac{V_\infty}{u_s - V_\infty}\right)^2\right] \qquad (3.F.1)$$

Here $\langle H'_2\rangle$ is the rms fluctuating total pressure behind a normal shock, $\langle P'_\infty\rangle$ is the rms fluctuating, freestream static pressure, and u_s is the sound-source velocity detected by the hot wire. The results from this equation gave excellent agreement with the fluctuating Pitot probe data, e.g., see Appendix I, Fig. 7. It is relevant to note here the conclusion reached by Anders, et al. (Ref. 14).

> "The hot wire and Pitot probe generally indicate the same trend and level with respect to the Reynolds number. This agreement is of great practical importance since the piezoelectric Pitot probe is a much more rugged instrument with simpler data reduction procedures than the hot-wire probe. For diagnostic studies, the Pitot probe can provide essentially the same information as the hot-wire probe with much less effort. However, the hot wire does have one particular advantage in the present investigation. That is, in a pure sound field the hot wire can distinguish between moving sources and fixed sources."

A similar comparison of hot wire data with fluctuating Pitot probe data has been reported by Grande and Oates (Ref. 39). However, a 1.78 mm (0.070 in.) diameter strain gage transducer was employed and data were obtained for $1.1 < M < 2.25$. Nondimensionalized power spectral densities obtained in a turbulent boundary layer and in the freestream were found to agree remarkably

*Dougherty and Steinle (Ref. 8) report that the accelerometer used in the AEDC transition cone has not detected any significant vibration effects during tests in a number of tunnels. However, Stainback, et al. (Ref. 35) did report significant probe vibration effects.

well. These authors conclude that "the frequency response characteristics of the stagnation pressure sensor are identical to those of the hot wire, i.e., it can be considered an ideal point sensor for fluctuations with spatial scales somewhat larger than the probe diameter."

To summarize the advantages and disadvantages of fluctuating Pitot probes, the following points are noted.

Disadvantages:

1. cannot separate the three possible flow disturbance modes of entropy, vorticity and pressure.
2. cannot deduce whether disturbance sources are stationary or moving.
3. shock modulation of disturbances may be unknown in some cases (e.g., see Ref. 39).

Advantages:

1. relatively inexpensive and off-the-shelf, commercial transducers are readily available.
2. speed and ease of measurement.
3. simpler data reduction.
4. durable, i.e., far less susceptible to particle damage compared to hot wires.
5. high signal to noise ratio.
6. reduced influence of flow perturbations associated with finite probe size (compared with the AEDC transition cone).
7. minimum wall-probe interference.
8. easily moved about to survey entire test section.

In conclusion, recent research with fluctuating Pitot probes indicates these instruments may be adequate for initial calibration of flow disturbances in transonic and supersonic tunnels. This type of measurement could serve as

a convenient and inexpensive standard to compare tunnel noise levels. It is also relevant to note that Dougherty of the Propulsion Wind Tunnel group at AEDC plans to use a fluctuating Pitot probe to monitor freestream disturbance levels during flight tests with the AEDC transition cone.

III.F. References

1. Dougherty, N. S.; Anderson, C. F.; and Parker, R. L.: "An Experimental Investigation of Techniques to Suppress Edgetones from Perforated Wind Tunnel Walls," AEDC-TR-75-88, Aug. 1975.

2. Hartzuiker, J. P.; Pugh, P. G.; Lorenz-Meyer, W.; and Fasso, G. E.: "On the Flow Quality Necessary for the Large European High-Reynolds-Number Transonic Windtunnel LEHRT," AGARD-R-644, March 1976.

3. McCanless, G. F. and Boone, J. R.: "Noise Reduction in Transonic Wind Tunnels," J. Acoust. Soc. Am., Vol. 56, No. 5, Nov. 1974.

4. Schutzenhofer, L. A. and Howard, P. W.: "Suppression of Background Noise in a Transonic Wind-Tunnel Test Section," AIAA Jour., Nov. 1975.

5. Mabey, D. G.: "Flow Unsteadiness and Model Vibration in Wind Tunnels at Subsonic and Transonic Speeds," C.P. No. 1155, Aero. Res. Coun., 1971.

6. Mabey, D. G.: "An Hypothesis for the Prediction of Flight Penetration of Wing Buffeting from Dynamic Tests on Wind Tunnel Models," RAE TR 70189, Oct. 1970.

7. Mabey, D. G.: "The Influence of Flow Unsteadiness on Windtunnel Measurements at Transonic Speeds," RAE Tech. Memo. Aero. 1473, 1973.

8. Dougherty, N. S. and Steinle, F. W.: "Transition Reynolds Number Comparisons in Several Major Transonic Tunnels," AIAA Paper No. 74-627, July 1974.

9. Westley, R.: "Problems of Noise Measurement in Ground-Based Facilities with Forward-Speed Simulation (High-Speed Wind Tunnel Noise)," Appendix 5 of AGARD-AR-83, Sept. 1975.

10. Riddle, C. D.: "Investigation of Free-Stream Fluctuating Pressures in the 16-Ft. Tunnels of the Propulsion Wind Tunnel Facility," AEDC-TR-67-167, Aug. 1967.

11. Boone, J. R. and McCanless, G. F.: "Evaluation of the Acoustic Sources of Background Noise in Wind Tunnel Facilities," NASA CR-98155.

12. Boone, J. R. and McCanless, G. F.: "Application of the Techniques for Evaluating the Acoustic Sources of Background Noise in Wind Tunnel Facilities," Tech. Rept. HSM-R05-69, Chrysler Huntsville Operations, Mar. 1969.

13. Credle, O. P.: "An Evaluation of the Fluctuating Airborne Environments in the AEDC-PWT 4-Ft. Transonic Tunnel," AEDC-TR-69-236, Nov. 1969.

14. Anders, J. B.; Stainback, P. C.; Keefe, L. R.; and Beckwith, I. E.: "Sound and Fluctuating Disturbance Measurements in the Settling Chamber and Test Section of a Small, Mach 5 Wind Tunnel," ICIASF '75, Int'l Congress on Instrumentation in Aerospace Simulation Facilities, Ottawa, Canada, Sept. 22-24, 1975, published by IEEE, 345 E. 47th Street, New York.

15. Anders, J. B.; Stainback, P. C.; Keefe, L. R.; and Beckwith, I. E.: "Fluctuating Disturbances in a Mach 5 Wind Tunnel," Proc. AIAA 9th Aerodynamics Testing Conference, June 1976.

16. Horstman, C. C. and Rose, W. C.: "Hot Wire Anemometry in Transonic Flow," NASA TM X-62495, Dec. 1975.

17. Donaldson, J. C. and Wallace, J. P.: "Flow Fluctuation Measurements at Mach Number 4 in the Test Section of the 12-Inch Supersonic Tunnel (D)," AEDC TR-71-143, Aug. 1971.

18. Lewis, T. L. and Dods, J. B.: "Wind-Tunnel Measurements of Surface-Pressure Fluctuations at Mach Numbers of 1.6, 2.0, and 2.5 Using 12 Different Transducers," NASA TN D-7087, Oct. 1972.

19. Fuchs, H. V.: "Measurement of Pressure Fluctuations Within Subsonic Turbulent Jets," J. Sound & Vib., Vol. 22, No. 3, 8 June 1972.

20. Willmarth, W. W.: "Pressure Fluctuations Beneath Turbulent Boundary Layers," Annual Review of Fluid Mechanics, Vol. 7, Annual Review Inc., Palo Alto, Calif., 1975.

21. Willmarth, W. W.: "Unsteady Force and Pressure Measurements," Annual Review of Fluid Mechanics, Vol. 3, Annual Review Inc., Palo Alto, Calif., 1971.

22. Hanly, R. D.: "Effects of Transducer Flushness on Fluctuating Surface Pressure Measurements, AIAA Paper No. 75-534, Mar. 1975.

23. Dods, J. B. and Hanly, R. D.: "Evaluation of Transonic and Supersonic Wind-Tunnel Background Noise and Effects of Surface Pressure Fluctuation Measurements," AIAA Paper No. 72-1004, Sept. 1972.

24. Credle, O. P. and Shadow, T. O.: "Evaluation of the Overall Root-Mean-Square Fluctuating Pressure Levels in the AEDC PWT 16-Ft. Transonic Tunnel," AEDC-TR-70-7, Feb. 1970.

25. Chevalier, H. L. and Todd, H. E.: "Measurement of the Pressure Fluctuations in the Test Section of the 16-Foot Transonic Circuit in the Frequency Range from 5 to 1000 cps," AEDC-TN-61-51 (AD 255 763), May 1961.

26. Karabinus, R. J. and Sanders, B. W.: "Measurements of Fluctuating Pressures in 8-by 6-Foot Supersonic Wind Tunnel for Mach Number Range of 0.56 to 2.07," NASA TM X-2009, May 1970.

27. Credle, O. P. and Carleton, W. E.: "Determination of Transition Reynolds Number in the Transonic Mach Number Range," AEDC-TR-70-218, Oct. 1970.

28. Dougherty, N. S., Jr.: "Prepared Comment on Cone Transition Reynolds Number Data Correlation Study," AGARD-CP-187, June 1975.

29. Whitfield, J. and Dougherty, N. S., Jr.: "A Survey of Transition Reynolds Number Work at AEDC," to be presented at AGARD Fluid Dynamics Panel Symposium on Laminar-Turbulent Transition, Copenhagen, Denmark, May 1977.

30. Pate, S. R. and Schueler, C. J.: "Radiated Aerodynamic Noise Effects on Boundary Layer Transition in Supersonic and Hypersonic Wind Tunnels," AIAA Jour., Vol. 7, No. 7, Mar. 1969.

31. Benek, J. A. and High, M. D.: "A Method for the Prediction of the Effects of Free-Stream Disturbances on Boundary-Layer Transition," AEDC-TR-73-158, Oct. 1973, also AIAA Jour., P. 1425, Oct. 1974.

32. Treon, S. L.; Steinle, F. W.; Hagerman, J. R.; Black, J. A., and Buffington, R. J.: "Further Correlation of Data from Investigations of a High-Subsonic-Speed Transport Aircraft Model in Three Major Transonic Wind Tunnels," AIAA Paper No.71-291, Mar. 1971.

33. Credle, O. P.: "Perforated Wall Noise in the AEDC-PWT 16-Ft. and 4-Ft. Transonic Tunnels," AEDC-TR-71-216, Oct. 1971.

34. Heller, H. H. and Clemente, A. R.: "Fluctuating Surface - Pressure Characteristics on Slender Cones in Subsonic, Supersonic, and Hypersonic Mach-Number Flow," NASA CR-2449, Oct. 1974.

35. Stainback, P. C.; Wagner, R. D.; Owen, F. K.; and Horstman, C. C.: "Experimental Studies of Hypersonic Boundary-Layer Transition and Effects of Wind-Tunnel Disturbances," NASA TN D-7453, Mar. 1974.

36. Siddon, T. E.: "On the Response of Pressure Measuring Instrumentation in Unsteady Flow," UTIAS Rept. No. 136, Institute for Aerospace Studies, Univ. of Toronto, Jan. 1969.

37. Strasberg, M.: "Measurements of the Fluctuating Static and Total-Head Pressures in a Turbulent Wake," David Taylor Model Basin Rept. 1779, (AD 428 700), Dec. 1963 (also AGARD Rept. 464).

38. Stainback, P. C. and Wagner, R. D.: "A Comparison of Disturbance Levels Measured in Hypersonic Tunnels Using a Hot-Wire Anemometer and a Pitot Pressure Probe," AIAA Paper No. 72-1003, Sept. 1972.

39. Grande, E. and Oates, G. C.: "Response of Miniature Pressure Transducers to Fluctuations in Supersonic Flow," Instrumentation for Airbreathing Propulsion, Progress in Astronautics and Aeronautics, AIAA Vol. 34, MIT Press, 1972.

III.G. TRANSONIC TUNNEL BOUNDARY CONDITIONS AND WALL INTERFERENCE

III.G.1. Conventional Ventilated Walls

The history of development of ventilated walls for transonic tunnels has been reviewed by Goethert (Ref. 1). The three primary milestones in this development were as follows:

1. Theoretical analyses in Germany, Italy, and Japan during the 1930's indicated tunnel walls with proper arrangement of longitudinal slots would provide wall-interference-free flow simulation. This work was interrupted by World War II.
2. During 1946, Wright and Ward (Ref. 2) developed a "subsonic theory for solid-blockage interference in circular wind tunnels with walls slotted in the direction of flow." Subsequently, a 12-in. diameter tunnel was designed with ten evenly spaced slots providing a total openness ratio of one-eighth. The tunnel was put into operation in 1947. This design did indeed prevent choking and enabled testing thru Mach one of a model with 8.5% blockage.
3. Unfortunately, the solid slats in slotted tunnels were found to cause significant reflections of bow shocks and expansion waves at supersonic speeds. Thus, around 1950 theoretical analyses at Cornell Aeronautical Laboratory* indicated better shock wave cancellation could be achieved with small-grain porous walls, Goodman (Ref. 3). Unfortunately, exploratory tests showed such walls clog easily, and even worse, the porosity needed to vary with each change in Mach number and/or shock strength. As an outgrowth of this work, the now familiar perforated wall was selected as a convenient compromise.

The early mathematical models of tunnel-wall-interference were based on the governing differential equation for perturbation velocity potential in subsonic, compressible flow, e.g., Baldwin, et al. (Ref. 4).

$$\beta \frac{\partial^2 \phi}{\partial x^2} + \frac{\partial^2 \phi}{\partial y^2} + \frac{\partial^2 \phi}{\partial z^2} = 0 \qquad (3.G.1)$$

*The current name of this facility is Calspan.

If the wall is solid, the boundary condition for no flow through the wall is

$$\frac{\partial \phi}{\partial n} = 0 \quad \text{at solid wall.} \tag{3.G.2}$$

In the case of an open-jet, there can be no pressure difference across the boundary; thus

$$\frac{\partial \phi}{\partial x} = 0 \quad \text{at open boundary.} \tag{3.G.3}$$

The corrections to measured values of model lift and pitching moment, which result when solving Eq. (3.G.1) with either solid or open-wall boundary conditions, are discussed in detail by Garner, et al. (Ref. 5). The theoretical results generally agree with experiments. In order to facilitate applications of this type of boundary-induced corrections, Heyson (Ref. 6) has compiled solutions in the form of curves and charts.

In the case of ventilated walls, the boundary conditions become more complex. In fact, the central problem of theoretical analysis of transonic-wall-interference is selection of the appropriate boundary conditions to use with Eq. (3.G.1). This is still an area of active research, and only a brief review of boundary conditions for ventilated tunnels will be given here.

An approximate boundary condition for porous walls was derived by Goodman (Ref. 3, Part II), viz.,

$$\frac{\partial \phi}{\partial x} + \frac{1}{R} \frac{\partial \phi}{\partial n} = 0 \quad \text{at ideal, porous wall.} \tag{3.G.4}$$

This boundary condition was derived by assuming the average velocity normal to the wall is proportional to the pressure drop through the wall (a linearized approximation to viscous flow through the wall), and that the pressure outside the wall is equal to freestream static. The value of R, for a given wall, is usually determined experimentally by measuring pressure drop and the associated mass flow through a wall sample (e.g. Ref. 7), i.e.,

$$R = -\frac{\phi_n}{\phi_x} = \frac{2\, v_n/U_\infty}{\Delta P/q_\infty} = \frac{2\, \dot{m}_w/\dot{m}_\infty}{\Delta P/q_\infty} \qquad (3.G.5)$$

An approximate, uniform boundary condition for slotted walls was derived by Baldwin, et al. (Ref. 4).

$$\frac{\partial \phi}{\partial x} + K \frac{\partial^2 \phi}{\partial x \partial n} = 0 \quad \text{at ideal, slotted wall} \qquad (3.G.6)$$

where K is related to slot geometry by

$$K = \frac{D_s}{\pi} \ln \{\csc (\frac{\pi}{2} \frac{W_s}{D_s})\} , \qquad (3.G.7)$$

and

D_s = distance between slot centers,

W_s = width of slots.

In an attempt to account for viscous effects, Baldwin, et al. suggested adding the porous boundary condition to Eq. (3.G.6) and measuring R for the slot of interest.

$$\frac{\partial \phi}{\partial x} + K \frac{\partial^2 \phi}{\partial x \partial n} + \frac{1}{R_s} \frac{\partial \phi}{\partial n} = 0 \text{ at viscous, slotted wall} \qquad (3.G.8)$$

Keller (Ref. 8) has recently suggested this boundary condition be extended to include varying slot width by replacing $1/R_s$ with $1/R_s + \partial K/\partial x$.

After more than two decades of testing and comparisons of theory with experimental results, it is now generally recognized that application of the linear boundary conditions, with constant values of K and/or R, is inadequate. As an example of this discrepancy, a brief summary of a typical case is presented here.

Lowe (Ref. 9) measured the wall porosity parameter for a wall with 22.5% porosity and normal holes. The standard porosity parameter, R, was determined experimentally by measuring the static pressure drop and mass flow across a

9-inch by 21-inch section of a sidewall of the General Dynamics 4-foot High Speed Wind Tunnel. Data were obtained for Mach numbers of 0.5, 0.7, and 0.9 and a corresponding unit Reynolds number range of 19.7 to 37.7 million (per meter). Using the measured values of R and the results of linear perturbation theory obtained by Lo and Oliver (Ref. 10), the upwash and streamline curvature corrections indicated the wall did not have the characteristics of an open jet. This contradicted the results of tests with an aircraft force model which,when corrected for open-boundary interference,agreed with data obtained with the same model in the Langley 8' Transonic Pressure Tunnel (Ref. 11)*. Thus, the results of Lowe, as well as others, indicate the measurement of R and use of the classical, linear perturbation theory is not very useful for calibrating the effects of transonic wind tunnel walls. If, in general, this approach to correcting for wall interference had proven successful, measurements of R for porous and slotted tunnels would have become a standard part of transonic tunnel calibration.

The current consensus is: the true, transonic-tunnel boundary conditions are dependent on the local flow conditions near the wall. This, in turn, means a dependence on both tunnel operating conditions and the particular model configuration, e.g., Newman and Klunker (Ref. 14). Recent efforts to obtain improved boundary conditions for fixed (passive) wall conditions include the study of variations in R between top and bottom perforated walls, Ref. 15, and nonlinear boundary conditions for walls with normal holes, Ref. 16, and slotted walls, e.g., Refs. 17 and 18. Of course, the basic objective of these studies is to attain data correction procedures which can reliably account for the effects of real, ventilated walls.

III.G.2. Adaptive Wall Studies

The difficulties in applying transonic wall corrections, which do not reduce to simple modifications of speed and angle of attack, are well known. Also, one of the conclusions obtained with the conventional, linear theory of wall effects is the impossibility of using uniform porosity to simultaneously

* The recent, supercritical airfoil tests of Blackwell and Pounds (Ref. 12) indicate the actual boundary condition shifts toward the free-jet as porosity increases, i.e., the transonic shock moves forward for a given Mach number. This same trend was also observed as a result of increased blockage in the supercritical cone-cylinder tests of Page (Ref. 13).

eliminate the effects of wall interference on both normal force and pitching moment, Ref. 16.

For these reasons, other procedures have been suggested and are currently being investigated. The theory developed by Ferri and Baronti (Ref. 19) and Sears (Ref. 20) seems to offer the promise of being more correct. These authors suggested that the pressure distribution and the streamline deflection angle be measured along the tunnel walls (outside the boundary layer) with a model in place. The scheme then involves calculation of (1) the flow-deflection angles which correspond to the measured pressure data and (2) the pressure distribution corresponding to the measured flow deflection angles. The difference between the measured and calculated pressure distributions and streamline deflections are then used to accomplish one of the following:

1. determine the wall porosity which eliminates wall interference for a given external pressure distribution,
2. provide the correct pressure distribution outside of the porous wall for a given porosity distribution,
3. determine wall contours to conform with free-air streamlines, or
4. calculate the wall corrections to be applied to the experimental results.

One of the advantages of this procedure is that it only requires the linearized perturbation equations to be valid near the wall. This means the procedure may be valid as long as supersonic pockets do not extend to the tunnel walls. The primary advantage of this procedure is that it uses data to establish the appropriate boundary conditions. However, as noted by Ferri and Baronti, the primary disadvantages are the requirements for "accurate measurements of flow deflections and pressure variations at several angular positions and at many stations along the test section."

In conjunction with the theory of Ferri and Baronti, an experimental program was begun in the 15" Trisonic Gasdynamics Facility at the Air Force Flight Dynamics Laboratory. Since streamline angles can be measured more accurately away from the wall, the theory was subsequently modified to use flow angles and static pressures measured at an intermediate "midfield" location between the model and wall. For angularity measurements, a new hot-film, 20 deg-wedge probe

was designed and fabricated. Calibration tests show it to be capable of resolving flow angles to within ±2 minutes of arc (Ref. 21). This probe, together with a conventional, cone-cylinder, static-pressure probe, provides the input required by the Ferri and Baronti theory.

Results of this work have demonstrated the feasibility of changing slotted-wall contour to minimize transonic-wall-interference with the flow over 6% thick biconvex airfoils at zero angle-of-attack. As expected, the results for nonzero angles-of-attack indicate the wall contour will need to be changed as changes in lift and/or model configuration are made. The study of lifting airfoil models is continuing. However, enough results are now available to conclude that this approach offers a decided advantage over the previous approach of measuring pressure drop and mass flow through a wall sample and then trying to use linear boundary conditions to estimate wall-model interference factors.

Work is also underway at the University of Southampton (England), Ref. 22, and ONERA (France), Ref. 23, on using adjustable, solid walls to conform with free-air streamlines.

Vidal, et al. (Ref. 24) have reported on recent progress with the Calspan one-foot, self-correcting tunnel. The conclusions regarding transonic cross-flow characteristics of perforated walls are quite interesting. The following is quoted from their paper.

> "The usual theoretical approach is to assume that the normal velocity component in the inviscid stream is linearly related to the velocity through the wall, which is linearly related to the pressure drop across the wall. Our results show that neither linear relation is applicable and that the wall boundary layer amplifies the normal velocity in the inviscid stream by a factor ranging at least from 1.15 to 6. It does not appear to be feasible to calibrate this boundary layer amplification because the latter will depend, in part, on the upstream history of the boundary layer. The main advantage to the flowmeter technique is that it is nonintrusive and does not produce disturbances in the flowfield. This one advantage is outweighed by the disadvantages cited above. Consequently, the flowmeter technique for inferring the normal velocity component has been discarded, and we are now using conventional pitch probes for this determination."

Thus, this is another case which shows the linear boundary condition at ventilated, transonic walls is basically incorrect.

The basic technique used to correct wall porosity is as follows. First, theoretical estimates of the unconfined, longitudinal, disturbance-velocities, are made at a chosen distance from the tunnel wall. The wall porosities are initially set to provide these distributions by monitoring the local static pressures with a long survey pipe. Second, the normal velocity components, at this same distance, are measured with small pitch probes and used as input for solutions of the transonic, small-disturbance equation which assume unconfined flow. The resulting solutions provide new approximations for the longitudinal velocity distributions. The wall porosities and/or plenum pressures are then adjusted to provide this new velocity distribution.* Next, the normal components are again measured, and the process continues until the differences between all the normal velocity components, measured at successive iterations, are less than 0.0005 V_∞. At this point, unconfined flow conditions are assumed to be achieved.

Experience with this iterative procedure has shown that the convergence criterion is unnecessarily stringent, and a better criterion is being considered. However, for the case of an NACA 0012 airfoil at $M = 0.55$, $\alpha = 4^\circ$ and 6°, and $M = 0.725$, $\alpha = 2^\circ$ convergence was obtained in five to seven iterations. The significant result was the measured airfoil pressure distribution, obtained in the one-foot tunnel with wall control, agreed very well with data obtained with the same airfoil in the 8-foot tunnel.

Although the Calspan results are encouraging, there are still a large number of problems to overcome before three dimensional models can be similarly tested, i.e., adequate theoretical models of 3D transonic flows and porosity adjustment of all four walls.

---

*The perforated walls are divided into ten segments on the top and eight on the bottom. The four central segments in the top wall and the two central segments in the bottom wall are designed to provide an adjustable porosity with linear variation in the streamwise direction. Each segment has a separate plenum for individual control of suction or blowing.

Recently, Kemp (Ref. 25) has suggested a hybrid scheme. He has proposed using limited adaptive-wall control to reduce interference to analytically correctable levels. In summary, reduction of transonic-wall-interference and improved data-correction methods are areas of active research in the USA, Canada, and Europe. Considerable progress is anticipated in the near future.

III.G.3. Boundary Layers and Wall Generated Noise

As noted by Pindzola, et al. (Ref. 16), slotted-wall tunnels generate less noise than do perforated walls. An illustration of the importance of this phenomena has been given by Cumming and Lowe (Ref. 11). In their tests, an F-111 aircraft model was tested in the same tunnel with both porous and slotted walls. Near-interference-free data and minimum drag were obtained over a Mach number of 0.60 to 0.80 with the slotted walls. With transition free, this corresponded to an observed rearward movement of boundary layer transition compared to the porous wall tests. Thus, this provides a specific case of wall-generated noise affecting boundary layer transition on an aircraft model.*

In the supersonic and hypersonic speed regimes Pate (Ref. 27) and Dougherty (Ref. 28) have developed correlations to relate tunnel wall boundary layer properties to radiated noise.** And in the transonic range, the recent tests of Vidal, et al. (Ref. 24) and Starr (Ref. 29) reaffirm the essential role the boundary layer plays in determining wall crossflow characteristics. These tests, among others, have also demonstrated that model-induced pressure gradients can significantly alter wall-boundary-layers in transonic tunnels. This means empty-tunnel boundary-layer surveys must be supplemented by taking additional surveys with models in place (particularly for high lift configurations). In summary, wall boundary layer surveys are a necessary part of calibrating both transonic and supersonic tunnels.

---

*The new National Transonic Facility at NASA Langley will have slotted walls because they generate less noise and interference at subsonic speeds, Ref. 26. Parker (Ref. 30) also found slotted walls, as opposed to perforated walls, provided a more uniform centerline Mach number distribution up to M = 1.1.

**Tunnel noise measurements are discussed in greater detail in Section III.F.

A review of various means for measuring boundary layer profiles has been given by Kenner and Hopkins (Ref. 31). These investigators obtained boundary layer measurements on a supersonic tunnel wall ($2.4 < M_{\infty} < 3.4$) with a single traversing probe, three different rakes, and a 12 deg. wedge with orifices in the leading edge. The interested reader may consult this reference for details of boundary layer probe designs and a discussion of the results that can be expected. Also, Allen (Ref. 32) has given a general discussion of the effects of Mach number on Pitot probe measurement errors in turbulent boundary layers.

III.G. References

1. Goethert, B. H.: Transonic Wind Tunnel Testing, Pergamon Press, 1961.

2. Wright, R. H. and Ward, V. G.: "NACA Transonic Wind-Tunnel Test Sections," NACA Report 1231, June 1955 (supercedes NACA RM L8J06, 1948).

3. Goodman, T. R.: "The Porous Wall Wind Tunnel: Part II - Interference Effect on a Cylindrical Body in a Two-Dimensional Tunnel at Subsonic Speed," Rept. No. AD-594-A-3, 1950, "Part III - Reflection and Absorption of Shock Waves at Supersonic Speeds," Rept. No. AD-706-A-1, Nov. 1950, "Part IV - Subsonic Interference Problems in a Circular Tunnel," Rept. No. AD-706-A-2, Aug. 1951, Cornell Aero. Lab., Inc.

4. Baldwin, B. S.; Turner, J. B.; and Knechtel, E. D.: "Wall Interference in Wind Tunnels with Slotted and Porous Boundaries at Subsonic Speeds," NACA TN 3176, May 1954.

5. Garner, H. C.; Rogers, E. W. E.; Acum, W. E. A.; and Maskell, E. C.: "Subsonic Wind Tunnel Wall Corrections," AGARDograph 109, Oct. 1966.

6. Heyson, H. H.: "Rapid Estimation of Wind-Tunnel Corrections with Application to Wind-Tunnel and Model Design," NASA TN D-6416, Sept. 1971.

7. Pindzola, M. and Chew, W. L.: "A Summary of Perforated Wall Wind Tunnel Studies at the Arnold Engineering Development Center," AEDC-TR-60-9, August 1960.

8. Keller, J. D.: "Numerical Calculation of Boundary-Induced Interference in Slotted or Perforated Wind Tunnels Including Viscous Effects in Slots," NASA TN D-6871, Aug. 1972.

9. Lowe, W. H.: "Subsonic Crossflow Calibration of a 22.5 Percent Perforated Wall," HST-TR-355-3, General Dynamics, presented at 39th STA Meeting, Mar. 1973.

10. Lo, C. F. and Oliver, R. H.: "Boundary Interference in a Rectangular Wind Tunnel with Perforated Walls," AEDC-TR-70-67, April 1970.

11. Cumming, D. P. and Lowe, W. H.: "Experimental Wall Interference Studies in a Transonic Wind Tunnel," AIAA Paper No. 71-292, Mar. 1971.

12. Blackwell, J. A., Jr. and Pounds, G. A.: "Wind Tunnel Wall Interference Effects on a Supercritical Airfoil at Transonic Speeds," Paper No. 1, Proc. AIAA 9th Aerodynamic Testing Conference, June 1976.

13. Page, W. A.: "Experimental Study of the Equivalence of Transonic Flow about Slender Cone-Cylinders of Circular and Elliptic Cross Section," NACA TN 4233, April 1958.

14. Newman, P. A. and Klunker, E. B.: "Numerical Modeling of Tunnel-Wall and Body-Shape Effects on Transonic Flow Over Finite Lifting Wings," Part II of Aerodynamic Analysis Requiring Advanced Computers, NASA SP-347, Mar. 1975.

15. Mokry, M.; Peake, D. J.; and Bowker, A. J.: "Wall Interference on Two-Dimensional Supercritical Airfoils, Using Wall Pressure Measurements to Determine the Porosity Factors for Tunnel Floor and Ceiling," NRC-13894, Nat'l. Aero. Estab., Ottawa, Canada, Feb. 1974.

16. Pindzola, M.; Binion, T. W.; and Chevallier, J. P.: "Design of Transonic Working Sections," App. 8 of A Further Review of Current Research Aimed at the Design and Operation of Large Wind Tunnels, AGARD-AR-83, Sept. 1975.

17. Berndt, S. B. and Sorensen, H.: "Flow Properties of Slotted Walls for Transonic Test Sections," Paper No. 17, Windtunnel Design and Testing Techniques, AGARD-CP-174, Mar. 1976.

18. Barnwell, R. W.: "Improvements in the Slotted-Wall Boundary Conditions," Paper No. 3, Proc. AIAA 9th Aerodynamic Testing Conference, June 1976.

19. Ferri, A. and Baronti, P.: "A Method for Transonic Wind-Tunnel Corrections," AIAA Jour., Jan. 1973.

20. Sears, W. R.: "Self Correcting Wind Tunnels," Aeronautical Jour., Vol. 78, Feb.-Mar. 1974.

21. Weeks, T. M.: "Reduction of Transonic Slotted Wall Interference by Means of Slat Contouring," AFFDL-TR-74-139, Mar. 1975.

22. Goodyer, M. J.: "The Low Speed Self Streamlining Windtunnel," Paper No. 13, Windtunnel Design and Testing Techniques, AGARD-CP-174, Mar. 1976.

23. Chevallier, J. P.: "Soufflerie Transsonique A Parois Auto-Adaptable," Paper No. 12, Windtunnel Design and Testing Techniques, AGARD-CP-174, Mar. 1976.

24. Vidal, R. J.; Erickson, J. C., Jr. and Catlin, P. A.: "Experiments with a Self-Correcting Windtunnel," Paper No. 11, Windtunnel Design and Testing Techniques, AGARD-CP-174, Mar. 1976. (Also see Calspan Report No. RK-6040-A-1, Jan. 1977.)

25. Kemp, W. B., Jr.: "Toward the Correctable Interference Transonic Wind Tunnel," Proc. AIAA 9th Aerodynamic Testing Conference, June 1976.

26. McKinney, L. W. and Howell, R. R.: "The Characteristics of the Planned National Transonic Facility," Proc. AIAA 9th Aerodynamic Testing Conference, June 1976.

27. Pate, S. R.: "Measurements and Correlations of Transition Reynolds Numbers on Sharp Slender Cones at High Speeds," AIAA Jour., Sept. 1971.

28. Dougherty, N. S.: "Correlation of Transition Reynolds Number with Aerodynamic Noise Levels in a Wind Tunnel at Mach Numbers 2.0 - 3.0," AIAA Jour., Dec. 1975.

29. Starr, R. F.: "Experiments to Assess the Influence of Changes in the Tunnel Wall Boundary Layer on Transonic Wall Crossflow Characteristics," Wind Tunnel Design and Testing Techniques, AGARD-CP-174, Mar. 1976.

30. Parker, R. L., Jr.: "Flow Generation Properties of Five Transonic Wind Tunnel Test Section Wall Configurations," AEDC-TR-75-88, Aug. 1975.

31. Keener, E. R. and Hopkins, E. J.: "Accuracy of Pitot-Pressure Rakes for Turbulent Boundary-Layer Measurements in Supersonic Flow," NASA TN D-6229, Mar. 1971.

32. Allen, J. M.: "Effects of Mach Number on Pitot-Probe Displacement in a Turbulent Boundary Layer," NASA TN D-7466, June 1974 (also see AIAA Jour., pp. 949-590, July 1975).

III.H. STANDARD MODELS

III.H.1. AGARD Force Models

The need for standard models was recognized early by the AGARD Wind Tunnel and Model Testing Panel. In 1952, this panel adopted AGARD Models A and B for the purpose of building and testing calibration models in supersonic tunnels, Ref. 1. It was thought that this would be "extremely useful in establishing standards of comparison between wind tunnels." It would also be useful in studying the effects of changes in Reynolds number, turbulence, model size and model fabrication tolerances.

AGARD Model A was an existing rocket body with fins which had been designed by NACA and had the prior designation of RM-10. AGARD Model B is a wing-body combination which consists of an ogive-cylinder and a delta wing with a symmetrical, 4% circular-arc airfoil. In 1954, the AGARD Model B was modified to include vertical and horizontal tail surfaces. This configuration was designated AGARD Model C and was designed "primarily for testing and calibration in the transonic speed range." The purpose of the tail was to have a model which would be more sensitive to flow curvature and wall reflections of shock and/or expansion waves.

The geometrical specifications for the various AGARD models are given in References 1, 2 and 3. The associated wind tunnel data is presented in Reference 4. Goethert (Ref. 5) also discusses some of the early AEDC data obtained for AGARD Models B and C. The following conclusion was derived from these early tests. Based on comparisons of data for models having 1.15% and 0.01% blockage in the PWT 16T Transonic Tunnel, it was concluded that satisfactory results could be achieved in transonic tunnels if aircraft models did not exceed about 1% blockage ratio. Responses to the questionnaire indicate this rule of thumb has been adopted almost universally. However, for precision testing, Goethert (Ref. 5) recommended blockage ratios be kept as small as 0.5% and with a wing span not exceeding half the tunnel width.

These early conclusions were based on the results of testing force models. The more recent testing of the past few years has employed models designed to measure pressure distributions. It is now known that aircraft models with 1% tunnel blockage can experience considerable wall interference, especially near

Mach one, even in the best ventilated tunnels. Thus, current studies of transonic wall interference require the use of pressure models to provide the necessary data.

III.H.2. Transonic Pressure Models: 2-D

In the past, a number of airfoils have been used in studies of transonic wall interference. What follows is a brief list of airfoils which have been employed recently.

Weeks (Ref. 6) has used a symmetrical, 6% circular-arc airfoil to study wall interference in a contoured, slotted-wall tunnel. In France, an NACA 64 A010 airfoil* has been used at ONERA (Ref. 7) for two-dimensional studies of solid, adjustable walls in transonic tunnels. Whereas, Calspan studies of walls with adjustable porosity have utilized the symmetrical NACA 0012 airfoil, Ref. 9. A 15.2 cm (6 in.) chord model has been tested in the Calspan 8-ft Tunnel to provide baseline force and pressure data which are wall-interference-free. Also, this airfoil has been found to be less sensitive to Reynolds number and tunnel flow quality. Thus, Pindzola, et al. (Ref. 10) have recommended the NACA 0012 airfoil be adopted as a standard 2-D model in order that transonic wall development work have a common basis.

III.H.3. Transonic Pressure Models: 3-D

A 20 deg cone-cylinder has been used in a number of transonic facilities (particularly for $M > 1$) to select operational values of wall porosity, wall angle and plenum pumping. Davis and Graham (Ref. 11) have described a typical case which illustrates this procedure. They have also reviewed the wall-interference-free, transonic data which is available for this model geometry.

At one time, it was thought that if the wall parameters were selected to give minimum interference on this model, through Mach one, this would be satisfactory for testing all types of models. However, a number of aircraft model tests have shown this is not the case. For example, Davis' (Ref. 12) transonic tests with an AGARD Model B indicated better agreement with the AGARD reference data could be obtained with different wall settings.

---

*Binion (Ref. 8) used a similar airfoil, NACA 64 A006, on a winged-body model.

Thus, care must be exercised in selecting a calibration model. In particular, it is now recognized that a calibration model must be "similar" to models which are to be tested. Unfortunately, precise criteria for how similar have not yet been defined. All that may be said at this time is: more than one type of standard calibration model is necessary for valid testing of missile, airfoil, and aircraft models in existing transonic tunnels.

The tests of Treon, et al. (Refs. 13 and 14) established the need for identical models and instrumentation when comparing results from different tunnels. In this study, a 0.0226-scale model of the Lockheed C-5A was tested in the Calspan 8-ft., the NASA Ames 11-by 11-ft., and the AEDC 16-ft. (16T) transonic wind tunnels. The same combination of model-support sting and internal force balance was used in each of the tunnels. This allowed analyses of small differences in blockage, buoyancy and Reynolds number effects which would not have been possible if different models had been used. In addition to forces and moments, seven orifices on the fuselage were used to measure local static pressure. This enabled comparisons of buoyancy and model-induced changes in effective freestream Mach number. The resulting corrections for relative buoyancy and effective Reynolds number* reduced the spread in axial force by 75 percent for Mach number below the drag rise value.** Finally, these tests permitted estimates of the "best expectancy agreement" between data obtained in the three facilities.

The utility of the AEDC transition cone (Refs. 15-17) has been discussed in Section III.F. and will not be repeated here. However, it should be noted that this study of the effects of tunnel environment on boundary layer transition was also based on the fundamental premise employed by Treon, et al. Namely, the same model, instrumentation, and support mechanism are essential for meaningful results.

A simplified, but versatile, aircraft model has been tested in the AEDC 16T and 4T transonic tunnels by Binion (Ref. 8). The model consists of two geometrically similar, centerbodies with rectangular-planform wings. The centerbodies have pointed, ogive-type noses and the wings have the NACA 63 A006 airfoil profile. The smaller body served as a tail and was mounted on a separate force

---

* See p. 150.

** Subsequent to this work, Binion and Lo (Ref. 15) showed, in some cases, wall interference can overshadow the effects of Reynolds number variations.

balance and sting. Four different model arrangements were tested in both tunnels, viz., the wing by itself, the tail by itself, and the wing with tail mounted close behind and at a more aft position.

After the force tests, the tests were repeated and pressure distributions were measured on the centerbodies and the wings. Angles of attack were repeated by duplicating the pressure difference across the model forebody which was initially calibrated as a function of α in the 16T.

The conclusions reached by Binion include the following.

1. Flow angularity can be induced into the tunnel flow which is a function of model configuration, model attitude, and tunnel configuration. This flow angularity is distinct from the usual upwash correction and varies nonlinearly with Mach number and model incidence. No existing theoretical corrections can account for this phenomena.

2. The movable tail feature confirmed the expected dependence of wall interference on model configuration in the transonic regime. Also, the more-aft tail position encountered wall-reflected disturbances at supersonic Mach numbers.

3. The attainment of an interference-free value of lift does not ensure an interference-free flow field.

4. There is no value of porosity, with the present AEDC 4T walls, which will yield interference-free pressure distributions for this aircraft model (0.9% blockage) when extensive regions of supercritical flow exists. The magnitude of wall interference appears to be a function of size and extent of supersonic pockets and the model-induced pressure gradient at the wall.

A transonic transport model has been designed and developed at ONERA and has been offered as a standard for transonic tunnel calibrations. A family of five different sizes has been fabricated so that an appropriate size is available for even small tunnels. However, only the largest model provides for measurements of wing pressure distributions. An equivalent body of revolution is also available for the large model. A description of the model geometry may be found in Reference 19.

Two sizes of this model (large M5 and 1/4 scale smaller M3) have recently been tested in the AEDC 16T and 4T tunnels and the NASA Ames 11-ft tunnel as part of a cooperative program with ONERA. The stated purposes of this study were "to provide an experimental data base for (1) the evaluation of theoretical or empirical wall-interference correction factors and (2) the establishment of guidelines to allow reasonable selection of wind-tunnel-to-model size ratios in the transonic speed regime." The test results and evaluation are reported by Binion (Ref. 19).

An unexpected result of these tests was the observed sensitivity to Reynolds number. In fact, the models were found to be more sensitive to Reynolds number when boundary layer transition was fixed than with free transition. Also, greater variation of the data from tunnel-to-tunnel occurred with fixed transition. Wing pressure data from the larger model showed these differences were caused by differences in shock-boundary layer interactions and trailing edge separation. Finally, even though state-of-the-art manufacturing tolerances were used to fabricate the models, there appears to be small differences in tail incidence between the two models. This precluded useful model-to-model comparisons of pitching moment. In summary, the ONERA models were found to be overly sensitive to Reynolds number and tunnel flow quality and exhibited insufficient model similarity for accurate studies of wall interference. Thus, the objectives of these tests were not achieved.

Based on experience with the AEDC simplified aircraft model and the ONERA models, the following criteria have evolved for a model to study transonic wall-interference problems.*

1. The aircraft model should have a small cylindrical centerbody with an ogive nose (the centerbody must house a force balance and provide a passage for surface pressure lines).
2. Surface pressures on the centerbody should be selected and calibrated to directly measure Mach number and angle of attack.
3. The wing should have an NACA 0012 airfoil, zero taper, and should be aligned with the centerbody axis. A variable sweep feature would be desirable in order to study the effect of lift on axial, interference gradients.

*Binion, T. W., Jr., personal communication, AEDC, March 1977.

4. The horizontal tail should be separately instrumented and geometrically similar to the wing.
5. Standardization of instrumentation and sting configuration is essential.
6. Both model forces and pressure distributions on wings and centerbody should be measured.

Work is continuing at AEDC to develop a model with these features.

In summary, a satisfactory aircraft model for calibrating transonic wind tunnels does not yet exist. Until wall interference effects are clearly defined and separable from Reynolds number and flow quality effects, a simplified aircraft model is required. Once this objective is realized, more realistic aircraft models, e.g., the ONERA transport models, can be utilized much more effectively for tunnel-to-tunnel comparisons.

III.H. References

1. "AGARD Wind Tunnel Calibration Models," AGARD Specification 2, Sept. 1958.

2. Fail, R. and Garner, H. C.: "Calibration Models for Dynamic Stability Tests," AGARD Report 563, 1968.

3. Curry, W. H., ed.: "The First Fifteen Years of the Supersonic Tunnel Association," Sandia Laboratories, Sept. 1969.

4. Hills, R., ed.: "A Review of Measurements on AGARD Calibration Models," AGARDograph 64, Nov. 1961.

5. Goethert, B. H.: Transonic Wind Tunnel Testing, Pergamon, 1961.

6. Weeks, T. M.: "Reduction of Transonic Slotted Wall Interference by Means of Slat Contouring," AFFDL-TR-74-139, March 1975.

7. Chevallier, J. P.: "Soufflerie Transsonique a' Parois Auto-Adaptables," Wind Tunnel Design and Testing Techniques, AGARD-CP-174, March 1976.

8. Binion, T. W., Jr.: "An Investigation of Three-Dimensional Wall Interference in a Variable Porosity Transonic Wind Tunnel," AEDC-TR-74-74, Oct. 1974.

9. Vidal, R. J.; Erickson, J. C., Jr.; and Catlin, P. A.: "Experiments with a Self-Correcting Wind Tunnel," Wind Tunnel Design and Testing Techniques, AGARD-CP-174, March 1976.

10. Pindzola, M.; Binion, T. W., Jr.; and Chevallier, J. P.: "Design of Transonic Working Sections," A Further Review of Current Research Aimed at the Design and Operation of Large Wind Tunnels, AGARD-AR-83, Sept. 1975

11. Davis, J. W. and Graham, R. F.: "Wind-Tunnel Wall Interference Effects for 20° Cone-Cylinders," AIAA Jour. Spacecraft & Rockets, Oct. 1973 (also see NASA TN D-7432).

12. Davis, J. W.: "AGARD Model B Transonic Blockage Investigation," NASA Marchall Space Flight Center, Huntsville, Ala., presented at 39th Semi-Annual STA Meeting, Mar. 1973 (referenced with author's permission).

13. Treon, S. L.; Steinle, F. W.; Hofstetter, W. R.; and Hagerman, J. R.: "Data Correlation from Investigations of a High-Subsonic Speed Transport Aircraft Model in Three Major Transonic Wind Tunnels," AIAA Paper No. 69-794, July 1969.

14. Treon, S. L.; Steinle, F. W.; Hagerman, J. R.; Black, J. A.; and Buffington, R. J.: "Further Correlation of Data From Investigations of a High-Subsonic-Speed Transport Aircraft Model in Three Major Transonic Wind Tunnels," AIAA Paper No. 71-291, March 1971.

15. Binion, T. W., Jr. and Lo, C. F.: "Application of Wall Corrections to Transonic Wind Tunnel Data," AIAA Paper No. 72-1009, Sept. 1972.

16. Dougherty, N. S., Jr. and Steinle, F. W.: "Transition Reynolds Number Comparisons in Several Major Transonic Tunnels," AIAA Paper No. 74-627, July 1974.

17. Dougherty, N. S., Jr.: "Prepared Comment on Cone Transition Reynolds Number Data Correlation Study," AGARD-CP-187, June 1975.

18. Whitfield, J. and Dougherty, N. S., Jr.: "A Survey of Transition Reynolds Number Work at AEDC," to be presented as Paper No. 25 at AGARD Fluid Dynamics Panel Symposium on Laminar-Turbulent Transition, Copenhagen, Denmark, May 2-4, 1977.

19. Binion, T. W., Jr.: "Tests of the ONERA Calibration Models in Three Transonic Wind Tunnels," AEDC-TR-76-133, Nov. 1976.

III.1. OPTICAL METHODS

III.1.1. Supersonic Tunnels

The use of schlieren and shadowgraph flow-visualization-methods to detect unwanted shocks in an empty test-section is well known (Ref. 1) and, in fact, may be designated a classical technique*. Obviously, the observance of a shock in the empty-tunnel indicates corrective action is necessary. These means of flow visualization are also helpful in assessing the performance of probes and rakes and their interaction with nearby boundaries. High quality pictures also enable flow separation on probes to be observed and thereby provide additional data to guide improved designs.

A third, classical method for flow visualization is the Mach-Zehnder interferometer. However, these instruments are seldom used for wind tunnel calibration because of their cost and hypersensitivity to vibration and alignment errors.

Detailed discussions of these methods may be found in a rather large number of references. References 2 thru 4 are representative of both older and newer literature which deals with these three methods of flow visualization.

III.1.2. Transonic Tunnels

As previously disucssed in Section III.D., movement of a transonic shock on a static pressure probe is strongly affected by blockage and wall characteristics. For example, the schlieren photographs of Page (Ref. 5) are quite instructive as to the effects on a probe caused by varying tunnel blockage from 0.25% to 0.005%.

In the case of supercritical flow about a hemisphere-cylinder probe, the shadowgraphs of Hsieh (Ref. 6) were very helpful in detecting boundary layer separation and interpreting the measured pressure distributions.

*Most of the respondents to the questionnaire indicated they routinely used one or both of these techniques.

At low supersonic speeds, schlierens and shadowgraphs are very useful in studies of the shock-cancellation properties of ventilated walls, e.g., Ref. 7. Also, Dougherty, et al. (Ref. 8) have very effectively used schlieren photographs to study the sound field generated by perforated walls when exposed to high-subsonic flows.

III.1.3. Newer Methods

Newer optical methods for flow visualization include laser Doppler velocimeters (LDV), holographic velocimeters (HV), and holographic interferometry (HI) for density measurements. The primary advantage of LDV's and HV's is their potential to measure three-dimensional flow fields without disturbing the flow. As we have seen, this is particularly important in transonic tunnels near Mach one.

The current state-of-the-art of LDV's and their application to tunnel calibration is reviewed in Appendix II. Since the accuracy of current LDV systems is approximately 0.4 - 0.5%, they are not yet superior to conventional probes which provide comparable accuracies of 0.1%.

The fundamentals of holographic velocimetry are reviewed by Shofner, et al. (Ref. 9). A very comprehensive review of the use of holography in wind tunnel testing has been compiled by Havener (Ref. 10). Progress (up to 1975) in automating HI data reduction is reported by Hannah and Havener (Ref. 11). Since this is still a developing technology, applications of holography to empty-tunnel calibration appears to be in the future.

Sparks and Ezekiel (Ref. 12) have recently demonstrated the usefulness of Laser Streak Velocimetry (LSV) for quantitative measurements of low-speed velocity fields near models. This technique has the advantage of providing, simultaneously, velocities on a plane as opposed to the point-by-point measurements required with LDV's. However, the accuracy of LSV's is currently insufficient for empty-tunnel calibrations. Finally, Sedney, et al. (Ref. 13) have given a review of flow tracer techniques and their applications in supersonic-flowfield diagnostics.

III.1. References

1. Pope, A. and Goin, K. L.: High-Speed Wind Tunnel Testing, Wiley, 1965.

2. Ladenburg, R. W.; Lewis, B.; Pease, R. N.; and Taylor, H. S. (editors): Physical Measurements in Gas Dynamic and Combustion, Princeton University Press, 1954.

3. Vasil'er, A. L.: Schlieren Methods, Transl. by A. Baruch, Israel Program for Scientific Translations, Jerusalem, New York and London, 1971.

4. Merzkirch, W.: Flow Visualization, Academic Press, 1974.

5. Page, W. A.: "Experimental Study of the Equivalence of Transonic Flow About Slender Cone-Cylinders of Circular and Elliptic Cross Section," NACA TN 4233, April 1958.

6. Hsieh, T.: "Hemisphere-Cylinder in Transonic Flow, M_∞ = 0.7 1.0," AIAA Jour., Oct. 1975 (also AIAA Paper No. 75-83, Jan. 1975).

7. Goethert, B. H.: Transonic Wind Tunnel Testing, Pergamon, 1961.

8. Dougherty, N. S., Jr.; Anderson, C. F.; and Parker, R. L., Jr.: "An Experimental Investigation of Techniques to Suppress Edgetones From Perforated Wind Tunnel Walls," AEDC-TR-75-88, Aug. 1975.

9. Shofner, F. M.; Menzel, R.; and Russell, T. G.: "Fundamentals of Holographic Velocimetry," AFFDL-TR-68-140, Nov. 1968.

10. Havener, A. G.: "A Users Guild on Pulse Laser Holography for Wind Tunnel Testing," ARL TR 75-0213, June 1975.

11. Hannah, B. W. and Havener, A. G.: "Applications of Automated Holographic Interferometry," Int'l Congress on Instrumentation in Aerospace Simulation Facilities, IEEE Pub. 75 CHO 993-6 AES, Sept. 1975.

12. Sparks, G. W., Jr. and Ezekiel, S.: "Laser Streak Velocimeter for Two-Dimensional Flows in Gases," AIAA Jour., Vol. 15, No. 1, Jan. 1977.

13. Sedney, R.; Kitchens, C. W., Jr.; and Bush, C. C.: "The Marriage of Optical, Tracer and Surface Indicator Techniques in Flow Visualization," BRL R-1763, USA Ballistic Research Laboratories, Feb. 1975.

III.J. Humidity Measurements

The effects of moisture condensation and the necessity for air drying have been discussed in Section II.C.7. Measurement and monitoring of the moisture content of the tunnel flow is therefore an essential part of tunnel calibration and operation.

The moisture content of a gas is expressed in a number of ways; relative humidity (ratio of moisture partial pressure to saturation pressure), dew point (or frost point) temperature at atmospheric pressure, specific humidity (mass of water per mass of dry gas), and volume ratio (parts of water vapor per million parts of air). The dew point or ice-point at atmospheric pressure is the most commonly used form of expression for wind tunnel operations.

A number of measurement systems are utilized by facilities responding to the questionnaire, extending from the visual observation of fog in the tunnel flow to completely automatic, continuously recording dew point systems. All dew point measurement instruments can be calssified according to the basic principles used.

One of the more basic non-continuous dew point measurement instruments operates on the principle of allowing a hand-pump pressurized sample of gas, at known pressure and temperature, to expand to room temperature (Ref. 1). If the expansion reduces the sample temperature to or below the dew point temperatures, fog is created which may be observed visually through a viewing window. A trial and error procedure is required to determine the initial sample pressure which will expand to create a just-visible fog. Since a known relationship exists between pressure and temperature ratios, the dew point can be determined using ambient as the final pressure. These instruments are low in cost, reasonably accurate and are widely used both as primary dew point monitors

and for monitoring the accuracy of less basic instruments. They provide only periodic or spot checks and are therefore not satisfactory for facilities where relatively sudden changes in dew point can occur. All readings must be manually recorded. Measurements below about -40C are difficult to make.

Continuous indicating and recording humidity sensors include the Dunmore type which changes resistance in a non-linear fashion with relative humidity. A modified form responds to dew point (Ref. 2). Each sensor has a limited range, so that several are required if the humidity range is large. The range extends downward to about -40 C.

An electrolytic humidity sensor is also available. These sensors utilize an element which electrolyzes water into hydrogen and oxygen, causing an electrolysis current to flow. The electrolytic instrument is usually calibrated in parts per million, with full scale ranges as low as 0 to 100 parts per million. This instrument, like the resistance device, can be configured to both indicate humidity and provide an electrical signal for an external recording device.

Dew point temperatures can be determined by controlling automatically the temperature of a polished metal mirror to the point that a trace film of condensation (or frost) is maintained. Several instruments based on this principle have been developed. More recent types are simplified in that the thermo-electric cooling effect is used to chill the mirror (with auxiliary refrigeration if necessary). The condensation film is automatically maintained by feedback control of the mirror temperature, utilizing an optical source reflectry light from the cooled mirror to a pair of photo-detectors forming a bridge circuit. The dew point temperature is measured by a thermocouple or

resistance-temperature detector attached directly to the mirror. The dew point is indicated by a meter or other indicator, and the temperature sensor output may also be recorded, supplied to the wind tunnel data system, etc. The range can extend to as low as 200 ^{o}K (-100 ^{o}F).

A continuous-recording, dew point monitor has obvious advantages both with regard to monitoring and control of tunnel measurements. They can also provide information on the performance of dryers and other tunnel equipment.

III.J. References

1. Pope, A.; and Goin, K. L.: High Speed Wind Tunnel Testing, pp. 223-226, John Wiley and Sons, New York.

2. Doeblin, E. O.: Measurement Systems; Application and Design, pp. 596-598, McGraw-Hill, New York.

3. Fraade, D. J.: "Measuring Moisture in Gases," Instruments and Control Systems, April 1963.

IV. ERROR AND UNCERTAINTY IN CALIBRATION MEASUREMENTS

Treatment of accuracy and sources of error in experimental data involves principles of statistics and probability. Unfortunately, each branch of science tends to develop specialized terminology, which impedes understanding and communication in comparing measurement results. An attempt will therefore be made to define and recommend basic terminology which may be used to advantage in evaluating, defining and communicating calibration accuracy. As a first step, a definition and classification of various types of errors will be stated.

IV.A. Random Error

Errors may be classified in two general categories: random and fixed. Random error is frequently referred to by the engineer in less precise terms as "scatter," "noise," etc., all implying that repeated measurements do not yield the same value. Most processes are such that if a sufficiently large number of measurements are made and the frequency with which each value is measured is plotted against the measured value, the resulting plot (the probability density function) will approach the familiar bell-shaped normal distribution curve. In this case, the arithmetic mean value, or average,

$$\bar{X} = \sum_{i=1}^{N} \frac{X_i}{N} \tag{4.A.1}$$

occurs at the peak of the curve. When plotted in normalized form, the area under the curve is unity. The precision, which is a measure of the scatter or random error, is specified by the standard deviation,

$$\sigma = \sqrt{\sum_{i=1}^{N} \frac{(X_i - \bar{X})^2}{N-1}} \tag{4.A.2}$$

if the distribution is based on a sufficiently large number of measurements, 68 percent of the measurements will lie within the range $\pm 1\ \sigma$, 95.4 percent within $\pm 2\ \sigma$ and 99.7 percent within $\pm 3\ \sigma$. A wide, flat distribution therefore corresponds to measurements with a large standard deviation, a large amount of scatter, a large random error, or a lack of precision, all of which refer to the same characteristics of the measurement. The random error is quantatively stated in terms of the standard deviation and error statements should always be specified as $1\ \sigma$, $2\ \sigma$, etc.

IV.B. Fixed Error

A second form of measurement error is referred to as systematic error, fixed error or bias. This component of error will be the same in each of many repeated measurements. The magnitude and sign of the bias may not be known a priori since these can be determined only by comparison with the true value of the measured quantity. As one example, an undetected change in the calibration of an instrument such as a pressure transducer will introduce a fixed bias of unknown magnitude and sign. Upon detection, this bias or fixed error can be removed by recalibration. Since unknown fixed errors are not correctable, unless detected, their minimization depends (1) upon careful monitoring of results, (2) routine pre-and post-test calibrations of instruments, in place, (3) end-to-end calibrations of instruments prior to and during tests, etc. This same philosophy can be applied to a basic instrument such as a pressure transducer or to the tunnel-flow calibration. The objective should be to eliminate all large, unknown fixed errors.

Some types of unknown fixed errors cannot be readily eliminated by calibration. An example might be the drag of a standard model, where no "true" value is known. Facility-to-facility comparisons allow only an estimate of the

probable maximum magnitude of the bias. Correction may be possible only to the extent that the comparison tests allow determination of and correction for the cause (or causes) of the bias (or a portion thereof).

The fixed error limit, which normally must be estimated, is the upper limit on the fixed error or bias, and may be symmetrical or non-symmetrical, i.e., it may be 0, + or 0, - rather than $\pm$.

IV.C. Uncertainty

The total uncertainty interval for a measurement represents the largest, reasonably-expected error (i.e., the true value should fall in the uncertainty interval) and is a combination of the precision (standard deviation) and the estimated bias.

A method described by Abernathy, et al. (Ref. 1) and recommended by the National Bureau of Standards expresses the uncertainty as the range centered about the mean value and defined as

$$U = \pm (B + t_{95}\, \sigma) \qquad (4.C.1)$$

Where U is the uncertainty, B the bias or fixed error limit, and t_{95} is the 95th percentile point for the Student "t" distribution. The value of t depends on the number of values used in computing σ ; for a large number of measurements the Student t distribution is identical to the normal distribution. The use of the t_{95} factor increases the uncertainty limit when small samples are used to calculate (or, more accurately, to estimate) σ . Abernathy, et al. recommended that a value of 2.0 be used for t_{95} for 31 or more samples (compared to 1.96 for an infinite number). Reference (1) and most statistics texts (e.g., Ref. 2) contain tables of Student's t distributions from which t_{95} can be obtained for less than 30 samples. Statistical methods employing the t distribution are frequently called small-sample methods for obvious

reasons. Although this example is simplified, it can be extended to include other error terms.

An additional problem in accurate determination of measurement error, not discussed above, is that the measured properties normally have small-amplitude variations with time. In addition to obtaining a statistically adequate number of samples, the sample interval must span at least one complete cycle of the lowest-frequency component of tunnel unsteadiness, as discussed by Muhlstein and Coe, (Ref. 3).

IV.D. Error Propogation

In essentially all cases, calibration parameters are determined from basic properties which are measured and a known function relating the measured quantities and the desired parameter. An obvious example would be the determination of Mach number in the test section from measured pressures. Random error sources would include the precision (standard deviations) of the pressure measurements. Static pressure probe uncertainty limits may be estimated as a fixed bias in the absence of a calibration. Another fixed bias could be the estimated uncertainty in γ . As an illustrative example, the random error in Mach number can be calculated from

$$\sigma_M = \sqrt{\left(\frac{\partial M}{\partial H_s}\ \sigma_{H_s}\right)^2 + \left(\frac{\partial M}{\partial P}\ \sigma_P\right)^2}\ , \qquad (4.D.1)$$

where the variations in H_s and P are taken to be uncorrelated. The fixed error or bias limit can similarly be calculated from

$$B_M = \sqrt{\left(\frac{\partial M}{\partial \gamma}\ B_\gamma\right)^2 + \left(\frac{\partial M}{\partial P}\ B_P\right)^2}\ , \qquad (4.D.2)$$

where B_γ and B_p are the estimated uncertainty limits for the ratio of specific heats and for the static probe error, respectively.

The results can be combined according to Eq. (4.C.1) to determine the total uncertainty interval for a specific (point) Mach number measurement.

$$U_M = \pm (B_M + 2\,\sigma_M) \qquad (4.D.3).$$

The uncertainty interval of an individual property measurement, such as a pressure, can also be estimated as above; where individual error sources such as the standard deviation of the transducer, the excitation power supply, the instrumentation amplifier and the analog-to-digital converter are all taken into account. Normally, however, the calibration is performed end-to-end utilizing all components so that all of the above factors are taken into account and attributed to the pressure transducer.

IV. References

1. Abernathy, R. B., et al and Thompson, J. W., Jr.: "Handbook; Uncertainty In Gas Turbine Measurements," AEDC-TR-73-5, February 1973 (also CPIA No. 180).

2. Hoel, P. G.: Introduction to Mathematical Statistics, pp 402-403, John Wiley and Sons, Inc., New York, 1966.

3. Muhlstein, L. Jr., and Coe, C. F.: "Integration Time Required to Extract Accurate Static and Dynamic Data From Transonic Wind Tunnel Tests," AIAA Paper 75-142, Pasadena, Calif., Jan. 1975.

V. CONCLUSIONS AND RECOMMENDATIONS

V.A. Summary of State-of-the-Art of Transonic and Supersonic Wind Tunnel Calibration

Reference has been made throughout the previous sections of this report to information obtained from the questionnaire survey, literature search and personal contacts. A condensation of this information has been presented where appropriate. Primarily, information has been summarized in an attempt to define "best state-of-the-art" calibration accuracy. Attention has been focused on the primary problems which were considered to be measurements of stagnation and static pressure and calculation of Mach number. A concluding summary of the questionnaire results is presented here for convenience.

Based on a judgment evaluation of data reported in the questionnaires, the best, current, pressure-measurement accuracy (on the basis of standard deviation) ranges from 0.025 to 0.10 percent. These accuracies were reported for both blowdown and continuous tunnels.

The best, transonic, Mach-number-measurement accuracy, again taken as the standard deviation, appears to range from 0.001 to 0.002. Several facilities claimed 0.001 measurement accuracy at a point, with variations ranging from 0.002 to 0.015.

The survey showed that approximately twice as many transonic tunnels use plenum chamber pressure for a reference to monitor Mach number, as opposed to test-section wall pressure. However, both types of measurements are used and both require a calibration(s) to relate the associated data to static pressure measurements along the centerline.

The most popular static-pressure-probe is a 10 deg cone-cylinder with static orifices located ten or more cylinder diameters downstream of the shoulder. The ten-deg-cone appears to be a trade-off between the requirements to minimize disturbance of the flow and, simultaneously, be easily fabricated and durable enough to be used repeatedly in a wind tunnel environment. Although at high subsonic speeds a shock forms on the cylinder and accurate measurement of the static pressure requires orifices at several stations, only a few of the probe designs submitted with the questionnaires have this feature. A smaller-angle cone not only has a lower, shock-attachment Mach number but it also generates a

weaker transonic shock on the cylinder and thus smaller deviations from free-stream conditions. Of the various static probe designs described in response to the questionnaire, a two-degree (total-included angle) cone was the smallest.

An additional source of error in calibrating transonic tunnels is the neglect of variations transverse to the flow. Almost without exception, in cases where measurements had been made, the questionnaires indicated greater Mach number gradients occur across the flow than along the tunnel centerline. This may be most significant in the determination of drag divergence and/or buffet onset for transonic aircraft models. However, the present state-of-the-art of wind-tunnel testing is to use off-centerline data exclusively as a diagnostic tool to detect unacceptably large variations. In which case nozzle and/or test section configurations are altered.

The most popular flow-angularity-probes appear to be the 30-deg-cone for simultaneous measurements of pitch and yaw. Wedges of various angles are often used for planar measurements. It appears feasible to design probes of this type (i.e., differential-pressure) which can resolve flow angles to ± 0.01 degree. (This objective was proposed in 1970 by the ad hoc Air Force-NASA Committee on Transonic Testing Techniques.) The quoted accuracy for flow angle measurements ranged from 0.01 deg to 0.04 deg. A spatial variation of $\pm 1/4$ deg was frequently mentioned.

Quoted stagnation-temperature accuracy usually ranged from 1 to 2 ^{o}C.

The majority of reporting facilities do not continuously monitor humidity. In order to achieve a Mach number accuracy of 0.001, humidity must be monitored continuously.

Nearly 50% of the tunnels have made noise measurements in either the stilling chamber, the tes section and/or the plenum chamber. In most cases, either miniature strain gauge transducers or condenser microphones were used to measure the noise data. The following techniques have been employed to measure freestream disturbances in transonic and/or supersonic wind tunnels.

1. High-frequency-response pressure transducers mounted near the tip of cones to measure fluctuating static pressures beneath a laminar boundary layer.

2. Pressure transducers mounted on wedges with the measurement surface aligned with the flow.
3. Pressure transducers mounted on the cylindrical portion of ogive-cylinders.
4. Pressure transducers mounted in Pitot probes to measure fluctuations in Pitot pressure.
5. Hot-wire and hot-film measurements.

Approximately 25% of the tunnels reported having made hot-wire or hot-film measurements of turbulence. However, in the majority of cases only very limited centerline and/or wall boundary layer measurements have been made. Only a few tunnels reported measurements of fluctuating Pitot pressure.

The majority of the tunnels reported that Schlieren systems were of value in detecting unwanted disturbances in the test section. When combined with high speed photography, this method also provides data on flow unsteadiness.

Most of the responding facilities have used one or more standard force models during calibration. However, comparisons with reference data are usually only qualitative and are of limited use in pinpointing undesirable flow characteristics.

The well known rule of thumb that the model cross section should not exceed 1% of the tunnel area for transonic testing appears to be universally accepted. A consequence of this criterion is that very few tunnel operators attempt to correct for wall interference. This also reflects the lack of an accepted theory for correcting for transonic wall interference.

Finally, the consensus on frequency of wind tunnel calibration is that a tunnel should be recalibrated or at least spot checked whenever:

1. tunnel configuration changes occur,
2. significant instrumentation modifications are made,
3. erroneous data is being obtained, or
4. in the absence of any of the above, once each year.

Static-pressure orifices should also be inspected before recalibrating.

V.B. TRANSONIC TUNNELS

The goal of Mach number calibrations in transonic tunnels should be to achieve an accuracy of ± 0.001, particularly in the transonic drag rise regime: $0.75 \leq M \leq 1.0$. For an air test medium, this requires the following constraint on total errors in total and static pressure measurements.

$$\frac{\Delta H}{H} - \frac{\Delta P}{P} \leq \frac{0.001}{M} \left[\frac{7M^2}{5 + M^2} \right]$$

However, changes in Reynolds number (Section II.B.2) or humidity level (Section II.C.7) can easily cause Mach number variations several times larger than 0.001. For this reason, considerable care should be taken to calibrate an empty-tunnel over the entire range of Reynolds number and humidity levels normally encountered during routine operations. Once the tunnel is calibrated for typical, operating humidity levels, a continuous monitoring of humidity is preferred, e.g., a strip recorder for subsequent reference. In addition, excessive spatial variations of total pressure (i.e., $\Delta H_s/H_s > 0.001$) across the stilling chamber may require corrective action, e.g., additional screens, honeycombs, etc. Finally, the assumption of an isentropic expansion from the stilling chamber to the test section should be evaluated by direct measurements in the test section, both on and off-centerline.

The long, static-pressure, survey pipe is well established as the standard for obtaining centerline measurements. Best results are achieved with the nose of the pipe located well upstream in the settling chamber; this is necessary in order to prevent passage of a transonic shock over the length of the pipe. In all cases, the resulting data should be carefully inspected for orifice-induced errors. Once the centerline data is determined to be free of orifice errors (Section III.D.1.), standard procedure is to use the static pressure data to calibrate either plenum chamber pressure or wall static taps. If plenum pressure is used for Mach number control, the possibility of departures from empty-tunnel calibrations should be carefully examined in cases of (1) large (> 1%) lifting models at high-subsonic speeds and (2) rapidly varying Mach number conditions such as occur during rapid changes in model orientation. If wall static taps are used for Mach number control, at least one should be located on

each wall, ahead of the model location, and averaged with a "piezometer ring"; this average is preferable to using only a single wall static pressure.

Since a long pipe is difficult to move about the test section and off-centerline data is important for aircraft-model testing, it is recommended that supplementary, off-centerline data be obtained with a conventional static pressure probe or rake of such probes, when M is <u>not</u> near one (Sec. III.D.2). Since the wing span of most transonic aircraft models is restricted to 60 percent, or less, of the tunnel width, both Mach number and flow angularity data should be obtained over this span in the vertical and horizontal planes.

Off-centerline measurements of flow angularity are sensitive indicators of errors caused by nozzle contour, wall settings, seal leaks, etc. The most accurate measurements of flow angularity can be obtained in the least amount of time with a probe consisting of two, orthogonal, symmetrical wings and a force balance housed in a small centerbody.*

In addition to measuring Mach number and flow angularity off-centerline, data should be taken at representative forward, center, and aft stations in the useable test section. It is suggested that the resulting data, at a given station, be expressed in terms of standard deviation from the mean of the centerline measurements. This type of data will provide more complete information on flow quality and should be considered when selecting wall porosity, wall angle or amount of plenum evacuation.

Unfortunately, no general constraints exist as to what are acceptable off-centerline variations. Jackson (AEDC) has suggested the following criteria for "good" uniformity in centerline Mach number:

$$2\,\sigma_M \leq 0.005 \text{ for } M < 1 \quad ,$$

$$2\,\sigma_M \leq 0.01 \text{ for } M > 1 \quad .$$

In the past, a criterion for acceptable flow angularity along the centerline has not been needed because a given model is usually run upright and inverted in order to establish the effective angle of incidence. This is a valid and

*Acceptable accuracy can also be obtained with conventional, differential-pressure probes, see Section III.E.

well-established testing practice; however, flow angularity in the yaw plane is frequently ignored. To summarize, standard criteria for flow uniformity need to be developed for representative (preferably standard) models in various kinds of tests, e.g., force, buffet, flutter, etc. These criteria should include standards for acceptable variations in Mach number and flow angularity, both on and off-centerline.

Unsteady disturbance measurements in transonic tunnels should be a standard part of tunnel calibration. Recent use of hot-wires in the test section of a transonic tunnel at NASA Ames indicates these may be useful for unsteady-flow calibration in at least some tunnels. However, as dynamic pressure increases hot-wires become more vulnerable to breakage and probably will be impractical for use in the new high-Reynolds-number facilities (except in the settling chamber). Based on extensive experience with the AEDC transition cone in twenty-one major windtunnels of the United States and Western Europe, this device has become an "unofficial" tunnel acoustic calibration model and is currently considered to be the best available disturbance calibration instrument However, there is a definite need for a less expensive instrument which can be easily reproduced and used in all sizes of facilities. The development of fluctuating Pitot probes appears to meet this need (Section III.F). This type of instrument can be used to measure centerline noise and to calibrate wall-mounted, dynamic pressure transducers. A wall transducer(s) can then be used as a permanent monitor of tunnel noise. The wall transducer(s) should be mounted approximately 0.025 cm (0.01 in.) below the plane of the tunnel wall and, preferably, should have a frequency response out to 30 kHz. By using two or more wall-mounted transducers, the direction of propagation of disturbances can be ascertained.

Although there are no general criteria for acceptable levels of flow unsteadiness, Mabey (RAE) has developed some noise guidelines for interference-free flutter and buffet tests (Section III.F.). The goal of transonic tunnel, noise-reduction research is to reduce unsteadiness to levels characteristic of turbulent boundary layers on solid walls, i.e., $\Delta C_p < 0.005$.

An accepted measure of wave-cancellation characteristics of ventilated walls is to obtain pressure distribution data on a 20 deg cone-cylinder and compare the results with wall-interference-free data. It is now apparent that the

traditional assumption of a linear boundary condition at ventilated, transonic walls is erroneous. Thus, this explains the failure of past attempts to theoretically calculate the effects of wall interference on model testing. Measurements of test-section-wall boundary layers, both with and without models in situ, are being made in efforts to gain a better understanding of ventilated walls and their cross-flow characteristics. Current research on transonic wall interference is focusing on three areas: (1) the derivation of more exact boundary conditions, (2) the development of a self-correcting wind tunnel with automatic control of longitudinally varying ventilation, and (3) varying wall contours to attain wall-interference-free flow about models.

The NACA 0012 airfoil is currently being used as a standard pressure model in two-dimensional tests. The ONERA transport aircraft models have been tested in a number of transonic tunnels and have been found to be extremely sensitive to flow quality. AGARD has not yet adopted a standard, transport-aircraft model. There is currently a genuine need for a standard, aircraft, pressure model (or models) to aid transonic wind tunnel calibration and data comparisons between tunnels.

Laser Doppler Velocimeters are an important addition to the tools available for wind tunnel calibration. The obvious advantage of an LDV is it does not perturb the flow. At Mach numbers near one, this is an important advantage. In addition, an LDV can be used not only for mean-flow velocity measurements but also can measure flow angularity and turbulence intensities greater than about one. LDV measurements of velocity and flow angularity are currently only 1/4 to 1/5 as accurate as the best conventional probes at high subsonic and low supersonic speeds. However, near Mach one an LDV is expected to provide superior data. At this time, the LDV is not being used to routinely calibrate empty-tunnels. However, we anticipate such use in the future.

V. C. SUPERSONIC TUNNELS

Mach number in supersonic tunnels should be calibrated by measuring two independent pressures in the test section. Accurate results can be obtained by measuring Pitot pressures in the freestream and behind the bow shock of a wedge. However, freestream Pitot and static pressures are preferable to only Pitot data and the assumption of isentropic flow from the settling chamber.

Since transverse gradients in Mach number are typically larger than axial variations, it is considered essential to calibrate both Mach number and flow angularity off-centerline. At least three cross-sections should be surveyed near the forward, center and aft portions of the useable test section. This type of data can be obtained most easily with Pitot and static probe rakes or arrays mounted on a traversing sting. This data should be used to calibrate a permanent Mach number probe which should be installed in supersonic tunnels for frequent, routine checks on calibration. In general, a calibrated Mach number accuracy of 0.5 to 1% is considered good. Industry standards need to be developed which define acceptable flow quality for particular kinds of testing, e.g., force and pressure tests of missiles and aircraft models.

As in transonic tunnels, centerline noise measurements should be obtained and used to calibrate one or more, wall-mounted, dynamic-pressure transducers. The AEDC transition cone is currently the only flow disturbance calibration device which has been tested in a large number of tunnels. A smaller and less expensive noise calibration device is needed to serve as a standard. Probes designed to measure fluctuating Pitot pressures should be considered for this purpose. Traditional Pitot surveys of tunnel-wall boundary layers not only establish the size and geometry of the inviscid flow but also aid correlations of facility noise.

In addition to keeping the total temperature high enough to avoid liquefaction of the test gas, the effects of typical levels of water vapor in the test gas should be carefully calibrated. As is well known, the primary effect of water condensation is a loss of total pressure and a rise in static pressure. Also, various operators have observed that pressure tests are more sensitive to humidity levels than force tests.

The number of surveys of supersonic flow fields with a laser Doppler velocimeter is increasing as some earlier problems have been resolved. In the future this new tool may enable more accurate calibrations of supersonic tunnels.

APPENDIX I

Hot Wires and Hot Films*

Introduction

A hot-wire anemometer is a means of measuring fluctuations in localized areas of the flow at frequencies up to 200 KHz. The sensor may be a small-diameter wire suspended between needle-like prongs or a thin metallic film on an insulative substrate that may be shaped in various geometries. It responds to cooling effects and thus measures both kinematic and thermodynamic fluctuations of the flow.

The hot-wire has been a generally accepted standard for measuring fluctuations in wind tunnel flow since the work of Dryden and Kuethe in 1929 (Ref. 1). Its use can be very tedious and thus has often been avoided. However, it has not been replaced because of its advantages that include: small sensor size, high frequency response and sensitivity to pressure, vorticity, and entropy fluctuations. Dr. Kovasznay (Ref. 2) opinioned in 1968 that the hot-wire has not been replaced by other methods because of its unique characteristics. Furthermore, significant developments in hot-wire methodology in the 1970's indicate continued use of this instrument in both specialized experiments and in wind tunnel calibrations.

Reference 3 is a recent textbook on hot-wire technology. References 4 and 5 provide further background and extended lists of references relative to measurements of fluctuating properties in wind tunnels. Reference 2 provides summaries of the early history and the technology up to 1968.

Useful application of hot-wires to incompressible flow is commonly dated as 1929 (Ref. 1). Experiments with hot wires in supersonic flows began in the mid 1940's. However, equipment and analysis techniques were not considered adequate until the mid 1950's (Refs. 6, 7, and 8). Applications to transonic flows encountered particular difficulty in separating the components of the output signal (Refs. 3 and 8). Recent reports of progress (Refs. 9 and 10) have outlined approaches for practical applications in the high-subsonic and transonic test regime.

---

*This section has been contributed by C. J. Stalmach, Jr., Vought Corporation.

Equipment Description and Operation

The sensor is electrically heated to maintain either a constant current or constant temperature (resistance). In the case of constant current, compensation for the thermal lag of the wire is obtained by an output amplifier whose gain with frequency is adjusted (during a square wave heating input) to compensate for decay of the output with increasing frequency. For large aspect ratios ($\ell/d \geq 150$) the wire exhibits a first order response that is simple to compensate electronically. Adjustment of the non-linear, compensating amplifier is required for each change in mean flow condition or sensor.

In the case of a constant temperature anemometer, a high-gain feedback system provides power to the wire in response to fluctuations in cooling caused by the flow such that the wire resistance (temperature) remains essentially constant. The square of the voltage required to maintain constant wire resistance is a direct measure of the heat transfer between the sensor and its environment. The constant temperature anemometer has several advantages compared to a constant current system including:

1. thermal lag not a problem since sensor temperature is constant,
2. automatic adjustment to large changes in mean flow conditions which reduces accidental burnouts and continues data acquisition during mean flow changes,
3. direct DC output as a function of mean velocity,
4. compatible with film and low ℓ/d wire sensors that have complex frequency response characteristics, and
5. output may be linearized and temperature compensated.

The constant current approach was initially preferred because it provided higher-frequency-response and signal-to-electronic-noise ratio. Solid state electronics, however, have permitted the constant temperature systems to have comparable performance and are the systems now generally preferred. An exception is measurement of temperature fluctuations independent of velocity and density effects. Here a minimum wire temperature is required that is best achieved with a constant current operation. Modern commercial units generally incorporate both circuits. Reference 3 and literature from commercial equipment suppliers provide further details on the power systems and commonly used sensor styles.

Response to Mean Flow

A wire or film sensor responds to changes in flow conditions that affects the heat transfer of the sensor to its environment. For steady flow the sensor response may be expressed as

$$Nu \sim A+B \sqrt{Re} \tag{1.1}$$

or

$$E^2 \sim [C+D\ (\rho u)^x]\ (T_w - T_e) \tag{1.2}$$

where x=0.5 for classical analysis (King's law) of flow around heated cylinders. Figure A.1.1 shows the response of a hot wire to the mean flow. For supersonic flow, the Nusselt number is evaluated behind the normal shock (Ref. 6).

Response to Fluctuations in the Flow

The simultaneous reaction of the heated sensor to density, velocity and temperature is the key both to the advantages and difficulties of the hot-wire anemometer approach to measuring flow fluctuations. It is an advantage to have one sensor measure both kinematic and thermodynamic fluctuations. In comparison, a laser Doppler velocimeter can only measure the fluctuating velocities and a microphone or pressure sensor responds only to the net sound or pressure fluctuations. Separation of the modes composing the output of the heated sensor is not simple and, in general, requires a priori knowledge of the flow characteristics being sampled.

The choice of techniques for separating the modes of a fluctuating hot-wire signal is somewhat dependent on the Mach number and Reynolds number of the test. As indicated in the summary curve of Fig. A.1.1, wire response to mean flow is well defined for the incompressible case. For isothermal, incompressible flow, a hot-wire responds only to velocity changes. The sensor output is well behaved for supersonic Mach numbers as indicated by the lower curve of Fig. A.1.1. The sensor output, however is Mach number dependent between these two bounds for the lower range of wire Reynolds number.

Test equipment and data analysis techniques are sufficiently developed to permit useful applications for tunnel calibrations over the Mach range of interest in this report ($0.4 \leq 3.5$). Research to improve equipment and analysis should continue however. In particular, additional work needs to be done in the areas of transonic flow applications and separation of the signal into its component modes.

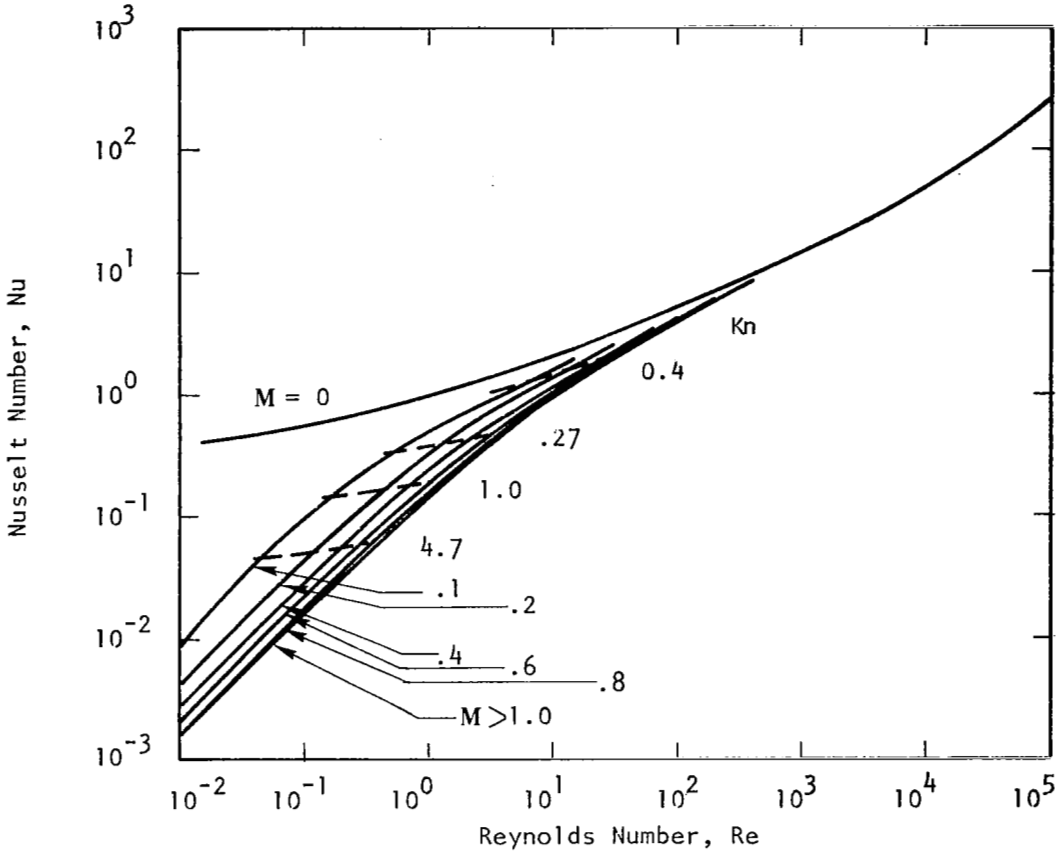

Figure A.1.1 CORRELATION OF CONVECTIVE HEAT TRANSFER FROM TRANSVERSE CYLINDERS. (Ref. 3)

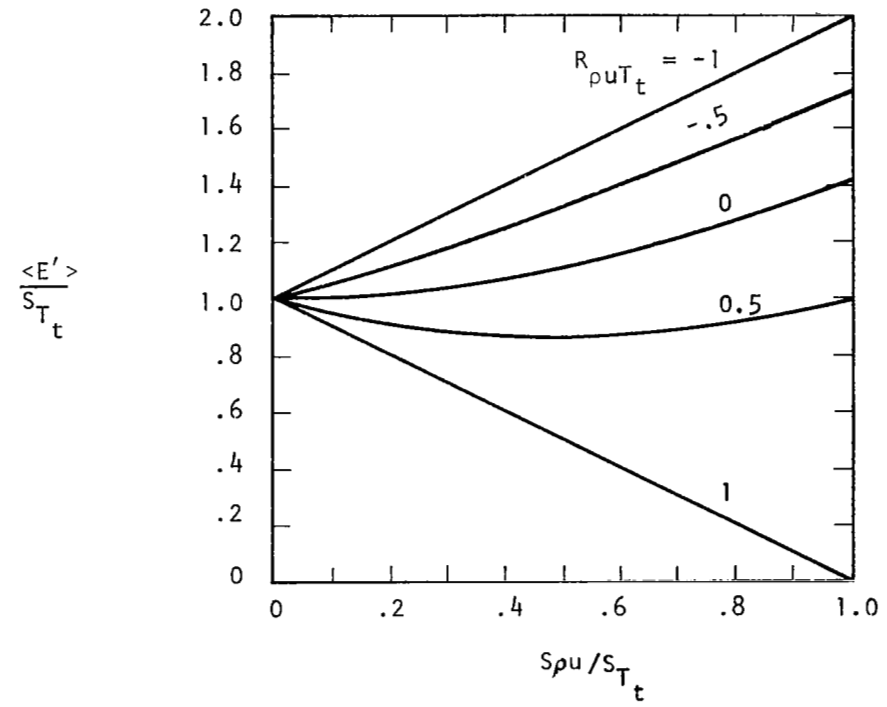

Figure A.1.2 FLUCTUATION DIAGRAM FOR 1 PER CENT MASS FLOW FLUCTUATIONS AND 1 PER CENT STAGNATION TEMPERATURE FLUCTUATIONS WITH VARYING DEGREES OF CORRELATION. (Ref. 7)

Separation of Modes in Fluctuating Flow

In supersonic flow the fluctuating voltage of a heated wire placed normal to the flow can be expressed in terms of the fluctuating velocity, density and total temperature (Refs. 3, 7, 8, and 10), (using the notation of Ref. 10):

$$\frac{E'}{\bar{E}} = - S_\rho \frac{\rho'}{\bar{\rho}} - S_u \frac{u'}{\bar{u}} + S_{T_t} \frac{T_t'}{\bar{T}_t} \tag{1.3}$$

The sensitivity coefficients for constant temperature sensor operation are:

$$S_\rho = \frac{1}{2}\left(\frac{\partial \ell n\, Nu_t}{\partial \ell n\, Re_t} - \frac{1}{\tau_{wr}} \frac{\partial \ell n\, \eta}{\partial \ell n\, Re_t}\right) \tag{1.4}$$

$$S_u = S_\rho + \frac{1}{2\alpha}\left(\frac{\partial \ell n\, Nu_t}{\partial \ell n\, M} - \frac{1}{\tau_{wr}} \frac{\partial \ell n\, \eta}{\partial \ell n\, M}\right) \tag{1.5}$$

$$S_{T_t} = \frac{K}{2 A'_w} + \frac{1}{2}(K - 1 - n_t) + m_t S_\rho + \frac{1}{2}(S_u - S_\rho) \tag{1.6}$$

For supersonic flow ($M > 1.2$), the heat loss is insensitive to Mach number, and sensitivity to velocity and density are essentially equal (Refs. 3, 6, 8).

$$\therefore S_u = S_\rho = S_{\rho u}$$

Thus for supersonic flow, Eq. (1.3) may be simplified to (Ref. 7):

$$\frac{E'}{\bar{E}} = - S_{\rho u} \frac{(\rho u)'}{\overline{\rho u}} + S_{T_t} \frac{T_t'}{\bar{T}_t} \quad . \tag{1.7}$$

The root-mean-square of the sensor output may be expressed as:

$$\frac{\langle E'^2 \rangle}{S^2_{T_t}} = \left(\frac{S_{\rho u}}{S_{T_t}}\right)^2 \left(\frac{\langle (\rho u)'^2 \rangle}{\overline{\rho u}}\right)^2 - 2 \frac{S_{\rho u}}{S_{T_t}} \left[\frac{\langle (\rho u)'^2 \rangle}{\overline{\rho u}} \frac{\langle T_t'^2 \rangle}{\bar{T}_t}\right] R_{\rho u T_t} + \left(\frac{\langle T_t'^2 \rangle}{\bar{T}_t}\right)^2 \tag{1.8}$$

where the correlation coefficient of mass flux and temperature is defined by:

$$R_{\rho u T_t} \equiv \frac{\overline{(\rho u)' \bar{T}_t'}}{\langle (\rho u)' \rangle \langle T_t' \rangle} \quad . \tag{1.9}$$

Sensor output, obtained at three different sensor temperatures, and sensor sensitivity, obtained from calibration, can provide solutions for the three unknowns $\langle(\rho u)'\rangle$, $\langle T_t'\rangle$ and $R_{\rho uT}$. The normal practice is to plot data, obtained at several wire overheat ratios, in modal diagrams as developed by Kovasznay (Ref. 7) and Morkovin (Ref. 8). A fluctuation diagram for varying degrees of correlation is given in Fig. A.1.2. The characteristic modal diagrams of Kovasznay for fluctuations in velocity, temperature, and sound are shown in Figs. A.1.3, A.1.4, and A.1.5.

Independent fluctuations which characterize the flow field are the vorticity (turbulence), entropy (temperature spottiness), and pressure (noise or sound) modes. The vorticity, entropy, and pressure sensitivity coefficients are related to the measured density, velocity, and total temperature sensitivity coefficients as follows (Ref. 8):

$$S_\tau = - S_u + \beta S_{T_t} \tag{1.10}$$

$$S_\sigma = S_\rho + \alpha S_{T_t} \tag{1.11}$$

$$S_\pi = - S_\rho - \frac{n_x}{M} S_u + \alpha (\gamma-1)(1+n_x M) S_{T_t} \tag{1.12}$$

Where n_x is the direction cosine of the normal to a plane sound wave front relative to the flow direction. If two or more measureable sound sources with distinct orientation exist, then a sound sensitivity coefficient would be required for each sound wave direction.

The modal diagram technique is an accepted means of distinguishing the primary characteristics of the sensor signal in supersonic and certain hypersonic flows. An important application of the modal diagram to wind tunnel calibration is to distinguish sound from a fixed source (such as caused by roughness or holes in the wall) as opposed to a moving sound source (such as eminating from a turbulent boundary layer on the tunnel wall).* This technique is effective only for flows where the temperature spottedness is negligible. The diagram for a fixed source of sound has an origin-intercept (see Fig. A.1.5) and the diagram for a moving source of sound has a positive ordinate-intercept similar to the temperature diagram of Fig. A.1.4.

---

* See Refs. 11, 12, 13, and 14 for examples.

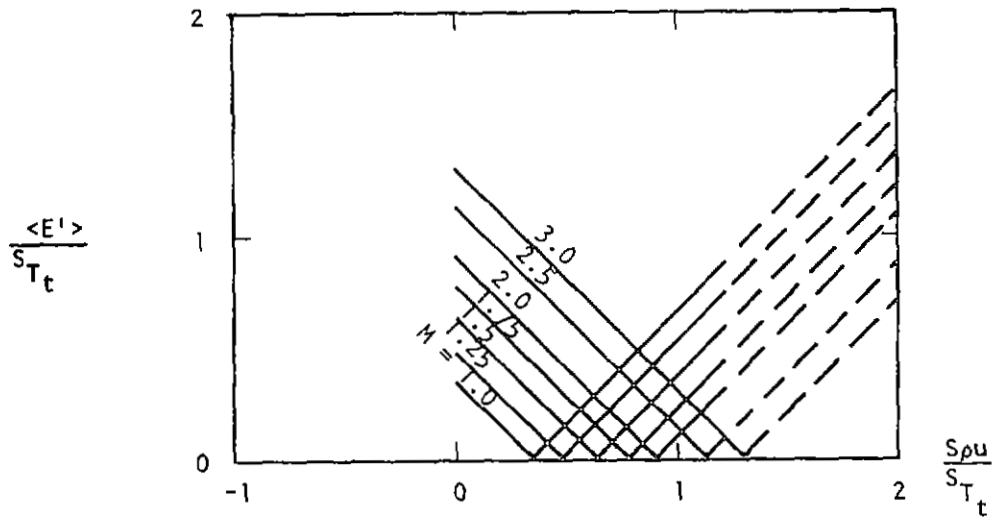

Figure A.1.3 FLUCTUATION DIAGRAM FOR 1 PERCENT TURBULENT VELOCITY FLUCTUATIONS (VORTICITY MODE). (Ref. 7)

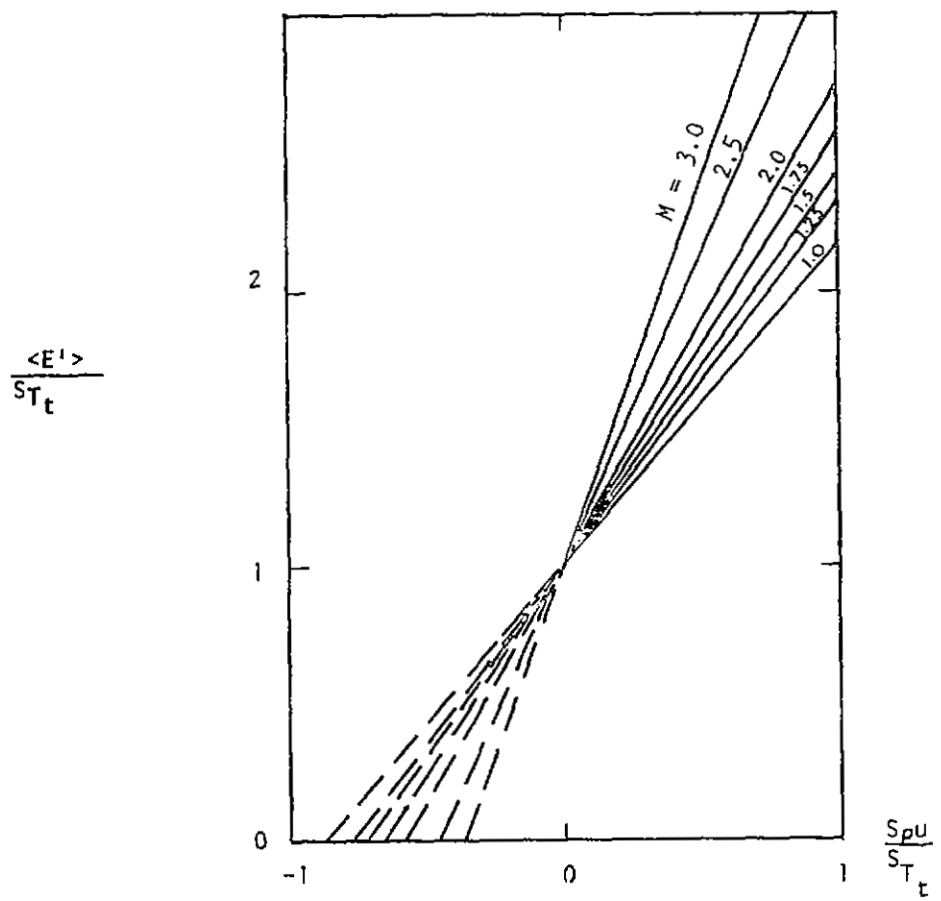

Figure A.1.4 FLUCTUATION DIAGRAM FOR 1 PER CENT TEMPERATURE SPOTTINESS (ENTROPY MODE). (Ref. 7)

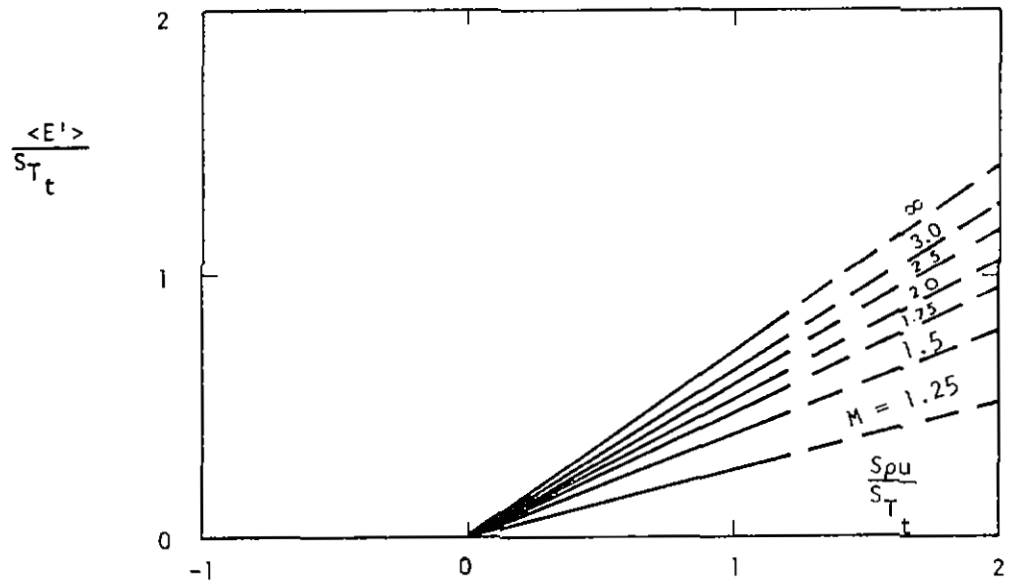

Figure A.1.5 FLUCTUATION DIAGRAM FOR SOUND WAVES THAT ARE ALMOST MACH WAVES HAVING 1 PER CENT PRESSURE FLUCTUATIONS (Ref. 7)

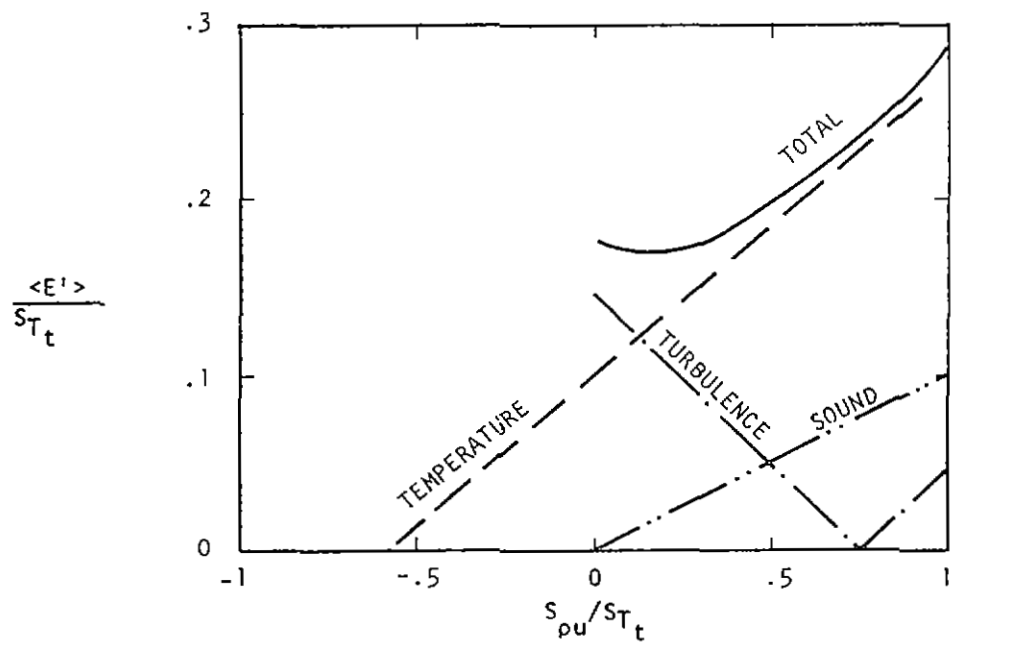

Figure A.1.6 FLUCTUATION DIAGRAM FOR UNCORRELATED MODES AT M = 1.75; TEMPERATURE SPOTTINESS 0.1 PER CENT; TURBULENT VELOCITY FLUCTUATIONS 0.2 PER CENT; SOUND WAVES (DETECTABLE) 0.1 PER CENT OF MASS FLOW FLUCTUATIONS. (DOTTED LINES SHOW SEPARATE CONTRIBUTIONS.) (Ref. 7)

When the dominate mode is sound, the following isentropic relations between pressure, density and temperature are appropriate (Ref. 11):

$$\frac{P'}{\overline{P}} = \frac{\rho'}{\overline{\rho}} = \frac{\gamma}{\gamma-1}\frac{T'}{\overline{T}} \tag{1.13}$$

$$\frac{(\rho u)'}{(\overline{\rho u})} = \frac{u'}{\overline{u}} + 1/\gamma\frac{P'}{\overline{P}} \tag{1.14}$$

$$\frac{T'_t}{\overline{T}_t} = \alpha(\gamma-1)\left(\frac{P'}{\gamma\overline{P}} + M^2\ \frac{u'}{\overline{u}}\right) \tag{1.15}$$

The resultant hot-wire equation and calculation of the fluctuation quantities in the freestream are given in References 11 and 12.

In Reference 15, an application of the diagram approach is shown which identifies temperature fluctuations in the wake of a wedge in hypersonic flow where the adjoining freestream signal level is low. If both temperature fluctuations and moving sound sources are likely present (Ref. 16), the interpretation of the diagrams becomes more difficult. An example of a hot-wire output, in a case where all three modes, are present is shown in Figure A.1.6. It is readily seen that in the absence of one dominant mode, separation of the component modes can be a problem. References 7, 8, and 12 may be consulted for more details concerning the modal diagram technique.

Transonic Flows

The modal diagram approach cannot be generally applied for compressible subsonic and transonic flows (see Fig. A.1.1) where the derivatives of the Nusselt number and recovery factor with respect to Mach number are not zero, and $s_u \neq s_\rho$ for all overheat ratios (Refs. 3, 8, and 10). Transonic operation at high dynamic pressures also increases problems with wire breakage.

The above problems help explain the limited usage of hot-wire systems in transonic wind tunnels. Recent developments, however, provide examples for overcoming these difficulties. The sensor failure problem may be alleviated with the use of shorter wires ($\ell/d \sim 100$), wires with insulative backing or film sensors (Ref. 10, 17, and 18). Heat losses to end supports or substrate and possible interference effects necessitate that each sensor be calibrated in a representative flow environment. The sensitivity coefficients S_ρ and S_u

have been systematically measured in transonic flow by independently varying density and velocity (Refs. 9 and 10). These results establish that S_ρ and S_u are approximately equal for all Mach numbers (including the troublesome transonic range) if the wire overheat ratio is greater than 0.5 and the wire Reynolds number is greater than 20. Operation within these restrictions again permits the use of the simplified expression of Eq. (1.7). For many transonic wind tunnels the total temperature fluctuations are negligible relative to the mass-flux term. In this case the hot-wire directly senses the fluctuations of the mass-flux. If the level of temperature fluctuation is unknown in a facility (such as a new cryogenic tunnel) the level may be ascertained with a sensor operated at constant current and near the recovery temperature.

Reduction of mass-flux measurements in a transonic flow into its elements requires further assumptions, e.g., possible application of the modal diagrams or an independent measurement with a laser velocimeter, pressure transducer or a special hot-film geometry. For boundary-layer flow, the pressure fluctuations can generally be neglected relative to vorticity. Operating within the above described wire and flow domain, boundary layer profiles of velocity, density and Reynolds shear stress were successfully obtained in Ref. 10 for a nominal Mach number of 0.8. For operation in the transonic freestream, it appears that the principle of modal diagrams can be applied to high-Reynolds-number flow by obtaining data at several over-heat ratios, all being greater than 0.5. Straight line fairings of the data, extrapolated to the ordinate, would then provide information on the dominate mode as in the supersonic case. Another approach for separation of the fluctuation modes is to employ a yet-to-be defined film sensor that has two (or more) films and a geometry such that one film responds to the mass-flux and a second film responds to pressure (geometrically shielded from velocity). An application of special sensor geometry, for direct correlation measurements, has been reported for hypersonic, boundary-layer flow (Ref. 17).

Comparison of Hot Wire to Other Systems

Hot-wire data have, in general, compared well with measurements from other devices. Agreement of velocity profiles obtained with hot wire and laser systems within a shock-wave/boundary-layer interaction (Ref. 19) gives credence to both systems and tends to validate the assumptions employed in

data reduction. In the freestream of many transonic and supersonic wind tunnels the sound mode generally dominates, and in such cases good agreement has been obtained between hot-wire and pressure transducer measurements (Refs. 14 and 20). An example comparison of Pitot and hot-wire measurements at M = 5 is shown in Fig. A.1.7. For diagnostic measurements of flows with noise dominated disturbances, a dynamic pressure transducer may sense such fluctuations with much less effort than a hot-wire system. A dynamic Pitot pressure survey may satisfy many wind tunnel calibration requirements. Another widely used calibration model is the AEDC developed, pressure-instrumented 10° cone. (See Section III.F.1.).

In summary, the hot-wire can provide more information than a dynamic pressure transducer, e.g., it can distinguish between moving and fixed sources of sound with a single sensor. The wire also provides a higher frequency response and, in general, has a more omnidirectional response to noise sources. The smaller sensor of a hot-wire system is important (in addition to the frequency aspect) if local fluctuating measurements in a shock or boundary layer are required. Further, the wire/film sensor may be located in areas hidden from the view of a laser Doppler velocimeter.

Other Data Analysis Techniques

Other data-reduction techniques for the fluctuating signal include time (autocorrelation) and spatial (location and direction) correlations of the signal. Spectral analysis provides the energy content at each frequency. These techniques and associated electronic equipment are fairly common and are described in the literature. (Suggested references include 3, 12, 14, and 21).

Sensor Choice and Calibration Requirements

In the past, the wire-breakage problem had encouraged minimizing calibration time. Minimum calibration requires maximum use of correlations of existing calibration data and end-loss corrections to predict the performance of a wire (Refs. 8, 12, 22, and 23). A more recent approach, that promises improved data gathering efficiency and data accuracy, is the use of more durable, rugged sensors. A rugged sensor may include a fine-diameter short wire ($\ell/d \sim 100$), a wire backed by an insulator, or a larger diameter film sensor (Refs. 10, 17, 18 and 24). The complex heat loss and possible support interferences with such sensors require individual sensor calibrations and the use of a constant temperature system.

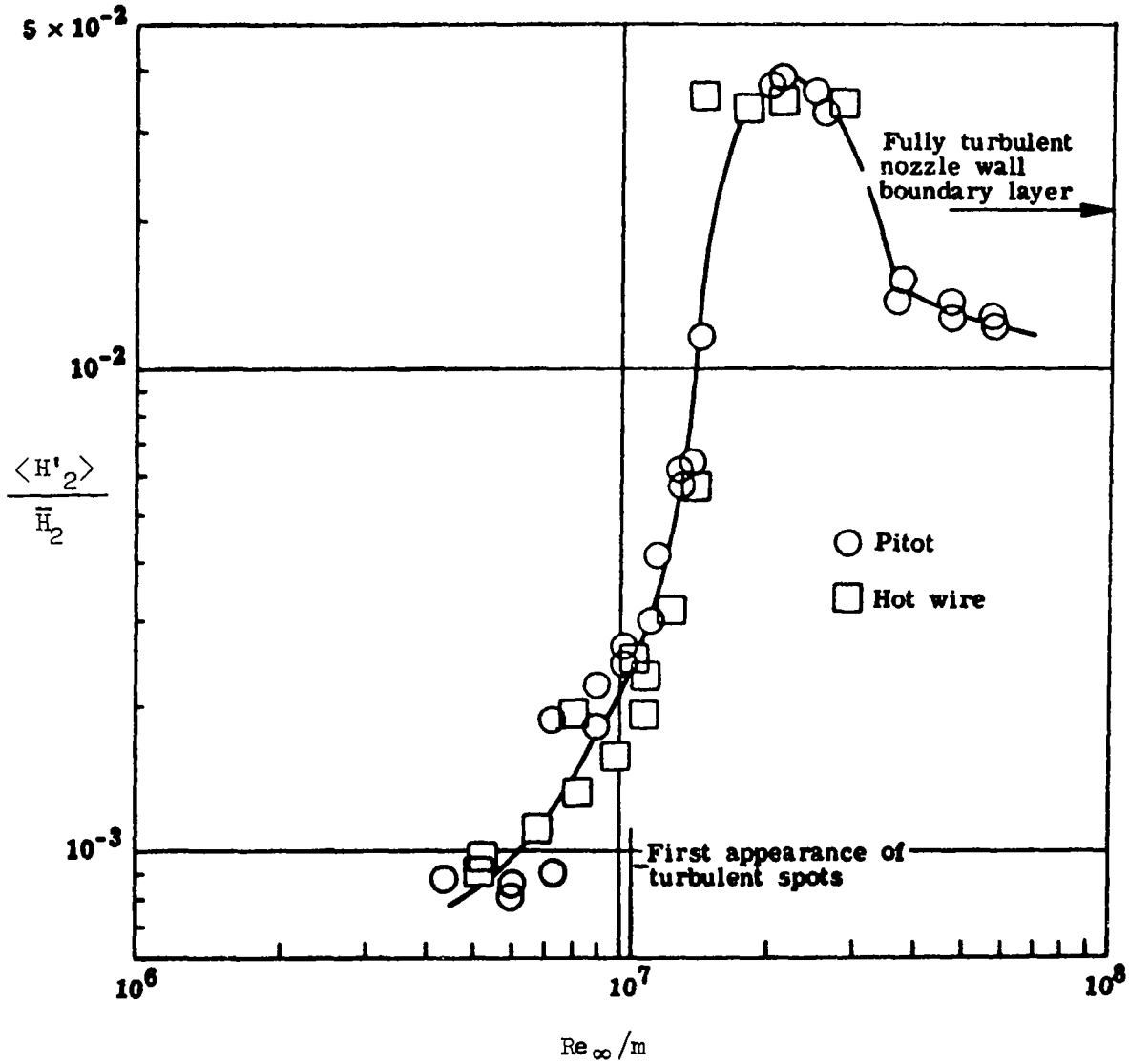

Figure A.1.7 COMPARISON OF PITOT PROBE AND HOT-WIRE MEASUREMENTS OF FREE-STREAM PRESSURE FLUCTUATIONS IN A CONVENTIONAL, MACH 5 NOZZLE, Ref. 14.

Calibration of a heated sensor may, in general, be obtained in situ by maintaining a constant Mach number and temperature and varying the total pressure (and thereby Reynolds number). For supersonic flow and for R > 20 in transonic flow, $S_\rho = S_u = S_{\rho u}$. Further discussions on such mean flow approaches to calibration and more-refined dynamic calibrations are given in References 3, 8, 9, 14, 18, 25, and 26.

Rose and Horstman have successfully used the rugged class of tungsten hot-wires in a transonic flow for over 16 hours without breakage.* Commercially available film sensors (such as 0.002 to 0.006-inch diameter cylinders) should also receive consideration for wind tunnel calibration because of the following advantages:

- superior resistance to particle damage,
- superior resistance to surface contamination and strain gaging,
- higher sensor Reynolds numbers (particularly important in transonic flow).

Compared to the rugged class of tungsten wire sensor, the platinum-film sensor has comparable capabilities in maximum overheat ratio (~one) and frequency response (~150K Hz).

*Private communication

Summary of Advantages and Disadvantages of Hot Wire System

The advantages and disadvantages of using a hot-wire system to measure the fluctuating flow properties during a wind tunnel calibration are summarized as follows.

Advantages

1. Small sensor size
2. High frequency response
3. High sensitivity
4. Sensitive to both kinematic and thermodynamic fluctuations
5. Distinguish between moving and stationary noise sources with a single sensor (in flows where temperature spottedness is negligible)
6. Reliable systems and sensors commercially available
7. Rugged sensors available, particularly film type

Disadvantages*

1. Possible frequent breakage of fine-wire sensor (due to air loads, vibrations, particle impingement, burnout, oxidation, accidents, etc.)
2. Possible false signal (usually apparent)due to strain guaging, contamination, or vibration of probe.
3. Calibration may be required in situ (facility time may be expensive).
4. Separation of signal into independent modes requires assumptions concerning flow characteristics or independent measurements
5. Analyses of signal particularly difficult for compressible subsonic or transonic flow, unless restricted to higher Reynolds numbers and wire temperatures.

*Since the original writing of this section, a review of hot-wire anemometry by Comte-Bellot has been published (Ref. 27). This reference provides additional discussion of problem areas.

NOMENCLATURE

A,B,C,D	constants
A'_w	overheat parameters, $1/2 \frac{\partial \ln R_w}{\partial \ln I}$
d	wire diameter
E	wire voltage
$\overline{H}_2$	time-averaged, total pressure behind a normal shock
h	heat-transfer coefficient
I	wire current
k	$d \ln R_w / d \ln T_w$
Kn	Knudsen number, n/d
ℓ	wire length
m	$d \ln \mu / d \ln T_w$
M	Mach number
n	$d \ln k / d \ln T_w$
n_x	direction cosine of normal to sound plane wave front relative to flow direction
Nu	Nusselt number, $\frac{hd}{k}$
p	static pressure
R	resistance
Re	Reynolds number, $\rho u d/\mu$
$R_{(\rho u)T_t}$	correlation coefficient of mass-flux and total temperature fluctuations, $\frac{\overline{\{ (\rho u)' T_t' \}}}{\overline{\{<(\rho u)'> < T_t'> \}}}$
S	sensor sensitivity coefficient
T	temperature
u	axial velocity
x	exponent in equation 2

α	$\frac{1}{\{1 + \frac{(\gamma - 1)}{2} M^2\}}$
β	$\frac{(\gamma - 1)M^2}{\{1 + \frac{(\gamma - 1)}{2} M^2\}}$
γ	ratio of specific heats, 1.40 used for air
n	recovery factor, T_r/T_t
λ	molecular mean free path
μ	viscosity
ρ	density
τ_{wr}	temperature overheat, $\frac{(T_w - T_r)}{T_r}$
$<( )>$	root mean square

Superscripts

$( )'$	fluctuating value
$\overline{( )}$	time averaged

Subscripts

e	environment
r	recovery of adiabatic wall
t	total or stagnation conditions
t_2	stagnation correction behind normal shock
T	temperature
u	velocity
w	wire
π	sound
ρ	density
ρu	mass flux
σ	entropy
τ	vorticity

A.1. REFERENCES

1. H. L. Dryden and A. M. Kuethe: "Effect of Turbulence in Wind Tunnel Measurements," NACA Tech. Rep. 342, 1930.

2. "Advances in Hot Wire Anemometry, Proceedings of the International Symposium on Hot Wire Anemometry," Edited by W. L. Melnik and J. R. Weske, University of Maryland, AFOSR No. 68 - 1492, USAF Office of Scientific Research, July, 1968.

3. V. A. Sandborn: Resistance Temperature Transducers, Metropology Press, Fort Collins, Colorado, 1972.

4. V. A. Sandborn: "A Review of Turbulence Measurements in Compressible Flow," NASA TM X-62,337, March 1974.

5. R. Westley: "Problems of Noise Measurements in Ground-Based Facilities with Forward-Speed Simulation," Appendix 5 of "A Further Review of Current Research Aimed at the Design and Operation of Large Wind Tunnels," Second Report of the Minilaws Working Group, AGARD-AR-83, Sept. 1975.

6. L. S. G. Kovasznay: "The Hot Wire Anemometer in Supersonic Flow," Jour. Aero. Sci., Vol. 17, No. 9, September, 1950.

7. L. S. G. Kovasznay: "Turbulence in Supersonic Flow," Jour. Aero. Sci., Vol. 20, No. 10, October, 1953.

8. M. V. Morkovin: "Fluctuations and Hot Wire Anemometry in Compressible Flows," AGARDograph, 24, November, 1956.

9. W. C. Rose and E. P. McDaid: "Turbulence Measurement in Transonic Flow," Proc. AIAA 9th Aerodynamic Testing Conference, June 1976.

10. C. C. Horstman and W. C. Rose: "Hot Wire Anemometry in Transonic Flow," NASA TM X-62,495, December 1975.

11. J. Laufer: "Aerodynamic Noise in Supersonic Wind Tunnels," Jour. Aero. Sci., Vol. 28, No. 9, September 1961.

12. J. C. Donaldson and J. P. Wallace: "Flow Fluctuations Measurements at Mach number 4 in the Test Section of the 12 Inch Supersonic Tunnel (D)," AEDC-TR-71-143, August 1971.

13. M. C. Fischer and R. D. Wagner: "Transition and Hot Wire Measurements in Hypersonic Helium Flow," AIAA Journal, Vol. 10, No. 10, October 1972.

14. J. B. Anders, P. C. Stainback, L. R. Keefe, and I. E. Beckwith: "Sound and Fluctuating Disturbance Measurements in the Settling Chamber and Test Section," ICIASF '75 Record, Int'l Congress on Instrumentation in Aerospace Simulation Facilities, Ottawa, Canada Sept. 22-24, 1975, published by IEE, 345 E. 47th Street, New York.

15. R. D. Wagner and L. M. Weinstein: "Hot Wire Anemometry in Hypersonic Helium Flow," NASA TN D-7465, June 1974.

16. P. C. Stainback, et al: "Experimental Studies of Hypersonic Boundary - Layer Transition and Effects of Wind Tunnel Disturbances," NASA TN D-7453, NASA Langley Research Center, March 1974.

17. V. Mikulla and C. C. Horstman: "Turbulence Stress Measurements in a Non-adiabatic Hypersonic Boundary Layer," AIAA Journal, Vol. 13, No. 12, December 1975.

18. W. C. Rose: "The Behavior of a Compressible Turbulent Boundary Layer in a Shock-Wave-Induced Adverse Pressure Gradient," NASA TN D-7092, NASA Ames Research Center, March 1974.

19. W. C. Rose and D. A. Johnson: "Turbulence in a Shock-Wave Boundary-Layer Interaction," AIAA Journal, Vol. 13, No. 7, July 1975.

20. E. Grande and G. C. Oates: "Response of Miniature Pressure Transducers to Fluctuations in Supersonic Flow," Instrumentation for Airbreathing Propulsion, AIAA Series on Progress in Astronautics and Aeronautics, Vol. 34, 1972.

21. R. K. Otnes and L. Enochson: Digital Time Series Analysis, Wiley, New York, 1972.

22. W. Behrens: "Total Temperature Thermocouple Probe Based on Recovery Temperature of Circular Cylinder," Int. J. Heat and Mass Transfer, Vol. 14, 1971.

23. C. F. Dewey, Jr.: "Hot Wire Measurements in Low Reynolds Number Hypersonic Flows," ARS Journal, Vol. 28, No. 12, December 1961.

24. E. L. Doughman: "Development of a Hot Wire Anemometer for Hypersonic Turbulent Flows," The Review of Scientific Instruments, Vol. 43, No. 8, August 1972.

25. R. F. Rosenberg: "Some Aspects on Hot Wire Anemometry Leading to a Special Calibration Method for Hot Wire Probes," ARL 71-0038, USAF Aerospace Research Laboratories, March 1971.

26. R. H. Kirchhoff and R. R. Safarik, "Turbulence Calibration of a Hot Wire Anemometer," AIAA Journal, Vol. 12, No. 5, May 1974.

27. Comte-Bellot, G.: "Hot-Wire Anemometry," Annual Reviews of Fluid Mechanics, Vol. 8, Palo Alto, Calif. 1976.

APPENDIX II
LASER DOPPLER VELOCIMETER MEASUREMENTS

The development of the laser was quickly followed by its application to the measurement of the velocity of a moving object by observing the Doppler shift in the frequency of the incident laser light. Liquid flow velocities were measured by Yeh and Cummins (Ref. 1) in 1964, utilizing Doppler radiation from small particles entrained in the flow. In 1965, the technique was refined and measurements were made in seeded gas flow by Foreman, George and Lewis (Ref. 2). Since that time very significant advances have been made both in the theoretical understanding of the technique, and in improved optical arrangements and signal processors. The Laser Doppler Velocimeter (LDV) technique has been applied to measurements of mean velocity, turbulent intensity and flow direction in a variety of flow fields and in both liquids and gases. By 1970 the velocity range over which measurements had been made extended from 10^{-4} cm/sec to 1000 m/sec (Ref. 3). This rapid rate of development continues. Literature on the subject is now extensive; a bibliography (Ref. 4) published in 1972 contains 190 references.

Laser velocimeter systems have been operated in several wind tunnels, e.g., Refs. 3, 5, 6, 7, 8, and their unique capabilities, especially for non-intrusive velocity and turbulence surveys around models in the tunnel, should insure their continued development and application. Although to the present, the LDV has not been widely applied to basic tunnel calibration measurements, this capability has been demonstrated and their availability to the wind tunnel operator will probably lead to this use. The discussion herein will be restricted primarily to consideration of the LDV technique for application to basic facility flow calibration measurements such as mean velocity (Mach number) distribution, turbulence intensity and flow angularity.

Basic Principles

Consideration of the advantages and disadvantages of laser velocimeter techniques require some discussion of the basic principles of the system.

The principle of the LDV can be described by both the Doppler effect and by an interference-fringe model. Since both approaches yield the same basic equations discussed in this report, the fringe model will be used since it aids visualization of the physical principles involved. Several optical arrangements are possible, but considerations will be limited to the dual-

beam or differential-Doppler system most commonly used for wind tunnel measurements.

For a single-component, dual-beam system, Fig. A.11.1, a laser beam is separated into two parallel beams of equal intensity separated by a distance Δ. These beams enter a lens which causes them to cross at the focal point of the lens where the measuring or probe volume is formed. In this region, the wavefronts interfere constructively and destructively to form stationary, alternate dark and bright regions or fringes, Fig. A.11.2. A particle moving through the measuring volume causes variations in the intensity of the light scattered by the particle. The scattered light is collected and focused by a second lens onto a photodetector, usually a photomultiplier tube.

The receiving optics and photodetector may be located on the same side of the measuring volume as the laser and transmitting optics or may be located on the opposite side. If located on the same side, the system utilizes light scattered in the backward direction by particles in the flow (backscatter mode). If laser and receiving optics are on opposite sides of the measuring volume, the system utilizes light scattered in the forward direction (forward-scatter mode). Obvious operational advantages are associated with the backscatter mode, particularly for wind tunnel application. However, since much more light is scattered in the forward direction, Fig. A.11.3, the signal-to-noise ratio is significantly higher with the forward-scatter system.

The photomultiplier tube generates an electrical signal at a frequency directly proportional to the velocity and inversely proportional to the fringe spacing, Fig. A.11.4, according to the relation

$$f_d = \frac{U}{\delta_f} \tag{11.1}$$

where f_d is the Doppler frequency, U the velocity component normal to the fringes and perpendicular to the bisector of the beam angle, and δ_f is the fringe spacing.

The fringe spacing can be determined from the system geometry and the wavelength of the laser as shown in Figs. A.11.1 and 2, i.e.,

$$\delta_f = \frac{\lambda}{2 \sin(\frac{\theta}{2})} \quad , \tag{11.2}$$

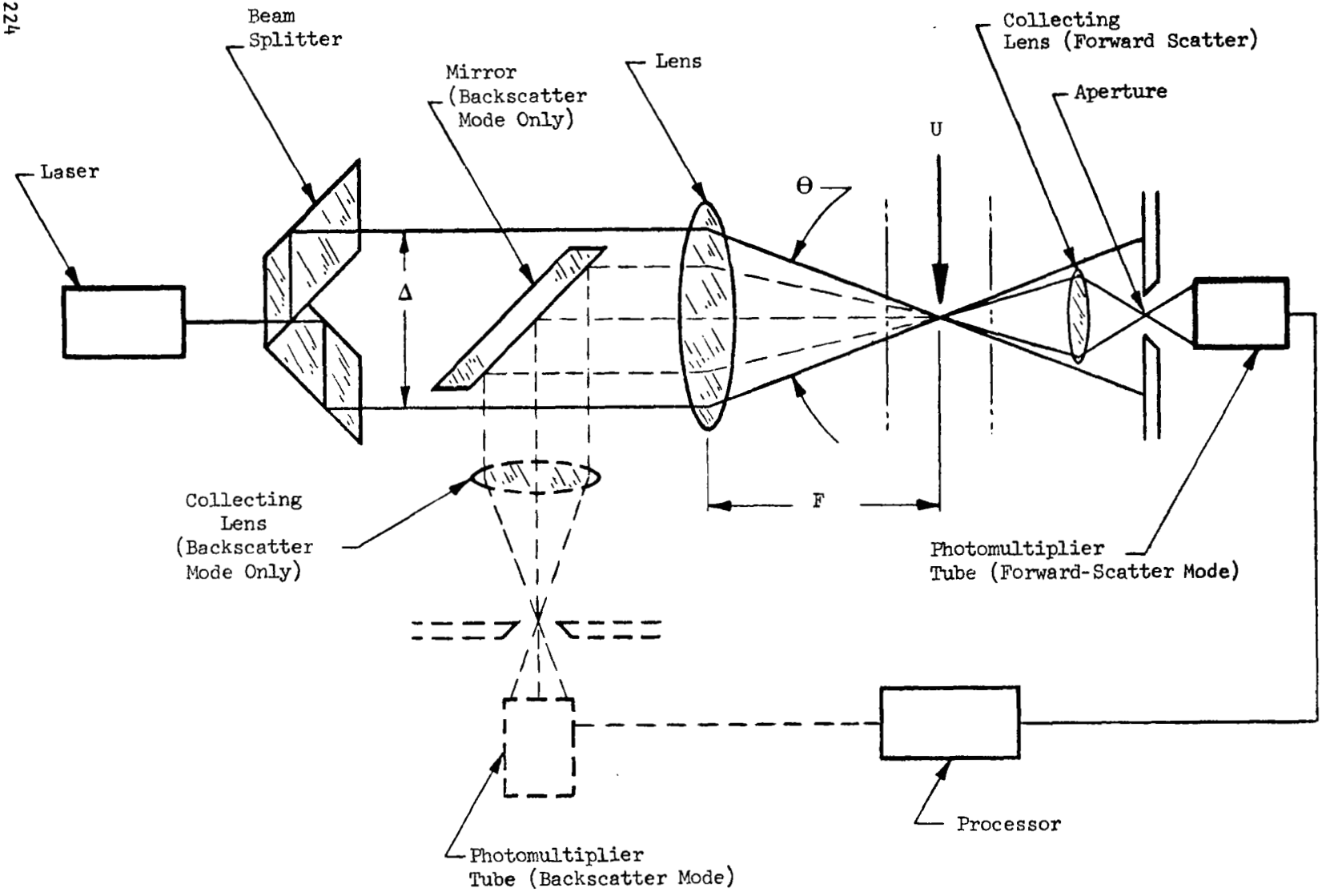

Figure A.11.1. DUAL BEAM LASER DOPPLER VELOCIMETER, WITH OPTIONAL FORWARD AND BACKSCATTER MODES

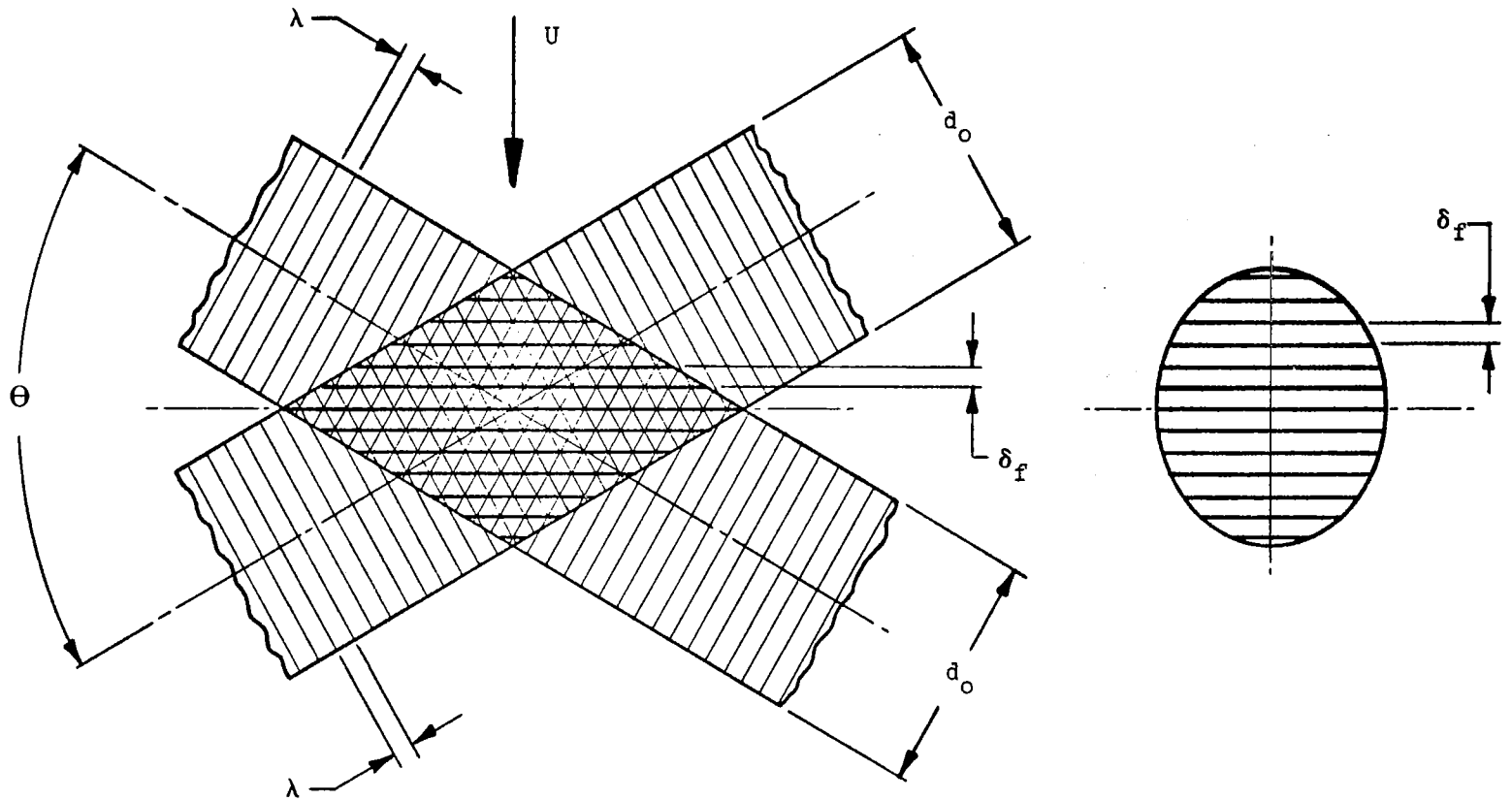

Figure A.11.2 GENERATION OF INTERFERENCE FRINGES IN MEASURING VOLUME OF DUAL BEAM LASER DOPPLER VELOCIMETER

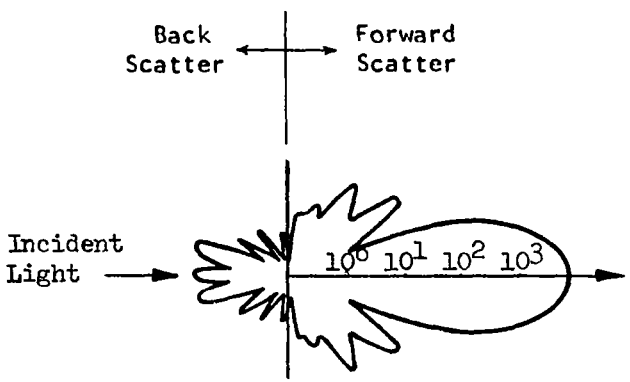

Figure A.11.3 LIGHT SCATTERED BY A SMALL PARTICLE

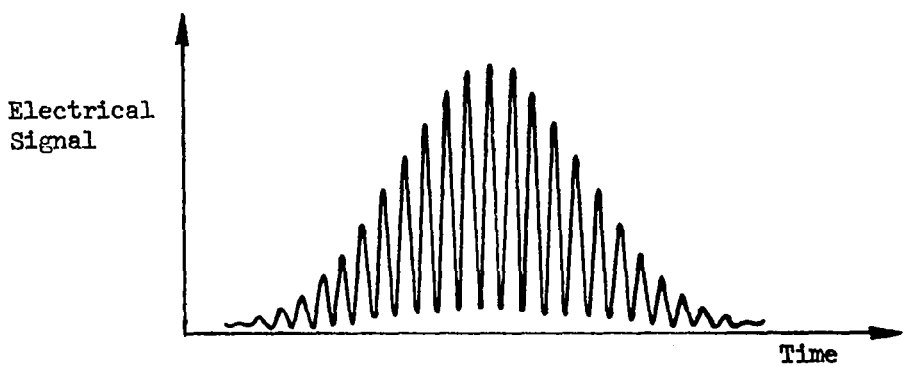

Figure A.11.4 LASER ANEMOMETER SIGNAL FROM PHOTODETECTOR

where λ is the wavelength of the laser and θ is the angle between the intersecting beams. From the above relations:

$$U = \frac{f_d \lambda}{2 \sin(\frac{\theta}{2})} \quad . \tag{11.3}$$

The measured velocity is the absolute value of the velocity of the particle which is not necessarily equal to that of the fluid. The problems of particle lag will be discussed in more detail later in this section. The ambiguity with regard to flow direction becomes a problem in turbulent flows at low, mean-component velocity where flow reversal may be encountered, but can be overcome by introducing an acousto-optic modulator (Bragg cell) into one of the two parallel laser beams. The Bragg cell introduces an accurately known frequency shift into one of the beams, which results in a moving rather than a stationary fringe system. Zero particle velocity then corresponds to the frequency shift; higher or lower velocities generate higher or lower output signal frequencies. In this manner the directional ambiguity can be eliminated and reversing flows can be measured. For main-stream, empty-test-section measurements in a wind tunnel the directional ambiguity will not normally be a problem, but the Bragg cell may still be useful at high flow velocities to down-shift the signal frequency to a range that can be more readily measured by the electronic signal processor.

The measuring or probe volume is an ellipsoid which may be defined by the contour where the light intensity decreases to 1/e times the maximum intensity at the center of the probe volume, Ref. 9. The width and length of the volume Fig. A.11.2 may be defined by

and $$w_v = \frac{d_o}{\cos(\frac{\theta}{2})} \approx d_o \quad , \tag{11.4}$$

and $$\ell_v = \frac{d_o}{\sin(\frac{\theta}{2})} \quad , \tag{11.5}$$

where d_o is the diameter of the intersecting laser beams at the focal point of the transmitting lens. The focused diameter, d_o, is related to the initial laser beam diameter, D_o, by

$$d_o = \frac{4}{\pi} \frac{F\lambda}{D_o} \quad , \tag{11.6}$$

where F is the transmitting lens focal length. Other relations may be derived for the dimensions of the probe volume, depending upon how the "effective" geometric boundaries are defined (Refs. 3, 10, 11). The above equation demonstrates that a large, original (or expanded) laser-beam diameter and a short-focal-length lens yield the minimum size measuring or probe volume. The focal length is also determined by the distance from the transmitting lens to the point of the flow where measurements are desired.

The selection of the measuring volume is a design problem during which conflicting requirements must be balanced. The initial restrictions are usually determined by the minimum number of fringes required for the signal processor to measure the frequency with adequate accuracy. Also, the Doppler signal frequency must not exceed the maximum which can be measured by the processor; this frequently is a function of the fringe spacing and the maximum velocity to be measured, as defined by Eq. (11.1). The required minimum number of usable fringes can be as low as eight with a counter system, but a somewhat larger number is normally preferred. The number of fringes can be determined from the width of the measuring volume, w_v, divided by the fringe spacing, δ_f, as defined by Eqs. (11.2), (11.4) and (11.6), i.e.,

$$N_{fr} = \frac{2\, d_o \sin\left(\frac{\theta}{2}\right)}{\lambda} \tag{11.7}$$

$$= \frac{8F \sin\left(\frac{\theta}{2}\right)}{\pi\, D_o} \quad . \tag{11.8}$$

From the optical configuration, Fig. A.11.1, it may be noted that the angle $(\theta/2)$ is normally small.

$$\sin\left(\frac{\theta}{2}\right) = \tan\left(\frac{\theta}{2}\right) = \frac{\Delta}{2F} \tag{11.9}$$

Here Δ is the beam separation distance at the transmitting lens. From Eqs. (11.8) and (11.9), the number of fringes can be expressed in terms of only the beam separation distance and the initial laser-beam diameter.

$$N_{fr} = \frac{4}{\pi} \frac{\Delta}{D_o} \tag{11.10}$$

Again note that the number of fringes can be increased by reducing the unfocused beam diameter, D_o, but this in turn increases the probe diameter. Increasing the beam separation, Δ, for a fixed transmitting lens focal length, is an effective means of increasing the number of fringes.

Based on the preceeding equations, it is of interest to calculate the dimensions of the measuring volume and other characteristics of a velocimeter system. Consider an Argon laser with a wavelength of 514.5 nm and an input beam diameter of 1.5 mm. If the transmitting lens focal length is 1.5 m and the beam spacing is 100 mm, the beam angle is 3.818°. From Eq. (11.6) the focused beam diameter is 0.65 mm which is also the maximum width of the probe volume. The length of the probe volume is, from Eq. (11.5), 19.7 mm. The fringe spacing is 7.7 μm and the maximum number of fringes is 84. At a velocity of 300 m/sec., the Doppler frequency (Eq. (11.1) will be 38.96 MHz. This system is not necessarily typical, but it illustrates application of the system relationships discussed previously.

To this point the measurement of a single velocity component (normal to the fringe pattern) has been described. The fringe pattern of a single-component LDV can be rotated by rotating the transmitting optics. This permits the measurement of velocity components at two or more angles such as $\pm$45 degrees to the nominal tunnel centerline. From the two velocity component measurements, the velocity vector in the tunnel plane normal to the bisector of the intersecting beams can be determined. Thus, flow angularity can be measured in addition to velocity and turbulence intensity.

Optical arrangements to yield simultaneous two-component measurements can be realized by using two pairs of intersecting beams, usually with the plane defined by the second pair of beams normal to that defined by the first beam pair. Separation of the two measurements can be achieved by splitting a laser beam into two pairs of beams, each pair polarized 90° to the other. Polarized filters on the two photodetectors allow each detector to see only the light scattered from the fringes formed by two of the four beams at the intersection point. Two wavelengths of laser light can also be used for two component measurements. The use of an Argon ion laser is particularly convenient for this purpose since two strong color bands, 488 nm (blue) and 514.5 nm (green) are available. Optical filters allow separation of the scattered light so each photodetector sees only the light of interest.

A third velocity component, parallel to the bisector of the intersecting beams, can also be measured simultaneously. For example, Orloff and Logan (Ref. 12) have described an LDV system for measuring all three velocity components which employs backscattering and a reference-beam method.

Signal Processors

The output signal from the photomultiplier tube, shown on Fig. A.11.4, is a frequency burst at the Doppler frequency with amplitude modulated according to the intensity distribution across the fringes. This amplitude-modulated envelope is commonly referred to as the "pedestal" and must be removed by high-pass filtering or optical means before processing. The number of cycles of the doppler signal and the modulation intensity about the pedestal envelope will vary according to the location at which the particle crosses the probe volume, the size of the particle and the number of particles present at one time within the probe volume. Signal bursts of measurable amplitude and the minimum required number of cycles occur at random time intervals, and phase reversals during a single signal burst will occur when multiple particles are present.

Several methods for processing the data from the photomultiplier have been used. These include:

- spectrum analyzers
- photon correlators
- filter banks
- frequency trackers
- counters

Only the last two types of processors produce essentially real-time velocity information directly and are currently used for most wind tunnel applications.

The frequency tracker, as the name implies, converts the Doppler frequency received from the photodetector into a proportional, analog voltage. The tracker circuit is implemented using phase or frequency locked loops, or a combination of the two. Both types of loops function by comparing the output frequency of a voltage-controlled oscillator (VCO) or a voltage-to-frequency converter (V/F) to the input signal frequency, and both utilize the difference in frequency to modify or adjust the ac input voltage to the internal frequency generator. The dc voltage is then proportional to the input frequency. Alternatively, the internally-generated frequency can be converted to a digital signal by means of a counter.

Tracker processors are characterized by the maximum frequency range, capture bandwidth, dynamic range and slew rate. If the change in velocity from one particle to the next exceeds the capture bandwidth or capture range, the tracker will lose lock and not track the particle or other particles which are outside the capture range.

Where Doppler signal tracking is interrupted by a drop-out, the last output voltage level is normally placed in "hold". If the signal returns during the hold period, tracking is resumed. If the signal is not recaptured during the hold period, the search or sweep mode is activated until the signal is re-acquired. Signals can be provided to external data systems to record mean velocity and ac or turbulent fluctuation signals, e.g., Ref. 13. Doppler frequencies can be measured from 2kHz to 50 MHz. Velocity changes over a 200:1 range can be followed, and in the search mode the frequency slew rate can be as high as 400 MHz/ms. Data-validation features are also normally incorporated. For example, one system requires tracking for 8 Doppler cycles and holding for 2 additional cycles without drop-out in order to be considered a valid data point. Thus, for heavily seeded flows, data rates up to 1×10^6 per second can be processed.

The counter or burst processor for laser-anemometer signals accurately measures the time required for a particle in the flow to travel across a fixed number of fringes in the measuring volume, i.e., a known distance. From these two quantities, a counter determines the Doppler frequency and thereby the particle velocity. The counter may be inherently a digital instrument, so drift and calibration problems which may be associated with analog processors, such as trackers, are avoided. Counter processors are normally configured to yield a direct digital output.

A counter functions by passing a laser signal burst through a threshold level detector which, when the adjustable amplitude-threshold is exceeded, enables a zero-crossing detector such as a Schmidt trigger. Those Doppler signals above the amplitude-threshold level are then converted into a train of square waves, with a frequency equal to the origianl signal frequency.

Many electronic frequency-counters function by counting each cycle of the unknown signal for an accurately-fixed time period, such as 0.1, 1.0 or 10 seconds. The readings are then converted to the signal frequency

in hertz. Since the maximum number of cycles available from the passage of a particle across the measuring volume of a LDV is extremely small, the accuracy of the direct counting procedure would be totally inadequate. To avoid this problem counter processors are period measurement devices, i.e., pulses from an accurate, high-frequency oscillator or clock are accumulated in a register during the time interval corresponding to a fixed number of pulses from the Schmidt trigger. Alternatively, the time intervals can be converted to voltage amplitudes which can be measured digitally. The time resolution for the n period ranges from 2 to 10 x 10^{-9} seconds, depending upon the clock frequency, e.g., 500 MHz corresponds to 2 x 10^{-9} seconds resolution. The counter processor also normally includes computational capabilities to convert the period information into either frequency or velocity units for digital display. The computation time is typically about 1 x 10^{-6} sec so that, even at high velocities where the Doppler frequency is 10 to 20 MHz, the total acquisition and computation time for one individual measurement can be as short as 2 to 3 x 10^{-6} sec. Data acquisition rates of 100,000 readings/sec are therefore theoretically possible (but far from common) with moderate concentration of particles, Ref. 14.

Counter processors include several data-validation features to allow the rejection of noise bursts, detect the loss of a bit or cycle during a processing cycle, reject signals from large particles, etc. The primary technique utilized to reject data sequences in which one or more cycles may be missing (cycle amplitude below threshold) consists of using two or more registers. The clock pulses are gated into both a high and low register on the first cycle. The clock pulses to the low register are gated off after N_L cycles, while the high register accumulates N_H cycles. A comparater then computes the ratio of the two time intervals, which should be equal, to the ratio N_H/N_L. If the error is within pre-set limits, the measurement is validated.

Asher (Ref. 14) demonstrates the advantage of an odd ratio, N_L/N_H, such as 5/8 or 10/16 over even ratios. Odd ratios such as 5/8 are commonly used. A counter processor using three different registers has been used at AEDC. None of these systems completely reject spurious signals, but they do greatly reduce the probability of such data being considered valid. Large particles, which may be lagging the fluid flow to an excessive degree, can be detected if the total input signal amplitude (pedestal plus Doppler frequency) exceeds

a pre-set limit. The adjustable threshold level (required to enable a zero-crossing detector) can be used to reject signals with inadequate signal-to-noise ratio. Setting the threshold level high, on the other hand, can bias the data acquired to large particles by rejecting low-level signals from small particles.

Most counter processors also include functions such as a digital indication of either the data rate (validated data points per second) or percent of total data signals processed that are validated. An output is normally provided to indicate each time a new data point is validated and processed. A digital output can be made available to allow introduction of the data directly into a computer or other digital recording system. An analog voltage output is also normally available.

Due to the difference in operating principles, the counter is not limited by slew rate or tracking rate performance. The counter is an extremely wide-band instrument, while the tracker is inherently narrow-band. Assuming the noise present is broadband, the noise rejection characteristics of the tracker is superior to that of the counter. However, since the tracker operates in the frequency domain, it is responsive to Doppler frequency spectrum broadening resulting from the finite duration of the signal burst. This broadening is similar to the modulation sidebands generated when a carrier frequency is amplitude modulated. The presence of multiple particles in the probe volume also generates phase reversals which cause spectrum broadening. Since the standard deviation about the mean velocity is a measure of turbulence and is related to the corresponding Doppler frequency deviation through Eq. (11.1), spectral broadening can interfere with turbulence measurements.

Particle Size and Distribution Effects

The size, size distribution, concentration, and physical characteristics of the particles in a transonic or supersonic tunnel flow field are of great importance, whether the particles are naturally present in the flow or the flow is seeded. In the presence of velocity gradients or turbulence, a significant velocity lag may exist between the fluid motion and the particle motion. Lag effects are most significant at high frequencies and in regions of rapid fluid acceleration or deceleration, as across a shock or expansion wave or along a streamline approaching a stagnation point. These environments, of interest in flow field surveys, would not normally be encountered in empty test section calibration measurements, but the ability of the particles to follow relatively small mean velocity perturbations and respond to low-to-moderate levels of turbulence are of interest.

The upper limit on particle size is determined by inertia or lag effects. and the lower limit, for high speed flows, may be determined by the reduced amount of light scattered by the particle which results in an unacceptably low signal-to-noise ratio.

Flow seeding may be required to obtain an adequate number of particles of controlled size, especially if a tracker processor is used. For measurements with a counter processor, naturally occuring particles in the flow may be utilized, Refs. 6 and 7. These particles are normally sparsely concentrated and result in no more than one particle in the measuring volume at the same time. However, seeding may be employed with a counter processor to control particle size and increase the data rate. Measurements in the 16-foot transonic tunnel at NASA Langley Research Center have been made using atomized oil to seed the flow, Ref. 5. Seeding in a continuous wind tunnel can create contamination problems which encourage the use of measurement procedures applicable to unseeded flows.

The motion of a spherical particle in a fluid flow has been reviewed by Hinze (Ref. 15). Soo (Ref. 16) also reviewed and summarized the equations describing particle motion. The complete equation, as given by Hinze is:

$$\frac{\pi}{6} d_p^3 \rho_p \frac{dV_p}{dt} = 3\pi\mu_g d_\rho (V_g - V_p) + \frac{\pi}{6} d_\rho^3 \rho_g \frac{dV_g}{dt} \qquad (11.11)$$

$$+ \frac{1}{2} \frac{\pi}{6} d^3 \rho_g \left(\frac{dV_g}{dt} - \frac{dV_p}{dt}\right)$$

$$+ \frac{3}{2} d_\rho^2 \sqrt{\pi\mu_g \rho_g} \int_{t_o}^{t} dt' \frac{\left[\frac{dV_g}{dt} - \frac{dV_p}{dt}\right]}{\sqrt{t - t'}} + F_e \, .$$

The subscript g refers to the gas and p to the particle; d_p is the diameter of the particle (assumed to be spherical), and t' is a dummy variable.

In this form the term on the left of the equality sign is the force required to accelerate the particle. The first term on the right is the drag force based on Stokes' law. The second term accounts for the pressure gradient in the fluid around the particle caused by acceleration of the fluid. The third term is the force required to accelerate the apparent mass of the particle relative to the ambient fluid.

The fourth term (designated the "Basset" term) accounts for the deviation of the flow pattern from steady state. The last term, F_e, represents body forces due to gravity, Lorentz force on a charged particle in an electric field, laser photon pressure, etc. Base (Ref. 17) reviews the complete equation as given by Hinze above but employs a more complex expression for drag (Oseen's law) to accommodate higher relative Reynolds numbers.

According to Hinze, the second, third and fourth terms on the right of Eq. (11.11) may be neglected if the density of the fluid is significantly less than the density of the particle, which is normally true. In the range of speeds encountered in transonic and supersonic tunnels, gravity effects are negligible compared to the drag force. Retaining only the Stokes' law drag term on the right side, Eq. (11.11) may be written

$$\frac{d^2\rho_p}{18\mu_g}\frac{dV_p}{dt} - (V_f - V_p) = 0 \quad . \tag{11.12}$$

This differential equation, which agrees with that given by Soo (Ref. 16), may be transformed into the standard transfer function form

$$\frac{V_p(S)}{V_f(S)} = \frac{1}{T_p S + 1} \quad ; \tag{11.13}$$

where S is the Laplace operator, and T_p is the time constant defined by

$$T_p = \frac{d_p^2\rho_p}{18\mu_g} \text{ (seconds)} \quad . \tag{11.14}$$

The steady state sinusoidal amplitude and phase response of the particle with respect to the gas may be expressed in the frequency domain by substituting $j\omega$ for S, where $j = \sqrt{-1}$.

$$\frac{V_p}{V_f} = \frac{1}{\left[T_p^2\omega^2 + 1\right]^{1/2}} \tag{11.15}$$

Here ω is the frequency of gas motion in radians per second. The phase angle, ϕ, by which the particle lags the fluid motion is

$$\phi = \tan^{-1}\frac{d_p^2\rho_p\omega}{18\mu_g} \quad . \tag{11.16}$$

The above equations based on Stokes' law agree with those given by Feller and Meyers (Ref. 18) and others. Mazumder, Hoyle and Kirsch (Ref. 19) and Yanta and Gates (Ref. 20) use a time constant expression similar to Eq. (11.14) except that a correction term is applied to the Stokes' drag coefficient to extend its applicability to the range of flow conditions where the Knudsen number ($K_n = \frac{\ell}{d_p}$) becomes appreciable. Epstein (Ref. 21) derived a correction term to Stokes' law from the kinetic theory viewpoint, as is discussed by Happel and Brenner (Ref. 22), but various forms and empirical constants have evolved. One of the simpler forms, used by Yanta and Gates (Ref. 20), results in a time constant expressed as

$$T_p = \frac{\rho_p d_p^2}{18\,\mu_g} \left(1 + k\,\frac{\ell}{d_p}\right) ; \qquad (11.17)$$

where k is the Cunningham constant (1.8 for air), and ℓ is the mean free path. From Eq. (11.17), the effect of increasing Knudsen number is to increase the time constant. The effect becomes significant (18%) for a ratio of mean free path to particle diameter of 0.1. Since the time constant increase can be significant for low density flows, Eq. (11.17) is more accurate for investigating particle response in these cases. This, of course, assumes Stokes' law to be valid. Thus, at this point, it is appropriate to discuss some of the limitations on the use of Stokes' law for particle drag in compressible flows.

A more detailed drag coefficient expression for large-differential Mach and Reynolds Number is given by Walsh (Ref. 23) and is based on experimental data. Walsh (Ref. 24) has compared results obtained using Stokes' drag coefficient equation with more complex expressions which account for a wide range of differential Reynolds and Mach numbers. Flow field studies included normal shocks in supersonic flow and velocity gradients up to 365 sec^{-1}. He concludes that the use of Stokes' law generally yields conservative results compared to the more accurate drag coefficient expressions, and it overpredicts the velocity lag by less than 10% for particle diameters less than 5 microns and velocity gradients up to 333 sec^{-1}. This overprediction decreases as the initial gas velocity increases, the velocity gradient decreases, and the particle size decreases. Considering other uncertainties,

such as the shape of the particle, the use of Stokes' drag coefficient is considered to be adequate for the purpose of this study; the exception being low density flows for which Eq. (11.17) is recommended.

The time constant defined by Eq. (11.14) is an extremely useful quantity for studying the particle lag problem. As in Eq. (11.15), it can be used to define the frequency response of the particle. In the time domain, the time constant is a measure of particle transient response. A step change in velocity lag, for example, is reduced to 1/e of its initial value in one time constant, $1/e^2$ in two time constants, etc. The relaxation length can also be determined by the product of the time constant and the gas velocity. As before, in one relaxation length the particle lag will reduce to 1/e of its initial velocity, etc.

According to Eq. (11.14), the fidelity with which particle motion represents fluid motion in a specific flow condition (test gas viscosity known) can be improved by reducing the particle diameter and density. Diameter reduction is particularly effective since the time constant increases according to diameter squared. As discussed previously, however, the minimum particle diameter is limited by the minimum acceptable signal-to-noise ratio.

An average particle density to 1 gm/cm^3 is commonly used for flow seeding at conditions typical of those encountered in transonic and supersonic wind tunnels. Seeding agents include dioctyl phthalate (DOP), silicone oil, and polystyrene latex (Ref. 19). A review of the several types of generators for introducing seeding particles of controlled size is given by Mazumder, Blevins and Kirsch (Ref. 25). For seeding high temperature gas flows, particles with higher melting points are necessary. Zirconium dioxide ($Zr\ O_2$), which has a melting point above 3000 K and a density of 5.9 gm/cm, and aluminum oxide ($Al_2\ O_3$) have been used for seeding high temperature gas flows, e.g., Ref. 26.

To demonstrate the effects of particle diameters, the frequency response of particles with a density of 1 gm/cm^3 and diameters ranging from 0.5 μm to 10 μm is shown in Fig. A.11.5 for Mach one flow and a stagnation temperature of 40 Celsius (104 ^oF). These response data clearly demonstrate the desirability of using particles with a diameter of approximately 0.5 μm. The time constants for particles with a density of 1 gm/cm^3 are shown in Fig. A.11.6 as a function

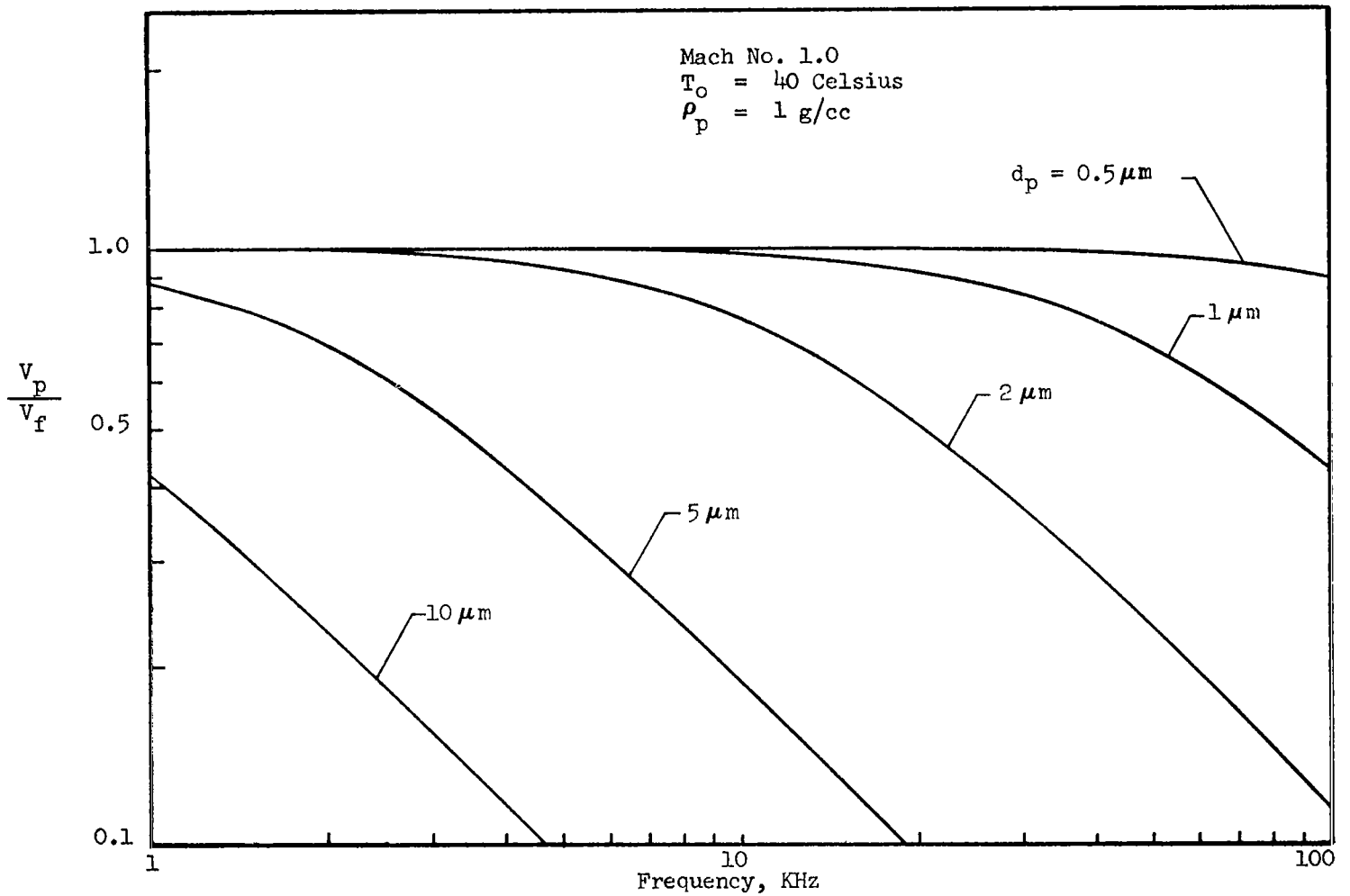

Figure A.11.5 EFFECT OF PARTICLE DIAMETER ON FREQUENCY RESPONSE

of particle diameter and with Mach numbers ranging from 0.5 to 3.0. From this Figure it may be seen that, for the assumed constant stagnation temperature, the time constant does not change significantly with Mach number. More effect would be apparent at Mach 2.0 and 3.0 for low density flow, in accordance with Eq. (11.17).

Various criteria may be chosen to define the required degree of fidelity of frequency response. If it is assumed that adequate measurements can be made when the particle lags the fluid motion by no more than 5%, i.e., $V_p/V_f = 0.95$, then from Eq. (11.15)

$$f_{0.95} = \frac{0.0523}{T_p}, \tag{11.18}$$

where $f_{0.95}$ is the upper frequency limit without realizing more than 5% attenuation of the particle velocity response to fluid motion. In Fig. A.11.7 this frequency limit is shown as a function of particle diameter and Mach number, again for a particle density of 1 gm/cm^3. In Figs. A.11.6 and 7, it is demonstrated that diameters of the order of 1 μm or less are required for measurements up to approximately 10 kHz, and that diameters less than 0.5 μm are necessary to extend accurate measurements to 100 kHz. These guidelines are obviously dependent on flow conditions and the definition of an acceptable amount of particle lag, but they are in general agreement with the conclusions of several investigations, based upon both experimental and analytical results. Pedigo and Stevenson (Ref. 27) state that for a particle to follow transonic flows with reasonable accuracy, the diameter should be less than 1 μm. Asher (Ref. 14), Mazumder, Hoyle and Kirsch (Ref. 19) and Seasholtz (Ref. 29) reach similar conclusions for rather widely varying flow conditions.

With regard to turbulence measurements in boundary layers, Yanta (Ref. 30) found that mean velocity and turbulence intensity distribution measurements with both 1 μm and 5 μm dioctyl phthalate particles were in very close agreement. These measurements were made in a Mach 3 flow channel operating at one atmosphere stagnation pressure. Yanta points out that in turbulent boundary layer flow, dominated by vortex motion, the particles are moving with the vortices and must respond to changes in velocity in a frame of reference moving with the flow (Lagrangian). A hot wire must respond to changes in velocity with respect to a fixed (Eulerian) frame of reference. As a consequence, larger particles can be used for turbulence measurements without particle lag effects.

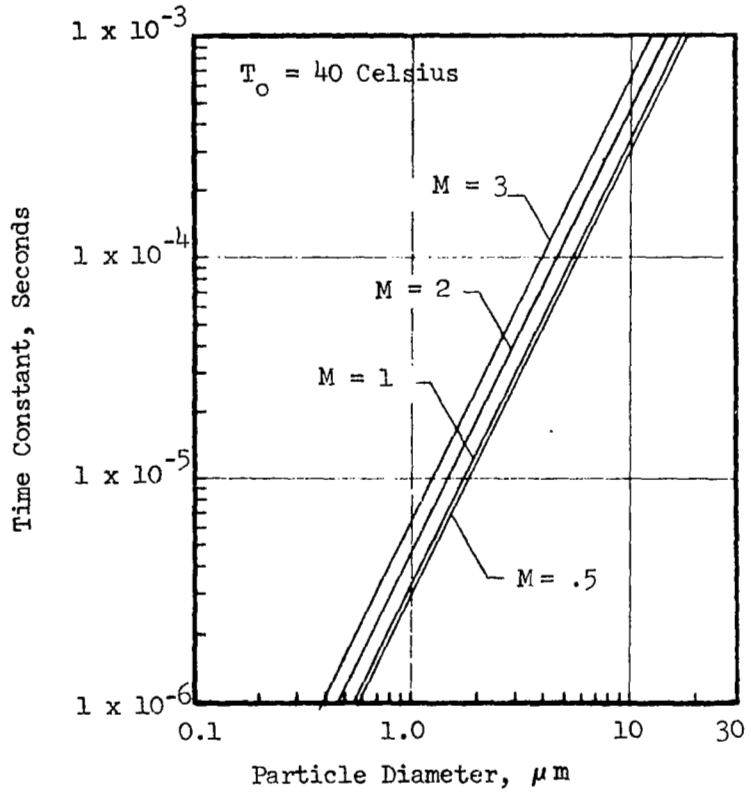

Figure A.11.6 TIME CONSTANT AS A FUNCTION OF PARTICLE DIAMETER FOR VARIOUS MACH NUMBERS, PARTICLE DENSITY = 1 gm/cc

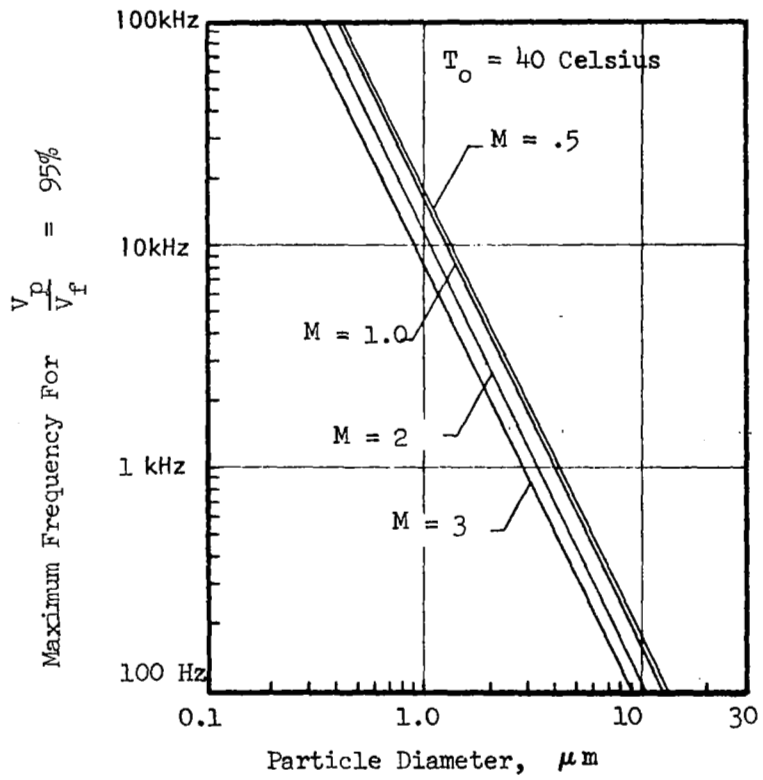

Figure A.11.7 MAXIMUM FREQUENCY FOR NO MORE THAN 5% ATTENUATION OF SINUSOIDAL VELOCITY VARIATIONS, PARTICLE DENSITY = 1 gm/cc

Data Analysis and Accuracy

The data normally obtained with a laser velocimeter include the mean velocity and the turbulence intensity in one, two or three components. By special analytical techniques, the spectrum of the turbulence can also be derived.

An individual measurement obtained from the velocimeter, U_i, is taken to represent the passage of an individual particle through the measuring volume (individual realization) since this occurence is typical of high-speed flows and counter-type processors. The individual measurement can deviate from the true mean velocity due to turbulence, noise and system resolution. The acquisition of a large number of measurements are therefore necessary to improve the accuracy of both the mean velocity and turbulence measurements.

The mean velocity as determined from a large number of individual measurements is

$$\overline{U} = \frac{\sum_{i=1}^{N} U_i}{N} \quad ; \tag{11.19}$$

where N is the number of values measured for a single test condition, and U_i is a single velocity measurement.

The standard deviation of the velocity probability distribution function is

$$\sigma_U = \left[\sum_{i=1}^{N} \frac{U_i^2}{N} - \overline{U}^2 \right]^{1/2} \tag{11.20}$$

If the effects of broadening of the Doppler frequency spectrum due to finite sample length and phase reversals (tracker processor) or, in general, apparent velocity fluctuations due to noise, etc., are negligibly small, the standard velocity deviation is equal to the root-mean-square turbulence velocity

$$\sigma_U = u' \quad ; \tag{11.21}$$

where $U = \overline{U} + u'$, and the turbulence intensity is $\frac{u'}{\overline{U}}$.

Correction of the measured turbulence velocity for the effects of Doppler spectral broadening (as occurs with a tracker processor) is discussed, for example, by George in (Ref. 31). The correction techniques for this type of bias are based on the white noise or broad-band characteristics of the intensity modulation of the Doppler frequency; whereas, the turbulence is band-limited.

Flack and Thompson (Ref. 32) have identified ten different biases which influence individual-realization, velocimetry measurements of mean velocity and turbulence. Magnitudes of the individual biases range from less than 0.1% to 31% for the turbulence component and from 0.1% to about 12% for the mean velocity component. The larger errors are associated with high turbulence intensities. The largest bias is due to the probability, in a turbulent flow, that more high velocity particles will be measured than low velocity particles.

This bias occurs because the individual measurements are not randomly distributed. If the scattering particles are uniformly distributed in the flow, the rate at which particles pass through the measuring volume is weighted linearly with velocity, Fig. A.11.8. This form of statistical bias is discussed by Barnett and Bentley (Ref. 33) and by McLaughlin and Tiederman (Ref. 34).

Velocity biasing can be corrected if a harmonic, rather than an arithmetic, mean is calculated, i.e.,

$$\overline{U} = \frac{N}{\sum_{i=1}^{N} \frac{1}{U_i}} \quad . \tag{11.22}$$

Barnett and Bentley derive the correction to the biased (arithmetic) mean in terms of the turbulence intensity as

$$\overline{U}_c = \frac{\sum_{i=1}^{N} U_i}{N} \left[\frac{1}{1 + (u'/\bar{U})^2} \right] \tag{11.23}$$

The correction to the arithmetic mean velocity for velocity bias is therefore significant only when the turbulent intensity is large; a turbulent intensity of 10% would result in a 1% correction to the mean velocity. It should be emphasized that Eqs. 11.22 and 11.23 are based on a one dimensional analysis and may not be generally applicable to all flows.

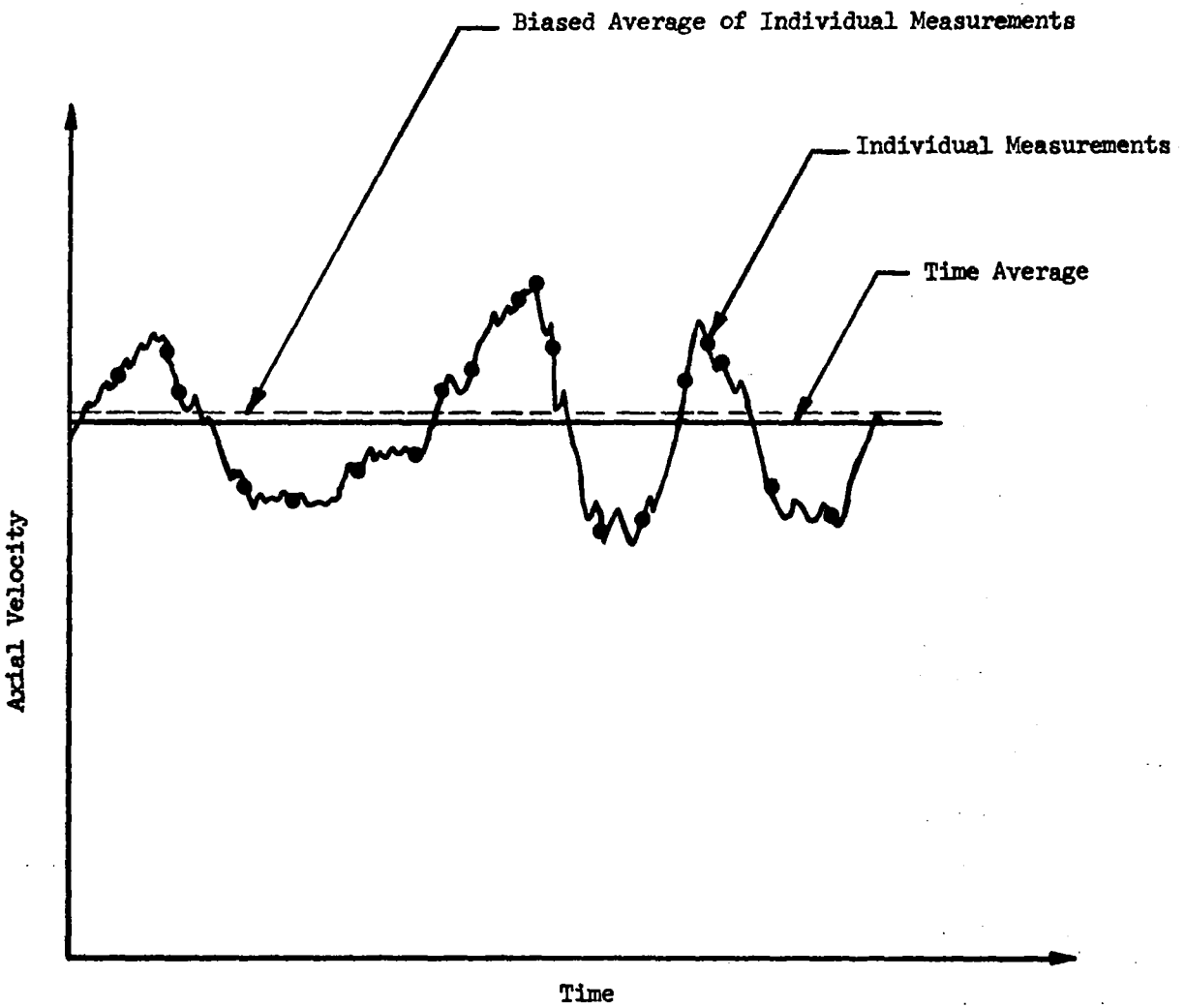

Figure A.11.8 EFFECT OF VELOCITY BIASING ON MEAN VELOCITY MEASUREMENT IN TURBULENT FLOW

The work to date on individual realization or velocity biasing has also been restricted to constant-density, velocity-fluctuation flows such as turbulent boundary layers. This work assumes uniform density of scattering particles. Further study is needed of other flow fields where the unsteadiness is dominated by unsteady shocks, acoustic sources, etc. In such cases, significant density variations occur, and density and velocity fluctuations may be correlated. For empty-test-section surveys of mean velocity in wind tunnels, turbulence is sufficiently low that the contribution of velocity biasing to the total measurement error would appear to be minor.

Yanta (Ref. 9) and Yanta and Smith, (Ref. 35) discuss the problem of determining the sample size, N, required to establish the uncertainty in a measured value, such as mean velocity, as a function of the turbulence intensity. For example,

$$N = \frac{Z^2 (u'/\overline{U})^2}{\left(\frac{\Delta \overline{U}}{\overline{U}}\right)^2} \quad . \tag{11.24}$$

When Z is the number of standard deviations corresponding to a desired confidence level (1.645, 1.96 and 2.58 for 90, 95 and 99-percent confidence limits, respectively), $\Delta\overline{U}/\overline{U}$ is the error in the mean value, and $u'/\overline{U}$ the turbulence intensity.

The confidence limits for the standard deviation of the velocity probability distribution (the rms turbulence, u') is given by

$$N = \frac{Z^2}{2(\Delta u'/u')^2} \quad . \tag{11.25}$$

Where $\Delta u'$ is the error in magnitude of the turbulence, and Z and N are as previously defined.

In the case of wind tunnel calibrations, the measurement period should be sufficiently long to average the lowest frequency component of tunnel flow unsteadiness. Therefore, the required measurement period will extend from one to more than 10 seconds, which may be of the same order of magnitude as the time required to obtain the necessary number of laser velocimeter measurements,

depending on the data rate. Some measurements in the AEDC Tunnel 1-T required several minutes per station.

An evaluation of the agreement between laser velocimeter and conventional, wind-tunnel-calibration measurements can be made from tests in several wind tunnels. Meyers, et. al., in Ref. (5) found that freestream velocities measured in the 4.9 m (16-foot) Langley Transonic Tunnel compared to the tunnel calibration measurements within $\pm 2\%$; where the uncertainty of the velocity based on the tunnel calibration is stated to be $\pm 1\%$. Although the particles used to seed the flow ranged in size from 10 to 15 microns, the authors did not consider particle lag to be a problem in the test section; although significant lag was present in the flow accelerating section of the tunnel.

Measurements in the 0.3 m (1-foot) AEDC Tunnel 1T in the Mach number range from 0.6 to 1.5 are reported by Smith et al. in Ref. (8). The error estimate for the conventional calibration data ranges from approximately two percent at Mach 0.6 to 0.5 percent at Mach 1.5. Multiple-point axial surveys of centerline calibration data, based on pressure measurements, were obtained only at Mach numbers 0.6 and 0.8, with a single-point, pressure-calibration, velocity measurement (at the same point on the tunnel centerline) of 2.5 to 2.7 percent. Comparison of the axial distributions obtained by both techniques at $M = 0.6$ showed the best agreement with an average difference of about 1.4 percent for a mean velocity of 216 mps, and the uncertainty bands overlapped. At Mach 0.8, the differences ranged from about 0.9 to 2.0 percent at a mean velocity of approximately 280 mps. Interestingly, all of the velocities measured with the laser velocimeter were higher than the velocities determined from pressure and temperature measurements. No explanation was offered for the difference, but obviously particle lag was not a factor. All measurements were made with naturally-present, light-scattering particles in the flow.

Flow angularity measurements were also made with the 2-component laser velocimeter, which demonstrated the ability to make angularity measurements with deviations ranging from $\pm .015$ degree to $\pm .25$ degrees. The deviations are a function of the rms deviations of the component velocities. No conventional angularity data were presented for comparison.

This test demonstrated the capability for measuring the flow angularity and an average of the flow fluctuations in both magnitude and direction.

The two tests described should be regarded as operational feasibility demonstrations only and should not be regarded as the best accuracy currently available. Further, since the laser velocimeter data are compared to conventional calibration data with a stated accuracy of approximately ± 0.5 to ± 2.0 percent, an absolute evaluation of the laser velocimeter accuracy cannot be made from these results.

Measurements by Johnson (Ref. 36), Johnson and Rose (Ref. 37), Yanta and Lee (Ref. 38) and Boutier and Lefevre (Ref. 39), provide additional evaluations of the agreement between flow velocity measurements by the laser velocimeter and by conventional Pitot and static probes. These freestream velocity measurements are somewhat limited in scope since they are obtained from boundary layer velocity profile measurements; nevertheless, agreement within 0.5% is demonstrated.

The laser velocimeter yields a direct measurement of flow velocity, while the Mach number is required for calibration of wind tunnels. A second measurement, the stagnation temperature, is therefore required. Using the energy equation, the local static temperature can then be determined from the measured velocity

$$T_\infty = T_o - \frac{V_\infty^2}{2 C_p} = T_o - \frac{V_\infty^2(\gamma - 1)}{2 \gamma R} \tag{11.25}$$

Where T_∞ is the test section temperature corresponding to V_∞, T_o is the stagnation temperature, C_p is the specific heat at constant pressure, R is the gas constant, and γ is the ratio of specific heats. The local Mach number can then be determined from

$$M = \frac{V_\infty}{a_\infty} \tag{11.26}$$

$$= \frac{V_\infty}{(\gamma R T_\infty)^{1/2}} \tag{11.27}$$

$$= \frac{V_\infty}{\{\gamma R (T_o - V_\infty^2/2C_p)\}^{1/2}} = \frac{V_\infty}{(\gamma R T_o - \frac{\gamma - 1}{2} V_\infty^2)^{1/2}} . \tag{11.28}$$

Sensitivity coefficients for measurements of both velocity and stagnation temperature are shown in Fig. A.11.9 for a stagnation temperature of 40° Celsius. From these data, measurement of Mach numbers to an accuracy of ±0.001 requires a velocity measurement accuracy of about 0.1% in the transonic speed range. This accuracy is not believed to be within the state-of-the-art at present.

Conclusions

The advantages and disadvantages of the laser velocimeter may be summarized as follows:

Advantages

1. No probe or other device introduced into the flow, i.e., non-pertubing.
2. Provides direct, linear measurement of velocity and velocity fluctuations; no calibration required.
3. Ability to measure reversing flows.
4. Ability to separate mean and fluctuating velocities into components.
5. Point measurements can be approached by proper control of measuring volume.
6. Can be realized as an inherently digital instrument.

Disadvantages

1. Complex, expensive equipment required
2. Measurement of high-velocity flows in large tunnels with an air test medium presents special problems with regard to single-to-noise ratio, frequency response, and sensitivity of equipment to tunnel vibration, temperature, etc.
3. Further development needed to improve signal processor, particularly with regard to data validation features, rejection of large particles, etc.
4. Light-scattering particles of size needed for good signal may not follow flow in regions of rapid velocity change.
5. Signal-to-noise ratio may preclude accurate turbulence intensity measurements at low levels, i.e., 0.1 to 1.0 percent.
6. Current accuracy attainable is not as good as with conventional techniques.
7. Takes excessive time to make the surveys required for wind tunnel calibration.

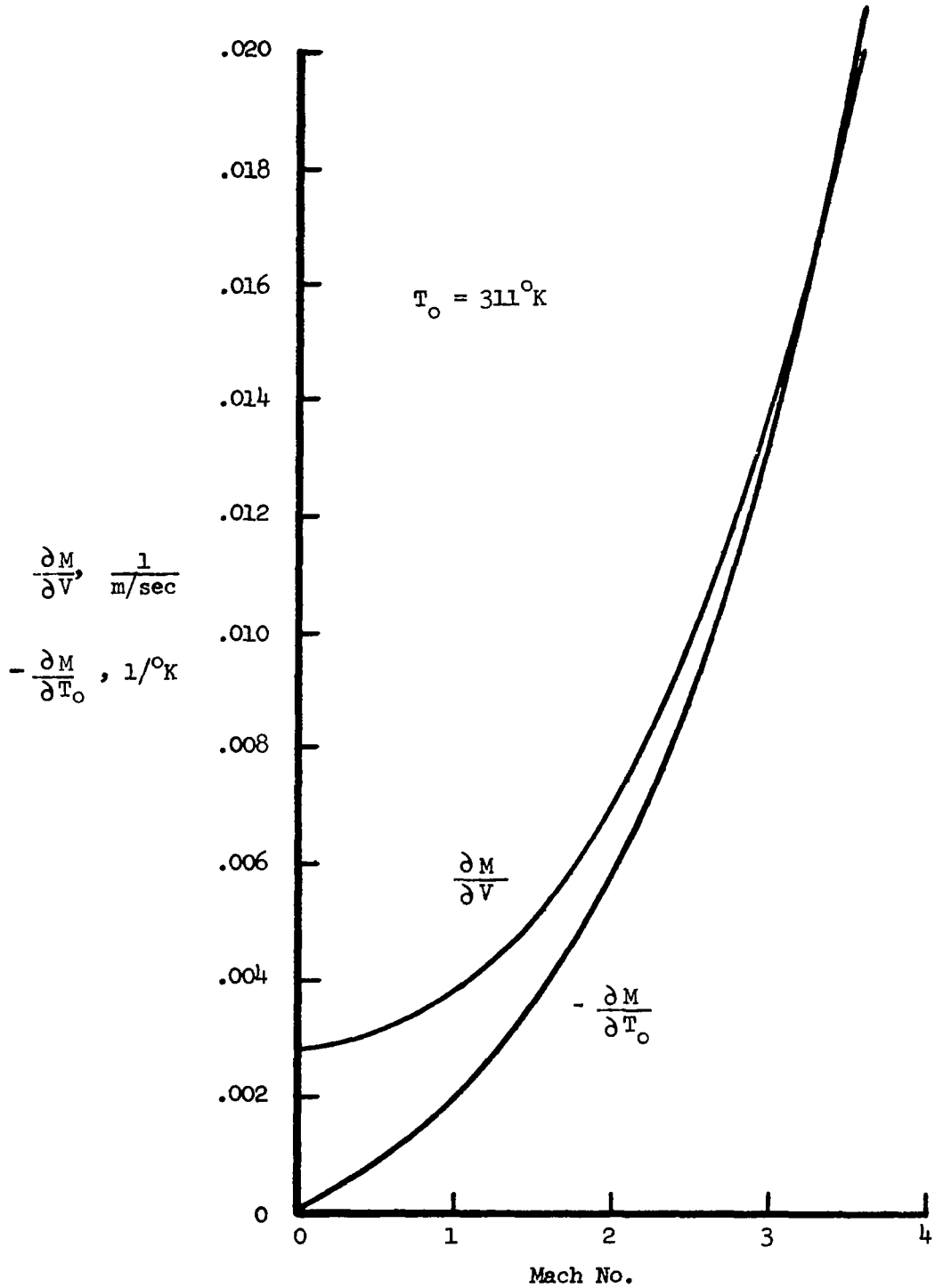

Figure A.11.9 SENSITIVITY COEFFICIENTS FOR DETERMINATION OF MACH NUMBER FROM VELOCITY AND STAGNATION TEMPERATURE MEASUREMENTS

Nomenclature

a_∞	free stream acoustic velocity
c_p	specific heat at constant pressure
D_o	initial diameter of laser beam
d_o	diameter of laser beams at the focal point of the transmitting lens
d_p	particle diameter
F	focal length of transmitting lens
F_e	body forces on particle (Eq. 11.11)
f_d	Doppler frequency, Hz
$f_{0.95}$	frequency at which particle motion is attenuated 5% relative to steady state sinusoidal fluid motion
j	$\sqrt{-1}$
K_n	Knudsen number
k	Cunningham constant (Eq. 11.17)
ℓ	mean free path
ℓ_v	length of measuring volume
M	Mach number
N	sample size
N_{f_r}	number of fringes in measuring volume
N_H	number of pulses counted in the high register of a counter processor
N_L	number of pulses counted in the low register of a counter processor
R	gas constant
S	Laplace operator
T_o	stagnation temperature

T_p	time constant defining particle response to variations in fluid flow velocity, seconds
T_∞	freestream temperature
t	time, seconds
t'	dummy variable (Eq. II.11)
U	velocity component normal to fringe pattern and to bisector of the angle formed by two intersecting laser beams
$\overline{U}$	mean velocity
$\overline{U}_c$	mean velocity, corrected for velocity bias
u'	rms turbulence velocity
$\Delta u'$	error in magnitude of turbulence velocity
V_g	gas flow velocity
V_p	particle velocity
V_∞	freestream velocity
w_v	width of measuring velocity
Z	number of standard deviations corresponding to a desired confidence level (Eq. II.24).

Greek

γ	ratio of specific heats
Δ	beam separation distance at the transmitting optics
δ_f	fringe spacing in measuring volume
θ	angle between laser beams at their intersection to form the measuring volume
λ	wavelength of laser light
μ_g	viscosity of gas
ρ_g	density of gas
ρ_p	density of particle
σ	standard deviation of velocity probability-distribution-function

phase angle, degrees

angular velocity, radians per second

REFERENCES

1. Yeh, Y. and Cummins, H. Z.: "Localized Fluid Flow Measurements with an He-Ne Laser Spectrometer," Vol. 4 pp 176-178, 1964.

2. Foreman, J. W.; George, W. W. and Lewis, R. O.: "Measurement of Localized flow Velocities in Gases With a Laser-Doppler Flowmeter," Applied Physics Letters, Vol. 7, pp 77-80, 1965.

3. Lennert, A. E.; Bragton, D. B.; Crosswy, F. L., et al: "Summary Report of the Development of a Laser Velocimeter to be Used in AEDC Wind Tunnels", AEDC-TR-70-101, July 1970.

4. Stevenson, W. H.; Pedigo, M. K. and Zamit, R. E.: "Bibliography on Laser Doppler Velocimeters: Theory, Design and Applications," U. S. Army Report No. RD-TR-72-8, 1972.

5. Meyers, J. F.; Crouch, L. M.; Feller, W. V. and Walsh, M. J.: "Laser Velocimeter Measurements in a Large Transonic Wind Tunnel," Proceedings of the Minnesota Symposium on Laser Anemometry, University of Minnesota, 1975.

6. Johnson, D. A.; Bochalo, W. D. and Modarress, D.: "Laser Velocimeter Supersonic and Transonic Wind Tunnel Studies," Proceedings of the Minnesota Symposium on Laser Anemometry, University of Minnesota, 1975.

7. Lo, C. F: "Transonic Flow Field Measurements Using a Laser Velocimeter," Proceedings of the Minnesota Symposium on Laser Anemometry, University of Minnesota, 1975.

8. Smith, F. H.; Lennert, A. E. and Hornkahl, J. O.: "Velocity Measurements in Aerodynamic Wind Tunnel (1T) Using a Laser Doppler Velocimeter," AEDC-TR-71-165, Feb. 1972.

9. Yanta, W. J.: "Turbulence Measurements with a Laser Doppler Velocimeter," TR 73-94, Naval Ordnance Laboratory, White Oak, Md., 1973.

10. Trolinger, J. D.: "Laser Instrumentation for Flow Field Diagnostics," AGARDograph No. 186, 1974.

11. Meyers, J. F.: "Investigation on Calibrations of Basic Parameters for the Application of the Laser Doppler Velocimeter, NASA TN D-6125, 1971.

12. Orloff, K. L. and Logan, S. E.: "Cofocal Backscatter Laser Velocimeter with On-Axis Sensitivity," Applied Optics, V. 12, No. 10, 1973.

13. Fridman, J. D. Young, R. M.; Seavey, R. E. and Orloff, K. L.: "Modular High Accuracy Trackers for Dual Channel Laser Doppler Velocimeter," Proceedings of the University of Minnesota Symposium on Laser Anemometry, 1975.

14. Asher, J. A.: "Laser Velocimeter System Development and Testing," Progress in Astronautics and Aeronautics, V. 34 pp 141-166, Massachusetts Institute of Technology, 1974.

15. Hinze, J. O.: Turbulence, An Introduction to its Mechanism and Theory, pp. 354-355, McGraw Hill, New York, 1959.

16. Soo, S. L.: Fluid Dynamics of Multiphase Systems, Blaisdell Publishing Co., Walthan, Mass., 1967.

17. Base, T. E.: "The Motion of Aerosol Particles in a Computed Turbulent Flow Model to Determine the Accuracy of a L.D.V. System," Proceedings of the Minnesota Symposium on Laser Anemometry, University of Minnesota, 1975.

18. Feller, W. W. and Meyers, J. F.: "Development of a Controllable Particle Generator for LV Seeding in Hypersonic Wind Tunnels," Proceedings of Minnesota Symposium on Laser Anemometry, University of Minnesota, 1975.

19. Mazumder, M. K.; Hoyle, B. D. and Kirsch, K. J.: "Generation and Fluid Dynamics of Scattering Aerosol in Laser Doppler Velocimetry," Proceedings of the Second International Workshop on Laser Velocimetry, Vol. II, Purdue University, March 1974.

20. Yanta, W. J. and Gates, D. F.: "The Use of a Laser Doppler Velocimeter in Supersonic Flows," AIAA Paper 71-287, Albuquerque, N.M., 1971.

21. Epstein, P. S.: Physical Review,V.23 (1924) p. 710.

22. Hoppel, T. and Brenner, H: Low Reynolds Number Hydrodynamics with Special Applications to Particulate Media, pp 50-51, Prentice-Hall, Englewood Cliffs, N. J., 1965.

23. Walsh, M. J., "Drag Coefficient Equations for Small Particles in High Speed Flows," AIAA Journal, V 13, No. 11, Nov., 1975.

24. Walsh, M. J.: "Influence of Drag Coefficient Equations on Particle Motion Calculations," Proceedings of the Minnesota Symposium on Laser Anemometry, University of Minnesota, 1975.

25. Mazumder, M. K.; Blevins, C. W. and Kirsch, K. J.: "Wind Tunnel Flow Seeding for Laser Velocimeter Applications," Proceedings of the Minnesota Symposium as Laser Anemometry, University of Minnesota, 1975.

26. Self, S. A., "Boundary Layer Measurements in High Velocity High Temperature MHD Channel Flows," Proceedings of the Second International Workshop on Laser Doppler Velocimetry, Purdue University, 1974.

27. Pedigo, M. K. and Stevenson, W. H., "The Design of a Laser Doppler Velocimeter for Transonic Flows," Purdue University, Prepared for Army Missile Command, AD-774 302, October 1973.

28. Haertig, J., Informal Presentation, Proceedings of the Second International Workshop on Laser Doppler Velocimetry, Purdue University, 1974.

29. Seasholtz, R. G., "Laser Doppler Velocimeter Measurements in a Turbine Stator Cascade Facility," Proceedings of the Second International Workshop on Laser Doppler Velocimetry, Purdue University, 1974.

30. Yanta, W. J., "Laser Doppler Velocimeter Measurements of Turbulence Properties of a Mach 3 Turbulent Boundary Layer," Proceedings of the Second International Workshop on Laser Velocimetry, Purdue University, 1974.

31. George, W. K., "The Measurement of Turbulence Intensities Using Real-Time Laser Doppler Velocimetry," Proceedings of the Second International Workshop on Laser Velocimetry, Purdue University, 1974.

32. Flack, R. D. and Thompson, H. D., "The LVD's Potential in Understanding Turbulent Structure," Proceedings of the Minnesota Symposium on Laser Anemometry, University of Minnesota, 1975.

33. Barnett, D. O. and Bentley, H. T., "Statistical Bias of Individual Realization Laser Velocimeters," Proceedings of the Second International Workshop on Laser Velocimetry, Purdue University, 1974.

34. McLaughlin, D. K. and Tiederman, W. G., "Biasing Correction for Individual Realization of Laser Anemometer Measurements in Turbulent Flows," The Physics of Fluids, Vol. 16, 1973.

35. Yanta, W. J. and Smith, R. A., "Measurement of Turbulence Transport Properties with a Laser Doppler Velocimeter," AIAA Paper No. 73-169, Jan. 1973.

36. Johnson, D. A., "Turbulence Measurements in a Mach 2.9 Boundary Layer Using Laser Velocimetry," AIAA Journal V 12 No. 5, pp 711-714, May 1974.

37. Johnson, D. A. and Rose, W. C., "Turbulence Measurements in a Transonic Boundary Layer and Free-Shear Flow Using Laser Velocimetry and Hot-Wire Anemometry Techniques," AIAA 9th Fluid and Plasma Dynamics Conference, Paper No. 76-399, July 1976.

38. Yanta, W. J. and Lee, R. E., "Measurements of Mach 3 Turbulence Transport Properties on a Nozzle Wall," AIAA Journal, V.14, No. 6, pp 725-729, June 1976.

39. Boutier, H. and Lefevre, J.: "Some Applications of Laser Anemometry in Wind-Tunnels," The Accuracy of Flow Measurements By Laser Doppler Methods, Proceedings of the LDA Symposium - Copenhagen, 1975.

APPENDIX III

EFFECTS OF VIBRATION OF A CYLINDRICAL PROBE ON STATIC PRESSURE MEASUREMENTS

In the process of collecting material for writing about mean static pressure measurements, the question arose as to how measured data would be affected by vibration of a probe. The problem of error in measured pressure caused by unsteady cross-flow has been previously considered by Siddon (Ref. 1). The following discussion is taken from this reference.

Some insight into the problem of a probe in an unsteady cross-flow can be obtained by use of an idealized flow model that ignores viscosity. Consider a cylindrical pressure probe of diameter d, subjected to a uniform, unsteady cross-velocity $V_n(t)$, see Fig. A.III.1. Any coupling effect of the axial velocity U(t) is neglected. Assuming the flow to be irrotational, the appropriate potential function is:

$$\phi = V_n \left(r + \frac{d^2}{4r}\right) \text{Cos } \eta .$$

The unsteady form of the Bernoulli equation gives:

$$P\ (r,\ \eta,\ t) - P_t(t) = \frac{1}{2}\rho\ (V_n^2 - v_r^2 - v_\eta^2) + \rho\ \frac{\partial \phi}{\partial t}$$

where,

$$v_r = -\frac{\partial \phi}{\partial r}\ , \qquad v_\eta = -\frac{1}{r}\frac{\partial \phi}{\partial \eta}\ .$$

$P_t(t)$ is the pressure which would have occurred at r = 0 in the absence of the probe (i.e., the 'true' pressure). At the surface of the probe (r = d/2), the pressure equation becomes:

$$P\ (\eta,t) - P_t(t) = \frac{1}{2}\rho\ V_n^2\ (1 - 4\ \text{Sin}^2\eta) + \rho \dot{V}_n d\ \text{Cos}\ \eta\ . \qquad \text{(III.1)}$$

The first term on the right hand side is recognized as the pressure distribution for steady potential flow. The second term arises from unsteadiness. For a pressure probe which registers the exact circumferential average of $P(\eta,t)$, (e.g., by means of a circumferential slit) the error will be:

$$P_m(t) - P_t(t) = -\frac{1}{2}\rho V_n^2 \quad ,$$

where $P_m(t)$ = measured unsteady static pressure.

In this ideal situation the part of the pressure distribution associated with the acceleration term $\dot{V}_n$ does not contribute to the error.

A real probe will not take an exact average over $P(\eta)$; therefore, an additional error proportional to $\dot{V}_n$ may arise.

$$P_m(t) - P_t(t) = -\frac{1}{2}\rho V_n^2 + K\rho \dot{V}_n d$$

Roughly speaking, the coefficient K (<1) represents the fractional inaccuracy of the average over $P(\eta)$. If we regard V_n as sinusoidal, the $\dot{V}_n$ error becomes increasingly important with frequency ($\dot{V}_n \sim \omega V_n$). Nevertheless, for a 0.318 cm (1/8 in.) diameter probe with an averaging inaccuracy of 5% and $V_n \cong 3.05$ m/sec (10 ft/sec), $K\rho \dot{V}_n d$ is less than 5% of the V_n^2 error at 100 Hz.

Based on responses to the questionnaire, many investigators have located a single row of orifices on either the top or side of a long pipe for tunnel calibrations. By using Eq. (III-1) with $\eta = 0$ (orifices on either top or bottom) and assuming the pipe oscillates sinusoidally, one can estimate the error in measured, mean static pressure, i.e.,

$$P(0, t) - P_t(t) = \frac{1}{2}\rho V_n^2(t) + \rho \dot{V}_n(t)\, d. \qquad \text{(III.2)}$$

Taking a time average over one cycle results in

$$\overline{P}_m(0) - \overline{P}_t = \frac{\rho}{2T}\int_0^T V_n^2(t)\, dt + \frac{\rho d}{T}\int_0^T \dot{V}_n(t)\, dt, \qquad \text{(III.3)}$$

where T = period of oscillation.

Before we can proceed any further, a characteristic frequency and amplitude must be assumed. For calculation purposes we here assume a frequency of 100 Hz.

Since we have previously established that it is desirable to measure mean static pressure to within 6.89 N/m^2 (0.001 psi), the amplitude of pipe oscillation will be calculated for the case $\overline{P}_m - \overline{P}_t = 6.89\ N/m^2$.

Hence, if the pipe oscillation is represented by

$$\text{Displacement} \equiv D = A \sin \omega t;$$

then

$$V_n = \dot{D} = A\omega \cos\omega t$$

$$\dot{V}_n = \ddot{D} = -A\omega^2 \sin\omega t.$$

Substituting into Eq. (III.3), we have

$$\overline{P}_m(0) - \overline{P}_t = 6.89 = \frac{\rho A^2}{2T}\int_0^T (\omega \cos\omega t)^2\, dt - \frac{\rho A d}{T}\int_0^T \omega^2 \sin\omega t\, dt$$

$$\therefore\ 6.89 = \frac{\rho A^2\omega^2}{2T}\int_0^T \frac{(1 + \cos 2\omega t)}{2}\, dt = \frac{\rho A^2\omega^2}{4} \qquad \text{(III.4)}$$

It may be noted from Eq. (III-4) that the required amplitude increases as frequency decreases. For the particular case of $\omega = 2\pi f = 200\pi$ and $\rho = 1.71\ N\ sec^2/m^4$ (0.00332 lbf sec^2/ft^4) [$P_0 = 2.41 \times 10^5\ N/m^2$ (35 psia), $T_0 = 311°K$ (560°R), M = 1], the amplitude required for significant pressure error is

$$A = \left[\frac{4\ (6.89)}{\rho\omega^2}\right]^{1/2} \cong 0.639\ cm\ (0.25\ in.) \qquad \text{(III.5)}$$

Therefore, a static pressure survey pipe with a single row of orifices, located on either the top or bottom, would have to oscillate at a frequency of 100 Hz and an amplitude of 0.639 cm in order to cause the measured pressure to be 6.89 N/m^2 (0.001 psi) too high.

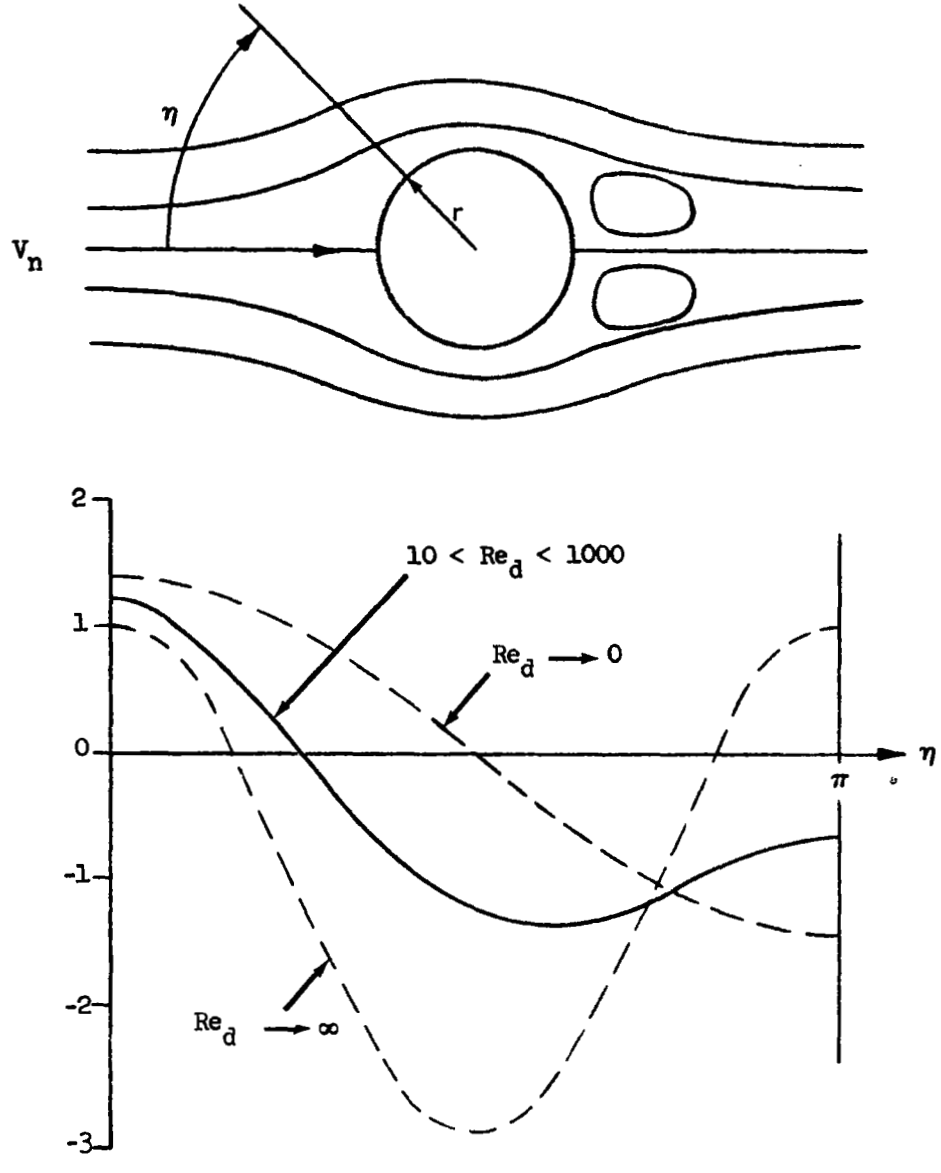

Figure A.III.1 PRESSURE DISTRIBUTION ON A CIRCULAR CYLINDER IN CROSSFLOW, Ref. 1

Going through the same procedure with $\eta = 90°$ (orifices on side of pipe), an amplitude of 0.368 cm (0.145 in.) is predicted to cause the measured, static pressure to be low by 6.89 N/m^2 (0.001 psi). Since large tension or compression loads are usually placed on static pressure survey pipes to minimize sag, it appears unlikely that pipe vibration is a significant source of error. Although this conclusion is based on an inviscid, incompressible analysis, it is considered to be conservative (i.e., gives a lower bound estimate of A) because of the neglect of pneumatic damping in tubing which connect orifices with pressure transducers.

A.III REFERENCES

1. Siddon, T. E., "On the Response of Pressure Measuring Instrumentation in Unsteady Flow," UTIAS Report No. 136, AD 682296, January 1969.

APPENDIX IV: FACILITIES RESPONDING TO QUESTIONNAIRE

TABLE I

Facility	Organization & Location	M	Re/m x 10^{-6} @ M = 1.0	Type	Cross-Section	Production Testing Began
4' Trisonic Blowdown	NAL Bangalore, India	0.2 - 4.0	24.6 - 60.7	Bd	1.22 m Sq.	1969
26" Transonic	GAC Grumman, A.C. Farmingdale, N.Y.	0.6 - 1.35	31 - 92	Bd	0.66 m Octagon	1957
16-Inch Supersonic WT	ETH Zurich, Switz.	0 - 0.95 1.2-2(2.5)	? - 7.5	Cont.	0.40 m Sq.	1935 (First, Cont. S.W.T)
High Speed WT	NLR Amsterdam, Holland	0 - 1.37	3.5 - 19	Cont.	1.6 x 2.0 m^2	1959
Continuous Supersonic WT	"	Insert.5-1.2 1.2 - 5.8	(M = 1.2) 30 - 50	Bd (Long Run Time)	0.27 x 0.27 m^2	1960
Pilot WT	"	0 - 1.0	14.1	Cont.	0.55 x 0.42 m^2	1956
Supersonic WT	"	1.2 - 4.0	21 - 54	Bd	Variable 1.2 x 1.2 m^2 0.9 x 1.2 m^2	1963
Supersonic Tunnel No. 1	U.S. Army Aberdeen, Md.	1.25 - 5.0	(M = 1.25) 4 - 23	Cont.	0.38 x 0.33 m^2	1956
Trisonic G.F.	USAF-FDL WPAB, Ohio	0.3 - 1.2 1.5 - 4.76	3.3 - 27	Cont.	0.38 x 0.38 m^2 0.61 x 0.61 m^2	N.A.
Mach 3 Hi-Re	USAF - ARL WPAFB, Ohio	2.97 - 3.03	33 - 359	Bd.	20.3 x 20.3 cm^2	1970
12" Trisonic	Sandia Albuquerque, N.M.	0.5 - 2.5	16.4	Bd	0.305 x 0.305 m^2	1956
8' x 6' SWT	NASA Lewis R.C. Cleveland, Ohio	0.36 - 2.1	15	Cont.	2.44 x 1.83 m^2	1949
10' x 10' SWT	"	2.0 - 3.5	(M = 2.0) 1 - 11	Cont.	3.05 x 3.05 m^2	1955
18-Inch	Aero. Res. Unit Pretoria, S.Afr.	0.6 - 4.2	12 - 30	Bd	0.45 x 0.45 m^2	1971

APPENDIX IV: FACILITIES RESPONDING TO QUESTIONNAIRE

TABLE I

Facility	Organization & Location	M	Re/m x 10^{-6} @ M = 1.0	Type	Cross-Section	Production Testing Began
1.2 m HSWT	BAC Preston, Eng.	0.4 - 4.0	21 - 74	Bd	1.22 x 1.22 m^2	1960
30" x 16" Suction W.T.	NAE Ottawa, Canada	0.4 - 2.0	15.1	Suction	0.76 x 0.41 m^2	1952
Trisonic Blowdown WT	"	0.1 - 4.4	16.4 - 62.3	Bd	1.52 x 1.52 m^2	1964
HRN-2DT	"	0.15 - 0.95	(M = 0.95) 26.25 - 131.2	Bd	0.38 x 1.52 m^2	1969
1/3 m Trans. Cryogenic Tun.	NASA Langley Res Ctr.Hampton, Va.	0.05 - 1.2	13.45 - 341	Cont.	0.34 m Octagon	1974
High Speed 7' x 10' Tun.	"	0.2 - 0.9	(M = 0.9) 11.8 - 16.1	Cont.	2.0 x 2.92 m^2	1946
4' x 4' Supersonic Press.T	"	1.25 - 2.20	(M = 1.25) 4.6 - 21.7	Cont.	1.37 x 1.37 m^2	1948
6" x 28" Transonic WT	"	0.3 - 1.20	32.8 - 98.4	Bd	15.2 x 72.4cm^2	1974
Transonic Dynamics Tun.	"	0 - 1.2	(1.05-2.53) air (8.04-19.7)Freon	Cont.	4.88 m x 4.88m 0.61 m corner fillets	1960
Unitary Plan WT	"	1.47 - 2.86 2.29 - 4.63	2.6 - 28 (M=1.5) 1.6 - 20 (M=2.3)	Cont.	1.22 x 1.22 m^2	1955
16' Transonic T	"	0.2 - 1.3	12 - 13.8	Cont.	4.72 m Oct.	1950
8' Transonic Pressure Tun.	"	0.2 - 1.3	1.3 - 15.9	Cont.	2.16 x 2.16 m^2	1952
2' Trisonic WT	Northrop Hawthorne, Ca.	0.20 - 1.35 1.5 - 3.0	0.28 - 49	Bd	0.61 m Sq.	1962
High Speed Subsonic WT	Picatinny Arsenal, Dover, N.J.	0.2 - 0.76	(M = 0.6) 11.12 - 12.96	Induction	0.61 m Diam.	N.A.

APPENDIX IV: FACILITIES RESPONDING TO QUESTIONNAIRE

TABLE I

Facility	Organization & Location	M	Re/m x 10^{-6} @ M = 1.0	Type	Cross-Section	Production Testing Began
16" Transonic WT	Picatinny Arsenal Dover, N.J.	0.3 - 1.25	20.5 - 25.9	Bd	0.42 x 0.41 m^2	N.A.
Compressible Flow Facility	Lockheed-Georgia Marietta, Ga.	0.2 - 1.2	22 - 203	Bd	0.71 x 0.51 m^2	1973
4" x 5" Supersonic WT	Univ. of Michigan Ann Arbor, Mich.	1.2 - 5.0	(M = 2) 0.72 - 78.7	Indraft	10.2 x 12.7 cm^2	1956
Trisonic WT S/T	Rockwell Int. Columbus, Ohio	0.3 - 1.3 1.7 - 3.0	6.6 - 72	Bd	0.66 m Sq.	1965
Polysonic WT	McDonnell-Douglas St.Louis, Mo.	0 - 5.82	23 - 54.5	Bd (Indraft Capability)	1.22 m Sq.	1960
Tunnel A	von Karman Gas Dyn Fac.AEDC/ARO Arnold AFS, Tenn.	1.5 - 6.0	(M = 1.5) 1.3 - 30	Cont.	1.02 m Sq.	1958
Tunnel D	"	1.5 - 5.0	(M = 1.5) 2 - 46.3	Bd	0.305 m Sq.	1955
Pilot HIRT	"	N.A.	N.A.	Ludwieg Tube	18.6x23.2 cm^2	N.A. (Research Only)
Transonic Induction WT	Technion Haifa, Israel	0.4 - 1.2	17.7	Induction	0.8 x 0.6 m^2	1968
30 cm SWT	"	1.5 - 2.25	(M = 1.5) 29.5 - 131	Bd	0.30 m Sq.	1960
40 x 50 cm SWT	"	1.5 - 4.0	(M = 1.5) 29.5 - 59	Bd	0.4 x 0.5 m^2	1968
7-Ft. Trisonic WT	Rockwell Int. El Segundo, Ca.	0.2 - 3.5	19.7 - 54.5	Bd	2.13 m Sq.	1958
8' x 9' Transonic WT	ARA Bedford, Eng.	0.35 - 1.4	11.2 - 17.7	Cont.	2.44 x 2.74 m^2	1956
2¼' x 2½' SWT	"	1.4 - 3.0	(M = 1.5) 5 - 13	Cont.	0.69x0.76 m^2	1959

APPENDIX IV: FACILITIES RESPONDING TO QUESTIONNAIRE

TABLE I

Facility	Organization & Location	M	Re/m x 10^{-6} @ M = 1.0	Type	Cross-Section	Production Testing Began
12" x 16" SWT	ARA Bedford, Eng.	4 - 5	(M = 4) 30	Bd	0.305x0.406m^2	1964
8" x 9" Transonic WT	"	0.3 - 1.3	15	Indraft	20.3x22.9 cm^2	1956
15-Inch SWT	WRE Salisbury, S. Aust.	0.4 - 1.0 1.4 - 2.8	3.3 - 0.38 m^2	Cont.	0.38x0.38 m^2	1957
S3 Bd WT	"	2.8 - 5.0	(M = 2.8) 16.4 - 65.6	Bd	17.8x15.2 cm^2	1966
Transonic WT	ARL Melbourne, Aust.	0.4 - 1.4	3.28 - 6.56	Cont.	0.81x0.53 m^2	1957
WT 1	Volvo Trollhatten Sweden	0.5 - 1.5	23 - 49	Bd	0.5 x 0.5 m^2	1952
WT 9	"	1.4 - 3.2	(M = 1.5) 29 - 55	Bd	0.5 x 0.5 m^2	1962
Boeing Supersonic WT	Boeing Seattle, Wash.	1.2 - 4.0	(M = 1.2) 19.7 - 45.9	Bd	1.22x1.22 m^2	1957
2D-TWT	"	0.2 - 1.25	26.25 - 77.1	Bd	0.305x0.91 m^2	1965
Boeing Transonic WT	"	0. - 1.11	12.7	Cont.	2.44 m x 3.66m 0.61 m corner fillets	1944
Lockheed Trisonic WT	Lockheed Saugus, Calif.	0.2 - 5.0	14.8 - 67.9	Bd	1.22x1.22 m^2	1960
HS - TWT	Hawker-Siddeley Hatfield,England	0.5 - 1.1	10.2 - 11.5	Cont.	0.76x0.61 m^2	1954
8' Transonic WT	Calspan Buffalo, N.Y.	0 - 1.34	1.3 - 18 28 - 42	Cont. @ low Re; Interm. @ high Re	2.44 m Sq.	1956
Ludwieg Tube	"	0.3 - 4.5	131	Ludwieg Tube	Variable Dia. 0.81m-1.52m	1966

APPENDIX IV: FACILITIES RESPONDING TO QUESTIONNAIRE

TABLE I

Facility	Organization & Location	M	Re/m x 10^{-6} @ M = 1.0	Type	Cross-Section	Production Testing Began
20" SWT	Jet Propulsion Lab.Pasadena,Ca.	0.3 - 0.9 1.3 - 5.6	(M = 1.5) 0.47 - 23.6	Cont.	0.51x0.46 m^2	1950
High Speed WT	Vought Corp. Dallas, Texas	0.5 - 5.0	21 - 44	Bd	1.22 m Sq.	1958
Aerodyn. WT - 1T	Propulsion WT Fac AEDC/ARO Tulla-homa, Tenn.	0.2 - 1.5	17	Cont.	0.305 m Sq.	1953
Aerodyn. WT - 4T	"	0.1 - 1.3, 1.6 & 2.0	1.3 - 22.5	Cont.	1.22 m Sq.	1968
Propulsion WT - 16T	"	0.2 - 1.6	1.3 - 23	Cont.	4.88 m Sq.	1957
Propulsion WT - 16S	"	1.5 - 4.75	(M = 2.0) 1.3 - 8.4	Cont.	4.88 m Sq.	1961
14" Trisonic WT	NASA Marshall SFC Huntsville,Ala.			Bd	0.356 m Sq.	1956
12' Pressure WT	NASA Ames RC Moffett Field,Ca.	0.- 0.98	2.1 - 5.4	Cont.	3.44 m Sq.	1946
14' Transonic WT	"	0.6 - 1.2	12 - 16.5	Cont.	4.11x4.18 m^2	1956
11' Transonic WT	"	0.4 - 1.4	6.7 - 32	Cont.	3.35 m Sq.	1956
2' Transonic WT	"	0.2 - 1.4	12 - 23.5	Cont.	0.61 m Sq.	1951
Injector-Driven Transonic WT	"	0 - 1.0, 1.2, 1.4	16.7 - 167	Cont.	15.24 cm Dia.	Pilot Model
9' x 7' Supersonic WT	"	1.55 - 2.5	(M = 2.0) 3 - 21.3	Cont.	2.74 x 2.13 m^2	1956
8' x 7' Supersonic WT	"	2.45 - 3.5	(M = 2.5) 3 - 17	Cont.	2.44 x 2.13 m^2	1956

APPENDIX IV: FACILITIES RESPONDING TO QUESTIONNAIRE

TABLE I

Facility	Organization & Location	M	Re/m x 10^{-6} @ M = 1.0	Type	Cross-Section	Production Testing Began
6' x 6' Supersonic WT	NASA Ames RC Moffett Field, Ca.	0.25 - 2.2	3.9 - 16	Cont.	1.83 m Sq.	1948
1' x 3' Supersonic WT	"	1.4 - 5.4		Cont.	0.864x0.305m^2 0.457x0.305m^2	1944
Supersonic Tunnel No. 1	Naval Surf.Weapons Cntr.,Silver Spg.	0.1 - 5.0	14.47	Indraft	0.4 m Sq.	1949
Supersonic Tunnel No. 2	"	0.3 - 1.1 1.5 - 5.0	7.2 - 16.4	Cont.	0.4 m Sq.	1949
Boundary Layer Channel	"	3 - 7	(M = 3) 0.66 - 32.8	Cont.Blow-down to a Vacuum	0.25x0.33 m^2	1966
NSWC Hypersonic Tunnel	"	1.2 - 3	(M = 1.2) 15.1 - 38.1	Bd	0.41 x 0.41 m^2 (Cir.Not.Avail)	1971 (low M capability)
Tunnel FFA-S4	Aero.Res.Inst. (FFA)Stockholm,Sw	0.5 - 1.9	16	Indraft	0.92 x 0.9 m^2	1955
Transonic Tunnel FFA-HT	"	0.3 - 1.3	4.2 - 14.0	Cont.	0.89 x 0.89m^2 Octagonal	1945 Modified 1960 & 1965
Trisonic Tunnel FFA-TVM 500	"	0.5 - 3.8	18 - 60	Bd	0.5 m sq.	1968
Tunnel FFA-S5	"	0.5 - 3.6	16	Indraft	0.46 x 0.48m^2	1956
8 x 6-Ft TWT	"	0.1 - 1.2	1.31 - 9.84	Cont.	2.44 x 1.83m^2	1956
3 x 4-Ft. SWT	Royal Airc.Est. Bedford,England	2.5 - 5.0	(M = 2,5) 1.64 - 11.1	Cont.	0.91 x 1.22m^2	1961
2 x 1.5-Ft TWT	"	0.5 - 1.4	2.84 - 7.87	Cont.	0.61 x 0.46m^2	1959
1 x 1 m TWT	DFVLR Gottingen,W.Ger.	0.5-2.2	17	Cont.	1 m Sq.	1965

APPENDIX IV: FACILITIES RESPONDING TO QUESTIONNAIRE

TABLE I

Facility	Organization & Location	M	Re/m x 10^{-6} @ M = 1.0	Type	Cross-Section	Production Testing Began
Trisonic Tunnel "B"	DFVLR Porz-Wahn, W. Germany	0.5 - 4.5	2 - 3.1	Bd.	0.6 m Sq.	1966
Transonic - Supersonic WT	DFVLR Braunschweigg W.G.	0.46 - 4	30 - 100	Bd	0.5 m Sq. (M>1) 0.6x0.34 m^2	NA
High Speed Cascade WT(HGK)	"	0.2 - 1.05	1.15 - 10	Cont.	(2-D Transonic) 0.25-0.50 m x 0.30 m	1956
Hi. Rey. No. Tube Tunnel	NASA Marshall SFC Huntsville,Ala.	0.4 - 2.0	630	Ludwieg Tube	0.81 m Dia.	1970

APPENDIX IV (Cont'd)

TABLE II: TEST SECTION CHARACTERISTICS

Facility	Cross-Section	Wall Type	Hole Size/Angle or Slot Width/Spacing	Porosity	Wall Angle	Venting of Plenum Chamber
NAL (India)	1.22 m Sq.	Perforated	1.27 cm, 90 SW 30° Top & Bot.	20% SW 6% T & B	1° to -2°	Ejector Flaps
GAC (NY)	0.66 m Octagon	Slotted		12% & 6%	0.08°	Ejector Flaps
ETH (Switz)	0.4 m Sq.	Solid				
NLR (HST Holland)	1.6 x 2 m^2	Slotted (T & B)	5 cm, 40 cm	12% T & B	0.13°	Fixed Ejector Slots
NLR (CSST)	0.27 x .27 m^2	Solid				
NLR (PT)	0.55 x 0.42 m^2	Slotted (T & B)	0.525 cm, 5.25 cm	10% T & B	0.22°	Fixed Ejector Slots
NLR (SST)	1.2 x 1.2 m^2	Solid				
U.S. Army (SST1)	0.38 x 0.33 m^2	Solid				
WPAFB (TGF)	0.38 x 0.38 m^2	Slotted	Width Variable	4 - 12%	0°	Ejector Flaps
WPAFB(M3HR)	20.3 x 20.3 cm^2	Solid				
Sandia (TWT)	0.305 x 0.305 m^2	Perforated	0.318 cm, 30°	6%	1°	Ejector Flaps
Lewis (8 x 6 SWT)	2.44 x 1.83 m^2	Perforated	2.54 cm, 30°	6%	0°	Auxiliary Pumps
Lewis (10 x 10 SWT)	3.05 x 3.05 m^2	Solid				
ARU (SWT)	0.45 x 0.45 m^2	Perforated		21%	0.6° T & B	Auxiliary Pumps

APPENDIX IV (Cont'd)

TABLE II: TEST SECTION CHARACTERISTICS

Facility	Cross-Section	Wall Type	Hole Size/Angle or Slot Width/Spacing	Porosity	Wall Angle	Venting of Plenum Chamber
BAC (HSWT)	1.22 x 1.22 m^2	Perforated	1.6 cm, 90°	19%	0°	Ejector Flaps
NAE (Su WT)	0.76 x 0.41 m^2	Slotted	0.58 cm, 4.7 cm		1°	
NAE (TBWT)	1.52 x 1.52 m^2	Perforated	1.27 cm, 90°	20.5%	-0.5° to-.25°	Ejector Flaps
NAE (2DT)	0.38 x 1.52 m^2	Perforated (T & B)	1.27 cm, 90°	20.5% T & B	0°	Venting to Atm.
ARA (TWT)	2.44 x 2.74 m^2	Perforated	1.27 cm, 90°	22.5%	0°	Auxiliary Pumps
ARA (SWT)	0.305 x 0.406 m^2	Solid				
ARA (TWT)	20.3 x 22.9 cm^2	Perforated	0.185 cm, 90°	22%	0°	Ejector Flaps
WRE (S1)	0.38 x 0.38 m^2	Slotted	2.54 cm, 12.38 cm	10% T & B	0°	Ejector Flaps
WRE (S3)	17.8 x 15.2 cm^2	Solid				
ARL (TWT)	0.81 x 0.53 m^2	Slotted		10 - 16%	0.5°	
Volvo (WT1)	0.5 x 0.5 m^2	Slotted (T & B)	?	4% T & B	0.21°	Ejector Flaps
Volvo (WT9)	0.5 x 0.5 m^2	Solid				
Boeing (SWT)	1.22 x 1.22 m^2	Solid				
Boeing (2D-TWT)	0.305 x 0.91 m^2	Perforated (T & B)	1.03 cm, 90°	34.1% T&B	0°	Ejector Flaps

APPENDIX IV (Cont'd)

TABLE II: TEST SECTION CHARACTERISTICS

Facility	Cross-Section	Wall Type	Hole Size/Angle or Slot Width/Spacing	Porosity	Wall Angle	Venting of Plenum Chamber
Boeing (TWT)	2.44 m x 3.66 m 0.61 m corner fillets	Slotted with inserts	7.45 cm, 70.41 cm T&B 47.31 cm SW	11% - 3.5%	0^{o}	Ejector Flaps
Lockheed (TWT)	1.22 x 1.22 m^2	Perforated	0.95 cm, 90^{o}	22%	-0.75^{o}	Auxiliary Pumps
Hawker Siddeley (TWT)	0.76 x 0.61 m^2	Slotted T&B Perf. Inserts	2.54 cm, 10.80 cm 0.10 cm, 90^{o}	3%	-0.17^{o}	Ejector Flaps
LRC (TDT)	4.88 m x 4.88 m 0.61 m Corner fillets	Slotted	6.35 cm, 148.6 cm	4.4%	0.067^{o} SW 0.167^{o} T&B	Ejector Flaps
LRC (UPWT)	1.22 x 1.22 m^2	Solid				
LRC (16' TT)	4.72 m Octagon	Slotted	7.62 cm, 1.95 m	3.9%	0^{o} - 0.75^{o}	Auxiliary Pumps
LRC (8' TPT)	2.16 x 2.16 m^2	Slotted	3.18 cm, 43.20 cm	3-6% T&B	0.083^{o} SW 0^{o} - 0.216^{o} T&B	Fixed Ejector Slots
LRC (1/3m TCT)	0.34 m Octagon	Slotted	Tapered from zero to 1.727 cm 14 cm	0-12%	0.083^{o}	Ejector Flaps or Venting to Atm.
LRC (HST)	2.0 x 2.92 m^2	Slotted	4.60 cm, 73.03 cm	4.8% T&B	0^{o}	Auxiliary Pumps & Ejector Flaps
LRC (4' SPT)	1.37 x 1.37 m^2	Solid				
LRC (6" TWT)	15.2 x 72.4 cm^2	Slotted	0.476 cm, 3.81 cm	12.5% T&B	0^{o}	Fixed Slots
NC (2' TWT)	0.61 m Sq.	Slotted Holes	0.318 x 2.54 cm, 1.91 cm	10%	$-2/3^{o}$ to $+1^{o}$	Ejector Flaps
PA (HSSWT)	0.61 m Dia.	Solid			0^{o} 10'	
PA (16" TWT)	0.42 x 0.41 m^2	Perforated	0.48 cm, 30^{o}	0.25 - 8%	NA	Valve Controls Diffuser Pumping

APPENDIX IV (Cont'd)

TABLE II: TEST SECTION CHARACTERISTICS

Facility	Cross-Section	Wall Type	Hole Size/Angle or Slot Width/Spacing	Porosity	Wall Angle	Venting of Plenum Chamber
L-G (CFF)	0.71 x 0.51 m^2	Perforated	0.635 cm, 30°	0-10%	0.25° T&B	Ejector Flaps
UM (4" x 5" SWT)	10.2 x 12.7 cm^2	Solid				
RI (TSWT)	0.66 m Sq.	Perforated	0.635 cm, 90°	23	0° to +.3°	Ejector Flaps
MD (PSWT)	1.22 m Sq.	Perforated	0.953 cm, 90°	25	-0.75° to 0°	Auxiliary Pumps
AEDC (Tunnel A)	1.02 m Sq.	Solid				
AEDC (Tunnel D)	0.305 m Sq.	Solid				
AEDC (Pilot HIRT)	18.6 x 23.2 cm^2	Perforated	.305 cm, 30°	0-10%	0°	Ejector Flaps and/ or Exhaust to Atm.
Technion (TIWT)	0.8 x 0.6 m^2	Perforated	.635 cm, 90°	21% T&B	+0.5°	Ejector Flaps
Technion (30 cm SWT)	0.3 m Sq.	Solid				
Technion (40 cm SWT)	0.4 x 0.5 m^2	Solid				
RI (TWT)	2.13 m Sq.	Perforated	0.635 cm, 90°	19.7%	0°	Ejector Flaps
Calspan (8' TWT)	2.44 m Sq.	Perforated	1.27 cm, 90°	22.7%	0° to 0.67°	Auxiliary Pumps & Venting to Atm.
Calspan (LT)	Variable Dia. 0.81 m - 1.52 m	Perforated				
JPL (SWT)	0.51 x 0.46 m^2	Solid				

APPENDIX IV (Cont'd)

TABLE II: TEST SECTION CHARACTERISTICS

Facility	Cross-Section	Wall Type	Hole Size/Angle or Slot Width/Spacing	Porosity	Wall Angle	Venting of Plenum Chamber
VC (HSWT)	1.22 m Sq.	Perforated	1.04 cm, 90°	22.5%	-0.33° T&B -0.42° SW	Ejector Flaps
AEDC (AWT-1T)	0.305 m Sq.	Perforated	0.318 cm, 30°	6% and 0 -10%	-0.67° to 0.5° T&B	Ejector Flaps & Steam Ejector Sys.
AEDC (AWT-4T)	1.22 m Sq.	Perforated	1.27 cm, 30°	0 - 10%	0 to 0.55° T&B	Ejector Flaps & Auxiliary Pumps
AEDC (PWT-16T)	4.88 m Sq.	Perforated	1.905 cm, 30°	6%	-1° to 0.3° T&B	Ejector Flaps & Auxiliary Pumps
AEDC (PWT-16S)	4.88 m Sq.	Solid				
NASA Marshall (14" TWT)	0.356 m Sq.	Perforated	0.556 cm, 30°	0-5.4%		Auxiliary Pumps
ARC (12' PWT)	3.44 m Sq.	Solid				
ARC (14' TWT)	4.11 x 4.18 m^2	Slotted with inserts	1.74 cm, 26.4 cm	5.6%	0.18° T&B	Ejector Flaps
ARC (11' TWT)	3.35 m Sq.	Slotted with inserts	1.59 cm, 26.4 cm	5.8%	0.19° SW	Ejector Flaps & Auxiliary Pumps
ARC (2' TWT)	0.61 m Sq.	Slotted with inserts	1.27 cm, 3.35 cm	22% with Throttle Bars	0° to 0.35°	Ejector Flaps
ARC (1-D TWT)	0.152 m Dia.	Solid				
ARC(7'x7' SWT)	2.74 x 2.13 m^2	Solid				
ARC(8'x7' SWT)	2.44 x 2.13 m^2	Solid				
ARC (6'x6' SWT)	1.83 m Sq.	Slotted T&B with inserts	1.03 cm, 28 cm	5.1%	0°	Auxiliary Pumps

APPENDIX IV (Cont'd)

TABLE II: TEST SECTION CHARACTERISTICS

Facility	Cross-Section	Wall Type	Hole Size/Angle or Slot Width/Spacing	Porosity	Wall Angle	Venting of Plenum Chamber
ARC(1'x3' SWT)	0.864 x 0.305 m^2 0.457 x 0.305 m^2	Solid				
NSWC (ST #1)	0.4 m Sq.	Perforated	0.15 cm, 90°	17.2%	NA	Auxiliary Pumps
NSWC(ST #2)	0.4 m Sq.	Transonic nozzle used in ST. #1 is available, but is not used routinely.				
NSWC (B-LC)	0.25 x 0.33 m^2	Solid			0.86°	
NSWC (H_yT)	0.41 x 0.41 m^2	Solid				
FFA-S4	0.92 x 0.90 m^2	Slotted	2.5 cm, 30 cm	6% T&B	0.15°	Ejector Flaps
FFA-HT	0.89 x 0.89 m^2 Octagonal	Slotted	3.4 cm, 37 cm	9.2%	0°	Ejector Flaps
FFA-TVM 500	0.5 m Sq.	Perforated	0.5 cm, 30°	6%	-6° to 0°	Auxiliary Pumps
FFA-S5	0.46 x 0.48 m^2	Slotted	0.21 cm, 5.3 cm	4% T&B	0.15°	Ejector Flaps
RAE(8'x6' TWT)	2.44 x 1.83 m^2	Slotted with inserts	3.94 cm, 35.4 cm	9.7%	-0.2° to 0.45°	Auxiliary Pumps
RAE(3'x4' SWT)	0.91 x 1.22 m^2	Solid				
RAE(2'x1.5' TWT)	9,5k x 9,45 m^2	Slotted	0.99 cm, 8.9 cm	9.75%	-0.4° to 0.9°	Ejector Flaps
DFVLR (1 m TWT)	1 m Sq.	Perforated	1 cm, 30°	6%	0° to 0.5°	Auxiliary Pumps Ejector Flaps
DFVLR (TT "B")	0.6 m Sq.	Perforated	0.6 cm, 30°	6%	-0.5 to 0°	Exhausted to Atm.

APPENDIX IV (Cont'd)

TABLE II: TEST SECTION CHARACTERISTICS

Facility	Cross-Section	Wall Type	Hole Size/Angle or Slot Width/Spacing	Porosity	Wall Angle	Venting of Plenum Chamber
DFVLR(T-S WT)	0.5 m Sq.(M > 1) 0.6 x 0.34 m^2	Slotted	0.8 cm, 6.8 cm	1 - 10%	0.05° to 0.1°	Exhausted to Atm.
DFVLR (HGK)	0.25 - 0.50 m x 0.30 m	Solid				
NASA Marshall (HRNTT)	0.81 m Dia.	Perf.	1.27 cm, 30°	Varies 1-10% along axis	0°	Ejector Flaps

1. Report No. NASA CR-2920	2. Government Accession No.	3. Recipient's Catalog No.
4. Title and Subtitle "Calibration of Transonic and Supersonic Wind Tunnels"		5. Report Date November 1977 6. Performing Organization Code
7. Author(s) T.D. Reed, T.C. Pope and J.M. Cooksey		8. Performing Organization Report No. 10. Work Unit No.
9. Performing Organization Name and Address Vought Corporation Dallas, Texas		11. Contract or Grant No. NAS 2-8606 13. Type of Report and Period Covered Contractor Report
12. Sponsoring Agency Name and Address National Aeronautics & Space Administration Washington, D.C. 20546		14. Sponsoring Agency Code

15. Supplementary Notes

16. Abstract

State-of-the art instrumentation and procedures for calibrating transonic ($0.6 < M < 1.4$) and supersonic ($M \leq 3.5$) wind tunnels are reviewed and evaluated. Major emphasis is given to transonic tunnels. Background information was obtained via a literature search, personal contacts, and a questionnaire which was sent to 106 domestic and foreign facilities. Completed questionnaires were received for 88 tunnels and included government, industry and university-owned facilities.

Continuous, blowdown and intermittent tunnels are considered. The required measurements of pressure, temperature, flow angularity, noise and humidity are discussed, and the effects of measurement uncertainties are summarized. Included is a comprehensive review of instrumentation currently used to calibrate empty-tunnel flow conditions. The recent results of relevant research are noted and recommendations for achieving improved data accuracy are made where appropriate. It is concluded, for general testing purposes, that satisfactory calibration measurements can be achieved in both transonic and supersonic tunnels. The goal of calibrating transonic tunnels to within 0.001 in centerline Mach number appears to be feasible with existing instrumentation, provided correct calibration procedures are carefully followed. A comparable accuracy can be achieved off-centerline with carefully designed, conventional probes, except near Mach 1. In the range $0.95 < M < 1.05$, the laser Doppler velocimeter appears to offer the most promise for improved calibration accuracy off-centerline.

With regard to procedures, tunnel operators are cautioned to: (1) verify by measurements that expansions from a settling chamber to a test section are indeed isentropic, and (2) obtain calibrations over the entire range of reynolds number and humidity levels. Also, it is suggested that calibration data should include off-centerline measurements of Mach number and flow angularity.

Finally, three problem areas for transonic tunnels are identified and discussed, viz. (1) the lack of standard criteria for flow uniformity and unsteadiness, (2) the undesirable noise generated by ventilated walls, and (3) wall interference.

17. Key Words (Suggested by Author(s))	18. Distribution Statement
Wind tunnels, Calibration, Testing	UNCLASSIFIED-UNLIMITED STAR Category 09

19. Security Classif. (of this report)	20. Security Classif. (of this page)	21. No. of Pages	22. Price*
UNCLASSIFIED	UNCLASSIFIED	287	$9.25

*For sale by the National Technical Information Service, Springfield, Virginia 22161

*U.S. GOVERNMENT PRINTING OFFICE: 1977 - 735-078/43